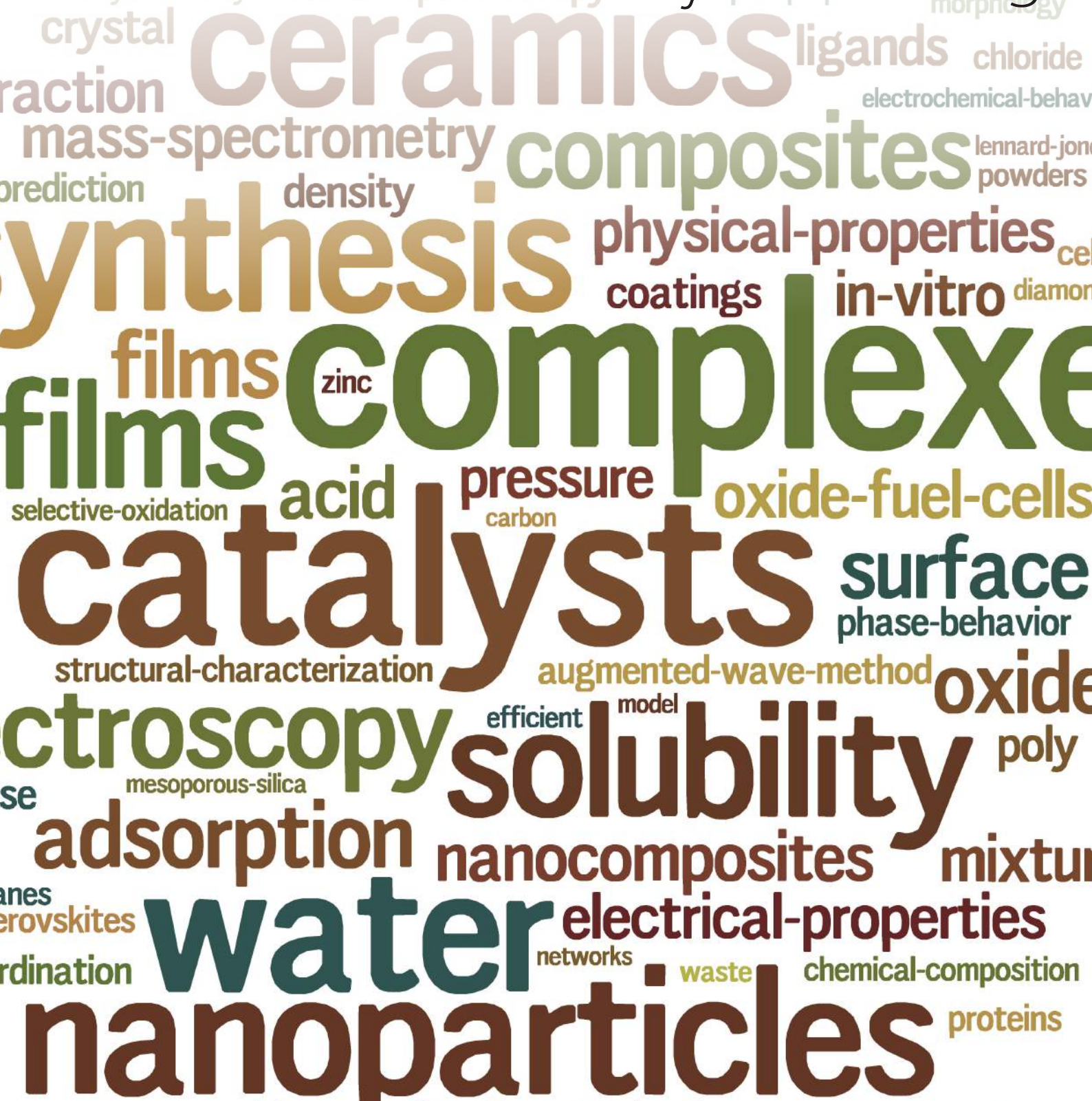


HIGHLIGHTING

# CICECO SCIENCE

The Associate Laboratory Review 2013



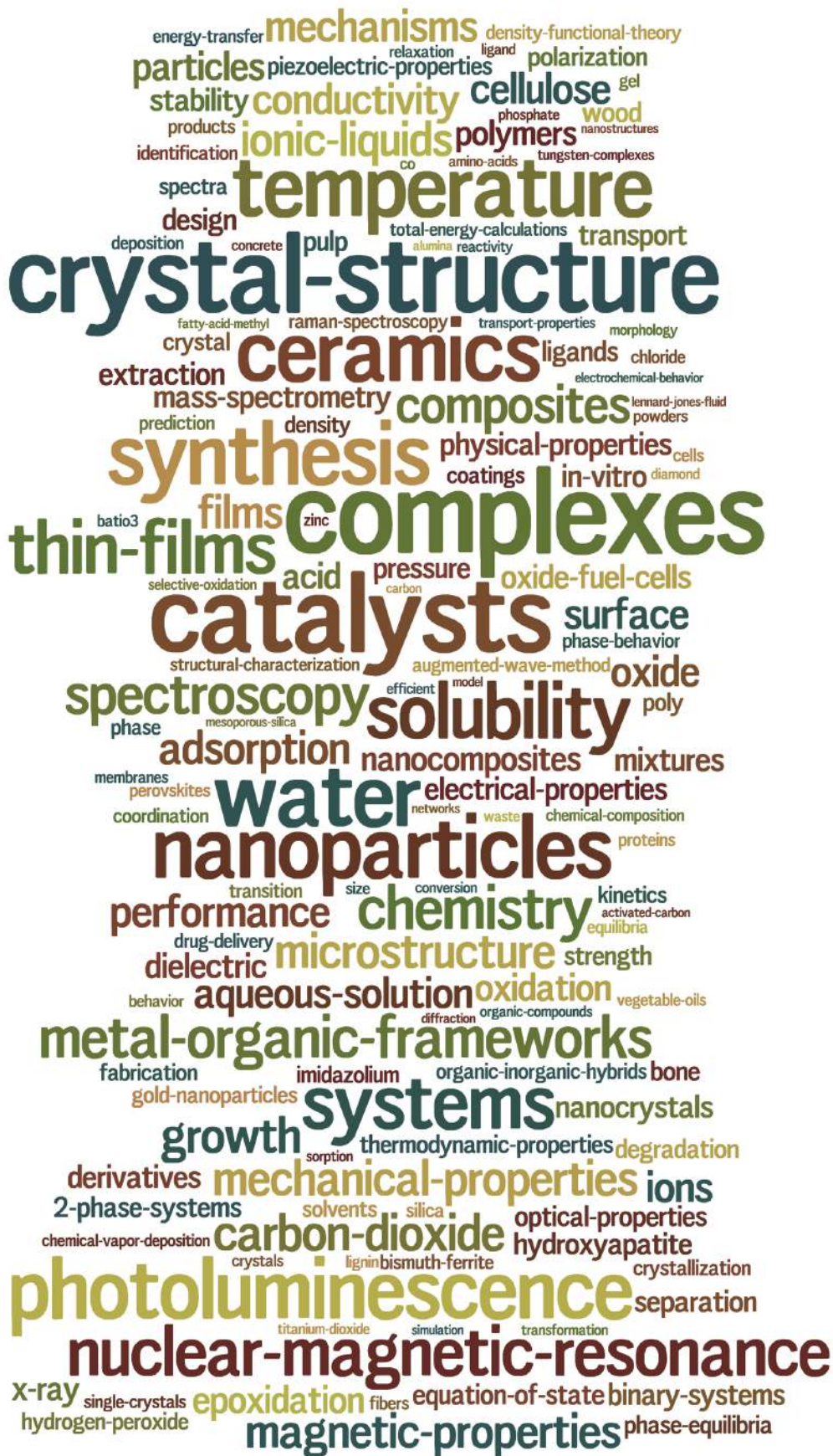


HIGHLIGHTING

**CICECO SCIENCE**

The Associate Laboratory Review 2013

free edition



## A WORD FROM THE DIRECTORS

A dozen years have passed since the associated laboratory CICECO was created in March 2002 at the University of Aveiro, Portugal. Entering the teenage years, we have matured and evolved into CICECO-Aveiro Institute of Materials, which better captures our present essence. Our Mission is developing the scientific and technological knowledge necessary for the innovative production and transformation of materials for a sustainable development and the benefit of society (from ceramics to soft matter and hybrids).

By the end of 2013 we were 48 academic staff, 32 full-time researchers, 91 post-doctoral associates, 119 Ph.D. students and 77 other students working in the Departments of Chemistry, Physics, Materials and Ceramic Engineering and Biology. We are organized in 3 research themes, Information and Communication Technology, Energy and Industrial Applications, Sustainability and Health, and 5 research groups, Inorganic Functional Nanomaterials and Organic-Inorganic Hybrids, Multifunctional Ferroic Ceramics and Nanostructures, Materials for Energy and Functional Surfaces, Biorefineries, Biobased Materials and Recycling, Biomedical and Biomimetic Materials.

These research highlights present some of the finest work done in the last three years. The word cloud in the cover and enclosed seizes some of the research areas where we are now most active. Words and papers we produce by the dozen but we never compromise with quality and are committed to continuously improve ourselves in the quest for scientific and cultural excellence.

Aveiro, July 2014.

João Rocha, Joaquim Vieira, Luís Carlos

# INDEX

## Nanomaterials and Nanostructures

- 8 DIRECT IMAGING OF JOULE HEATING DYNAMICS AND TEMPERATURE PROFILING INSIDE A CARBON NANOTUBE INTERCONNECT**  
Costa PMFJ, Gautam UK, Bando Y, Golberg D
- 8 GALVANIC REPLACEMENT REACTIONS IN METAL OXIDE NANOCRYSTALS**  
Oh MH, Yu T, Yu SH, Lim B, Ko KT, Willinger MG, Seo DH, Kim, BH, Cho MG, Park JH, Kang K, Sung YE, Pinna N, Heyeon T
- 9 ALL-IN-ONE HEATER-THERMOMETER NANOPATFORM OPERATIVE FROM 300 to 2000 K BASED ON  $Er^{3+}$  EMISSION AND BLACKBODY RADIATION**  
Debasu ML, Ananias D, Pastoriza-Santos I, Liz-Marzan LM, Rocha J, Carlos LD
- 10 SENSING ACTIVE COATING ON THE BASIS OF NANOREACTORS CONTAINING pH INDICATING AGENT**  
Maia F, Tedim J, Bastos AC, Ferreira MGS, Zheludkevich ML
- 11 DRY FERROFLUIDS**  
Sousa FL, Trindade T, Silva NJD
- 12 SILVER-MODIFIED NANO-TITANIA AS AN ANTIBACTERIAL AGENT AND PHOTOCATALYST**  
Tobaldi DM, Piccirillo C, Pullar RC, Gualtieri AF, Seabra MP, Castro PML, Labrincha JA
- 13 METAL-ORGANIC FRAMEWORKS BASED ON A PHOSPHONATE POLYMERIC ORGANIC LINKER**  
Silva P, Vieira F, Gomes AC, Ananias D, Fernandes JA, Bruno SM, Soares R, Valente AA, Rocha J, Paz FAA
- 14 CHIRAL TRANSPOSING FROM DIPHOSPHONATE METAL-ORGANIC FRAMEWORK PRECURSORS TO POROUS LANTHANIDE PYROPHOSPHATES**  
Shi FN, Paz FAA, Ribeiro-Claro P, Rocha J
- 15 MULTIFUNCTIONAL LANTHANIDE-ORGANIC FRAMEWORKS BASED ON A TRIPODAL PHOSPHONATE ORGANIC LINKER: PHOTOLUMINESCENCE AND HETEROGENEOUS CATALYSIS**  
Vilela SMF, Firmino ADG, Mendes RF, Fernandes JA, Ananias D, Gomes AC, Valente AA, Ott H, Carlos LD, Rocha J, Tomé JPC, Paz FAA
- 16 FUNCTIONAL NANOSTRUCTURED COMPOSITE MATERIALS BASED ON BACTERIAL CELLULOSE**  
Freire CSR, Silvestre AJD, Barros-Timmons A, Neto CP
- 16 SOFT NANOCOMPOSITES FOR STRONG SIGNAL ENHANCEMENT IN RAMAN SPECTROSCOPY**  
Fateixa S, Daniel-da-Silva AL, Nogueira HIS, Trindade T
- 18 LANTHANOPOLYOXOMETALATE BASED COMPOSITE MATERIALS**  
Nogueira HIS
- 19 EVIDENCE FOR ENTANGLEMENT AT HIGH TEMPERATURES IN AN ENGINEERED MOLECULAR MAGNET**  
Brandão P, Moreira dos Santos A, Reis MS

- 20 USE OF INNOVATIVE ECO-BUILDING MATERIALS**  
Tobaldi DM, Pullar RC, Seabra MP, Labrincha JA
- 21 SYNTHESIS AND STRUCTURE OF NOVEL INORGANIC LAYERED MATERIALS**  
Lin Z, Wu ZY, Zhang XS, Brandão P, Dong JX
- 22 ANOMALY ON THE GRAIN GROWTH AND DIELECTRIC RESPONSE OF TI-RICH STRONTIUM TITANATE CERAMICS**  
Amaral L, Fernandes M, Reaney IM, Harmer MP, Senos AMR, Vilarinho PM
- 23 CAN POROSITY BE AN ADVANTAGE? YES, IT CAN!**  
Ferreira P, Castro A, Laberty C, Boissière C, Grosso D, Sanchez C, Rodriguez B, Vilarinho PM
- 24 LOCAL BIAS INDUCED FERROELECTRICITY IN MANGANITES WITH COMPETING CHARGE AND ORBITAL ORDER STATES**  
Figueiras FGN, Bdkin IK, Amaral VBS, Kholkin AL
- 25 AQUEOUS PROCESSING OF LEAD FREE  $0.5Ba(Zr_{0.2}Ti_{0.8})O_3-0.5(Ba_{0.7}Ca_{0.3})TiO_3$  PIEZOELECTRIC CERAMIC MICRO-COMPONENTS FROM A POWDER SURFACE TREATED AGAINST HYDROLYSIS**  
Kaushal A, Olhero SM, Ferreira JMF
- 26 NANOSCALE FERROELECTRICITY IN CRYSTALLINE  $\Gamma$ -GLYCINE**  
Heredia A, Kholkin AL, Bdkin I, Gracio J, Meunier V, Balke N, Tselev A, Agarwal P, Sumpster BG, Kalinin SV
- 26 SYNERGISTIC CORROSION INHIBITION ON GALVANICALLY COUPLED MATERIALS**  
Kallip S, Bastos AC, Ferreira MGS, Zheludkevich ML

## Energy, Lighting and Photonics

- 30 {3 + 3} DIMENSIONAL 'HYPERCUBIC' OXIDE-IONIC CONDUCTOR: TYPE II  $Bi_2O_3-Nb_2O_5$**   
Ling CD, Schmid S, Blanchard PER, Petříček V, McIntyre GJ, Sharma N, Maljuk A, Yaremchenko AA, Kharton VV, Gutmann M, Withers RL
- 30 MATERIALS AND CONCEPTS FOR CARBON LEAN STEELMAKING BY PYROELECTROLYSIS**  
Kovalevsky AV, Ferreira NM, Yaremchenko AA, Costa FM, Frade JR
- 31 SrTiO<sub>3</sub>-BASED THERMOELECTRICS FOR EFFICIENT HIGH TEMPERATURE WASTE HEAT CONVERSION**  
Kovalevsky AV, Yaremchenko AA, Populoh S, Weidenkaff A, Frade JR
- 32 Pr-SUBSTITUTED SrTiO<sub>3</sub> AS PROSPECTIVE SOLID OXIDE FUEL CELL ANODE MATERIAL**  
Yaremchenko AA, Patrício SG, Frade JR
- 33 OXYGEN-ION TRANSPORT IN  $Ba_{0.5}Sr_{0.5}Co_{0.8}Fe_{0.2}O_{3-\delta}$ : DEVELOPMENTS OF ASYMMETRIC/MULTILAYER AND HOLLOW-FIBER CERAMIC MEMBRANES FOR OXYGEN SEPARATION**  
Kovalevsky AV, Yaremchenko AA, Kolotygin VA, Buysse C, Middelkoop V, Snijkers F, Buekenhoudt A, Frade JR

- 34 CERAMIC TILES WITH CONTROLLED POROSITY AND LOW THERMAL CONDUCTIVITY BY USING PORE-FORMING AGENTS**  
Novais RM, Seabra MP, Labrincha JA
- 35 MODULATING THE PHOTOLUMINESCENCE OF BRIDGED SILSESQUIOXANES FOR LUMINESCENT SOLAR CONCENTRATORS**  
Correia SFH, André PS, Ferreira RAS, Carlos LD
- 35 PHOTONIC-ON-A-CHIP: A THERMAL ACTUATED MACH-ZEHNDER INTERFEROMETER AND A MOLECULAR THERMOMETER BASED ON A SINGLE DI-UREASIL ORGANIC-INORGANIC HYBRID**  
Ferreira RAS, Brites CDS, Vicente CMS, Lima PP, Carlos LD, André PS
- 36 NOVEL BIFUNCTIONAL MAGNETIC-NEAR-INFRARED LUMINESCENT NANOCOMPOSITES: NEAR-INFRARED EMISSION FROM Nd and Yb**  
Yu SY, Fu LS, Zhou YJ, Su

## Catalysis and Separation

- 40 SUPPORTED IONIC LIQUID SILICA NANOPARTICLES ARE EXCELLENT HETEROGENEOUS CATALYSTS FOR THE DEHYDRATION OF FRUCTOSE TO 5-HYDROXYMETHYLFURFURAL**  
Sidhpuria KB, Daniel-da-Silva AL, Trindade T, Coutinho JAP
- 41 TARGETING BIO-DERIVED CHEMICALS BY TUNING THE PROPERTIES OF SOLID ACID CATALYSTS**  
Antunes MM, Lima S, Neves P, Russo PA, Wiper PV, Fernandes A, Ferreira LR, Abrantes JP, Veiga JM, Pillinger M, Mafra L, Portugal I, Evtuguin DV, Pinna N, Rocha SM, Ribeiro MF, Valente AA
- 42 INVESTIGATION OF A DICHLORODIOXOMOLYBDENUM(VI)-PYRAZOLYLPIRIDINE COMPLEX AND A HYBRID DERIVATIVE AS CATALYSTS IN OLEFIN EPOXIDATION**  
Amarante TR, Neves P, Paz FAA, Valente AA, Pillinger M, Gonçalves IS
- 43 IRON-SUBSTITUTED POLYOXOTUNGSTATES AND THEIR CATALYTIC APPLICATIONS**  
Cavaleiro AMV, Nogueira HIS
- 44 COPPER(II) BIS(OXAZOLINE)-TYPE LIGANDS IMMOBILIZED ONTO MESOPOROUS SILICAS AND THEIR CARBON REPLICAS AS EFFICIENT ASYMMETRIC HETEROGENEOUS CATALYSTS FOR ORGANIC TRANSFORMATIONS**  
Silva AR, Carneiro L, Guimarães V, Carvalho AP, Pires J
- 45 INTERCALATION OF MOLYBDENUM CARBONYL COMPLEXES IN LAYERED DOUBLE HYDROXIDES**  
Gomes AC, Bruno SM, Gamelas CA, Valente AA, Abrantes M, Gonçalves IS, Romão CC, Pillinger M
- 46 CO<sub>2</sub> ADSORPTION AND ACTIVATION BY AMINE-MODIFIED NANOPOROUS MATERIALS STUDIED BY NMR AND <sup>13</sup>C<sub>2</sub>O<sub>2</sub> ADSORPTION**  
Pinto ML, Mafra L, Guil JM, Pires J, Rocha J

**47 CARBOHYDRATES AND IONIC LIQUIDS IN AQUEOUS MEDIA: A MAJOR PATH TOWARDS A SUSTAINABLE DEVELOPMENT**

Freire MG, Louros CLS, Rebelo LPN, Coutinho JAP

**48 ZEOLITIC INORGANIC MEMBRANES**

Lin Z, Cardoso SP, Silva CM

**49 MODELING TRACER DIFFUSION COEFFICIENTS IN LIQUIDS, GASES AND SUPERCRITICAL FLUIDS**

Vaz RV, Magalhães AL, Gomes JRB, Silva CM

**49 IONIC LIQUIDS MICROEMULSIONS: THE KEY TO CANDIDA ANTARCTICA LIPASE B SUPERACTIVITY**

Ventura SPM, Santos LDF, Saraiva JA, Coutinho JAP

**50 SCALE-UP STUDIES OF THE SUPERCRITICAL FLUID EXTRACTION OF TRITERPENOIDS FROM EUCALYPTUS BARK**

Melo MMR, Silvestre AJD, Silva CM

**Biorefineries and Materials from Renewable Sources**

**54 2<sup>nd</sup> GENERATION BIOETHANOL PRODUCTION FROM DIFFERENT LIGNOCELLULOSIC RESIDUES**

Pereira SR, Fernandes MC, Gorwa-Grauslund MF, Evtuguin DV, Serafim LS, Xavier AMRB

**55 ADVANCED CELLULOSE/SILICA HYBRID MATERIALS**

Evtuguin DV, Portugal I

**56 TARGETED MODIFICATION OF CELLULOSIC MATERIALS USING ULTRAHIGH PRESSURE PROCESSING**

Evtuguin DV, Saraiva JA

**56 POTENTIOMETRIC CHEMICAL SENSORS FROM LIGNIN-DERIVED NANOCOMPOSITES**

Rudnitskaya A, Evtuguin DV, Costa LC, Graça MPF, Correia, MRP, Fernandes AJ

**57 GETTING VALUE FROM WASTES: BIOLOGICAL PRODUCTION OF BIODEGRADABLE PLASTICS**

Queirós DC, Xavier AMRB, Evtuguin DV, Rossetti S, Serafim LS

**58 PLANT OIL-BASED LONG-CHAIN MONOMERS AND THEIR POLYMERS**

Vilela C, Silvestre AJD, Meier MAR

**59 TWO STEPS FORWARD IN THE DEVELOPMENT OF FURAN-BASED POLYESTERS**

Sousa AF, Matos M, Freire CSR, Silvestre AJD, Coelho JFJ

**Biomedical Materials and Applications**

**62 SLOW RELEASE OF NO BY MICROPOROUS TITANOSILICATE ETS-4**

Pinto ML, Rocha J, Gomes RJB, Pires J

**63 QUANTIFYING WEAK PACKAGING INTERACTIONS IN THE HYDRATED AND ANHYDROUS FORMS OF ANTIBIOTIC CIPROFLOXACIN**

Mafra L, Santos SM, Siegel R, Alves I, Paz FAA, Dudenko D, Spiess HW

**64 BACTERIAL CELLULOSE AS TRANSDERMAL DRUG DELIVERY SYSTEMS**

Silva NHCS, Silvestre AJD, Freire CSR, Neto CP

**65 PHOTOTHERMALLY ENHANCED DRUG RELEASE BY HYDROGELS REINFORCED WITH CARBON NANOTUBES**

Estrada AC, Daniel-da-Silva AL, Trindade T

**65 NOVEL BINUCLEAR COPPER COMPLEXES AS ALTERNATIVE ANTI-TUMORAL DRUGS: SYNTHESIS, CHARACTERISATION AND CYTOTOXIC STUDIES**

Brandão P, Ferreira BJML, Santos TM, Meireles M, Félix V

**66 BONE MECHANICAL STIMULATION WITH PIEZOELECTRIC MATERIALS**

Reis J, Frias C, Silva FC, Potes J, Simões JA, Botelho ML, Castro CC, Marques AT

**67 POLARIZATION SWITCHING IN HYDROXYAPATITE: BONES CAN GROW FASTER**

Lang SB, Tofail SAM, Kholkin AL, Wojta D M, Gregor M, Wang Y, Bauer S, Krause M, Plecenik A

**69 CARBON NANOTUBE/BIOCERAMIC COMPOSITES FOR IN SITU ELECTRICAL STIMULATION OF BONE**

Mata D, Oliveira FJ, Neto MA, Bastos AC, Lopes MA, Gomes PS, Fernandes MHV, Silva RF

**71 MODULATING CELLULAR RESPONSE WITH ENGINEERED HAP NANOPARTICLES**

Costa MEV, Almeida MM, Santos C

**72 PIEZOELECTRIC PLLA AS A PLATFORM FOR TISSUE GROWTH**

Barroca N, Vilarinho PM, Daniel-da-Silva AL, Wu A, Fernandes MHV, Gruverman A

**73 A NEW APPROACH TO THE PREPARATION OF PDMS-SiO<sub>2</sub> BASED HYBRIDS - A STRUCTURAL STUDY**

Almeida JC, Castro AGB, Salvado IMM, Margaca FMA, Fernandes MHV

**74 SELECTIVE, ULTRASHARP, BORON DOPED DIAMOND MICROELECTRODES**

Silva EL, Bastos AC, Neto MA, Silva RF, Ferreira MGS, Zheludkevich ML, Oliveira FJ

**75 BIOMATERIALS FROM THE VALORISATION OF WASTE COD FISH BONES WITH APPLICATIONS IN PHOTOCATALYSIS, POLLUTION REMEDIATION AND SELF-STERILISING MATERIALS**

Piccirillo C, Pullar RC, Silva MF, Tobaldi DM, Pereira SIA, Braga da Cruz I, Marques APGC, Jorge R, Durnill CW, Parkin IP, Labrincha JA, Castro PML, Pintado MM

**76 SECOND TRIMESTER MATERNAL URINE FOR THE DIAGNOSIS OF TRISOMY 21 AND PREDICTION OF POOR PREGNANCY OUTCOMES**

Diaz SO, Barros AS, Goodfellow BJ, Duarte IF, Galhano E, Pita C, Almeida MC, Carreira IM, Gil AM

**77 METABOLOMICS OF BLOOD PLASMA AND URINE SHOWS PROMISE IN LUNG CANCER DIAGNOSIS**

Rocha CM, Carrola J, Barros AS, Gil AM, Goodfellow BJ, Carreira IM, Bernardo J, Gomes A, Sousa V, Carvalho L, Duarte IF

**78 POTENTIAL MARKERS OF CISPLATIN TREATMENT RESPONSE UNVEILED BY NMR METABOLOMICS OF HUMAN LUNG CELLS**

Duarte IF, Ladeirinha AF, Lamego I, Gil AM, Carvalho L, Carreira IM, Melo JB

**Computational Methods and Theory**

**82 HALOGEN-BONDING IN ANION RECOGNITION**

Costa PJ, Félix V, Beer PD

**82 DEVELOPMENT OF SYNTHETIC ANION CARRIERS FOR REPLACEMENT THERAPIES: A COMPUTATIONAL APPROACH**

Félix V, Marques I, Colaço AR, Costa PJ, Busschaert N, Gale PA

**84 DINUCLEAR RUTHENIUM(II) COMPLEXES FOR STABILIZING AND IMAGING AN ANTIPARALLEL FOLDED HUMAN TELOMERE SEQUENCE**

Félix V, Costa PJ, Williamson MP, Thomas JA, Wilson T

**85 SIMPLE DESCRIPTORS FOR PREDICTING THE CATALYTIC ACTIVITY OF TRANSITION METAL SURFACES FOR O-H BOND DISSOCIATION REACTIONS**

Fajin JLC, Cordeiro MNDS, Illas F, Gomes JRB

**86 ON THE ORIGINS OF THE MOLECULAR-SCALE PERIODICITY IN THE PORE WALLS OF PERIODIC MESPOROUS ORGANOSILICAS**

Futamura R, Jorge M, Gomes JRB

**87 COMBINING QUANTUM MECHANICS WITH MOLECULAR SIMULATION FOR PREDICTING ADSORPTION IN MOFS WITH UNSATURATED METAL SITES**

Jorge M, Fischer M, Gomes JRB

**88 AB-INITIO VALIDATION OF A RELATION BETWEEN LOCAL ELECTRIC FIELD AND GLOBAL POLARIZATION IN FERROELECTRICS**

Gonçalves JN, Stroppa A, Correia JG, Butz T, Picozzi S, Fenta AS, Amaral V

**Outreach**

**90 "THE CHEMISTRY OF THINGS" MULTIMEDIA PROJECT**

Ribeiro-Claro P

**91 WEBCAM-BASED SPECTROGRAPH FOR A STUDENT PROJECT**

Ferreira RAS, André PS

**91 BRING DISCOVERY INTO THE CLASSROOM: HOW TO EVALUATE PLANCK'S CONSTANT USING SIMPLE EQUIPMENT**

Ferreira RAS, André PS



# **Nanomaterials and Nanostructures**

# DIRECT IMAGING OF JOULE HEATING DYNAMICS AND TEMPERATURE PROFILING INSIDE A CARBON NANOTUBE INTERCONNECT

Costa PMFJ<sup>1</sup>, Gautam UK<sup>2</sup>, Bando Y<sup>2</sup>, Golberg D<sup>2</sup>

Resistive heating is a common phenomenon when electronic components are exposed to high current densities. It leads to an accentuated waste of energy and favours electromigration, a frequent cause of circuit failure. Knowing how the building blocks of nanoscaled electronic circuits respond to such electrical stress is essential for their future use in devices. Carbon nanotubes (CNTs) have been widely touted as superior wires to connect the various components of next-generation integrated circuits. Despite almost two decades of intense effort, insight into the internal structural and thermal responses of these structures when subjected to resistive heating has been lacking. On the 9<sup>th</sup> of August 2011, in a report published by Nature Communications, P. Costa from the University of Aveiro and colleagues from the National Institute for Materials Science, Japan, described how it was possible to directly image the dynamics of Joule heating and extract temperature profiles from the interior of CNTs acting as interconnects.

In general, electrical probing studies of CNTs had been performed in the absence of information concerning its internal

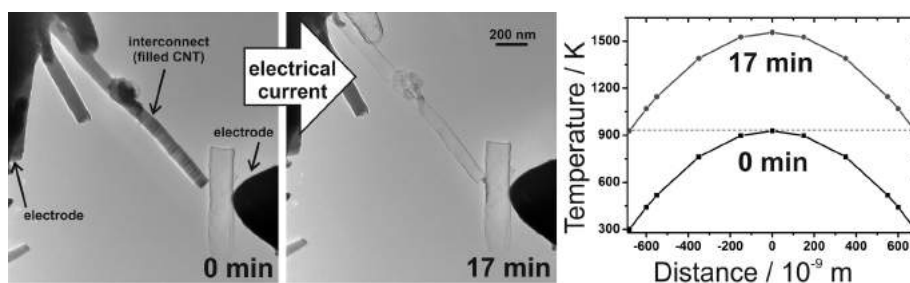


Figure 1. Electrically-driven sequential removal of Ga-doped ZnS from the interior of a carbon nanotube and estimation of the longitudinal temperature profiles in the initial (filled) and final (empty) states.

structure, with relatively low spatial resolution and often not resolved in time. Consequently, what happened in the tubular channel during the Joule heating process remained a mystery. Working with a transmission electron microscope and an electrical probing sample holder, Costa *et al.* were able to locate the hottest points inside an electrically-heated nanotube due to the solid-to-vapour phase transitions that took place in a carbon-encapsulated semiconductor nanowire (Fig. 1).<sup>[1]</sup> In addition, the team also followed the migration of these hot-spots and their evolution. The sublimation fronts of the confined nanowire acted as temperature markers to understand how heat is distributed along and across the tube.

Besides CNTs, the method reported may be used to evaluate the resistive heating behaviour of other nanoscaled tubular interconnects. Eventually, it may also be envisaged as a test-bed for the study of phase transitions occurring in confined spaces such as nanometer-sized channels of porous materials.

<sup>1</sup> Department of Materials and Ceramic Engineering, CICECO, University of Aveiro, 3810-193 Aveiro, Portugal.

<sup>2</sup> National Institute for Materials Science, Ibaraki 305-0044, Japan.

## Reference

[1] Costa PMFJ, Gautam UK, Bando Y, Golberg D, *Nature Communications*, 2011, 2, 421.

## GALVANIC REPLACEMENT REACTIONS IN METAL OXIDE NANOCRYSTALS

Oh MH<sup>1,2</sup>, Yu T<sup>3</sup>, Yu SH<sup>1,2</sup>, Lim B<sup>4</sup>, Ko KT<sup>5</sup>, Willinger MG<sup>6</sup>, Seo DH<sup>7</sup>, Kim BH<sup>1,2</sup>, Cho MG<sup>1,2</sup>, Park JH<sup>5,8</sup>, Kang K<sup>7</sup>, Sung YE<sup>1,2</sup>, Pinna N<sup>2,9,10</sup>, Heyeon T<sup>1,2</sup>

The galvanic replacement reaction is the most versatile method of preparing hollow metallic nanostructures with controllable pore structures and compositions<sup>[1]</sup>. These reactions involve a corrosion process that is driven by the difference in the electrochemical potentials of two metallic species. The hollow interior is generated from the oxidative dissolution of the metal nanocrystals

that are used as reactive templates. This strategy has also been used for the production of hollow semiconductor nanostructures. However, the chemical transformation of ionic systems via galvanic reactions has remained elusive. We demonstrated that a galvanic replacement reaction can occur in oxide nanocrystals as well and can produce hollow oxide nanostructures.

Hollow oxide nanocrystals have attracted much interest because of their potential for application in energy storage, catalysis, and medicine. Considerable advances have been made in the synthesis of hollow oxide and semiconductor nanocrystals. The Kirkendall effect has been exploited to produce complex hollow nanostructures of metal oxides and chalcogenides. However, synthesizing hollow nanocrystals of multimetallic oxides still remains a substantial challenge<sup>[2]</sup>.

Recently, in collaboration with Korean and German colleagues, we have shown that by using a nanoscale galvanic replacement reaction, monometallic oxide

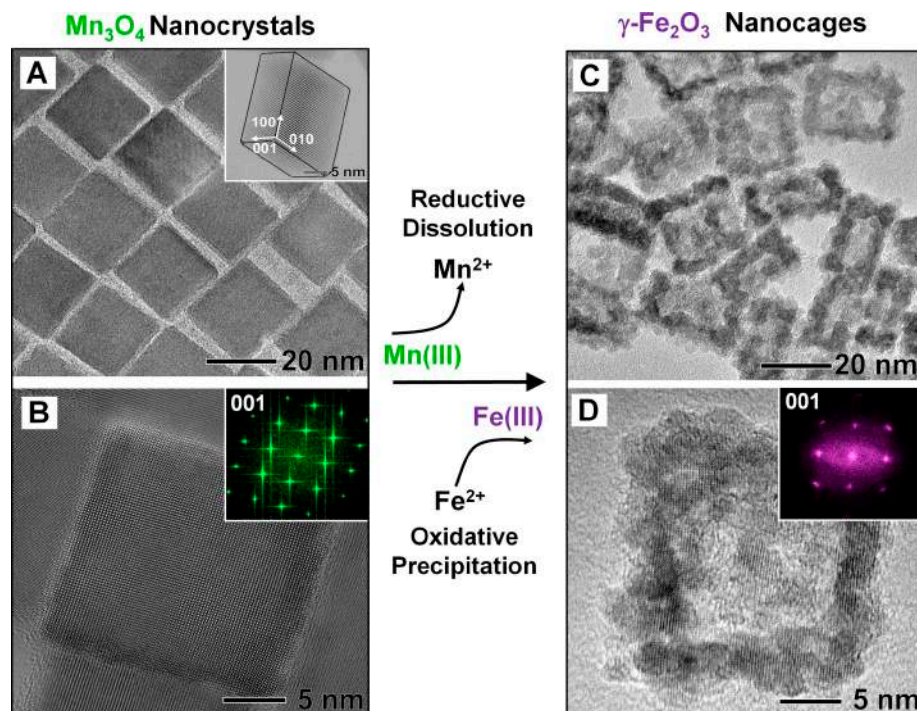


**Figure 1.** (A and B) TEM image of Mn<sub>3</sub>O<sub>4</sub> NCs. (A) Low magnification image of Mn<sub>3</sub>O<sub>4</sub> NCs. The inset shows the corresponding HRTEM image of a single NC recorded along the [111] axis. (B) HRTEM image of a single Mn<sub>3</sub>O<sub>4</sub> NC recorded along the [001] axis. The inset shows the corresponding FT pattern. (C and D) (C) Low magnification TEM and (D) HRTEM image of the  $\gamma$ -Fe<sub>2</sub>O<sub>3</sub> nanocages synthesized by reacting the Mn<sub>3</sub>O<sub>4</sub> NCs with 1 mL of 2.0 M aqueous iron(II) perchlorate solution. The inset shows the corresponding FT pattern.

nanocrystals could be completely transformed into hollow multimetallic oxide nanostructures<sup>[3]</sup>. Contrary to what occurs in metallic systems, a redoxcouple reaction between multivalent metallic ions took place, replacing the higher-

oxidation-state ions in the nanocrystals with lower-oxidation-state metal ions from solution. We focus here on one example, hollow heterostructured nanocrystals of manganese oxide/iron oxide (Mn<sub>3</sub>O<sub>4</sub>/ $\gamma$ -Fe<sub>2</sub>O<sub>3</sub>) with a boxlike shape

(‘nanoboxes’), which we transformed into cage-shaped iron oxide ( $\gamma$ -Fe<sub>2</sub>O<sub>3</sub>) nanocrystals (‘nanocages’). We also showed that these hollow, structured, multimetallic oxide nanostructures exhibit synergistic properties that make them attractive for use as anode materials in lithium ion batteries.

<sup>1</sup> Center for Nanoparticle Research, Institute for Basic Science, and School of Chemical and Biological Engineering, Seoul National University, Seoul 151-742, Korea.

<sup>2</sup> World Class University Program of Chemical Convergence for Energy and Environment and School of Chemical and Biological Engineering, Seoul National University, Seoul 151-742, Korea.

<sup>3</sup> Department of Chemical Engineering, College of Engineering, Kyung Hee University, Yongin 446-701, Korea.

<sup>4</sup> School of Advanced Materials Science and Engineering, Sungkyunkwan University, Suwon 440-746, Korea.

<sup>5</sup> c-CCMR and Department of Physics, Pohang University of Science and Technology, Pohang 790-784, Korea.

<sup>6</sup> Department of Inorganic Chemistry, Fritz Haber Institute of the Max Planck Society, Berlin 14195, Germany.

<sup>7</sup> Department of Materials Science and Engineering, Research Institute of Advanced Materials, Seoul National University, Seoul 151-742, Korea.

<sup>8</sup> Division of Advanced Materials Science, Pohang University of Science and Technology, Pohang 790-784, Korea.

<sup>9</sup> Department of Chemistry, CICECO, University of Aveiro, Aveiro 3810-193, Portugal.

<sup>10</sup> Institut für Chemie, Humboldt-Universität zu Berlin, Berlin 12489, Germany.

#### References

- [1] Sun Y, Xia Y, *Science*, 2002, 298, 2176.
- [2] Zhang Q, Wang W, Goebel J, Yin Y, *Nano Today*, 2009, 4, 494.
- [3] Oh MH, Yu T, Yu SH, Lim B, Ko KT, Willinger MG, Seo DH, Kim BH, Cho MG, Park JH, Kang K, Sung YE, Pinna N, Hyeon T, *Science*, 2013, 340, 964-968.

## ALL-IN-ONE HEATER-THERMOMETER NANOPLATFORM OPERATIVE FROM 300 to 2000 K BASED ON Er<sup>3+</sup> EMISSION AND BLACKBODY RADIATION

Debasu ML<sup>1,2</sup>, Ananias D<sup>1</sup>, Pastoriza-Santos I<sup>3</sup>, Liz-Marzan LM<sup>3,4,5</sup>, Rocha J<sup>1</sup>, Carlos LD<sup>2</sup>

Light-induced thermal heating of noble metal nanostructures has found many applications in biological detection, remote release of encapsulated material, photothermal therapy, sensors, photovoltaic and plasmonic devices. In particular, there is a growing interest in developing plasmonic-induced nanoheaters for applications in nanomedicine. Moreover, the precise measurement of the surface-temperature increments of nanoheaters (for example in hyperthermia) caused by thermo-plasmonics is crucial to regulate the heat released to

the surrounding medium, thereby allowing adjusting the irradiation parameters and guiding the therapy. The local temperature increase avoids the need for macroscopic heating, with the concomitant attenuation of collateral effects arising from heating of healthy tissues. Measuring the temperature at the nanoscale with high spatial (10<sup>-6</sup> m) and temperature (10<sup>-1</sup> degree) resolution is very challenging and an exciting field of research (e.g., in intracellular temperature fluctuations and temperature mapping of microcircuits).

Suitable nanoplatforms integrating heaters and thermometers, however, have not yet been realized, despite their great potential in nanophotonics and biomedicine. At the University of Aveiro we have addressed this issue during the last 5 years and recently in collaboration with Spanish colleagues from Vigo and Donostia - San Sebastián reported a step forward towards assessing the local temperature of laser-excited gold nanostructures using an all-in-one nanoplatform comprising (Gd,Yb,Er)<sub>2</sub>O<sub>3</sub> nanorods (thermometers) that were surface-decorated with gold nanoparticles (heaters), Figure 1<sup>[1]</sup>.

The local temperature is calculated using either Boltzmann’s distribution (300 – 1050 K) of the Er<sup>3+</sup> up-conversion <sup>2</sup>H<sub>11/2</sub> → <sup>4</sup>I<sub>15/2</sub>/<sup>4</sup>S<sub>3/2</sub> → <sup>4</sup>I<sub>15/2</sub> intensity ratio and from the Planck’s law (1200 – 2000 K) for a white-light emission ascribed to

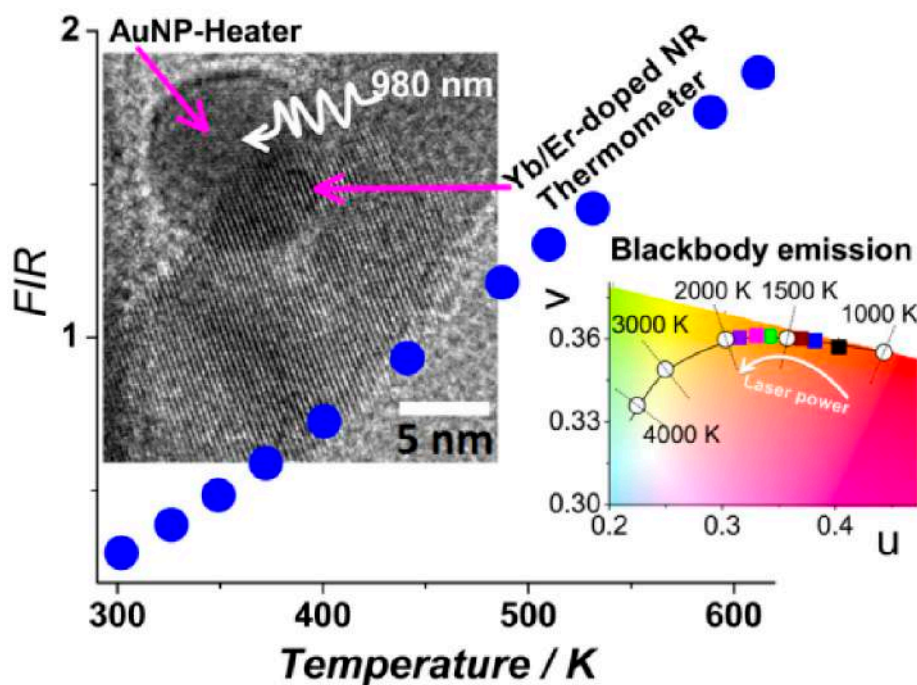


Figure 1. TEM image of AuNP heaters and Yb/Er thermometers [top left]. The up-conversion emission of this nanoplatform is a function of temperature [main plot], and the CIE chromaticity diagram [bottom right] shows that the variation of the emission color coordinates as a function of the laser pump power follows the Planckian locus.

the blackbody radiation. Increasing the amount of AuNPs increases the surface temperature of the  $(\text{Gd,Yb,Er})_2\text{O}_3$  nano-

rods and the operating range of the nano-thermometers. An outstanding result of this study is the unambiguous attribution

of the white-light emission to an incandescence process, which settles the existing controversy on the subject.

A maximum relative sensitivity up to 1.5 % K (resolution 1K) in the temperature range of physiological interest (301 – 350 K) is demonstrated with NRS-AuNPs-1.25 under low-power ( $32 - 86 \text{ W cm}^{-2}$ ) near-infrared light (980 nm) excitation in the therapeutic window. This offers much potential for biological applications in laser-induced controlled hyperthermia and in deep-tissue optical bioimaging, while avoiding thermal damage of the surrounding healthy tissues as well as background fluorescence. Work along these lines is in progress.

<sup>1</sup> Department of Physics, CICECO, University of Aveiro, 3810-193 Aveiro, Portugal

<sup>2</sup> Department of Chemistry, CICECO, University of Aveiro, 3810-193 Aveiro, Portugal

<sup>3</sup> Departamento de Química Física, Universidade de Vigo, Spain

<sup>4</sup> Bionanoplasmonics Laboratory, CIC biomaGUNE, San Sebastián, Spain

<sup>5</sup> Ikerbasque, Basque Foundation for Science, Bilbao, Spain

#### Reference

[1] Debasu ML, Ananias D, Pastoriza-Santos I, Liz-Marzan LM, Rocha J, Carlos LD, *Advanced Materials*, 2013, 35, 4868-4874.

## SENSING ACTIVE COATING ON THE BASIS OF NANOREACTORS CONTAINING A pH INDICATOR

Maia F<sup>1</sup>, Tedim J<sup>1</sup>, Bastos AC<sup>1</sup>, Ferreira MGS<sup>1</sup>, Zheludkevich ML<sup>1</sup>

The main idea of this work is to create a novel functionality on active coatings able to sense the initiation of corrosion under the coating or in defects. The goal is to significantly reduce the maintenance costs in many industrial applications. The indication of corrosion activity by such coatings allows optimizing the maintenance operations, avoiding excessive and unnecessary preventive operations.

The present development involves a new sensing active coating on the basis of nanoreactors containing a pH-indicating agent (Fig. 1). An important feature of these nanostructures is that the indicating molecules are not released from them, thereby preventing the spontaneous leaching and ensuring a long service time.

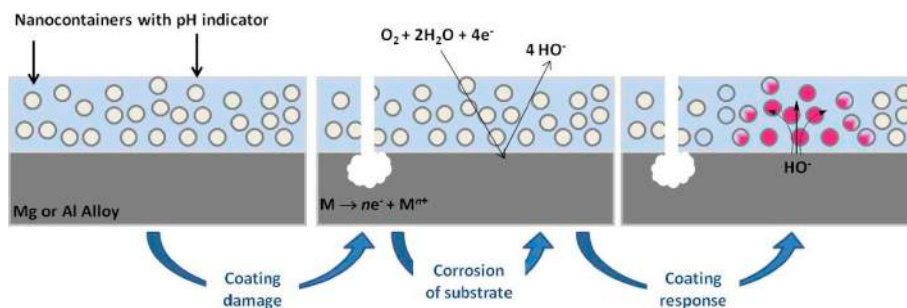


Figure 1. Scheme of pH sensing response from coating.

Mesoporous silica nanocontainers were synthesized and loaded with phenolphthalein (pH indicator) in a one-stage process. The resulting system was mesoporous, which together with the bulkiness of the indicator molecules limits the leaching of the latter (Fig. 2). Moreover,

the penetration of water molecules and ions inside the mesopores is possible, allowing the hydroxide ions formed on cathodic areas to react with the pH indicator. Colour change is used to detect and locate the active corrosion spots in the coated system.

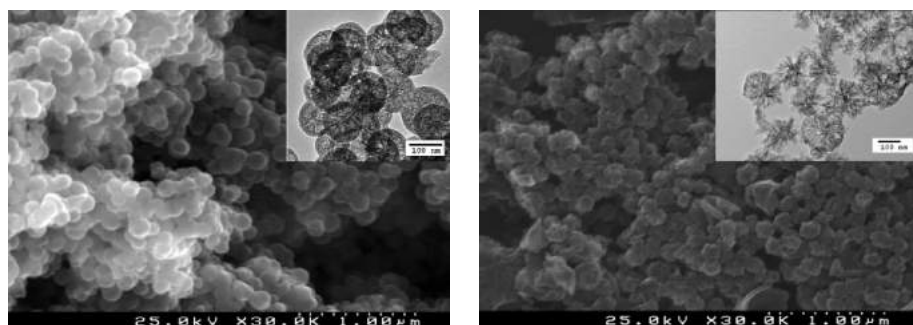


Figure 2. SEM images of Si<sub>3</sub>N<sub>4</sub>: (left) empty [inset: TEM picture of Si<sub>3</sub>N<sub>4</sub> with scale bar of 100 nm] and (right) with PhPh [inset: TEM picture of Si<sub>3</sub>N<sub>4</sub>-PhPh with scale bar of 100 nm].

The corrosion sensing functionality of the protective coatings with nanocontainers was proven for aluminium and magnesium based metallic substrates. The developed nanocontainers show high potential to be used in the new generation of active high performance multifunctional protective coatings.

<sup>1</sup> Department of Materials and Ceramic Engineering, CICECO, University of Aveiro, 3810-193 Aveiro, Portugal

#### Reference

<sup>[1]</sup> Maia F, Tedim J, Bastos AC, Ferreira MJS, Zheludkevich ML, *Nanotechnology*, 2013, 24, 415502.

## DRY FERROFLUIDS

Sousa FL<sup>1</sup>, Trindade T<sup>1</sup>, Silva NJO<sup>2</sup>

The concept of “Dry Ferrofluids” was developed here by encapsulating micro-drops of aqueous dispersions of magnetic nanoparticles in amorphous silica shells. The resulting system can be regarded as a “nanogyroscope” or as “magnetic micro-eggs”, behaving as a powder at the micro-scale and as a magnetic fluid at the nano-scale.

Ferrofluids and dry magnetic particles are two distinct classes of magnetic materials being their most noticeable difference the rotational degree of freedom of the particles present in the ferrofluids. This degree of freedom is externally controlled by a magnetic field and is locally dependent on the interactions between the particles and their surrounding media. For many applications of ferrofluids, the vis-

cosity of the surrounding media can vary, for example by changing the pH and aggregation state of the particles, which in turn leads to ferrofluids with an unstable and unpredictable magnetic response. In principle, this could be avoided by encapsulating the ferrofluid, which would be in this case shielded from changes in the viscosity of the surrounding media. This has been experimentally demonstrated by the encapsulation of magnetite aqueous ferrofluids into highly hydrophobic silica, where micrometer-sized drops of the ferrofluid are surrounded by a protective silica shell<sup>[1]</sup>. The ferrofluid comprises magnetite nanoparticles (~10 nm) electrostatically stabilized in water by surface citrate anions. The high stability of this ferrofluid is apparent in Fig.1a: in the

presence of a magnetic field gradient the fluid moves as a whole towards higher field values and the meniscus becomes oblique. The encapsulated ferrofluid is also attracted toward higher fields but in this case the individual silica capsules containing the ferrofluid are free to approach the top of the magnet, defeating gravity. Fig.1b shows a SEM image of a silica capsule containing the magnetic particles stabilized in water in a egg-like fashion.

In summary, dry-ferrofluids are a new member of the magnetic materials family combining properties of the parent ferrofluids and powdered magnetic nanoparticles. This results in an unprecedented stabilization of the magnetic response of the ferrofluids, controlling their heating capability. This capability can be further explored together with the container functionality typical of capsules for the release of drugs and gases.

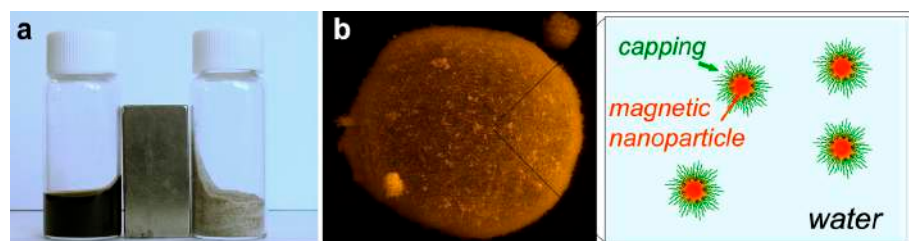


Figure 1. (a) Digital photograph of the magnetite ferrofluid (left) and dry-ferrofluid (right) in the presence of a NdFeB magnet; (b) Environmental scanning electron microscopy image of a dry-ferrofluid capsule about 40 nm diameter and scheme illustrating the anatomy of the encapsulated magnetite ferrofluid.

<sup>1</sup> Department of Chemistry, CICECO, University of Aveiro, 3810-193 Aveiro, Portugal

<sup>2</sup> Department of Physics, CICECO, University of Aveiro, 3810-193 Aveiro, Portugal

#### Reference

<sup>[1]</sup> Sousa FL, Bustamante R, Millan A, Palacio F, Trindade T and Silva NJO, *Nanoscale*, 2013, 5, 7229.

#### Acknowledgments

This work was performed in collaboration with researchers from Instituto de Ciencia de Materiales de Aragón (Zaragoza, Spain).

# SILVER-MODIFIED NANO-TITANIA AS AN ANTIBACTERIAL AGENT AND PHOTOCATALYST

Tobaldi DM<sup>1</sup>, Piccirillo C<sup>2</sup>, Pullar RC<sup>1</sup>, Gualtieri AF<sup>3</sup>, Seabra MP<sup>1</sup>, Castro PML<sup>3</sup>, Labrincha JA<sup>1</sup>

Nanopowders of titania modified with silver were made by a green nano synthesis technique, based upon environmentally benign aqueous sol-gel techniques. The effect of Ag on the microstructure and phase composition of the prepared samples was characterized using advanced X-ray powder diffraction methods. Due to its large size, silver could not enter the titania lattice and did not modify the titania unit cell parameters. This led to a slight decrease of the anatase, rutile, and brookite average crystalline domain size. Increasing the calcination temperature to 600 °C led to a common increase of the average domain size. On the other hand, the presence of Ag retarded the anatase-to-rutile phase transition (ART) – the modification with 2 mol % Ag delaying the ART to a greater extent.

As for the functional applications, considering the photocatalytic activity, 2 mol % was the optimum amount of Ag for methylene blue photodegradation – using both UV- and visible light irradiation – with both thermal treatment tempera-

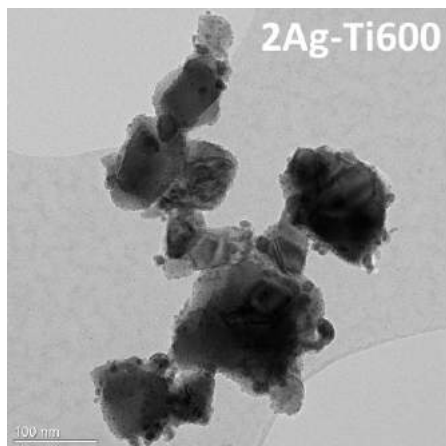


Figure 1. TEM image of titania NPs with 2 mol% Ag doping after heating to 600°C (mostly rutile phase with some metallic Ag<sup>0</sup> NPs)

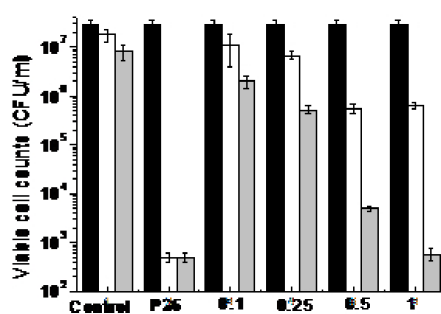


Figure 2. XRD pattern and whole powder pattern modelling to show crystallite domain sizes for the rutile and anatase phases ( $\approx 10$  nm).

tures. In the case of antibacterial activity, when using a UV-light source, samples showed a much greater activity toward *E. coli* (Gram-negative) than MRSA (Gram-positive). It was observed that UV light caused a change in the oxidation

state of silver, from ionic silver to metallic ( $\text{Ag}^+ \rightarrow \text{Ag}^0$  NPs), this being detrimental for the antibacterial activity. However, under artificial white light irradiation this did not occur and the material kept its excellent antibacterial properties (higher activity than commercial P25); because of this, it could be suitable for use in health care, helping to greatly reduce the spread of Gram-negative type bacteria such as *E. coli*.

<sup>1</sup> Department of Materials and Ceramic Engineering, CICECO, University of Aveiro, Campus Universitário de Santiago, 3810-193 Aveiro, Portugal

<sup>2</sup> CBOF/Escola Superior de Biotecnologia, Universidade Católica Portuguesa, Rua Dr. António Bernardino de Almeida, 4200-072 Porto, Portugal

<sup>3</sup> Dipartimento di Scienze Chimiche e Geologiche, Università di Modena e Reggio Emilia, Via S. Eufemia 19, I-41121 Modena, Italy

## Reference

[1] Tobaldi DM, Piccirillo C, Pullar RC, Gualtieri AF, Seabra MP, Castro PML, Labrincha JA, *The Journal of Physical Chemistry C*, 2014, 118, 4751–4766.

## Acknowledgments

We thank FCT [PEst-C/CTM/LA0011/2013, PEst-OE/EQB/LA0016/2011, FCT Ciência 2008 programs and SFRH/BPD/86483/2012 research grant].

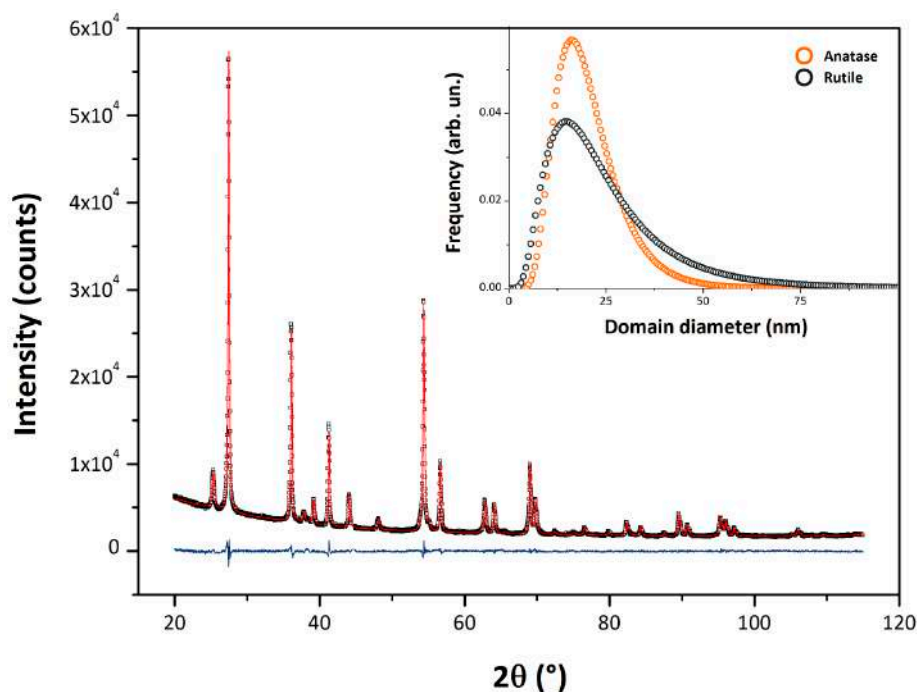


Figure 3. Antibacterial activity against *E. coli* under visible/white light (x axis = concentration in mg/L).

# METAL-ORGANIC FRAMEWORKS BASED ON A PHOSPHONATE POLYMERIC ORGANIC LINKER

Silva P<sup>1</sup>, Vieira F<sup>1</sup>, Gomes AC<sup>1</sup>, Ananias D<sup>1</sup>, Fernandes JA<sup>1</sup>, Bruno SM<sup>1</sup>, Soares R<sup>2</sup>, Valente AA<sup>1</sup>, Rocha J<sup>1</sup>, Paz FAA<sup>1</sup>

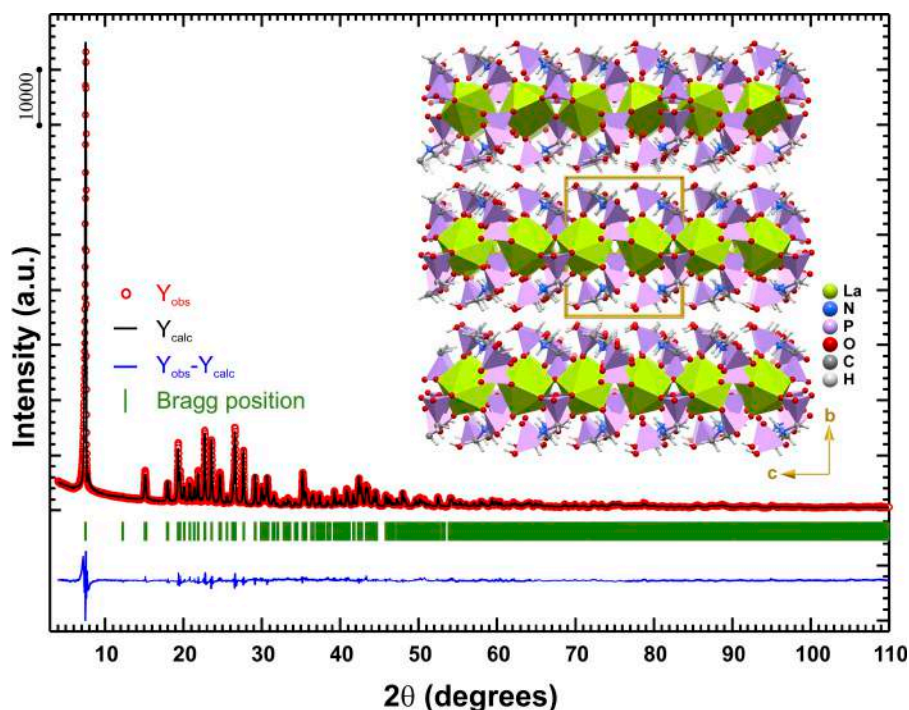


Figure 1. Crystal structure of  $[\text{La}(\text{H}_3\text{nmp})]$  (1) determined from powder X-ray diffraction.

Metal-Organic Frameworks (MOFs) and, in a more wide sense, coordination polymers are nowadays one of the most studied topics in synthetic chemistry. Mainly driven by porosity and surface area-based applications, MOFs are promising materials for gas storage, uptake and separation of gases, and good candidates to per-

form catalytic reactions, especially in an heterogeneous fashion.

Our research group has been investigating the utilization of highly flexible organic ligands based on chelating phosphonic acid groups: (carboxymethyl)iminodi(methyl-phosphonic acid) and nitrilotris(methylenephosphonic acid) ( $\text{H}_6\text{nmp}$ ).

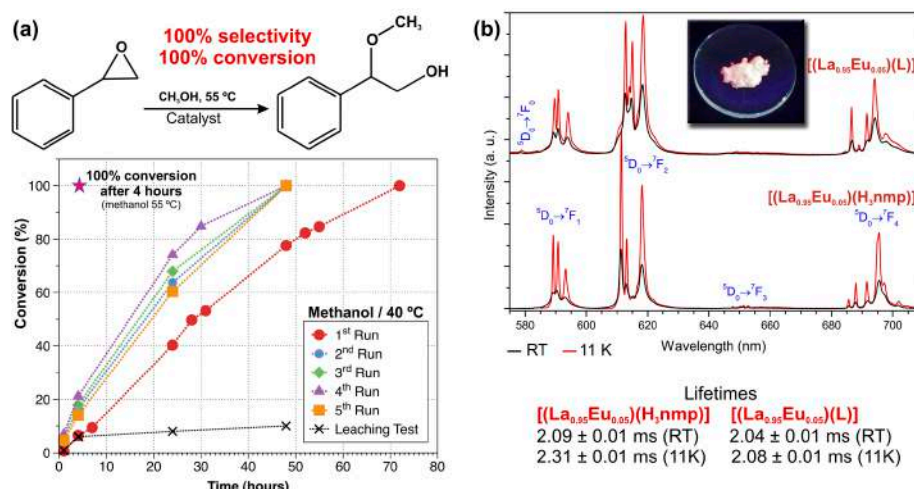


Figure 2. (a) Catalytic activity of compound 1 compared with that of 2 (pink star). (b) Emission spectra of 1-LaEu and 2-LaEu, with excitation at 393 and 394 nm, respectively, recorded at ambient temperature [RT] and at 11 K. The inset depicts the characteristic red emission of  $\text{Eu}^{3+}$  when 1-LaEu is irradiated with a laboratory UV lamp (wavelength of 254 nm).

The self-assembly of these molecules with rare-earth cations has led to the preparation of several families of photoluminescent materials, many of which also exhibit interesting heterogeneous catalytic activity or can be employed as potential MRI contrast agents.

One of the most striking and unusual discovered materials resulted from the use of the polyphosphonic  $\text{H}_6\text{nmp}$  ligand that led to the preparation and structural characterization of two novel 2D MOFs:  $[\text{La}(\text{H}_3\text{nmp})]$  (1) (Fig. 1) and  $[\text{La}(\text{L})]$  (2) (where  $\text{L}^{3-} = [-(\text{PO}_3\text{CH}_2)_2(\text{NH})(\text{CH}_2\text{PO}_2)(\mu\text{-O})_2]^{3-}$ ). Compound 1 undergoes a microcrystal-to-microcrystal phase transformation above  $300^\circ\text{C}$ , being transformed into 2. Heating induces a transformation at the level of the coordinated  $\text{H}_3\text{nmp}^{3-}$  anionic organic ligand: a polymerization (condensation) reaction occurs in situ, forming a novel and unprecedented 1D polymeric organic ligand. Photoluminescent materials were engineered by selectively including stoichiometric amounts (5%) of optically active  $\text{Eu}^{3+}$  and  $\text{Tb}^{3+}$  centers into the  $\text{La}^{3+}$  matrices: red and green-emitting materials ( $[(\text{La}_{0.95}\text{Eu}_{0.05})(\text{H}_3\text{nmp})]$  (1-LaEu) and  $[(\text{La}_{0.95}\text{Eu}_{0.05})(\text{L})]$  (2-LaEu), and  $[(\text{La}_{0.95}\text{Tb}_{0.05})(\text{H}_3\text{nmp})]$  (1-LaTb), respectively) were isolated. The photoluminescent properties of 1-LaEu and 2-LaEu showed the presence of a single crystallographic lanthanide center with lifetimes ranging from  $2.04 \pm 0.01$  to  $2.31 \pm 0.01$  ms for both materials (at ambient and low temperature) (Fig. 2).

Both compounds behave as effective heterogeneous catalysts in the ring-opening reaction of styrene oxide, under mild conditions ( $40\text{-}70^\circ\text{C}$  range). Materials exhibit excellent regioselectivity toward the  $\beta$ -alkoxy alcohol products (formed in quantitative yields) even in the presence of water, and they may be recycled without the need for regeneration treatments. Remarkably, material 2 showed a much higher catalytic activity than the parent compound 1, most likely due to the formation of structural defects during the calcination procedure. These results are currently helping us to design new materials which also evidence high catalytic activity, while photoluminescence is boosted by the inclusion of aromatic rings within the organic linker core.

<sup>1</sup> Department of Chemistry, CICECO, University of Aveiro, 3810-193 Aveiro, Portugal.

<sup>2</sup> Central Analytical Laboratory, CICECO, University of Aveiro, 3810-193 Aveiro, Portugal.

#### Reference

[<sup>1</sup>] Silva P, Vieira F, Gomes AC, Ananias D, Fernandes JA, Bruno SM, Soares R, Valente AA, Rocha J, Paz FAA, *Journal of the American Chemical Society*, 2011, 133, 15120-15138.

#### Acknowledgments

This research was funded by the European Union (QREN, COMPETE) and FCT (PTDC/QUI-QUI/098098/2008 – FCOMP-01-0124-FEDER-010785).

## CHIRAL TRANSPOSING FROM DIPHOSPHONATE METAL-ORGANIC FRAMEWORK PRECURSORS TO POROUS LANTHANIDE PYROPHOSPHATES

Shi FN<sup>1</sup>, Paz FAA<sup>1</sup>, Ribeiro-Claro P<sup>1</sup>, Rocha J<sup>1</sup>

The synthesis of chirally-pure porous solids from achiral building blocks is an intriguing, nontrivial, and much promising field. The real challenge for chemists encompasses ensuring that only one of the possible enantiomorphs is formed in the syntheses. Among chiral inorganic materials most work has been concentrated on zeolites, some of which present chiral polymorphs, viz., zeolite-beta, SU-32 and ITQ-37. ETS-10, a porous titanosilicate, also exhibits chiral polymorphs. In zeolite synthesis, chiral templating by addition of an organic molecule or cation to the synthesis medium has been a method of choice (although with limited success) to attempt imprinting the molecule's chirality onto the inorganic framework. Chiral templating and chiral induction (the use of chiral solvents or chiral additives) methods utilized to engineer homochirality in porous solids have been reviewed recently [<sup>1</sup>].

We have reported the synthesis of chiral porous inorganic materials, lanthanide (Ln) pyrophosphates, from chiral porous Metal-Organic Framework (MOF) precursors, which upon thermal decomposition transpose their chirality and porosity onto the inorganic framework [<sup>2</sup>]. The crux of this single-crystal to single-crystal transformation lies in that the key structural modifications take place at a specific crystallographic site and, as a result, the topological features of the parent MOFs are transposed to the final crystalline inorganic frameworks, via an intermediate (also hybrid) material. Although the materials reported here possess relatively narrow pores they may be of interest for H<sub>2</sub> storage or separation from gas mixtures.

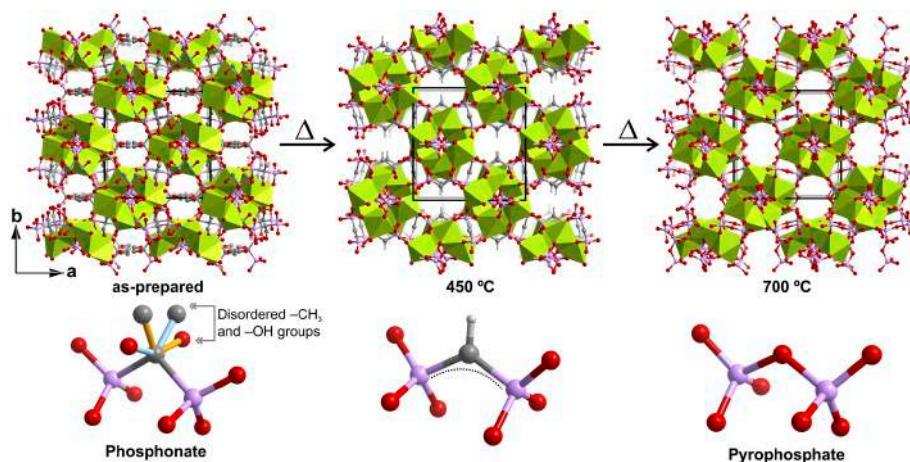


Figure 1. Structural transformation of the frameworks and ligands, from room temperature to ca. 700 °C: as-prepared [Er<sub>4</sub>(Hhedp)<sub>3</sub>(H<sub>2</sub>O)<sub>2</sub>] MOF 1 transforms into the hybrid [Er<sub>4</sub>(PO<sub>3</sub>-CH=PO<sub>3</sub>)<sub>3</sub>] network 2 at ca. 450 °C, which upon further heating yields the purely inorganic [Er<sub>4</sub>(PO<sub>3</sub>-O-PO<sub>3</sub>)<sub>3</sub>] network 3 at ca. 700 °C.

The hydrothermal reaction of etidronic acid (H<sub>2</sub>hedp) and lanthanide chlorides afforded a series of isotypical materials formulated as [Ln<sub>4</sub>(Hhedp)<sub>3</sub>(H<sub>2</sub>O)<sub>2</sub>] (Ln=Y<sup>3+</sup>, Ho<sup>3+</sup>, Dy<sup>3+</sup> and Tb<sup>3+</sup>) on the basis of single-crystal X-ray diffraction. A case in point, [Er<sub>4</sub>(Hhedp)<sub>3</sub>(H<sub>2</sub>O)<sub>2</sub>] (1) crystallizes in the chiral cubic I<sub>2</sub>3 space (Figure 1). Heating 1 from ambient temperature to ca. 700 °C results in intriguing structural transformations, whose epicentre is the ligand itself (Figure 1). At ca. 450 °C, the water molecule coordinated to Er<sub>2</sub> is released and the Hhedp<sup>4-</sup> ligand decomposes around the central carbon atom (located on the two-fold axis) by releasing the -OH and -CH<sub>3</sub> groups, which are replaced by a C-H group. A new hybrid material forms, [Er<sub>4</sub>(PO<sub>3</sub>-CH=PO<sub>3</sub>)<sub>3</sub>] (2), retaining the connectivity of the parent framework. At ca. 700 °C, 2 transforms into a purely inorganic pyrophosphate material, with the central C-H bond re-

placed by an oxygen atom, [Er<sub>4</sub>(PO<sub>3</sub>-O-PO<sub>3</sub>)<sub>3</sub>] (3). Again, this structural transformation occurs at the two-fold site (C-H bond), with no modification of the overall network connectivity. Because the thermal structural modifications take place primarily at a specific crystallographic site, the topological features of the parent MOF material are imprinted onto the final crystalline inorganic framework 3, via the intermediate hybrid 2.

We submit that it is worth considering extending these ideas to the synthesis of other chiral porous inorganic solids. Work along these lines is in progress.

<sup>1</sup> Department of Chemistry, CICECO, University of Aveiro, 3810-193 Aveiro, Portugal

#### References

[<sup>1</sup>] Morris, RE, Bu XH, *Nature Chemistry*, 2010, 2, 353-361.

[<sup>2</sup>] Shi F, Paz FAA, Ribeiro-Claro P, Rocha J, *Chemical Communications*, 2013, 49, 11668-11670.

# MULTIFUNCTIONAL LANTHANIDE-ORGANIC FRAMEWORKS BASED ON A TRIPODAL PHOSPHONATE ORGANIC LINKER: PHOTOLUMINESCENCE AND HETEROGENEOUS CATALYSIS

Vilela SMF<sup>1,2</sup>, Firmino ADG<sup>1,2</sup>, Mendes RF<sup>1</sup>, Fernandes JA<sup>1</sup>, Ananias D<sup>1</sup>, Gomes AC<sup>1</sup>, Valente AA<sup>1</sup>, Ott H<sup>3</sup>, Carlos LD<sup>4</sup>, Rocha J<sup>1</sup>, Tomé JPC<sup>2</sup>, Paz FAA<sup>1</sup>

Metal-Organic Frameworks (MOFs), also known as Coordination Polymers, are constructed from the self-assembly between metallic centers and organic ligands. This new class of materials opens the window to customizable high porosity materials, with high surface area, thermal, mechanical and chemical robustness, and to the design of luminescent, magnetic and catalytic devices. Because of this rich versatility MOFs may find applicability in distinct fields such as gas storage and separation, ion-exchange, heterogeneous catalysis, magnetism, as optical sensors, among others. Our research group have been interested in the preparation of multifunctional Lanthanide-Organic Frameworks (LnOFs) based on multipodal phosphonate organic linkers. We have designed and prepared two families of LnOFs containing the new (benzene-1,3,5-triyl(methylene)triphosphonic acid ( $H_6bmt$ ) ligand (Figure 1):<sup>[1, 2]</sup> 1D  $[Ln(H_4bmt)(H_5bmt(H_2O))_2] \cdot 3H_2O$  materials [where  $Ln^{3+} = La^{3+}, (La_{0.97}Eu_{0.03})^{3+}$

and  $(La_{0.97}Eu_{0.03})^{3+}$ ] prepared using microwave irradiation (40 ffc for 5 min); 3D  $[Ln_2(H_3bmt)_2(H_2O)_2] \cdot H_2O$  frameworks [where  $Ln^{3+} = La^{3+}, Ce^{3+}, Pr^{3+}, Nd^{3+}, (La_{0.95}Eu_{0.05})^{3+}$  and  $(La_{0.95}Tb_{0.05})^{3+}$ ] prepared using both hydrothermal conditions (100 ffc for 1 day) or microwave irradiation (150 °C for 5 min). Isotypical 3D materials can be fully dehydrated under heating (above ca. 100 °C), with or without vacuum, while their crystalline structures remain unaltered. When kept in contact with atmospheric air, the dehydrated compounds are easily rehydrated. The zeolitic behaviour of the 3D  $Eu^{3+}$ -based material led to an increase of the quantum efficiency in ca. 3.6 times (from ca. 15 to 54%). Both 1D and 3D  $Tb^{3+}$ -based MOFs have remarkable absolute emission quantum yields (ca. 44 and 46%).

The heterogeneous catalytic activity of the 1D  $[La(H_4bmt)(H_5bmt(H_2O))_2] \cdot 3H_2O$  and the 3D  $[La_2(H_3bmt)_2(H_2O)_2] \cdot H_2O$  materials were investigated in the ring-opening

reaction of the styrene oxide (PhEtO). Both MOFs exhibited excellent regioselectivity towards 2-methoxy-2-phenylethanol (always as the sole reaction product). They further showed to be truly heterogeneous catalysts that could be recycled by simple and efficient regeneration processes. Noteworthy, the 1D  $[La(H_4bmt)(H_5bmt(H_2O))_2] \cdot 3H_2O$  material has much higher catalytic activity (conversion of 100% of PhEtO at 55 °C in only 30 min) than the 3D  $[La_2(H_3bmt)_2(H_2O)_2] \cdot H_2O$  material (conversion of 80% of PhEtO at 55 °C in 24 h). The outstanding catalytic activity of the 1D MOF catalyst is related with the amount of active sites available in its structure that are likely to be of Brønsted type.

<sup>1</sup> Department of Chemistry, CICECO, University of Aveiro, 3810-193 Aveiro, Portugal

<sup>2</sup> Department of Chemistry, OOPNA, University of Aveiro, 3810-193 Aveiro, Portugal

<sup>3</sup> Bruker AXS GmbH, Oestliche Rheinbrueckenstr, 49, 76187 Karlsruhe, Germany

<sup>4</sup> Department of Physics, CICECO, University of Aveiro, 3810-193 Aveiro, Portugal

## References

[1] Vilela SMF, Ananias D, Gomes AC, Valente AA, Carlos LD, Cavaleiro JAS, Rocha J, Tomé JPC, Paz FAA, *Journal of Material Chemistry*, 2012, 22, 18354-18371.

[2] Vilela SMF, Firmino ADG, Mendes RF, Fernandes JA, Ananias D, Valente AA, Ott H, Carlos LD, Rocha J, Tomé JPC, Paz FAA, *Chemical Communications*, 2013, 49, 6400-6402.

## Acknowledgments

This research was funded by the European Union (OREN, COMPETE) and FCT (PTDC/QUI-QUI/098098/2008 – FCOMP-01-0124-FEDER-010785).

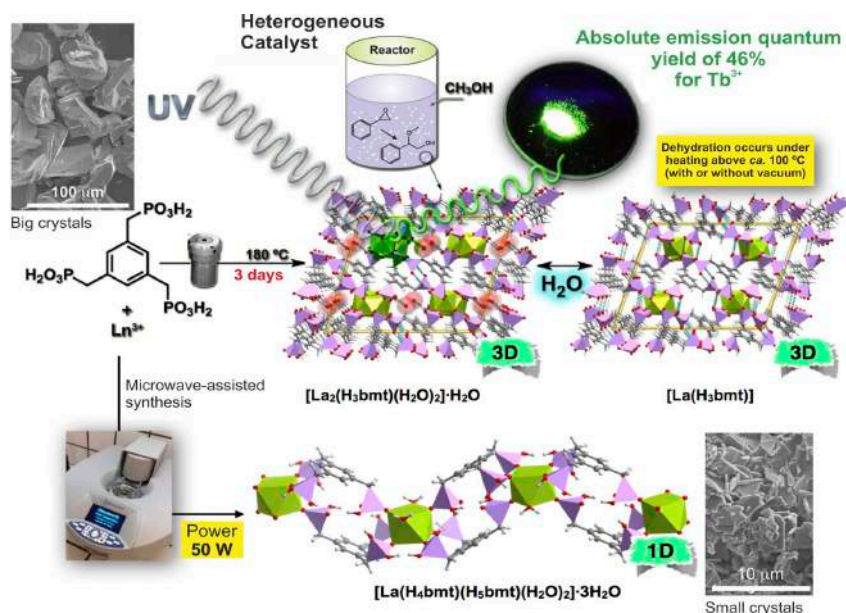
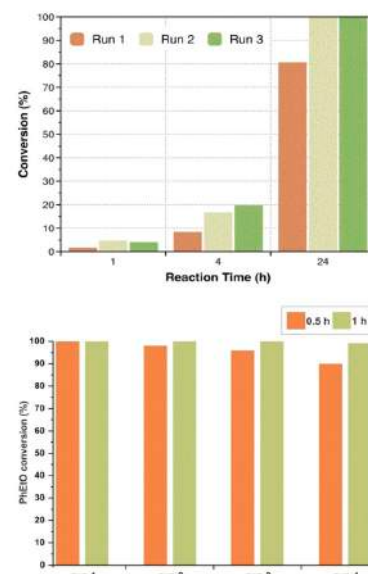


Figure 1. (left) Schematic representation of the preparation of the 3D  $[La_2(H_3bmt)_2(H_2O)_2] \cdot H_2O$  and its dehydrated form  $[La(H_3bmt)]$ , and of the 1D  $[La(H_4bmt)(H_5bmt(H_2O))_2] \cdot 3H_2O$  polymer. (right) Catalytic activity of  $[La_2(H_3bmt)_2(H_2O)_2] \cdot H_2O$  (on the top) and of  $[La(H_4bmt)(H_5bmt(H_2O))_2] \cdot 3H_2O$  (at the bottom) in the ring-opening reaction of styrene oxide with methanol at 55 °C.



## FUNCTIONAL NANOSTRUCTURED COMPOSITE MATERIALS BASED ON BACTERIAL CELLULOSE

Freire CSR<sup>1</sup>, Silvestre AJD<sup>1</sup>, Barros-Timmons A<sup>1</sup>, Neto CP<sup>1</sup>

In the last decades there has been an increasing awareness in the search for bio-based alternatives as sources of novel (nano)composites for application in several fields such as packaging, biomedical products and devices, as well as in high technology domains. Nanocellulose forms like bacterial cellulose (BC), bio-synthesized by several bacteria as a 3D network of nano- and micro-fibrils, have gained particular attention in this context because of its unique features, namely high purity, water holding capacity,

crystallinity, tensile strength and Young modulus, that can be successfully exploited in the development of innovative nanostructured composite materials.<sup>[1]</sup> Bacterial nanocellulose based composite materials can be prepared following different strategies, including compounding with synthetic thermoplastic matrices<sup>[2]</sup>, combination/blending with other natural polymers<sup>[3,4]</sup> and *in situ* polymerization with different monomers<sup>[5-8]</sup>; resulting in functional materials with improved thermal stability and mechanical per-

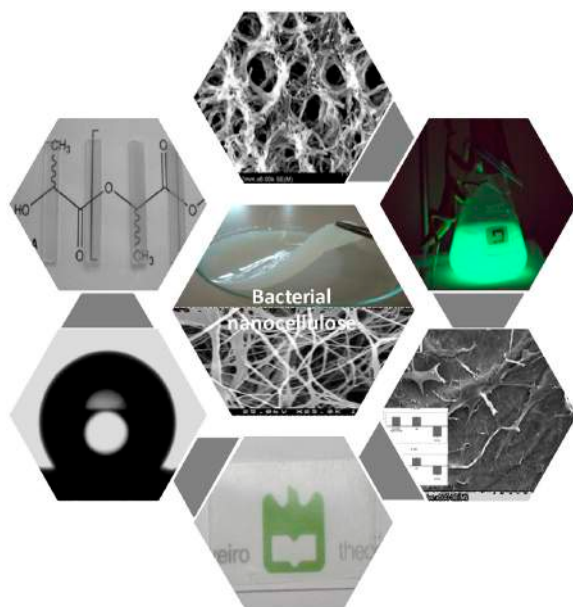


Figure 1. Examples of nanostructured composites prepared using bacterial nanocellulose and different methodologies.

## SOFT NANOCOMPOSITES FOR STRONG SIGNAL ENHANCEMENT IN RAMAN SPECTROSCOPY

Fateixa S<sup>1</sup>, Daniel-da-Silva AL<sup>1</sup>, Nogueira HIS<sup>1</sup>, Trindade T<sup>1</sup>

The Surface-Enhanced Raman Scattering (SERS) effect refers to a method of Raman spectroscopy (Fig.1) in which some chemical species exhibit strong Raman signal enhancement when interacting

with metal surfaces, typically silver and gold.<sup>[1]</sup> The high sensitivity of SERS, that in certain conditions can reach the molecular level, associated to specifically designed plasmonic nanostructures makes

performance and bearing properties such as transparency, biocompatibility, bioactivity, hydrophobicity, conductivity, among others (Figure 1).

It is clearly demonstrated that bacterial nanocellulose is a suitable biopolymer for the development of innovative nanostructured composites following different approaches. The final properties of the nanocomposites can be tailored by changing the monomer type, the ratio polymer/BC or the modification approach. These nanostructured porous composites could find applications in several fields namely in controlled release of drugs or other bioactive compounds, electronic devices, among others.

<sup>1</sup> Department of Chemistry, CICECO, University of Aveiro, 3810-193 Aveiro, Portugal

### References

- [1] Figueiredo ARP, Vilela C, Neto CP, Silvestre AJD, Freire CSR, *Bacterial cellulose based nanocomposites: a roadmap for innovative materials*, in: *Nanocellulose Polymer Nanocomposites: Fundamentals and Application* (Kumar V. Ed.), Wiley, in press. ISBN: 978-1-118-87190-4.
- [2] Tomé LC, Pinto RJB, Trovatti E, Freire CSR, Silvestre AJD, Neto CP, Gandini A, *Green Chemistry*, 2011, 13, 419-427.
- [3] Trovatti E, Fernandes SCM, Rubatat L, Freire CSR, Silvestre AJD, Neto CP, *Cellulose*, 2012, 19, 729-737.
- [4] Tomé LC, Fernandes SCM, Perez DS, Sadocco P, Silvestre AJD, Neto CP, Marrucho IM, Freire CSR, *Cellulose*, 2013, 20, 1807-1818.
- [5] Fernandes SCM, Sadocco P, Alonso-Varona A, Palomares T, Eceiza A, Silvestre AJD, Mondragon I, Freire CSR, *ACS Applied Materials and Interfaces*, 2013, 5, 3290-3297.
- [6] Lacerda PSS, Barros-Timmons AMMV, Freire CSR, Silvestre AJD, Neto CP, *Biomacromolecules*, 2013, 14, 2063-2073.
- [7] Figueiredo A, Figueiredo A, Alonso-Varona A, Fernandes SCM, Palomares T, Rubio E, Barros-Timmons A, Silvestre AJD, Neto CP, Freire CSR, *BioMed Research International*, 2013, article number 698141.
- [8] Gadim TDO, Figueiredo A, Vilela C, Rosero-Navarro NC, Gamelas JAF, Barros-Timmons A, Neto CP, Silvestre AJD, Freire CSR, Figueiredo FML, *ACS Applied Materials and Interfaces*, 2014, 6, 10, 7864-7875.

this a technique of choice for a number of nanotechnologies of practical interest in medicine and environmental monitoring. However, the widespread use of this technique is still dependent on a number of requisites, which include the availability of analytical platforms that are user friendly and easily processed using standard technologies. Our interest in this research problem led us to investigate the development of new nanocomposites as



Figure 1. The Nobel Prize in Physics (1930) was awarded to the scientist Chandrasekhara Venkata Raman for research on the scattering of light and for the discovery of the effect named in his honor.

new analytical platforms for SERS. These nanocomposites comprise a polymer matrix containing metal nanoparticles. Furthermore, we have been interested in exploiting new functionalities that might arise in these nanocomposites but not ob-

served in the original components. Two selected examples of our recent research in this topic are described below, that involve the use of a synthetic and a natural polymer as the matrices, and Ag nanoparticles as the fillers.

Organically capped Ag nanoparticles (average diameter  $\sim 11$  nm) have been used as nanofillers in poly(*t*-butylacrylate) composites prepared by *in situ* polymerization via miniemulsions.<sup>[2,3]</sup> This synthetic strategy enabled the dual use of the final composites as SERS substrates, both as aqueous emulsions and as cast films, using thiosalicylic acid and adenine as molecular probes (Fig.2). The Ag/PtBA materials still showed SERS activity when submitted to temperature cycles ( $-60^{\circ}\text{C}$  to  $65^{\circ}\text{C}$ ), which suggests that the adsorbates were retained at Ag sites eventually protected by the surrounding polymer layers. This

work demonstrated the potential of this approach to fabricate nanocomposites that can be regarded as scalable, versatile and handy SERS substrates contributing to the implementation of Raman analytical tools in a wider context.

Carrageenan hydrogels containing Ag nanoparticles have been investigated as new colloidal platforms for SERS using 2,2'-dithiodipyridine as the analytical probe (Fig.3). These studies have been performed for a series of nanocomposites in which the gel strength was varied by using several strategies, including the increase of the polysaccharide content in the gel, the addition of KCl as cross-linker, and the variation of the type of carrageenan network. This research led to the first report of a direct correlation between the gel strength of a hydrogel composite used as substrate and its analytical SERS sensitivity.<sup>[2,4]</sup> A mechanism has been suggested for these findings that considers an increasing number of hot spots due to the formation of Ag particles nanojunctions when the biopolymer matrix tends to rearrange into stronger gels (Fig.3).

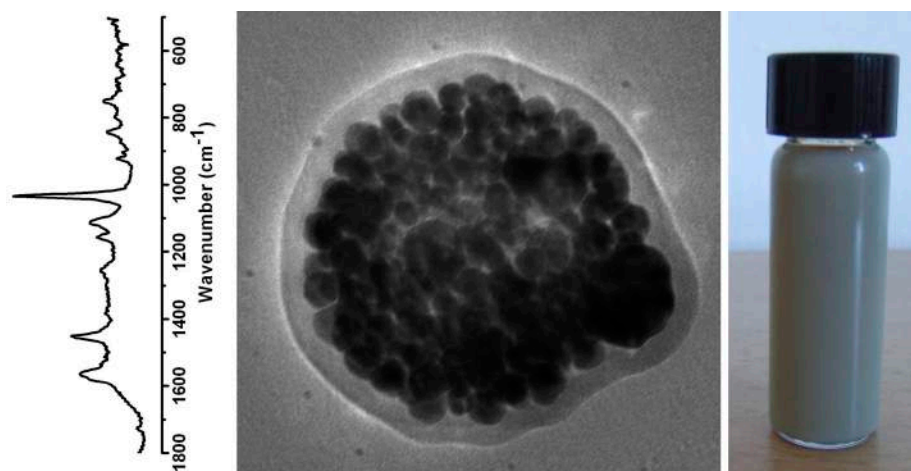


Figure 2. SERS active nanocomposites in the form of an aqueous emulsion containing poly(*t*-butylacrylate) beads encapsulating Ag nanoparticles.

<sup>1</sup> Department of Chemistry, CICECO, University of Aveiro, 3810-193 Aveiro, Portugal

#### References

- [1] Nogueira HIS, Teixeira-Dias JJC, Trindade T, *Encyclopedia of Nanoscience and Nanotechnology*, H. S. Nalwa (Ed), ASP, 2004, 7, 699.
- [2] Fateixa S, PhD Thesis, 2013, University of Aveiro.
- [3] Fateixa S, Girão AV, Nogueira HIS, Trindade T, *Journal of Materials Chemistry*, 2011, 21, 15629.
- [4] Fateixa S, Daniel-da-Silva AL, Nogueira HIS, Trindade T, *The Journal of Physical Chemistry C*, 2014, 118 (19), 10384-10392.

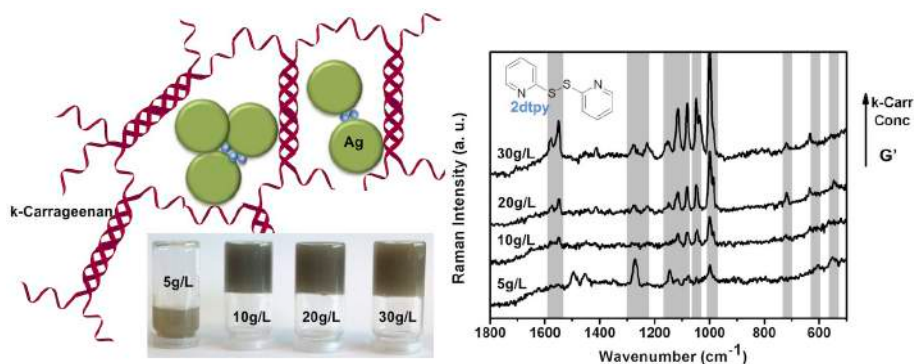


Figure 3. Carrageenan hydrogels containing Ag nanoparticles and variable polysaccharide content that show SERS sensitivity dependent on the induced gel strength.

## LANTHANOPOLYOXOMETALATE BASED COMPOSITE MATERIALS

Nogueira HIS<sup>1</sup>

Polyoxometalates (POMs) are discrete cluster anions of metal oxides with a range of dimensions that goes from less than 1 nm (small anions with a few metal atoms like  $[\text{Mo}_7\text{O}_{24}]^{6-}$ ) to large anionic clusters in the nanometer range (one of the biggest being  $[\text{H}_x\text{Mo}_{368}\text{O}_{1032}(\text{H}_2\text{O})_{240}(\text{SO}_4)_{48}]^{48-}$  ( $x \approx 16$ ) with 5.4 nm width, the “nano-hedgehog”). POMs show very extensive and versatile properties, due to the variety on its composition and structural motifs. The idea of tailor-made POM design in synthetic chemistry is not far from what is achieved in current research. Still there is a big gap between POMs design and its specific applications. The assembly of these inorganic clusters in hybrid materials of adequate processability and stability, that keep the POM functionality, is a big challenge in POM research.

There has been great interest on the use of lanthanopolyoxometalates (LnPOMs) as functional units in nanostructured composite materials. The presence of the lanthanide confers specific functionalities to LnPOM compounds, in particular the photoluminescent properties. We have reported a number of new photoluminescent materials based on LnPOMs incorporated into layered double hydroxides, layer-by-layer assemblies and Langmuir-Blodgett thin films or encapsulated in core-shell silica nanoparticles. Organic-inorganic hybrid materials were prepared using LnPOM anions as inorganic building blocks and organic ligands such as 3-hydroxypicolinate<sup>[1]</sup>; in these materials intra-4f emission of Ln(III) (Ln = Eu, Tb and Er) ions is sensitized both by the 3-hydroxypicolinate ligand and the POM moiety. The preparation of LnPOM/graphene composites (Fig. 1) has been explored and the effect of graphene grafting on the luminescent properties studied<sup>[2]</sup>. Detailed photoluminescence studies have shown that there is efficient emission from the LnPOMs in those composite materials, in particular for the europium derivatives, with excitation paths that involve  $\text{O} \rightarrow \text{Eu}$  and  $\text{O} \rightarrow \text{W}$  ligand-to-metal charge-transfer transitions.

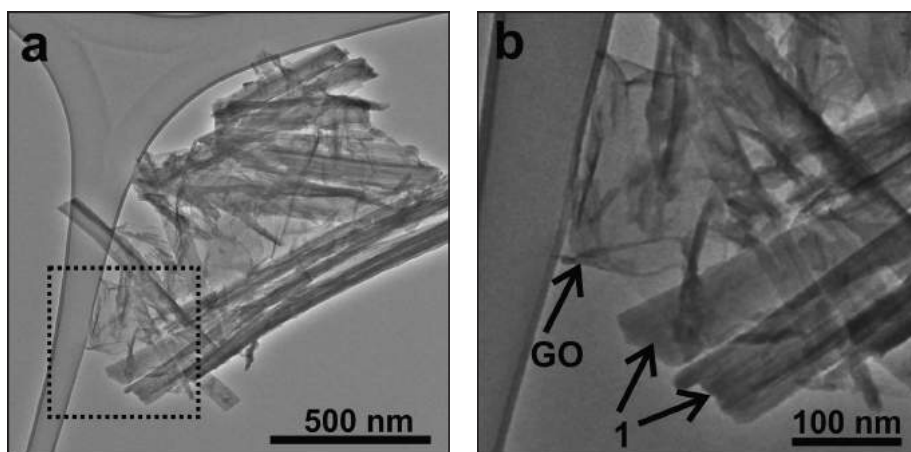


Figure 1. (a) TEM image of the composite LnPOM/Graphene-Oxide where the presence of elongated structures [1- LnPOM rods] is visible. (b) A magnified view of the area boxed in [a].

A series of polysaccharide-based transparent composite films containing LnPOMs was prepared<sup>[3]</sup> using a water-soluble cationic chitosan derivative (HTCC = *N*-(2-hydroxypropyl)-3-trimethylammonium chitosan chloride) and pullulan (PUL). HTCC was more adequate than pure

chitosan due to its positive charge and solubility in water at a broad range of pH values. LnPOMs of  $[\text{Ln}(\text{W}_5\text{O}_{18})_2]^{9-}$  (Ln(III) = Eu and Tb) type were incorporated in the polysaccharides (Fig. 2). EuPOMs encapsulated in amorphous silica shells were also incorporated in the polysac-

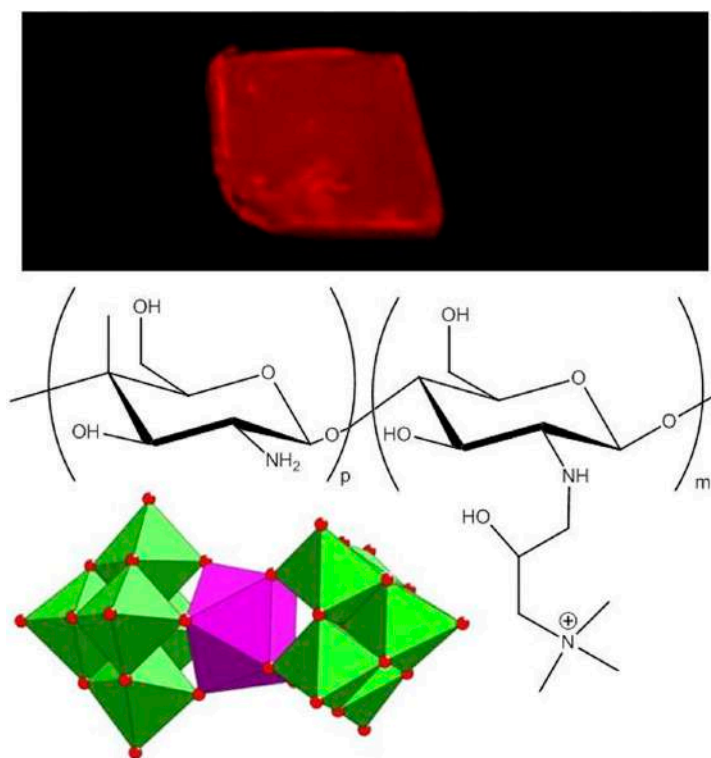
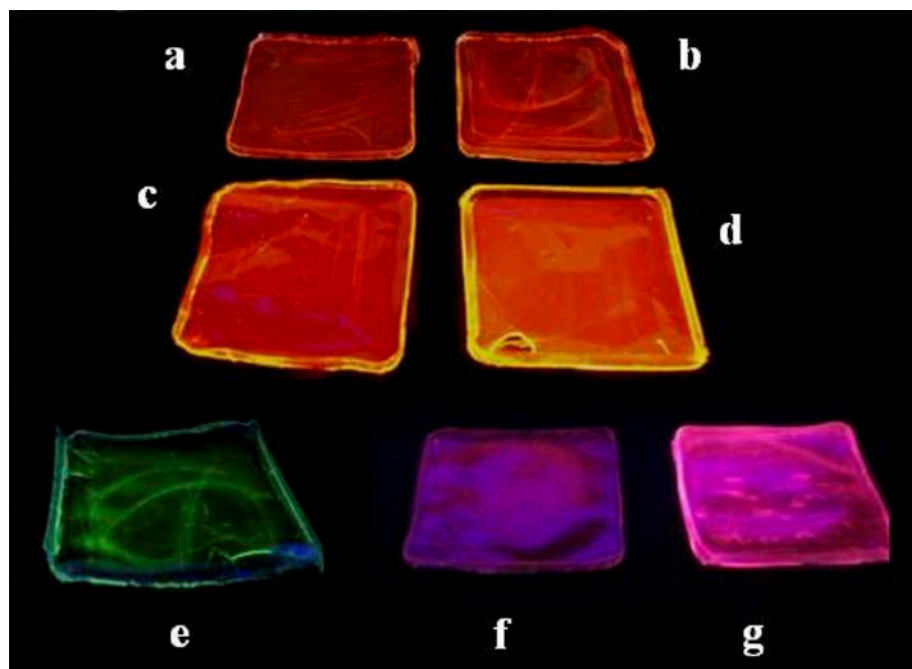


Figure 2. Incorporation of lanthanopolyoxometalates such as  $[\text{Eu}(\text{W}_5\text{O}_{18})_2]^{9-}$  (bottom structure) in a chitosan derivative (HTCC, top structure) originates clear transparent films that show the lanthanide emission under UV (photograph under 366 nm excitation).



**Figure 3.** Photographs of PUL films with different EuPOM loadings [a] 2.5%, [b] 5%, [c] 10%, [d] 40% and loadings of [e] TbPOM, [f] EuPOM@SiO<sub>2</sub> and [g] EuL@SiO<sub>2</sub>, taken under 366 nm radiation. Films size is approximately 5 cm x 5 cm.

charides, in order to test the effect on the film processing of having a nanoparticles loading instead of LnPOM anions. The incorporation of LnPOMs or LnPOM-silica core-shell nanoparticles in either HTCC or PUL polysaccharides originated clear transparent films. These composite films are transparent under daylight exhibiting visible emission while under UV excitation (Fig. 3).

<sup>1</sup> Department of Chemistry, CICECO, University of Aveiro, 3810-193 Aveiro, Portugal

#### References

- [<sup>1</sup>] Granadeiro CM, Ferreira RAS, Soares-Santos PCR, Carlos LD, Nogueira HIS, *European Journal of Inorganic Chemistry*, 2009, 5088-5095.
- [<sup>2</sup>] Granadeiro CM, Cruz SMA, Gonçalves G, Marques PAAP, Costa PMFJ, Ferreira RAS, Carlos LD, Nogueira HIS, *RSC Advances*, 2012, 2, 9443-9447.
- [<sup>3</sup>] Pinto RJB, Granadeiro CM, Freire CSR, Silvestre AJD, Neto CP, Ferreira RAS, Carlos LD, Cavaleiro AMV, Trindade T, Nogueira HIS, *European Journal of Inorganic Chemistry*, 2013, 1890-1896.

#### Acknowledgments

This work has been funded by FCT (Portugal) and COST Action CM1203.

## EVIDENCE FOR ENTANGLEMENT AT HIGH TEMPERATURES IN AN ENGINEERED MOLECULAR MAGNET

Brandão P<sup>1</sup>, Santos AM<sup>2</sup>, Reis MS<sup>3</sup>

Entanglement, a sort of quantum correlation, plays an important role in quantum information science because it can be used as resource for many quantum information processing protocols<sup>[1]</sup>. Therefore, the study of entanglement in solid-state physics is of great relevance to the area of quantum information, since many proposals of quantum processors are solid-state based. The recent demonstration that entanglement can change the thermodynamic properties of solids, such as magnetic susceptibility, shows that entanglement can be related to significant macroscopic effects. Hence, this subject establishes an interesting connection between quantum information theory and condensed-matter physics, because magnetization, heat capacity, and

internal energy can also be used to reveal spin entanglement among constituents of a solid. Quantum entanglement at elevated temperatures has been studied in several physical systems and the recent work by Vedral<sup>[2]</sup> summarizes this scenario. In that work it is recognized that some molecular magnets remain entangled at surprisingly high temperatures. Besides presenting robust entangled states, such materials can be engineered to enhance their quantum features and, consequently, to be better suited for quantum information applications. As an example, it was recently shown, through magnetic susceptibility measurements, that certain families of molecular magnets are entangled up to 630 K, and have the maximum

degree of entanglement at temperatures as high as 100 K<sup>[3]</sup>.

In order to obtain systems with the highest entanglement temperature, which should contain antiferromagnetically coupled magnetic ions with the highest possible spin states, a systematic study of molecular iron compounds was made, which resulted in the preparation of a new di-iron complex with formula [Fe<sub>2</sub>(μ<sub>2</sub>-oxo)(C<sub>3</sub>H<sub>4</sub>N<sub>2</sub>)<sub>6</sub>(C<sub>2</sub>O<sub>4</sub>)<sub>2</sub>]. The crystal structure consists of a di-nuclear μ-oxo Fe(III) complex where the bridging oxygen atom is at the crystallographic inversion center and the metal-to-metal distance is of 3.594(9) Å with a Fe–O–Fe angle of 180°. The Fe(III) center is six-coordinated in a distorted octahedra coordination in which the equatorial plane is composed of three nitrogen donors from imidazole ligands (2.095(2), 2.147(2) and 2.168(2) Å), and one oxygen atom of oxalate ligand (2.042(2) Å). The apical positions are occupied by the μ-oxo bridging atom (1.797(5) Å) and by the other oxalate oxygen (2.152(2) Å), as shown in figure 1. The magnetic susceptibility of this compound was measured from

2 to 300 K. The analysis of the susceptibility data using protocols developed for other spin singlet ground-state systems indicates that the quantum entanglement would remain at temperatures up to 732 K, significantly above the highest entanglement temperature reported to date<sup>[4]</sup>. The large gap between the ground state and the first-excited state (282 K) suggests that the spin system may be somewhat immune to decohering mechanisms. Our measurements strongly suggest that molecular magnets are promising candi-

date platforms for quantum information processing.

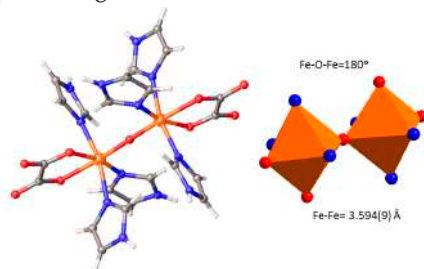


Figure 1. Crystal structure details of  $[\text{Fe}_2(\mu_2\text{-oxo})(\text{C}_2\text{H}_4\text{N}_2)_2(\text{C}_2\text{O}_4)_2]$ ; left - Molecular structure; right - iron dimer polyhedral representation.

<sup>1</sup> Department of Chemistry, CICECO, University of Aveiro, 3810-193 Aveiro, Portugal

<sup>2</sup> NSSD, Oak Ridge National Laboratory, Oak Ridge, Tennessee 37831-6475, USA

<sup>3</sup> Instituto de Física, Universidade Federal Fluminense, 24210-340, Rio de Janeiro, Brasil

#### References

[1] Vedral V, Introduction to Quantum Information Science [Oxford University Press], 2006.

[2] Vedral V, *Scientific American*, 2011, June issue, 2011, 38.

[3] Souza AM, Soares-Pinto DO, Sarthour RS, Oliveira IS, Reis MS, Brandão P, Santos AM, *Physical Review B*, 2009, 79, 054408.

[4] Reis MS, Soriano S, Santos AM, Sales BC, Soares-Pinto DO, Brandão P, *EPL*, 2012, 100, 50001.

## USE OF INNOVATIVE ECO-BUILDING MATERIALS

Tobaldi DM<sup>1</sup>, Pullar RC<sup>1</sup>, Seabra MP<sup>2</sup>, Labrincha JA<sup>3</sup>

The energy efficiency and the carbon footprint of modern building are highly reduced. On the other hand, these airtight and sealed environments have created unexpected side effects, realising potentially harmful chemicals in the air, hence potentially causing negative impacts on human being.



Figure 1. Banner of the ECO-SEE project ([www.eco-see.eu](http://www.eco-see.eu)).

Our research group, involved in the European project ECO-SEE (ECO-innovative, Safe and Energy Efficient wall panels and materials for a healthier indoor environment), aims at addressing that emerging health problem, associated with modern low carbon buildings. The goal is to study the use of innovative eco-building materials that will not only address poor air quality, but also will radically improve the energy efficiency of buildings.

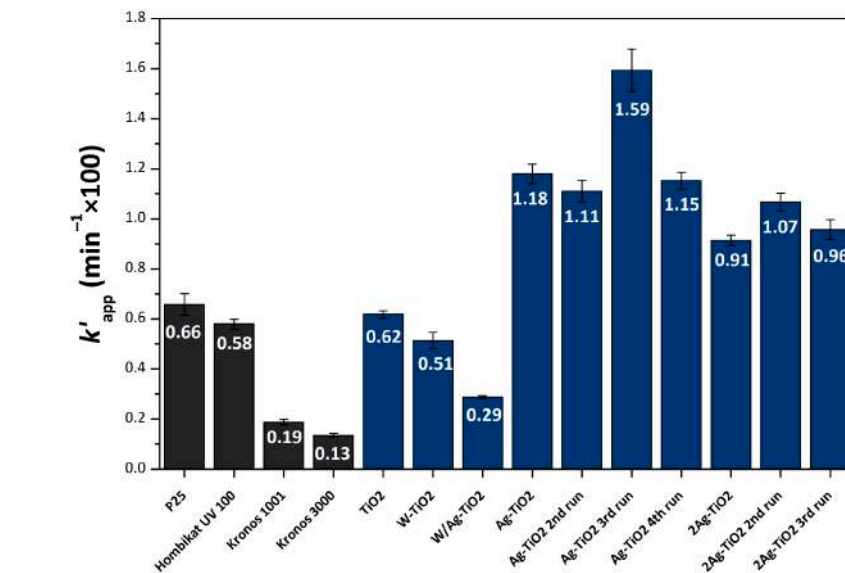


Figure 2 Photocatalytic results, depicting the initial [20 min] pseudo-first order kinetic constants for some commercial (dark grey), and synthesised nano  $\text{TiO}_2$  samples (blue). The model pollutant was  $\text{NO}_x$ , the light source a white-light lamp (irradiance =  $7 \text{ Wm}^{-2}$ ), simulating an indoor environment.

One of our group involvements is the full development of highly novel photocatalytic coatings by the use of nanoparticle technology, which will decompose harmful chemicals when exposed to sunlight (simulating an outdoor environment) or visible light (recreating real indoor situation), preventing them from being released into the air.

<sup>1</sup> Department of Materials and Ceramic Engineering, CICECO, University of Aveiro, 3810-193 Aveiro, Portugal

#### References

[1] Tobaldi DM, Pullar RC, Seabra MP, Labrincha JA, *Materials Letters*, 2014, 122, 345–347.

[2] Tobaldi DM, Pullar RC, Sever Škapin A, Seabra MP, Labrincha JA, *Materials Research Bulletin*, 2014, 50, 183–190.

#### Acknowledgments

We thank the European Union's Seventh Framework Programme (grant agreement n° 609234) and FCT (PEst-C/CTM/LA0011/2013 and Ciência2008 programmes).

# SYNTHESIS AND STRUCTURE OF NOVEL INORGANIC LAYERED MATERIALS

Lin Z<sup>1</sup>, Wu ZY<sup>1</sup>, Zhang XS<sup>2</sup>, Brandão P<sup>1</sup>, Dong JX<sup>2</sup>

The development of a new technology requires a continuous search for new materials and/or new properties of traditional materials. With the advent of the nanotechnology era, the increasing interest turns to the use of layered materials for device applications. Layered materials have been delaminated. The exfoliated layers have thickness at nano scale and can be used as additives to improve the gas selectivity of polymer membrane and as a solid lubricant additive to improve the load-carrying capacity. On the other hand, the knowledge on the structure will help us to explain properties and to predict the applications. Copper zirconium phosphate ( $\text{CuZr}(\text{PO}_4)_2 \cdot 4\text{H}_2\text{O}$ ) was usually prepared by high temperature Cu(II) ion exchange from  $\text{Zr}(\text{HPO}_4)_2 \cdot \text{H}_2\text{O}$  and was used in different application for long time although its structure is not clearly known yet. Rare earth borates are important due to their excellent properties, especially for optics. The synthesis research showed that their formation is sensitive to the synthesis conditions.

By hydrothermal synthesis, high crystalline copper zirconium phosphate [with more precise chemical formulae from the structure point of view,  $\text{Cu}(\text{OH})_2\text{Zr}(\text{HPO}_4)_2 \cdot 2\text{H}_2\text{O}$ ,  $\text{Cu-}\alpha\text{-ZrP}$ ] has been directly obtained. Its crystal structure has been determined initially by using laboratory powder X-ray diffraction data, showing a laminar structure with  $\text{ZrPO}$  layers and Cu(II) between them. In the structure, Cu(II) was located in an exchangeable position and was certified to be exchangeable by the proton.  $\text{Cu-}\alpha\text{-ZrP}$  was evaluated as an additive of grease in a four ball test, showing better effect in improving the load-carrying capacity of lithium grease than  $\text{MoS}_2$ , a typical solid lubricant additive. The maximum non-seizure load ( $P_B$ , represent the load-carrying capacity) of base grease containing  $\text{Cu-}\alpha\text{-ZrP}$  was increased from 353 N to 1235 N. The

excellent load-carrying capacity can be explained by its easier cleavage and adherence to the worn surface forming the tight protective layer (Fig.1).<sup>[1]</sup>

By careful selection of synthesis conditions, three samarium polyborates have been prepared hydrothermally in very similar experimental conditions, of which two [ $\text{SmB}_6\text{O}_8(\text{OH})_3 \times \text{B}(\text{OH})_3$  (1),  $\text{SmB}_6\text{O}_8(\text{OH})_3 \times \text{B}(\text{OH})_3 \times \text{H}_2\text{O}$  (2)] possess new structures and their structures have been determined by single-crystal X-ray diffraction data.<sup>[2]</sup> The two layered materials are structurally related and constituted by hexaborate chains. The hexabo-

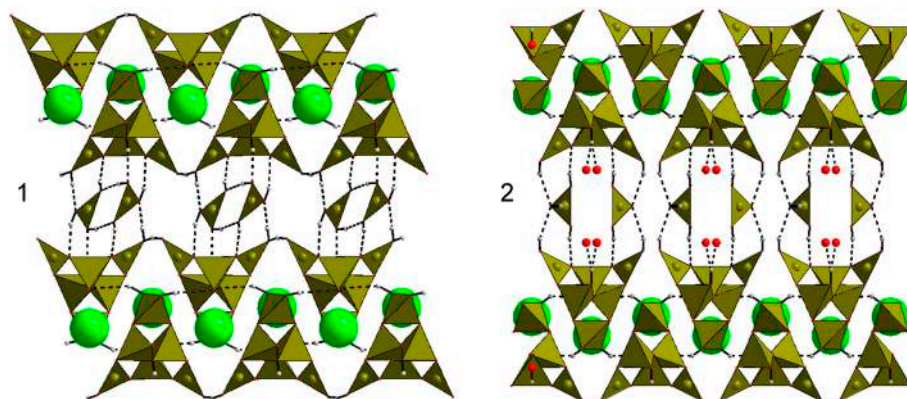


Figure 2. Crystal packing of compounds 1 and 2. Green balls represent samarium while dashed lines represent O-H...O hydrogen bond interactions.

rate chains are connected by samarium polyhedra, forming dense sheets which further interact with each other by hydrogen bonding via isolated boric acid between these sheets (Fig.2). The compound 2 also has hydrogen bonded water molecules between dense sheets. From structure point of view, the new layered samarium borate compound 2 may be able to transform to compound 1 and  $\text{NaNdB}_6\text{O}_9(\text{OH})_4$  by careful selection of treatment conditions. The distance between dense sheets of compound 2 can be easily altered by heating or ion exchange with Na, being expected easy cleavage of layers.

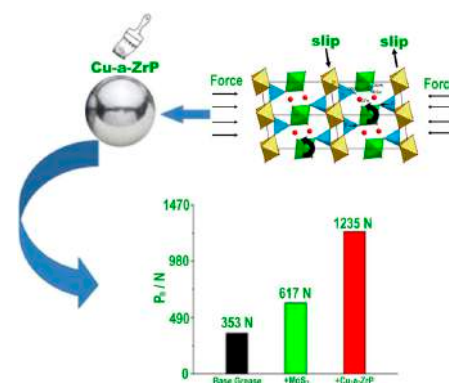


Figure 1.  $\text{Cu}(\text{OH})_2\text{Zr}(\text{HPO}_4)_2 \cdot 2\text{H}_2\text{O}$  structure and its application to improve the load-carrying capacity of lithium grease.

<sup>1</sup> Department of Chemistry, CICECO, University of Aveiro, 3810-193, Aveiro, Portugal

<sup>2</sup> Research Institute of Special Chemicals, Taiyuan University of Technology, Taiyuan, 030024, Shanxi, P. R. China

## References

- [<sup>1</sup>] Zhang XS, Xu H, Zuo ZJ, Lin Z, Ferdov S, Dong JX, *Applied Materials & Interfaces*, 2013, 5, 7989-7994.  
 [<sup>2</sup>] Wu ZY, Brandão P, Lin Z, *Inorganic Chemistry*, 2012, 51, 3088-3093.

# ANOMALY ON THE GRAIN GROWTH AND DIELECTRIC RESPONSE OF TI-RICH STRONTIUM TITANATE CERAMICS

Amaral L<sup>1</sup>, Fernandes M<sup>1</sup>, Reaney IM<sup>2</sup>, Harmer MP<sup>2</sup>, Senos AMR<sup>1</sup>, Vilarinho PM<sup>1</sup>

Strontium titanate based materials have a great interest for a wide range of applications in microelectronics namely in tunable microwave devices, due to the high electric-field dependence of the permittivity and more recently as a possible thermoelectric material where special attention is being paid to the important role of grain boundaries to improve the figure of merit of this material.

Grain boundaries in ceramics are mainly formed during the sintering process and are moving, enabling the coarsening of the microstructures by grain growth. We have investigated the grain growth of 0.5 mol% Ti-rich SrTiO<sub>3</sub> composition over a wide range of sintering temperatures, from 1400 up to 1650 °C, in air, and the evolution of bulk and grain boundary electrical response with the sintering temperature was assessed by impedance spectroscopy. This technique allows to

address separately the grain boundary impedance response and therefore to detect changes in the grain boundary dielectric properties.

A grain growth anomaly in Ti-rich strontium titanate ceramics is here reported: discontinuities on the evolution of grain growth with the sintering temperature were observed, defining four grain growth regimens with transitions at temperatures around 1500, 1550 and 1605 °C (Figures 1 and 2). These transitions correspond to grain size decreases, despite the increasing sintering temperature. We also show that similar discontinuities can be observed in the dependence of the grain boundary activation energy for conductivity and in the grain boundary thickness, assessed by impedance spectroscopy (Figure 2). These notable coincidences are reported for the first time and strongly support the formation

of different grain boundary complexions in polycrystalline oxides with transitions in between the observed grain growth regimens, which may be correlated to different grain boundary mobility and dielectric properties. Grain boundary dielectric response was much more affected by the sintering temperature than that of the bulk counterpart, strongly reinforcing the idea of the key role played by the grain boundaries in the anomaly in the

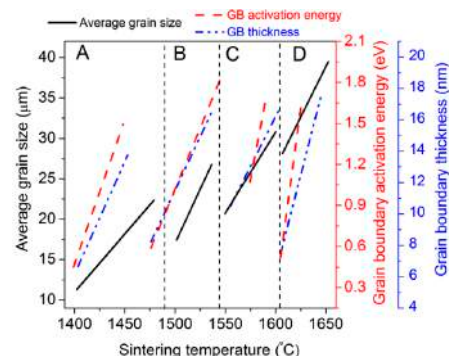


Figure 2. Illustration of the similar trends observed for the dependence of the average grain size, grain boundary activation energy for conductivity and grain boundary thickness on the sintering temperature.

grain growth observed for Ti-rich SrTiO<sub>3</sub>. We postulate that this anomalous behavior is directly related to a 1<sup>st</sup> order reverse change of complexions driven by the temperature effect on the grain boundary wettability and electrostatic potential. These new insights have great scientific and technological relevance in tailoring the microstructure and dielectric response of SrTiO<sub>3</sub>-based materials and related systems and using grain boundary complexion behavior for materials properties design.

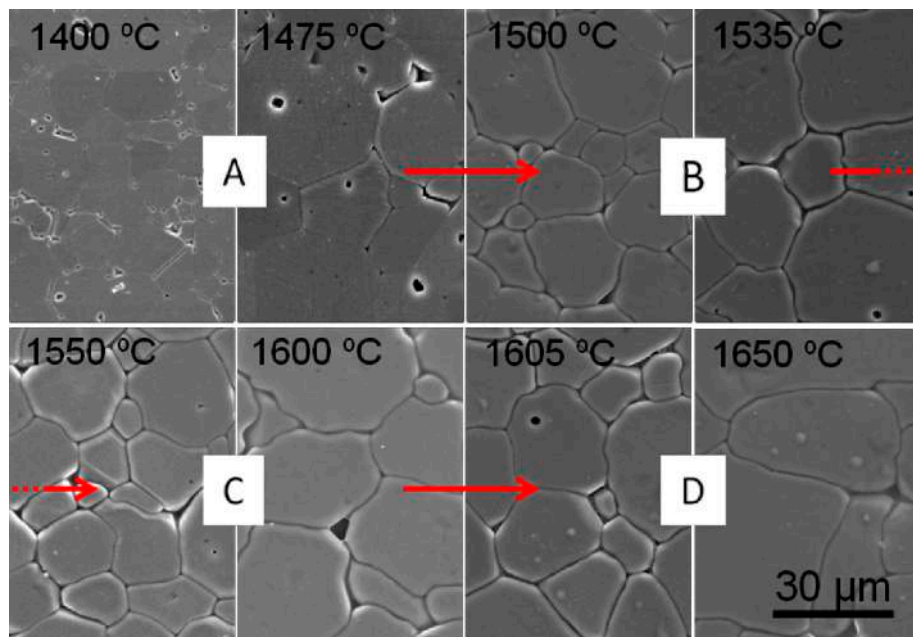


Figure 1. SEM microstructures of samples sintered at several temperatures [indicated on the images]. In spite of the continuous increase of the sintering temperature, the decrease of the grain size is obvious. Arrows signalize the regimen transitions with decreasing of the grain size.

<sup>1</sup> Department of Materials and Ceramic Engineering, CICECO, University of Aveiro, 3810-193 Aveiro, Portugal

<sup>2</sup> Center for Advanced Materials and Nanotechnology, Lehigh University, Bethlehem, Pennsylvania 18015, United States

<sup>3</sup> Department of Engineering Materials, University of Sheffield, Sheffield, S1 3JD, UK

## References

- [1] Amaral L, Fernandes M, Senos AMR, Vilarinho PM, Harmer MP, *Microscopy and Microanalysis*, 2012, 18 (S5), 123-124.
- [2] Amaral L, Fernandes M, Reaney IM, Harmer MP, Senos AMR, Vilarinho PM, *The Journal of Physical Chemistry C*, 2013, 117 (47), 24787–24795.

## CAN POROSITY BE AN ADVANTAGE? YES, IT CAN!

Ferreira P<sup>1</sup>, Castro A<sup>1</sup>, Laberty C<sup>2</sup>, Boissière C<sup>2</sup>, Grosso D<sup>2</sup>, Sanchez C<sup>2</sup>, Rodriguez B<sup>3</sup>, Vilarinho PM<sup>1</sup>

In 1965, Moore's predicted that the number of transistors per integrated circuit will double approximately every two years. This trend, known as Moore's law has been verified up to recently, however due to size and thermal management, this miniaturization trend is reaching the limits. Indeed a new trend emerged in the Semiconductor Industry Roadmap encompassing functionalities that do not necessarily scale, but provide additional value to the end customer in different ways, allowing the development of value-added systems.

The Electroceramics group has been actively engaged in developing strategies to prepare porous ferroic films to be used as startup matrices for multifunctional materials, namely for multiferroics. Multiferroic materials have been actively studied as a route to control magneto-electric coupling and to enable a range of applications whereby magnetism can be controlled by an electric field. Single phase, room temperature multiferroics are rare, because of that a variety of approaches to prepare composite multiferroic materials have been tried.

In a collaboration involving Researchers from Group 2 of CICECO, the University Pierre et Marie Curie, France and the University College Dublin, Ireland we have successfully prepared porous ferroelectric thin films<sup>[1]</sup> and systematically studied the effect of porosity on the local electric properties.<sup>[2]</sup> Nanoporous piezo- and ferro- electric barium titanate and lead titanate thin films (~100 nm calculated from ellipsometric data) were prepared starting from sol-gel solutions modified with a commercially available block-copolymer and evaporation-induced self-assembly methodology. The tuning of the thermal treatment followed by in situ ellipsometry allows the decomposition of the organic components and of the structuring agent leading to the formation of porous tetragonal crystal-

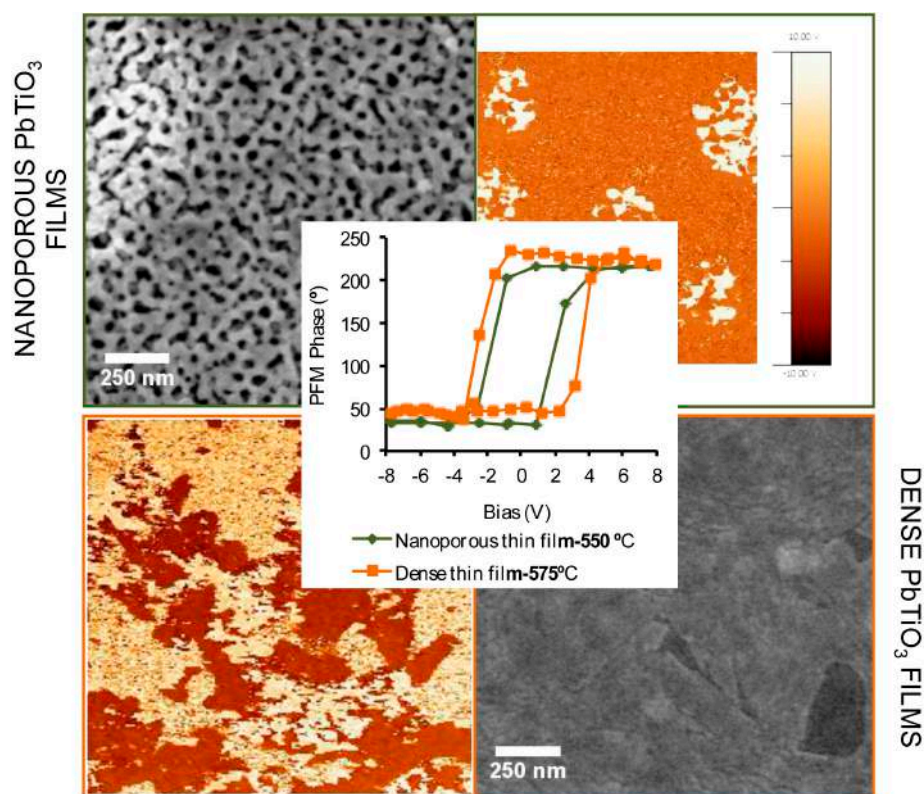


Figure 1. SEM, topographic and PFM images and local hysteresis loops obtained in nanoporous and dense  $\text{PbTiO}_3$  films after thermal treatment at: 550 and 575 °C, respectively. Ferroelectric properties are enhanced in nanoporous films.

line perovskite structures as observed by XRD, HRTEM, SEM, and ellipsometry. Both nanoporous barium titanate and lead titanate thin films present local piezoelectric and ferroelectric behavior measured by piezoresponse force microscopy (PFM). A recent study aiming the understanding of the effect of porosity on the electric properties at the nano-scale demonstrated the crystallization of the tetragonal phase at lower temperatures in porous than in dense films. Nanoporous films with improved tetragonality exhibit enhanced piezoelectric coefficients, switchable polarization and low local coercivity (Figure 1). By providing a means of achieving enhanced properties, nanoporosity may have a broad impact in applications of ferroelectric thin films by themselves and also as platforms to reach multifunctional devices.

<sup>1</sup> Depart. Materials and Ceramics Engineering, CICECO, University of Aveiro, 3810-193 Aveiro, Portugal

<sup>2</sup> Lab. Chimie de la Matière Condensée de Paris, UMR-7574 CNRS, UPMC Université, Paris 06, France

<sup>3</sup> School of Physics, University College Dublin, Dublin, Ireland

### References

[1] Ferreira P, Hou RZ, Wu A, Willinger MG, Vilarinho PM, Mosa J, Laberty-Robert C, Boissière C, Grosso D, Sanchez C, *Langmuir*, 2012, 28, 2944.

[2] Castro A, Ferreira P, Rodriguez BJ, Vilarinho PM, *Journal of Materials Chemistry C*, 2014, accepted.

### Acknowledgments

This work was funded by FCT, FEDER, European Union through the projects FCOMP-01-0124-FEDER-009356 (ReP. FCT PTDC/CTM/098130/2008) and FCOMP-01-0124-FEDER-037271 (ReP. FCT PEst-C/CTM/LA0011/2013).

# LOCAL BIAS INDUCED FERROELECTRICITY IN MANGANITES WITH COMPETING CHARGE AND ORBITAL ORDER STATES

Figueiras FGN<sup>1</sup>, Bdikin IK<sup>2</sup>, Amaral VBS<sup>1</sup>, Kholkin AL<sup>3</sup>

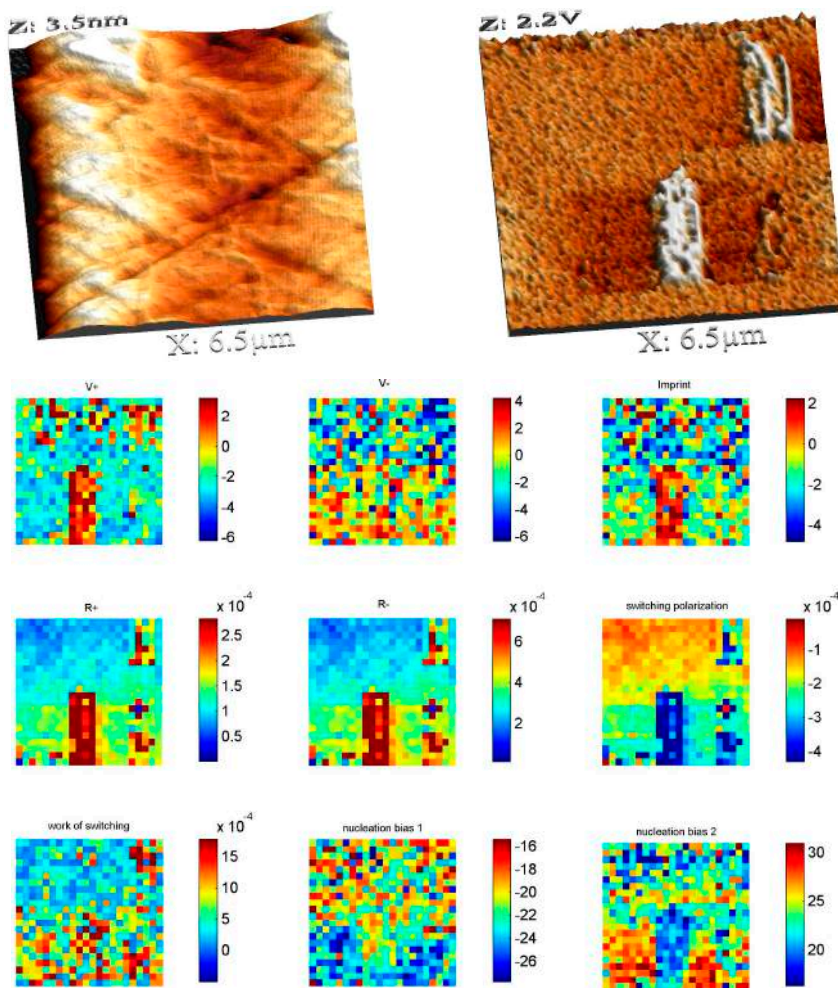


**Figure 1.** (top left) Topographic and (top right) piezo contrast surface scans after performing bias lithographic paths: Top corner  $+20 V_{dc}$ ; Low center  $-15 V_{dc}$ ; Bottom corner  $-20 V_{dc}$ ; (under)  $3 \times 3 \mu m^2$  detail of the respective BEPS maps results for the single crystal  $Pr_{0.60}Ca_{0.40}MnO_3$  sample.

Our experimental work investigated a complementary paradigm for ferroelectricity, a property of some dielectric materials, having a spontaneous polarization that can be reversed by an external electric field and that is technologically relevant in the essence of MRAMs and flash drives devices. We analyzed a partic-

ular set of materials based in perovskite-type manganites, such as  $Pr_{1-x}Ca_xMnO_3$ ,  $La_{1-x}Ca_xMnO_3$  and  $La_{1-x}Sr_xMnO_3$  solid solutions. Conventionally, the finite conductivity of such manganites hinders the observation of macroscopic ferroelectricity, even though polarization may still exist in nanoscale volumes.

We use Piezoresponse Force Microscopy (PFM) to probe local bias induced modifications of electrical and electromechanical properties at the manganites surface. Clear bias-induced piezocontrast and local hysteresis loops are observed at room temperature in compounds close to a charge-order (CO/OO) state providing convincing evidences of the existence of locally induced polar states, while reference samples without CO/OO behavior showed no ferroelectric-like response. This sets forth a new case study of ferroelectricity formation by mechanisms associated with the metastable appearance of site- and bond-centered charge/orbital ordering (CO/OO) which breaks structural inversion symmetry. The co-existence of intrinsic magnetism usually found in manganites and ferroelectricity due to the CO/OO states induced under locally applied electric field opens up a new pathway to expand the phase diagrams of such systems and to achieve spatially localized multiferroic effects. Induced metaphases within a single compound at the nanometer scale can raise multifunction material and interface effects with a technological potential to be used in new generations of memory cells and data processing circuits. Lithographic induced Structural/Electro-chemical phase transitions can be an alternative technological process for manufacturing permanent or temporary nano circuit chips from a single base material.

<sup>1</sup> Department of Physics, CICECO, University of Aveiro, 3810-193, Aveiro-Portugal

<sup>2</sup> Department of Mechanical Engineering, TEMA, University of Aveiro, 3810-193, Aveiro-Portugal

<sup>3</sup> Department of Materials and Ceramic Engineering, CICECO, University of Aveiro, 3810-193, Aveiro-Portugal

## Reference

[1] Figueiras FGN, Bdikin IK, Amaral VBS, Kholkin AL, *Physical Chemistry Chemical Physics*, 2014, 16 (10), 4977–4981.

## Acknowledgments

Work supported by FCT research projects (PTDC/FIS/105416/2008) and Grants SFRH/BD/25011/2005 and SFRH/BPD/80663/2011 and performed in collaboration with researchers from Oak Ridge National Laboratory (TN, USA)

# AQUEOUS PROCESSING OF LEAD FREE $0.5\text{Ba}(\text{Zr}_{0.2}\text{Ti}_{0.8})\text{O}_3-0.5(\text{Ba}_{0.7}\text{Ca}_{0.3})\text{TiO}_3$ PIEZOELECTRIC CERAMIC MICRO-COMPONENTS FROM A POWDER SURFACE TREATED AGAINST HYDROLYSIS

Kaushal A<sup>1</sup>, Olhero SM<sup>1</sup>, Ferreira JMF<sup>1</sup>

Aqueous processing of multicomponent electroceramics relies on achieving their various functional properties unaffected from the odds of ionic leaching in water.  $0.5\text{Ba}(\text{Zr}_{0.2}\text{Ti}_{0.8})\text{O}_3-0.5(\text{Ba}_{0.7}\text{Ca}_{0.3})\text{TiO}_3$  (BZT–BCT) has been reported as the lead free ferroelectric system that exhibits highest piezoelectric coefficient  $d_{33} \sim 620\text{pC/N}$  and has been regarded as future replacement of lead based

$\text{Pb}[\text{Zr}_x\text{Ti}_{1-x}]\text{O}_3$  (PZT) piezoelectric ceramics. The dispersion of powders in suitable liquid media to obtain stable colloidal suspensions with high solids loading is one of the most demanding processing steps. They would enable consolidating bulk green shapes with homogeneous microstructures.

We reported in 2013, all the essential steps for consolidating defect free green ceramic bodies from: (i) solid state reaction synthesis of pure phase BZT–BCT; (ii) deagglomeration to obtain a fine powder; (iii) assessment of the solid/liquid interfacial reactions and how they can be controlled/prevented through a suitable surface treatment of the powder particles; (iv) preparation of high solids loading suspensions; (v) evaluating the effects of surface coating, dispersant type and amount, solids volume fraction, and aging time on rheology and colloidal stability. Surface treatment consisted in adding 100 g of the attrition milled BZT–BCT powder to 200 cm<sup>3</sup> of 2 wt.% aqueous solutions of aluminium di-hydrogen phosphate,  $\text{Al}(\text{H}_2\text{PO}_4)_3$ , at 60 °C under magnetic stirring for 30 minutes. In order to assess the efficiency of the surface treatment, aqueous suspensions containing 5 wt.% of non-treated (BZT–BCT–NT) and surface treated (BZT–BCT–ST) powders were kept under magnetic stirring at room temperature and the pH variations as a function of time were monitored for along 7 days (168 h). The pH values fluctuate within the range of 8.3–9.4 for BZT–BCT–NT suspension, whereas significantly smaller pH variations between 8.8–9.1 have been registered for BZT–BCT–ST suspension. This hypothesis of ionic leaching in aqueous media was confirmed by ICP analysis of centrifuged supernatants derived from suspensions aged for one week as shown in Fig. 1. We have shown that: (i) the ex-

tent of leaching is 4–5 times higher for the NT powder; (ii) the leaching process is somewhat enhanced in the presence of dispersant (D); (iii) the leached amounts of Ba are 15–16 times higher than those of Ca. This hydrolysis and non-stoichiometric dissolution reactions will alter the composition of BZT–BCT powder and is confirmed from corresponding XRD pattern (Fig. 2). The presence of extra impurity phase peaks corresponding to  $\text{Ba}(\text{OH})_2 \cdot \text{H}_2\text{O}$  and  $\text{BaZrO}_3$  for the BZT–BCT–NT powder aged for 1 week under constant stirring in water confirms the occurrence of hydrolysis and degradation of the original BZT–BCT–NT powder with change of desired pure single perovskite-type tetragonal phase to multiple phase system. Furthermore, suspensions with solid loadings ( $\Phi$ ) up to 60 vol.%, pseudoplastic flow behaviours and long term colloidal stability could be achieved from the surface treated powder. The concentrated and stable suspensions represent a stride for successful processing functional BZT–BCT ceramic components via various aqueous colloidal shaping methods (slip casting, gel-casting, etc.) for large scale industrial applications. This stable aqueous suspension of high solid loading results in successful gel-casting and de-moulding of three dimensional (3D) micropatterning with interesting features, including

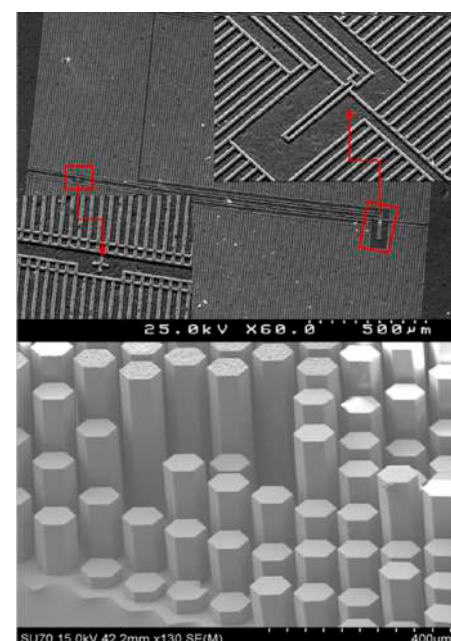


Figure 3. 3D multiscale ordered complex micro components of aqueous processed BZT–BCT electroceramics obtained by gel-casting process.

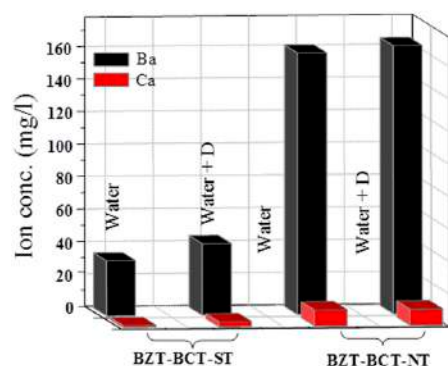


Figure 1. ICP analysis showing Ba and Ca concentrations in centrifuged supernatants from 5 wt.% aqueous solutions of BZT–BCT–ST and BZT–BCT–NT powder kept for 1 week in water in the absence and in the presence of dispersant (D).

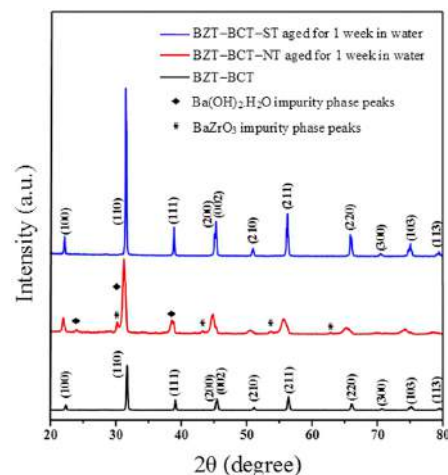


Figure 2. XRD patterns of the BZT–BCT–NT powder, before (a) and after aging in water for one week (b), and of the BZT–BCT–ST powder after being in contact with water for the same time period (c).

complex structures with a periodic variations through their length and, multi-scale array of hexagonal shaped pillars of different aspect ratios (AR) (max AR  $\approx$  9

with approx  $\sim$  360  $\mu\text{m}$  of height and side length  $\sim$  40  $\mu\text{m}$ ) with smooth side wall features along height (Fig. 3).

## NANOSCALE FERROELECTRICITY IN CRYSTALLINE $\gamma$ -GLYCINE

Heredia A<sup>1</sup>, Kholkin AL<sup>1</sup>, Bdikin I<sup>2</sup>, Gracio J<sup>2</sup>, Meunier V<sup>3</sup>, Balke N<sup>3</sup>, Tselev A<sup>3</sup>, Agarwal P<sup>3</sup>, Sumpster BG<sup>3</sup>, Kalinin SV<sup>3</sup>

Ferroelectrics are multifunctional materials that reversibly change their polarization under an electric field. Recently, the search for new ferroelectrics has focused on organic and bio-organic materials, where polarization switching is used to record/retrieve information in the form of ferroelectric domains. This progress has opened a new avenue for data storage, molecular recognition, and new self-assembly routes. Crystalline glycine is the simplest amino acid and is widely used by living organisms to build proteins.

In this work, it has been shown that  $\gamma$ -glycine, which is known to be piezoelectric since 1954, is also *ferroelectric*, as evidenced by local electromechanical measurements and by the existence of as-grown and switchable ferroelectric domains in microcrystals grown from the solution (Fig. 1). Molecular simulations help rationalizing the experimental results by showing that the polarization vector in glycine is easily switched at the nanoscale under a moderate electric field (Fig. 2). The discovery of ferroelectricity

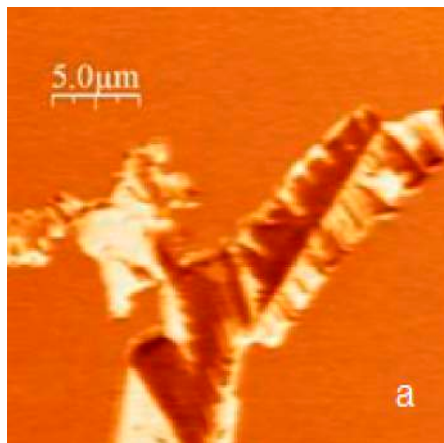
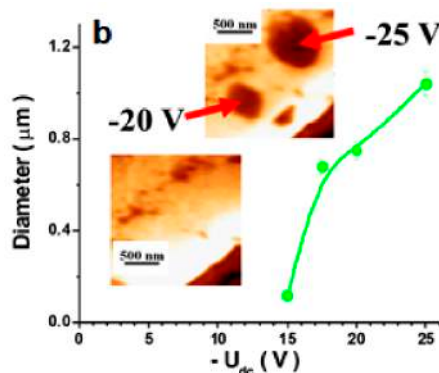


Figure 1. (a) As-grown ferroelectric domains in glycine; (b) polarization switching (shown by arrows) after application of moderate electric field.



<sup>1</sup> Department of Materials and Ceramic Engineering, CICECO, University of Aveiro, 3810-193, Aveiro-Portugal

### Reference

[1] Kaushal A, Olhero SM, Ferreira JMF, *Journal of Materials Chemistry C*, 2013, 1, 4846-4853.

in amino acids offers avenues to novel classes of bioelectronic logic and memory devices, where polarization switching is used to record and retrieve information in the form of ferroelectric domains. Ferroelectric-based memory may be built, for example, using the synergy with DNA-based conductors and organic transistors. Beyond information storage, these studies open up a set of interesting possibilities regarding the role of glycine piezoelectricity and ferroelectricity in the genesis of life (*e.g.*, protein formation), as well as emerging properties in peptides, from the biophysical point of view.

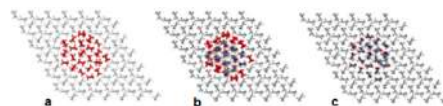


Figure 2. Molecular switching of glycine molecules under increasing bias field: (a) 0.434, (b) 4.10 and (c) 9.55 V/nm.

<sup>1</sup> Department of Materials and Ceramic Engineering, CICECO, University of Aveiro, 3810-193 Aveiro, Portugal

<sup>2</sup> Nanotechnology Research Division, TEMA, University of Aveiro, 3810-193 Aveiro, Portugal

<sup>3</sup> Oak Ridge National Laboratory, Oak Ridge, TN 37830, USA

### Reference

[1] Heredia A, Kholkin AL, Bdikin I, Gracio J, Meunier V, Balke N, Tselev A, Agarwal P, Sumpster BG, Kalinin SV, *Advanced Functional Materials*, 2012, 22, 2996-3003.

## SYNERGISTIC CORROSION INHIBITION ON GALVANICALLY COUPLED MATERIALS

Kallip S<sup>1</sup>, Bastos AC<sup>1</sup>, Ferreira MGS<sup>1</sup>, Zheludkevich ML<sup>1</sup>

Multi-material combinations are actively introduced nowadays to different ap-

plications especially in the transport industry where light weight structures are

very attractive from standpoint of energy saving and reduction of carbon footprint. In the case of joining dissimilar conductive materials the galvanic corrosion can become a limiting factor. Since the current anti-corrosion approaches are mainly suitable for single-material structures, the need for development of new strategies of active and passive corrosion

protection for the multi-material applications is evident.

The seek for successful inhibitor candidates in our group has resulted with unique combination of two well known corrosion inhibitors, that has a superior performance especially for active galvanic systems, while on single material corrosion the elevated advantage does not appear.

The driving idea for the present work was to combine an anodic corrosion inhibitor with a cathodic one in scope of synergistic suppression of galvanic corrosion on Zn-Fe model couple. 1,2,3-benzotriazole (BTA) inhibitor was chosen as the anodic inhibitor, while cerium (III) nitrate was selected as the cathodic one. BTA has mostly known of its adsorption based corrosion inhibition mechanism especially on copper and copper containing alloys, but has been proved as an effective specie for Zn passivation as well. Cerium cations are known cathodic inhibitors, forming

blocking hydroxide precipitates due to local pH increase at cathodic sites.

Additionally to conventional Electrochemical Impedance Spectroscopy (EIS) method the Scanning Vibrating Electrode Technique (SVET) was used especially for monitoring of galvanic corrosion [1-3]. The data has been systematically analysed in respect of calculated inhibition efficiencies and synergistic parameters. As a new development the recently proposed multi-electrode cell for SVET [1] was modified for standalone Zn and Fe electrodes and separate galvanic combination. The usage of SVET allows to detect separately and non-destructively the local anodic and cathodic activities and can thereby complement significantly the conventional electrochemical techniques, where the evaluation of galvanic systems has been traditionally a more sophisticated task.

It can be seen on Fig. 1 how the measured ionic currents depend on selected inhibi-

tor solutions. With the combination solution, both anodic and cathodic currents are suppressed and almost invisible on the SVET map, while the inhibitors alone ( $\text{Ce}^{3+}$ ) can act even as corrosion promoters. The synergy factor calculated from measured ionic currents in this case was significantly above 1 ( $S = 36.5$ ) demonstrating a high synergy between BTA and  $\text{Ce}^{3+}$  cations for corrosion suppression on Zn+Fe galvanic system. The synergy is based on dedicated cooperation of selected inhibitors. The optimal conditions on Zn for BTA and on Fe for  $\text{Ce}^{3+}$  are created. At the cathodic areas (Fe), due to the local pH increase, the deposition of cerium hydroxide occurs:  $\text{Ce}^{3+} + 3\text{OH}^- \rightarrow \text{Ce}(\text{OH})_3 \downarrow$ . Concurrently in anodic areas, especially at lower pH values the BTA is acting as an adsorption based inhibitor which results with a very high synergistic inhibiting action for Zn+Fe galvanic couple.

The presented approach can be used to design highly effective active corrosion protection systems for multi-material assemblies used in different industries, particularly in the case of galvanised steel.

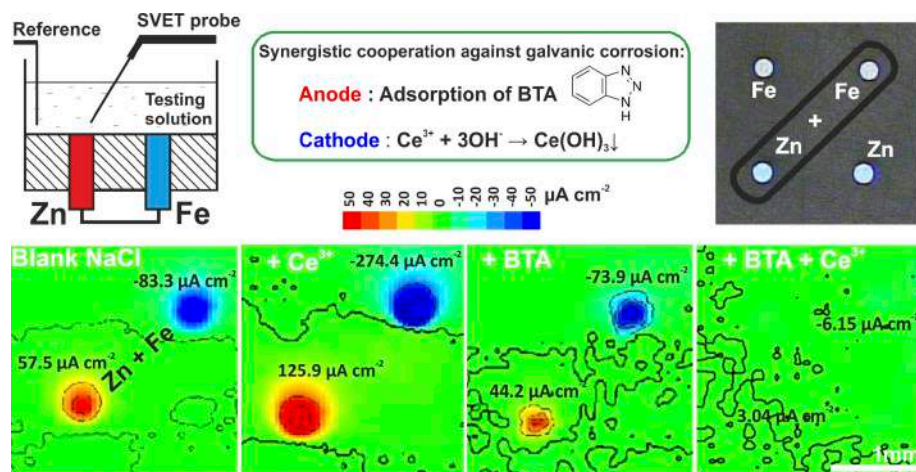


Figure 1. Diagram of SVET micro-electrode cell concept for Zn+Fe galvanic system, microphotograph of the galvanic cell configuration and obtained SVET maps taken after 2h of immersion in different inhibitor solutions with Fe and Zn electrodes electrically coupled in 0.05M NaCl and addition of corrosion inhibitor 0.005M  $\text{Ce}(\text{NO}_3)_3$ , 0.005M BTA and combination of 0.0025M  $\text{Ce}(\text{NO}_3)_3$  + 0.0025M BTA.

<sup>1</sup> Department of Materials and Ceramic Engineering, CICECO, University of Aveiro, 3810-193 Aveiro, Portugal.

#### References

- [1] Kallip S, Bastos AC, Yasakau KA, Zheludkevich ML, Ferreira MGS, *Electrochemistry Communications*, 2012, 20, 101-104.
- [2] Kallip S, Bastos AC, Zheludkevich ML, Ferreira MGS, *Corrosion Science*, 2010, 52, 3146-3149.
- [3] Serdechnova M, Kallip S, Ferreira MGS, Zheludkevich ML, *Electrochemistry Communications*, 2014, 41, 51-54.

#### Acknowledgments

This work has been funded by FCT Portugal (PTDC/CTM/108446/2008, IF/00856/2013 and SFRH/BPD/64580/2009) and by EU FP7 projects "MUST" (NMP3-LA-2008-214261) and "PROAIR" (PIAPP-GA-2013-612415).



# Energy, Lighting and Photonics

## (3 + 3) – DIMENSIONAL ‘HYPERCUBIC’ OXIDE-IONIC CONDUCTOR: TYPE II $\text{Bi}_2\text{O}_3 - \text{Nb}_2\text{O}_5$

Ling CD,<sup>1</sup> Schmid S,<sup>1</sup> Blanchard PER,<sup>1</sup> Petříček V,<sup>2</sup> McIntyre GJ,<sup>3</sup> Sharma N,<sup>1</sup> Maljuk A,<sup>4</sup> Yaremchenko AA,<sup>5</sup> Kharton VV,<sup>5</sup> Gutmann M,<sup>6</sup> Withers RL<sup>7</sup>

The high-temperature cubic form of bismuth oxide,  $\delta\text{-Bi}_2\text{O}_3$ , is the best intermediate-temperature oxide-ionic conductor known. The well-established way of stabilizing  $\delta\text{-Bi}_2\text{O}_3$  to room temperature, while preserving a large part of its conductivity, is by doping with higher valent transition metals to create wide solid-so-

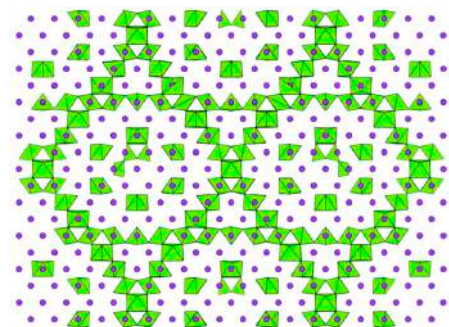


Figure 1. Refined structure of Type II  $(\text{Bi}_2\text{O}_3)_{0.795}(\text{Nb}_2\text{O}_5)_{0.205}$ ; view along the  $\langle 110000 \rangle$  direction, drawn over  $8 \times 8 \times 8$  fluorite-type subcells. Bi atoms are purple, and Nb atoms and polyhedra are green.

lutions fields with exceedingly rare and complex (3+3)-dimensional incommensurately modulated ‘hypercubic’ Type

II structures. These materials remain poorly understood because no such structure has ever been quantitatively solved and refined, due to the complexity of the problem and lack of adequate experimental data. In the present work, this was addressed by growing a large (centimeter scale) crystal using a novel refluxing floating-zone method, collecting high-quality single-crystal neutron diffraction data, and treating its structure together with X-ray diffraction data within the superspace symmetry formalism<sup>[1]</sup>. The Type II structure can be understood as an ‘inflated’ pyrochlore, in which the corner-connected  $\text{NbO}_6$  octahedral chains move smoothly apart to accommodate the solid solution. While some oxide vacancies are ordered in these chains, others are distributed throughout a continuous three-dimensional network of wide  $\delta\text{-Bi}_2\text{O}_3$ -like channels (Figure 1), explaining the superior oxide-ionic conductivity of incommensurate Type II phase compared to commensurately modulated Type III phases in the same pseudobinary system (Figure 2).

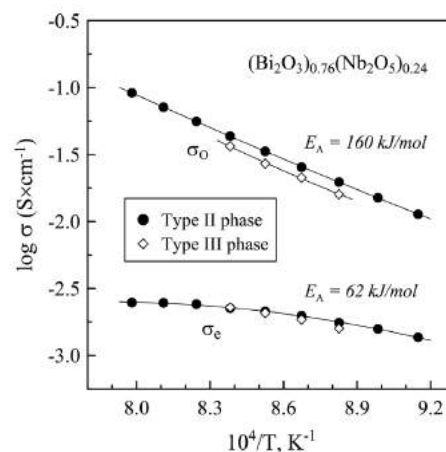


Figure 2. Partial oxide-ionic  $[\sigma_0]$  and electronic  $[\sigma_e]$  conductivities for the ceramic samples of Type II and Type III  $(\text{Bi}_2\text{O}_3)_{0.76}(\text{Nb}_2\text{O}_5)_{0.24}$ .

<sup>1</sup> School of Chemistry, The University of Sydney, Australia

<sup>2</sup> Institute of Physics, ASCR, v.v.i., The Academy of Sciences of the Czech Republic

<sup>3</sup> Institut Laue-Langevin, Grenoble, France

<sup>4</sup> Leibniz Institute for Solid State and Materials Research Dresden, Germany

<sup>5</sup> Department of Materials and Ceramic Engineering, CICECO, University of Aveiro, 3810-193 Aveiro, Portugal

<sup>6</sup> ISIS, Science and Technology Facilities Council, Rutherford Appleton Laboratory, UK

<sup>7</sup> Research School of Chemistry, Australian National University, Canberra, Australia

### Reference

[1] Ling CD, Schmid S, Blanchard PER, Petříček V, McIntyre GJ, Sharma N, Maljuk A, Yaremchenko AA, Kharton VV, Gutmann M, Withers RL, *Journal of the American Chemical Society*, 2013, 135, 6477-6484.

## MATERIALS AND CONCEPTS FOR CARBON LEAN STEELMAKING BY PYROELECTROLYSIS

Kovalevsky AV<sup>1</sup>, Ferreira NM<sup>1,2</sup>, Yaremchenko AA<sup>1</sup>, Costa FM<sup>2</sup>, Frade JR<sup>1</sup>

Pyroelectrolysis emerged as a key factor for feasible production of aluminium and is also providing breakthrough approaches for production of strategic metals from molten halite/oxide systems. Expected gains in energy efficiency by thermal activation at very high temperatures also raise prospects for challenging low- $\text{CO}_2$  steelmaking, to overcome the environmental impact of classical extractive metallurgy. However, this requires challenging new concepts to meet harsh conditions imposed by very high tem-

peratures and very corrosive nature of molten media, such as consumable anode materials, freeze lining cathodes and autothermal self regulation.

One proposed the concept of consumable anodes relying on slowly consumable magnetite-based spinels, to tackle the materials challenges of electrical conductivity and other required properties, without undue contamination of the molten electrolyte and produced steels, and acting as a supplementary raw material. However, the redox stability of

magnetite is insufficient for prospective operating conditions (temperature, oxidizing atmospheres and anodic polarization). Thus, one demonstrated strategies for higher refractoriness and enhanced redox stability over wider ranges, by co-doping of magnetite with redox stable Mg and Al oxides in the concentration range where aluminium provides improvement of refractoriness without significant deterioration of electric properties, whilst magnesium increases tolerance against oxidative decomposition.<sup>[1]</sup> Guidelines for improved compromise between stability and electrical properties were also drawn for  $(\text{Fe,Mg})_3\text{O}_4$  spinels, with additions of transition metal oxides. The oxidation state of substituting cation, and preference for tetrahedral or octahedral

coordination determine the fractions of  $\text{Fe}^{2+}$  in spinel lattice, with impact on tolerance to oxidative decomposition, and effects on  $\text{Fe}^{2+}:\text{Fe}^{3+}$  ratio in octahedral sites, which determines electronic transport. Trade-off relations (Fig. 1) show good prospects for application of  $(\text{Fe,Al,Mg})_3\text{O}_4$  and  $(\text{Fe,Ti,Mg})_3\text{O}_4$  spinels as slowly consumable ceramic anodes.<sup>[2]</sup> Preliminary electrochemical studies of such electrodes in contact with mol-

ten magnesium aluminosilicate glass showed that the level of anodic polarization must also be controlled to ensure redox and chemical stability in molten electrolyte.

One also demonstrated an alternative concept of pyroelectrolysis based on yttria-stabilized zirconia cells (Fig. 1), and used this configuration to study mechanisms and possible limitations of iron extraction by pyroelectrolysis. Electrochemical

measurements and post-mortem SEM/EDS analyses indicated that high current yields are possible in electron-blocking mode using the solid electrolyte membrane. Faradaic efficiency was assessed by integrating the time dependence of electrolysis current; this revealed limitations imposed by parasitic electrochemical processes, mainly on lowering the Fe concentration in the molten electrolyte. These results suggest that the concept of solid electrolyte membrane for separation of cathodic and anodic compartments may become essential, if one seeks pyroelectrolysis with high current yields. They also show that the concentration of iron oxide in the molten electrolyte may be optimized.

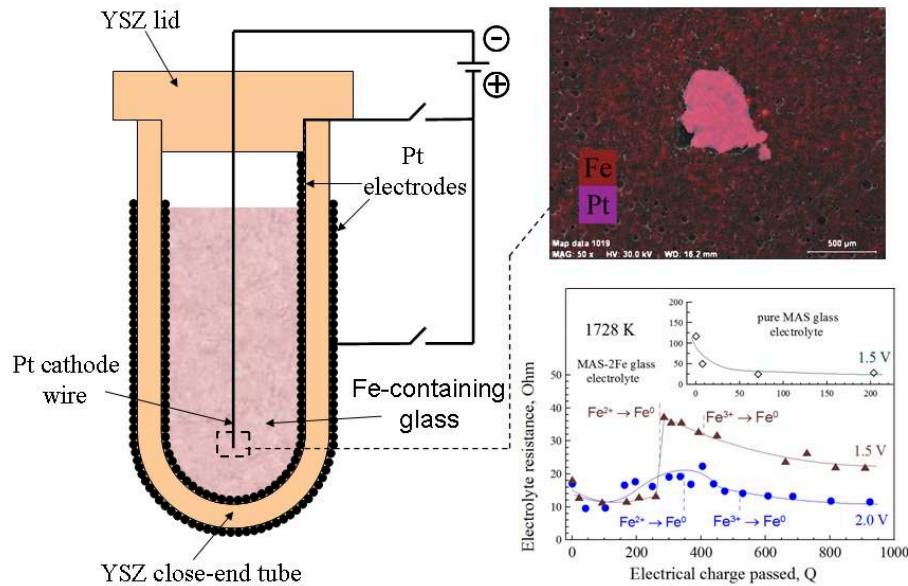


Figure 1. (under right) Total electrical conductivity in air for  $\text{Fe}_{2-x}\text{Me}_{x-1}\text{Mg}_{3-x}\text{O}_4$  spinel-type materials; (left and upper right) Electrochemical YSZ cell for assessing the mechanism of pyroelectrolysis process and representative results.

<sup>1</sup> Department of Materials and Ceramic Engineering, CICECO, University of Aveiro, 3810-193 Aveiro, Portugal

<sup>2</sup> i3N, Department of Physics, University of Aveiro, 3810-193 Aveiro, Portugal

#### References

- [1] Kovalevsky AV, Yaremchenko AA, Naumovich EN, Ferreira NM, Mikhalev SM, Costa FM, Frade JR, *Journal of the European Ceramic Society*, 2013, 33, 2751-2760.  
 [2] Ferreira NM, Kovalevsky AV, Naumovich EN, Yaremchenko AA, Zakharchuk KV, Costa FM, Frade JR, *Journal of the European Ceramic Society*, 2014, 34, 2339-2350.

#### Acknowledgments

This work was supported by FCT, Portugal and by the European Union Research Fund for Coal and Steel [RFCS].

## $\text{SrTiO}_3$ -BASED THERMOELECTRICS FOR EFFICIENT HIGH TEMPERATURE WASTE HEAT CONVERSION

Kovalevsky AV<sup>1</sup>, Yaremchenko AA<sup>1</sup>, Populoh S<sup>2</sup>, Weidenkaff A<sup>2</sup>, Frade JR<sup>1</sup>

Thermoelectric materials are very flexible for thermoelectric cooling and raise good prospects for natural or waste heat recovery. Thermoelectric conversion requires both p-type and n-type materials. Their dimensionless figure of merit ( $ZT = \sigma \alpha^2 T / \kappa$ ), which increases with electrical conductivity ( $\sigma$ ) and Seebeck coefficient ( $\alpha$ ), and decreases with thermal conductivity ( $\kappa$ ), determines the gap between the actual efficiency of thermoelectric generation and Carnot efficiency  $\eta_c = 1 - T_c / T_h$ . This implies that efficiency increases rapidly with temperature of heat source  $T_h$  for its effects on Carnot

efficiency and figure of merit, provided that this is not limited by thermal and/or redox stability. Thus, oxides are best suited for high temperature waste heat recovery due to stability limitations of Te- or Se-based thermoelectric materials, skutterudites and related intermetallic compounds.

Donor-substituted strontium titanate is, probably, the most promising n-type oxide thermoelectrics. One engineered its thermoelectric properties by defect chemistry and structural changes, accomplished by A-site substitution with rare-earth elements or B-site substitution with Nb, and

high temperature firing under reducing conditions. One demonstrated enhanced thermoelectric performance of  $\text{SrTiO}_3$  by A-site substitution with praseodymium<sup>[1]</sup>, attaining maximum figure of merit for  $\text{Sr}_{0.90}\text{Pr}_{0.10}\text{TiO}_3$  ( $ZT \sim 0.23$  at 670 K and  $\sim 0.34$  at 1170 K). One also addressed, for the first time, A-site cation deficiency as a structural engineering approach yielding higher thermoelectric performance<sup>[2]</sup>. Formation of oxygen vacancies was found to suppress lattice thermal conductivity at low and intermediate temperatures. For both Pr- and Nb- substituted titanates, nominal A-site deficiency results in significant enhancement of thermoelectric performance (Fig. 1).

The positive impact of oxygen deficiency on thermoelectric properties inspired further studies of other rare-earth substituted strontium titanate ceramics, pre-

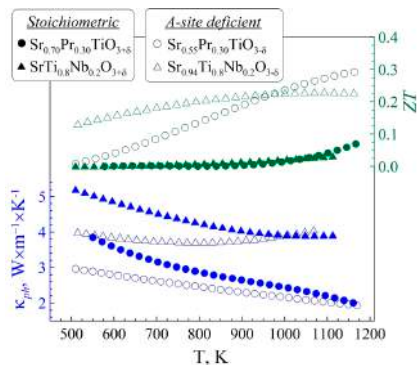


**Figure 1.** Temperature dependence of the dimensionless figure of merit and lattice counterpart of the thermal conductivity for A-site stoichiometric and deficient (Sr,Pr)TiO<sub>3±δ</sub> and Sr<sub>1-x</sub>Pr<sub>x</sub>TiO<sub>3±δ</sub>

pared in strongly reducing conditions. A marked improvement in performance was observed for Sr<sub>0.9</sub>R<sub>0.1</sub>TiO<sub>3±δ</sub> (R= Nd, Sm, Dy) by sintering in 10%H<sub>2</sub>-90%N<sub>2</sub> at 1773 K for 10 h, reaching ZT values as

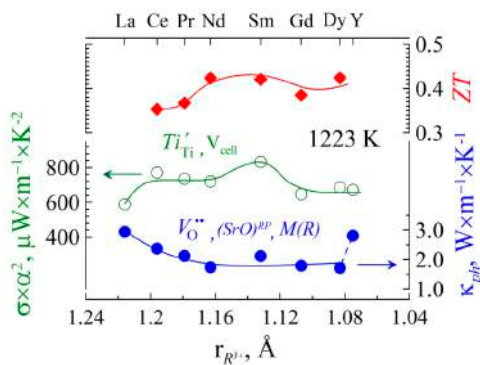


**Figure 2.** Thermoelectric properties of Sr<sub>0.9</sub>R<sub>0.1</sub>TiO<sub>3±δ</sub> titanates, prepared in strongly reducing conditions.

high as 0.42 at 1190-1225 K (Fig. 2). This performance exceeds previous limits for SrTiO<sub>3</sub>-based bulk thermoelectrics and is attributed to enhanced phonon scattering in oxygen-deficient perovskite layers.

## Pr-SUBSTITUTED SrTiO<sub>3</sub> AS PROSPECTIVE SOLID OXIDE FUEL CELL ANODE MATERIAL

Yaremchenko AA<sup>1</sup>, Patrício SG<sup>1</sup>, Frade JR<sup>1</sup>

Donor-doped strontium titanate is known to be stable in both oxidizing and reducing conditions and to exhibit substantial electronic conductivity (if reduced at high temperatures), and, therefore, is considered as a prospective sulfur-tolerant component for solid oxide fuel cell anodes. The present work was focused on appraisal of praseodymium-substituted SrTiO<sub>3</sub> for possible application in SOFC anodes, with emphasis on phase relationships and structural stability under different conditions, electrical transport properties, thermochemical expansion and its compatibility with solid electrolytes, and dimensional stability in redox cycles.

Sr<sub>1-x</sub>Pr<sub>x</sub>TiO<sub>3±δ</sub> and Sr<sub>1-1.5x</sub>Pr<sub>x</sub>TiO<sub>3±δ</sub> (x = 0.02-0.30) ceramic samples were prepared by conventional solid-state reaction route and sintered under either oxidizing (air, 1600-1750°C) or reducing (10%H<sub>2</sub>-N<sub>2</sub>, 1400-1500°C) conditions. XRD studies confirmed the formation of single-phase ceramic materials with perovskite-like structure in both oxidizing and reducing

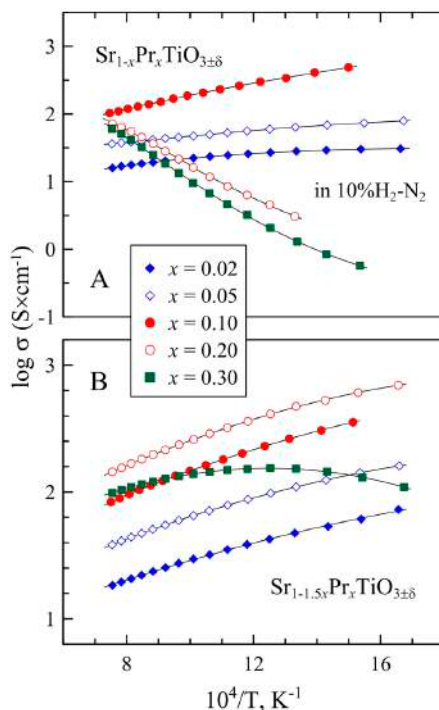


**Figure 1.** Temperature dependence of electrical conductivity of reduced Sr<sub>1-x</sub>Pr<sub>x</sub>TiO<sub>3±δ</sub> (A) and Sr<sub>1-1.5x</sub>Pr<sub>x</sub>TiO<sub>3±δ</sub> (B) ceramics in 10%H<sub>2</sub>-N<sub>2</sub> atmosphere ( $p_{\text{O}_2}$  ff 10<sup>-15</sup> atm at 900°C).

These results also show that highly-reducing conditions are needed for micro/nanostructural engineering to suppress thermal conductivity, without undue effects on electrical conductivity and Seebeck coefficient, and while retaining outstanding thermal and redox stability.

<sup>1</sup> Department of Materials and Ceramic Engineering, CICECO, University of Aveiro, 3810-193 Aveiro, Portugal

<sup>2</sup> Empa, Solid State Chemistry and Catalysis, Ueberlandstr. 129, CH-8600 Duebendorf, Switzerland

### References

- [1] Kovalevsky AV, Yaremchenko AA, Populoh S, Weidenkaff A, Frade JR, *Journal of Applied Physics*, 2013, 113, 053704.
- [2] Kovalevsky AV, Yaremchenko AA, Populoh S, Weidenkaff A, Frade JR, *The Journal of Physical Chemistry C*, 2014, 118, 4596-4606.

### Acknowledgments

This work was supported by FCT, Portugal.

atmospheres, although microstructural studies indicated a minor precipitation of TiO<sub>2</sub> in reduced Sr-deficient ceramics with high Pr content. XPS analysis in combination with XRD demonstrated that praseodymium cations substitute into strontium sublattice in mixed 4+/3+ oxidation state (~1:1 ratio) and are essentially insoluble in titanium sublattice under applied conditions. Taking into account the lattice electroneutrality condition, all oxidized materials exhibit oxygen excess correlated with praseodymium content and accommodated, most likely, in a form of extended defects (such as rock-salt layers characteristic for Ruddlesden-Popper structures of Sr<sub>n+1</sub>Ti<sub>n</sub>O<sub>3n+1</sub>). Thermogravimetric analysis showed that under reducing conditions Sr<sub>1-x</sub>Pr<sub>x</sub>TiO<sub>3±δ</sub> solid solutions retain overall oxygen overstoichiometry, while Sr<sub>1-1.5x</sub>Pr<sub>x</sub>TiO<sub>3±δ</sub> are characterized with minor oxygen deficiency. Reduction at elevated temperatures results in 2-3 orders of magnitude increase of n-type electronic conductivity with respect to oxidized materials. The electrical conductivity of Sr<sub>0.90</sub>Pr<sub>0.10</sub>TiO<sub>3±δ</sub> and Sr<sub>1-1.5x</sub>Pr<sub>x</sub>TiO<sub>3±δ</sub> (x = 0.10-0.20) at 600-800°C under reducing conditions reaches as high as 130-340 S/cm (Fig.1). TGA and electrical studies (Fig.2) demonstrated however very slow reduction kinetics at tempera-

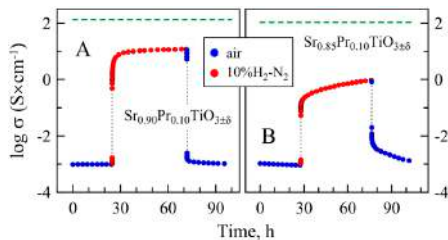


**Figure 2.** Variations of electrical conductivity of porous oxidized  $\text{Sr}_{0.90}\text{Pr}_{0.10}\text{TiO}_{3-d}$  [A] and  $\text{Sr}_{0.85}\text{Pr}_{0.10}\text{TiO}_{3-d}$  [B] ceramic samples in one redox cycle at  $900^\circ\text{C}$ . Thick green line indicates the conductivity value for dense reduced ceramics in  $10\%\text{H}_2\text{-N}_2$  atmosphere at  $900^\circ\text{C}$ .

tures below  $1273\text{ K}$  associated mainly with nearly frozen equilibrium in cation sublattice and low oxygen vacancy concentration in oxidized materials. All oxidized and reduced materials exhibit moderate almost  $p(\text{O}_2)$ -independent thermal expansion coefficients  $((11.3\text{-}12.6)\times 10^{-6}\text{ K}^{-1}$  at  $25\text{-}1100^\circ\text{C}$ ), which ensure the compatibility with common solid electrolytes, and favorably small chemical expansion on reducing oxygen partial pressure.

<sup>1</sup> Department of Materials and Ceramic Engineering, CICECO, University of Aveiro, 3810-193 Aveiro, Portugal

#### Reference

[1] Yaremchenko AA, Patricio SG, Frade JR, *Journal of Power Sources*, 2014, 245, 557-569.

#### Acknowledgments

This work was supported by the FCT, Portugal (projects BPD/75943/2011, PTDC/CTM-CER/118933/2010 and PEst-C/CTM/LA0011/2011, and Ciência-2008 program).

## OXYGEN-ION TRANSPORT IN $\text{Ba}_{0.5}\text{Sr}_{0.5}\text{Co}_{0.8}\text{Fe}_{0.2}\text{O}_{3-d}$ : DEVELOPMENTS OF ASYMMETRIC/MULTILAYER AND HOLLOW-FIBER CERAMIC MEMBRANES FOR OXYGEN SEPARATION

Kovalevsky AV<sup>1</sup>, Yaremchenko AA<sup>1</sup>, Kolotygin VA<sup>1</sup>, Buysse C<sup>2</sup>, Middelkoop V<sup>2</sup>, Snijkers F<sup>2</sup>, Buekenhoudt A<sup>2</sup>, Frade JR<sup>1</sup>

Dense ceramic membranes with mixed ionic and electronic conductivity provide a viable alternative to cryogenic distillation for oxygen separation, and are expected to offer significant economic benefits if integrated in industrial energy

conversion processes such as coal gasification and oxyfuel combustion. Oxygen transport across ceramic membrane occurs via diffusion of oxygen ions in the crystal lattice of oxide material, thus providing absolute theoretical selectivity of oxygen separation. This work addresses several factors determining the performance of ceramic membranes made of  $\text{Ba}_{0.5}\text{Sr}_{0.5}\text{Co}_{0.8}\text{Fe}_{0.2}\text{O}_{3-d}$  (BSCF, a perovskite-like oxide with highest reported oxygen permeability) and relevant for the developments of membranes with multi-layer supported architecture and capillary (or hollow-fiber) geometry.

The oxygen transport studies of dense BSCF ceramic membranes demonstrated that the permeation rate is predominantly controlled by surface exchange kinetics when the membrane thickness is smaller than  $1.00\text{ mm}$ . In order to improve oxygen exchange, an asymmetric membrane concept including two porous layers (with one thick porous layers acting as a support) and one thin dense central layer was implemented (Fig.1A). The amount of graphite as a pore-forming additive, powder compaction and sintering conditions were optimized to produce three-layer membranes having appropriate mechanical strength and microstructure. Comparison of the data on oxygen permeation through three-layer and dense

$1.00\text{ mm}$  thick symmetric membranes indicated that a moderate improvement of the overall performance was achieved due to asymmetric architecture. The oxygen fluxes through the membrane with  $170\text{ }\mu\text{m}$  dense layer and porous layers with thicknesses of  $1.05\text{ mm}$  and  $100\text{ }\mu\text{m}$  at  $900^\circ\text{C}$  were found to be  $\sim 1.5\text{-}1.8$  times higher compared to  $1.00\text{ mm}$  thick symmetric membrane. Analysis of oxygen permeability data suggests however that three-layer architecture introduces additional permeation-limiting factor – gas diffusion in porous layers, thus indicating a need for further microstructural optimization.

Another issue relates to the effect of sulphur contamination on the performance of BSCF membranes. Capillary and hollow-fiber ceramic membranes are commonly prepared by phase-inversion process using polysulphone or polyether-sulphone as a binder. The decomposi-

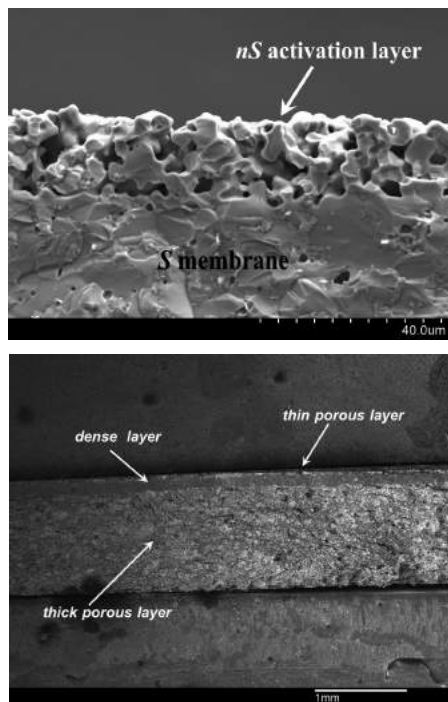


**Figure 1.** SEM micrographs of fractured cross-section of [A] asymmetric three-layer BSCF membrane [thick porous layer:  $1.05\text{ mm}$ , dense layer:  $170\text{ }\mu\text{m}$ , thin porous layer:  $60\text{ }\mu\text{m}$ ], and [B] sulphur-contaminated BSCF membrane with sulphur-free BSCF porous surface layer.

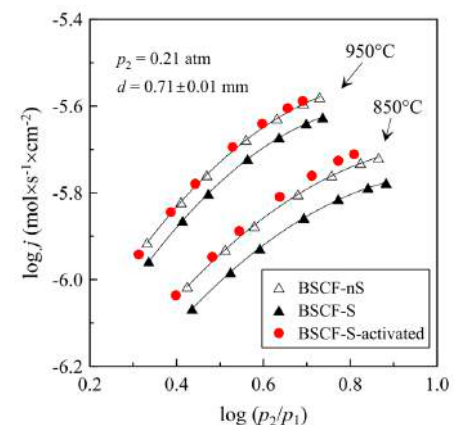


**Figure 2.** Comparison of the oxygen permeation fluxes ( $j$ ) through sulphur-free (nS) and sulphur-contaminated non-modified (S) and surface-activated (S-activated) BSCF membranes at  $950$  and  $850^\circ\text{C}$ .  $p_2$  and  $p_1$  are feed-side and permeate-side oxygen partial pressures, respectively, and  $d$  is the membrane thickness.

tion of the sulphur-containing binder during the calcination/sintering leads to the formation of sulphates, which negatively affect the oxygen permeation through the membrane. In present work, the comparative analysis of the oxygen transport through sulphur-free and sulphur-contaminated BSCF membranes indicated that sulphates decrease the permeation rate mostly due to the partial blocking of the surface oxygen exchange, whilst the bulk ambipolar conductivity remains essentially unchanged. SEM/EDS studies revealed segregation of  $\text{BaSO}_4$  at the grain boundaries, which

are presumably responsible for the fast surface oxygen exchange in phase-pure BSCF. The negative impact of sulphur contamination on oxygen permeation was more pronounced at temperatures below  $850^\circ\text{C}$ . It has been demonstrated that by surface activation (i.e. application of thin porous layer of S-free BSCF at the membrane surface (Fig.1B)) the oxygen flux through sulphur-contaminated BSCF membranes can be increased to the level characteristic for sulphur-free membranes (Fig.2).

## CERAMIC TILES WITH CONTROLLED POROSITY AND LOW THERMAL CONDUCTIVITY BY USING PORE-FORMING AGENTS

Novais RM<sup>1</sup>, Seabra MP<sup>1</sup>, Labrincha JA<sup>1</sup>

This work reports the influence of two pore forming agents (polypropylene – PP, and polymethyl methacrylate – PMMA), their incorporation content and particle size distribution on the bi-layered ceramics porosity, mechanical resistance and thermal conductivity. The porosity level was independent of porogen particle size distribution; nevertheless, pore area and number were heavily dependent on the porogen's particle size distribution. Smaller pore formers prompted a high number of pores, while larger particles had the opposite effect. The upper-layer (dense layer) of the bi-layered ceramic showed typical microstructure of a commercial product, thus the release of gases from the bottom layer did not induce additional porosity.

The incorporation of porosity into the bi-layered ceramics promotes thermal conductivity attenuation and simultaneously decreases the ceramics mechanical resistance, however maintaining suitable mechanical strength. The thermal conductivity attenuation is adjustable as a function of volume and size of the generated pores. Attenuation up to 79% was achieved in comparison with standard porcelain stoneware compositions.

These results demonstrate that bi-layered ceramics can be prepared with variable thermal conductivity, tailored for specific applications. The prepared tiles limit the energy loss, in comparison with conventional stoneware tiles, thus increasing the thermal comfort inside buildings, and

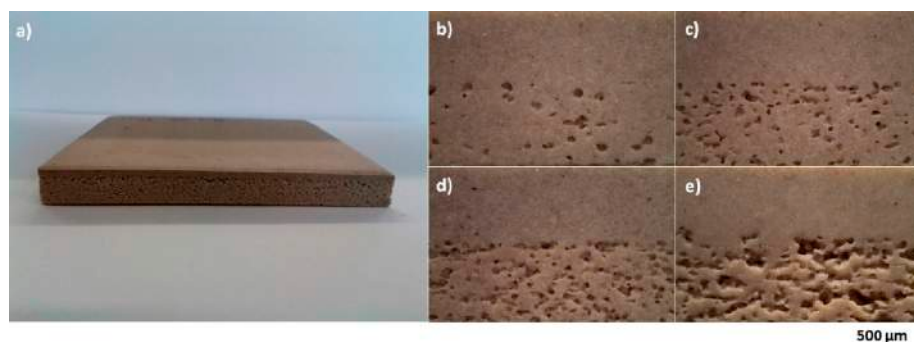


Figure 1. a) Image of a bi-layered ceramic tile (10x10 cm) and optical microscopy characterization of the sintered discs containing distinct PMMA content in the bottom part: b) 2.5 wt%, c) 10 wt%, d) 15 wt% and e) 20 wt%.

<sup>1</sup> Department of Materials and Ceramic Engineering, CICECO, University of Aveiro, 3810-193 Aveiro, Portugal

<sup>2</sup> Flemish Institute for Technological Research, VITO NV, Boeretang 200, B-2400 Mol, Belgium

### References

[1] Kovalevsky AV, Yaremchenko AA, Kolotygin VA, Shaula AL, Kharton VV, Snijders FMM, Buekenhoudt A, Frade JR, Naumovich EN, *Journal of Membrane Science*, 2011, 380, 68-80.

[2] Yaremchenko AA, Buysse C, Middelkoop V, Snijders F, Buekenhoudt A, Frade JR, Kovalevsky AV, *Journal of Membrane Science*, 2013, 428, 123-130.

### Acknowledgments

This work was supported by the FCT, Portugal (projects PTDC/CTM/64357/2006 and PEst-C/CTM/LA0011/2011, and Ciência-2008 program), Belgian Federal Science Policy foundation (FOD Science policy), and the German Helmholtz Alliance project "MEM-BRAIN".

energy savings. The nature of the pore forming agent did not affect the bi-layered ceramics properties, and both PMMA and PP generated, after burn out, high open porosity levels. Even if PMMA is most frequently used as a pore forming agent, our work demonstrated that PP presents similar behavior, and thus great potential as a pore forming agent. The large scale

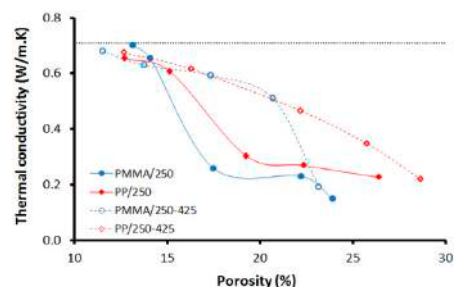


Figure 2. Thermal conductivity of the porous ceramic, prepared with PMMA and PP, as function of porosity.

production and availability of PP reduce its production costs, which represent an important asset in comparison with other pore forming agents.

<sup>1</sup> Department of Materials and Ceramic Engineering, CICECO, University of Aveiro, Campus Universitário de Santiago, 3810-193 Aveiro, Portugal

### Reference

[1] Novais RM, Seabra MP, Labrincha JA, *Ceramics International*, 2014, 40, 8, A, 11637–11648.

### Acknowledgments

We thank Portuguese Innovation Agency (ThermoCer, project n° 23143) and FCT (PEst C/CTM/LA0011/2013).

# MODULATING THE PHOTOLUMINESCENCE OF BRIDGED SILSESQUOXANES FOR LUMINESCENT SOLAR CONCENTRATORS

Correia SFH<sup>1,2</sup>, André PS<sup>3</sup>, Ferreira RAS<sup>1</sup>, Carlos LD<sup>1</sup>

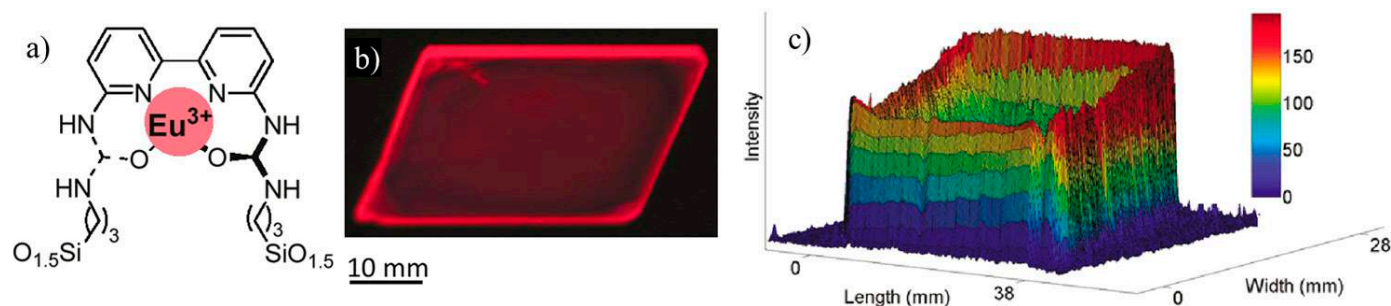


Figure 1. a) Schematic representation of the possible interactions between the Eu<sup>3+</sup> ion (full circle) and one di-ureido-2,20-bipyridine ligand. b) Photograph and c) intensity map of the red pixel of the Eu<sup>3+</sup>-based film excited at 365 nm. The top edge of the photograph corresponds to the more intense profile in the intensity map.

In the framework of a collaboration with Institut Charles Gerhardt, Montpellier, France, new urea-bipyridine derived bridged organosilanes have been synthesized in the presence of Eu<sup>3+</sup> [1,2] and Tb<sup>3+</sup> [2] salts led to luminescent thin films (thickness *ca.* 50 nm). The Eu<sup>3+</sup>-derived films (Figure 1) exhibit one of the highest emission quantum yields reported so far for films of Eu<sup>3+</sup>-containing hybrids (0.34±0.03) and an interesting potential as new luminescent solar concentrators (LSCs) with an optical conversion efficiency of ~4%. The ratio between the light guided to the film edges and the one emitted by the surface of the film was quantified through the mapping of

the intensity of the red pixels (in the RGB color model) from a film image. This quantification enabled a more accurate estimation of the transport losses due to the scattering of the emitted light in the film (0.40), thereby correcting the initial optical conversion efficiency to a value of 1.7% [1]. This is a very rare example of the use of Ln<sup>3+</sup>-containing hybrid thin films for LSCs. Moreover, through the optimization of the optical conversion efficiency by increasing the Eu<sup>3+</sup> concentration, film thickness, and geometry, opens the possibility of increasing the photocurrent generated by solar cells coupled to the LSC edges, relative to the same cells facing the sun.

<sup>1</sup> Department of Physics, CICECO, University of Aveiro, 3810-193 Aveiro, Portugal

<sup>2</sup> Instituto de Telecomunicações, University of Aveiro, 3810-193, Aveiro, Portugal

<sup>3</sup> Department of Electric and Computer Engineering and Instituto de Telecomunicações Instituto Superior Técnico, Universidade de Lisboa, Lisbon, Portugal

## References

[1] Graffion J, Cattoën X, Chi-Man MW, Fernandes VR, André PS, Ferreira RAS, Carlos LD, *Chemistry of Materials*, 2011, 23, 4773.

[2] Graffion J, Cojocariu AM, Cattoën X, Ferreira RAS, Fernandes VR, André PS, Carlos LD, Chi-Man MW, Bartlett JR, *Journal of Materials Chemistry*, 2012, 22, 13279.

## Acknowledgments

Funding was provided by Fundação para a Ciência e a Tecnologia (FCT), FEDER, COMPETE, under contracts PEst-C/CTM/LA0013/2011 and PTDC/CTM/101324/2008 and SFRH/BD/91263/2012 (SFRH).

# PHOTONIC-ON-A-CHIP: A THERMAL ACTUATED MACH-ZEHNDER INTERFEROMETER AND A MOLECULAR THERMOMETER BASED ON A SINGLE DI-UREASIL ORGANIC-INORGANIC HYBRID

Ferreira RAS<sup>1</sup>, Brites CDS<sup>1</sup>, Vicente CMS<sup>1,2</sup>, Lima PP<sup>1</sup>, Carlos LD<sup>1</sup>, André PS<sup>3</sup>

In the framework of collaboration with Instituto de Telecomunicações and the VTT Technical Research Centre of Finland an integrated photonic-on-a-chip device based on a single organic-inorganic di-ureasil hybrid was fabricated for opti-

cal waveguide and temperature sensing. The device is composed by a thermal actuated Mach-Zehnder (MZ) interferometer patterned on the surface of the di-ureasil films operating with a switching power of 0.011 W and a maximum temperature dif-

ference between branches of 0.89 °C. The MZ interferometer is covered by a Eu<sup>3+</sup>/Tb<sup>3+</sup> co-doped di-ureasil luminescent molecular thermometer with a temperature uncertainty of 0.1 °C and a spatial resolution of 13 μm. This is an uncommon example in which the same material (an organic-inorganic hybrid) that is used to fabricate a particular device (a thermal-actuated MZ interferometer) is also used to measure one of the device intrinsic properties (the operating temperature). Moreover, the photonic-on-a-chip example discussed here can be applied to sense temperature gradients with a resolution of 10<sup>-3</sup> °C · μm<sup>-1</sup> in chip-scale heat engines

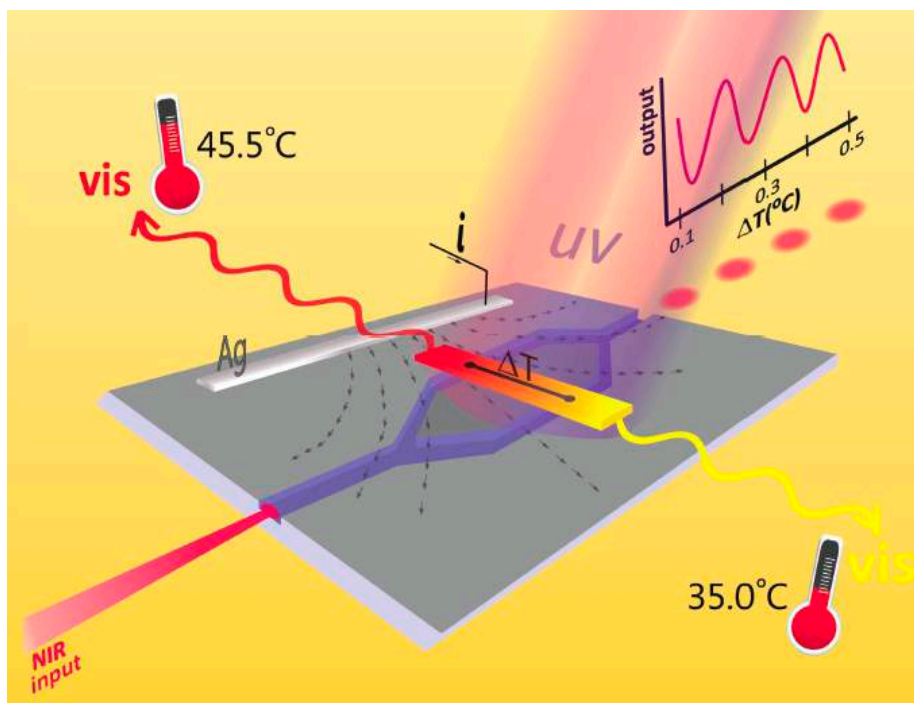


Figure 1. Schematic representation of the MZ interferometer geometry showing the metallic contacts, (light grey), MZ interferometer (blue) and di-ureasil layer thermometer (red). Image selected by the publisher as back-cover of the reference paper.

or refrigerators, magnetic nanocontacts and energy-harvesting machines, for instance.

<sup>1</sup> Department of Physics, CICECO, University of Aveiro, 3810-193 Aveiro, Portugal

<sup>2</sup> Instituto de Telecomunicações, University of Aveiro, 3810-193, Aveiro, Portugal

<sup>3</sup> Department of Electric and Computer Engineering and Instituto de Telecomunicações Instituto Superior Técnico, Universidade de Lisboa, Lisbon, Portugal

#### Reference

[1] Ferreira RAS, Brites CDS, Vicente CMS, Lima PP, Bastos ARN, Marques PG, Hiltunen M, Carlos LD, André PS, *Laser & Photonics Reviews*, 2013, 7, 1035.

#### Acknowledgments

Funding was provided by Fundação para a Ciência e a Tecnologia (FCT), FEDER, COMPETE, under contracts PEst-C/CTM/LA0013/2013, PTDC/CTM/101324/2008, SFRH/BPD/34365/2006 (PPL), SFRH/BPD/87473/2012 (CV) and SFRH/BPD/89003/2012 (CDSB). The Organic Electronics group from Instituto de Telecomunicações-Portugal is gratefully acknowledged to make available a materials inkjet printing.

## NOVEL BIFUNCTIONAL MAGNETIC-NEAR-INFRARED LUMINESCENT NANOCOMPOSITES: NEAR-INFRARED EMISSION FROM Nd AND Yb

Yu SY<sup>1,2</sup>, Fu LS<sup>2</sup>, Zhou YJ<sup>2</sup>, Su<sup>1</sup>

In recent years, research toward near-infrared (NIR) emitting systems based on lanthanide (Ln) complexes, such as neodymium (Nd), ytterbium (Yb), and erbium (Er), has become increasingly prevalent, even though visible fluorophores still dominate the luminescence field. However, for many applications, it is quite troublesome for lanthanide-based NIR materials to separate small particles from liquid. Considerable attention has been drawn to the nanoparticles with magnetic property, as a type of important functional material, because of their great potential applications in magnetic fluids, catalysis, biotechnology/biomedicine, magnetic resonance imaging (MRI), magnetic recording devices, and environmental remediation. Among magnetic particles, magnetite ( $\text{Fe}_3\text{O}_4$ ) has received more attention because of its potential applica-

tions in nanobiotechnology. Therefore, Ln-based NIR materials combined with  $\text{Fe}_3\text{O}_4$  magnetic nanoparticles can be conveniently separated from the aqueous

phase by application of an external magnetic field.

Herein, we report the synthesis of novel magnetic-NIR luminescent bifunctional nanomaterials, in which  $\text{Fe}_3\text{O}_4$  magnetic particles were embedded in the silica nanospheres and Nd-PABI and Yb-PABI (PABI = *N*-(4-benzoic acid-yl)-*N'*-(propyltriethoxysilyl)urea) complexes were covalently bonded to the surface of magnetic silica.<sup>[1]</sup> The synthesis process is shown in Fig. 1.

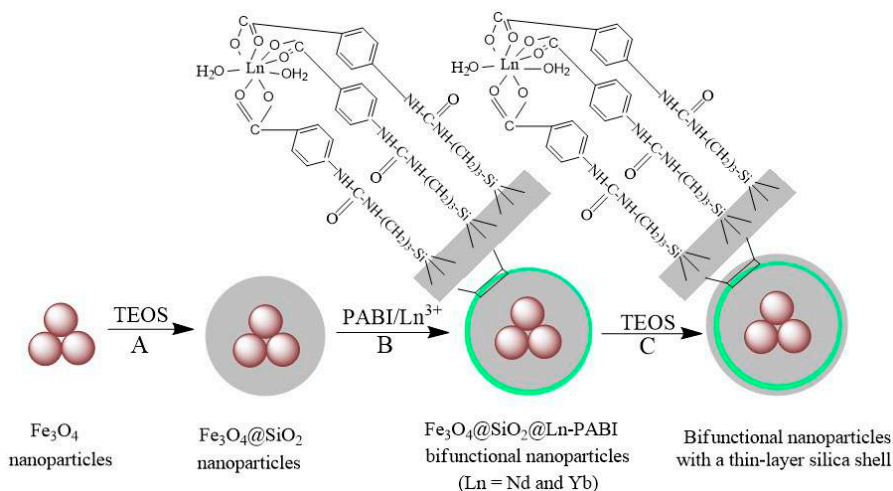


Figure 1. Synthesis of bifunctional magnetic-optical nanoparticles.

The TEM images of bifunctional magnetic-NIR luminescent nanoparticles  $\text{Fe}_3\text{O}_4@\text{SiO}_2@\text{Ln-PABI}$  (Ln = Nd, Yb) show the two kinds of particles with diameter ranged from 150 to 180 nm. The presence of core  $\text{Fe}_3\text{O}_4$  nanoparticles and the core-shell structure are also confirmed, which show obvious differences in terms of contrast between the core and its surroundings.

The magnetic properties of these two nanocomposites were characterized using a VSM with fields of up to 1 T. The saturation magnetizations of the  $\text{Fe}_3\text{O}_4@\text{SiO}_2@\text{Nd-PABI}$  and  $\text{Fe}_3\text{O}_4@\text{SiO}_2@\text{Yb-PABI}$  nanoparticles at room temperature reach the saturation moment of 12.5 and 14.8 emu per gram, respectively.

The more obvious proof for the magnetic properties could be found in the following designed experiments (Fig. 2). When a handheld magnet was placed close to

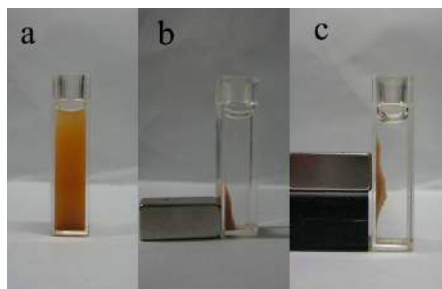


Figure 2. An aqueous suspension of bifunctional magnetic-optical nanoparticles [a], after magnetic capture [b], and movement of the magnet dragging the concentrated nanoparticles [c].

the glass vial, the bifunctional nanoparticles were attracted toward the magnet very quickly. We can easily drag the nanoparticles from the bottom to the middle of glass vial by elevating the magnets. This observation further proves the bifunctional materials will be easy to control.

The emission spectra of  $\text{Fe}_3\text{O}_4@\text{SiO}_2@\text{Ln-PABI}$  nanocomposites were

measured by excitation of the  $\text{Nd}^{3+}$  and  $\text{Yb}^{3+}$  ion at 355 nm. For Nd material, the emission spectrum consists of three bands at 895, 1065, and 1325 nm, attributed to the  ${}^4\text{F}_{3/2} \rightarrow {}^4\text{I}_{9/2}$ ,  ${}^4\text{I}_{11/2}$ , and  ${}^4\text{I}_{13/2}$  transitions, respectively. For Yb material, the typical  ${}^2\text{F}_{5/2} \rightarrow {}^2\text{F}_{7/2}$  transition at 980 nm was detected. These bifunctional nanocomposites exhibit superparamagnetic behaviour, high fluorescence intensity and color purity.

<sup>1</sup> College of Chemistry & Chemical Engineering, Inner Mongolia University, Hohhot 010020, PR China

<sup>2</sup> Department of Physics, CICECO, University of Aveiro, 3810-193, Aveiro, Portugal

#### Reference

[1] Yu SY, Fu LS, Zhou YJ and Su HQ, *Photochemical & Photobiological Sciences*, 2011, 10 (4), 548-553.

#### Acknowledgments

This work was supported by FCT (Portugal) and NSFC (China).



# Catalysis and Separation

# SUPPORTED IONIC LIQUID SILICA NANOPARTICLES CATALYZE THE DEHYDRATION OF FRUCTOSE TO 5-HYDROXYMETHYLFURFURAL

Sidhpuria KB<sup>1</sup>, Daniel-da-Silva AL<sup>1</sup>, Trindade T<sup>1</sup>, Coutinho JAP<sup>1</sup>

Diminishing fossil fuel reserves and growing concerns about global warming have fostered the development of alternative sources of energy and chemicals. Renewable biomass resources are promising alternatives for the sustainable supply of liquid fuels and chemical intermediates. The catalytic conversion of biomass is important to develop alternatives to crude oil derivatives. Among the many biomass-derived chemicals, 5-hydroxymethylfurfural (HMF) is a particularly valuable intermediate for fine chemicals, pharmaceuticals and in bio-fuel and polymer chemistry. Hence, the acid catalyzed dehydration of fructose to HMF has received substantial attention. Homogeneous-acid catalyzed processes achieve only up to 90% fructose conversion with a moderate HMF yield, and have severe drawbacks in terms of equipment corrosion, separation and recycling. While existing heterogeneous acid catalysts may be recycled they have high HMF selectivity but very low fructose conversion, even after a very long reaction time. Consequently, there is the need to develop more efficient catalytic systems for the selective production of HMF from fructose.

We have recently developed supported ionic liquid nanoparticles based on amorphous SiO<sub>2</sub>. Each sample was characterized by a distinct average particle size (300 to 600 nm) that depended on the ammonia concentration used in the sol-gel synthesis. The silica surfaces were chemically modified with an ionic liquid by covalent attachment using a silicon alkoxide linker. The supported ionic liquid nanoparticles quickly (<30 minutes

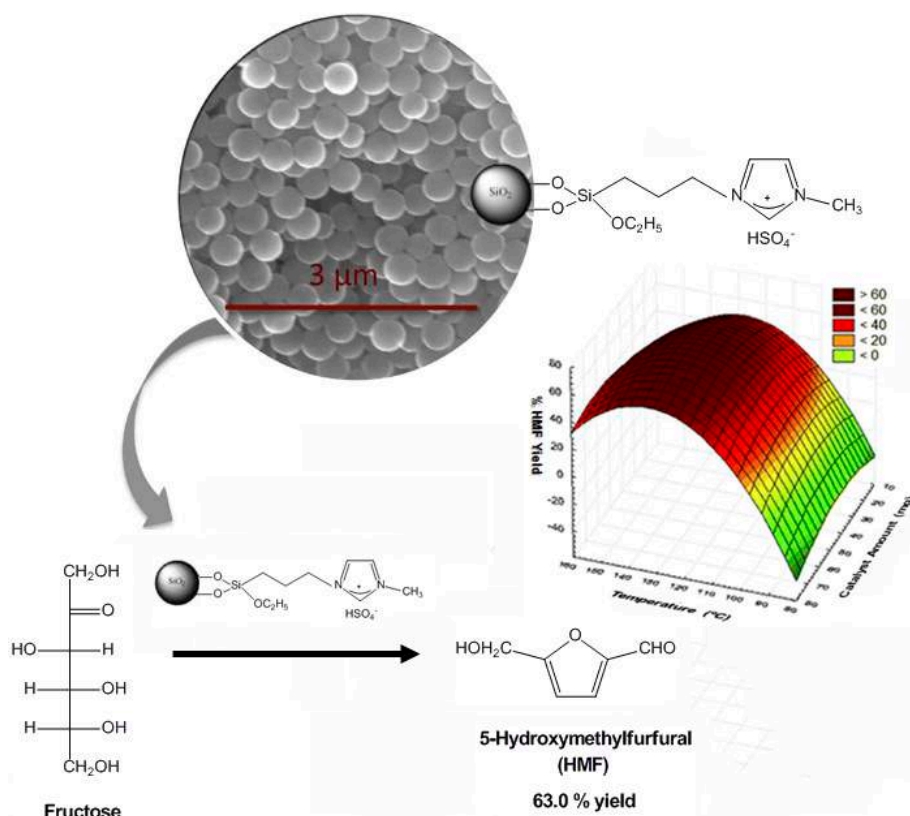


Figure 1. Scheme illustrating the application of SILNPs in the catalysis of the dehydration of fructose to HMF and 3D response surface plot of the % HMF yield against reaction temperature and catalyst amount.

reaction time) and efficiently (99.9% conversion) convert fructose into HMF with yields of 63% under optimized reaction conditions (130 °C). These heterogeneous catalysts presented improved performances as compared with zeolites and strong acid ion exchange resins, and were shown to be efficiently and easily recycled without any significant loss in fructose conversion and HMF yield. These new catalysts, allowing the conversion of the biomass fraction into valuable

products, contribute to make the biorefinery dream come true, minimizing our dependency on crude oil derivatives and advancing the world's sustainability.

<sup>1</sup> Department of Chemistry, CICECO, University of Aveiro, 3810-193 Aveiro, Portugal

## Reference

[1] Sidhpuria KB, Daniel-da-Silva AL, Trindade T, Coutinho JAP, *Green Chemistry*, 2011, 13, 340-349.

# TARGETING BIO-DERIVED CHEMICALS BY TUNING THE PROPERTIES OF SOLID ACID CATALYSTS

Antunes MM<sup>1</sup>, Lima S<sup>1</sup>, Neves P<sup>1</sup>, Russo PA<sup>1</sup>, Wiper PV<sup>1</sup>, Fernandes A<sup>2</sup>, Ferreira LR<sup>1</sup>, Abrantes JP<sup>1</sup>, Veiga JM<sup>1</sup>, Pillinger M<sup>1</sup>, Mafra L<sup>1</sup>, Portugal I<sup>1</sup>, Evtuguin DV<sup>1</sup>, Pinna N<sup>1</sup>, Rocha SM<sup>2</sup>, Ribeiro MF<sup>2</sup>, Valente AA<sup>1</sup>

The production of non-petroleum derived energy, fuels and chemicals is nowadays a global concern, principally due to oil depletion and the climatic impacts of

anthropogenic CO<sub>2</sub> emissions. Plant biomass is a widespread, abundant, renewable carbon source that through chemical and/or biological transformations

can give a plethora of bio-products as alternatives to petrochemicals. Valente and co-workers<sup>[1]</sup> have been investigating catalytic routes for the chemical valorisation of carbohydrates which are the major components of plant biomass (Fig. 1). The hydrolysis of di/polysaccharides gives primarily hexoses and pentoses, and the dehydration of the latter gives 5-hydroxymethyl-2-furfural (HMF) and furfural (Fur), respectively, which have wide application profiles. In particular, Fur is produced on an industrial scale and its major market is furfuryl alcohol (FA), produced via the hydrogenation of Fur. The acid-catalysed reactions of FA and HMF give furanic ethers (FEs) and levulinic esters (LEs), which are interesting solvents, plasticizing agents, oxygenated fuel extenders, etc.

Our research has been directed towards developing heterogeneous acid catalytic routes for producing Fur, HMF, FEs and LEs.<sup>[2-5]</sup> An important issue in these studies is the understanding of the influence of the structure/texture and acid properties of the solid acids on the overall reaction processes. The reaction mechanisms are complex, and the various elementary steps depend differently on the catalytic properties. The identification of reaction products by comprehensive two-dimensional gas chromatography combined with time-of-flight mass spectrometry has allowed mechanistic insights into these complex reaction processes.<sup>[2,3]</sup> By focussing on specific families of materials and modifying their physicochemical properties, structure-activity relationships have been established. Zirconium-tungsten mixed oxides (ZrW),<sup>[3]</sup> aluminosilicates of the type TUD-1 (Al-TUD-1)<sup>[4]</sup>, and sulfonated carbons (e.g. partially reduced graphene oxide (S-RGO))<sup>[5]</sup> are fairly stable solid acids, and their texture and acid properties can be fine-tuned through different synthesis approaches and conditions. The texture properties of ZrW materials were modified using a templating agent in order to enhance the surface area and tune the mesoporosity.<sup>[3]</sup> This led to superior catalytic performances of ZrW in the dehydration of xylose to Fur (faster reaction; higher Fur yields), in comparison to related materials prepared by conventional co-condensation. The acidity

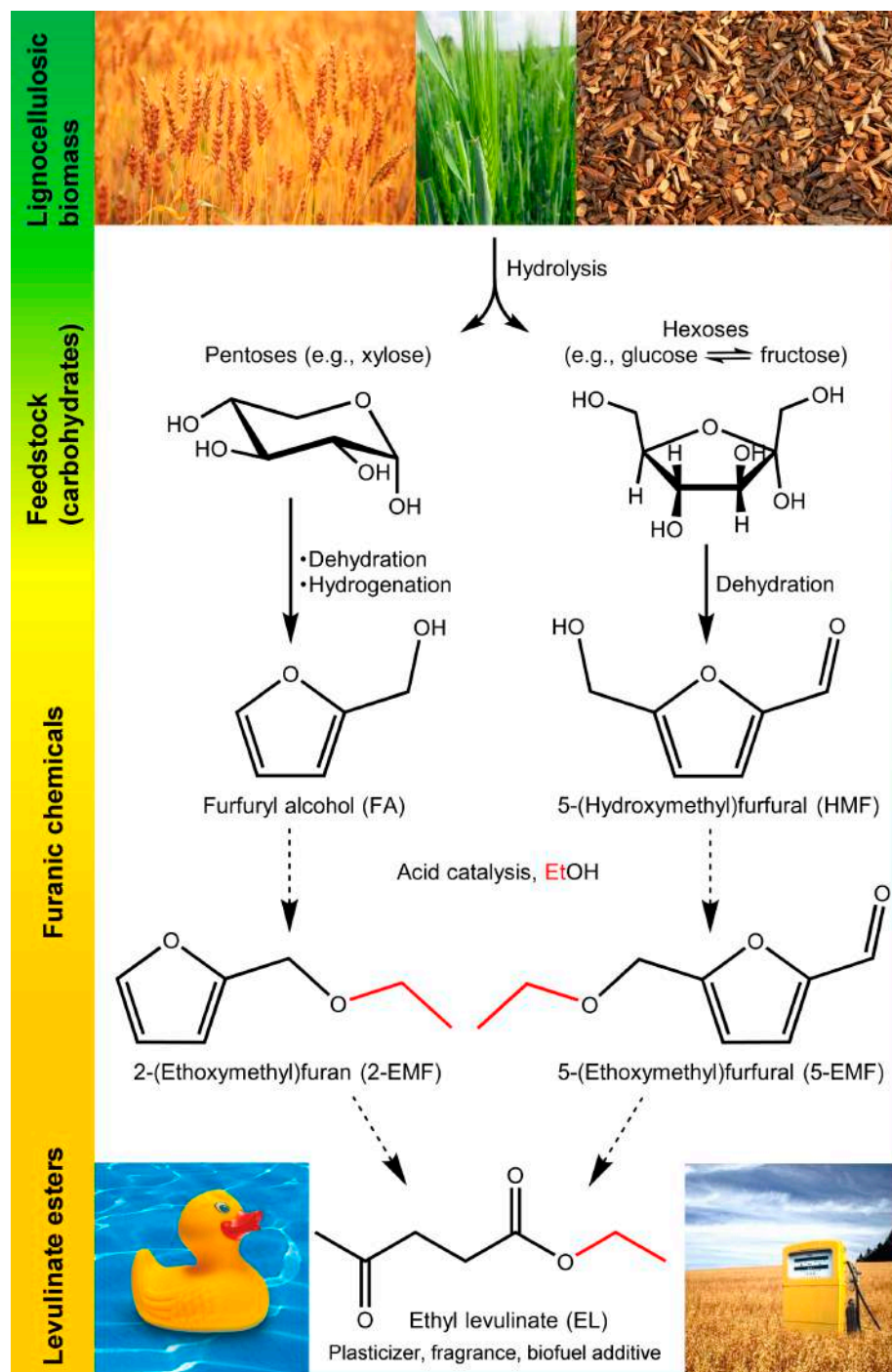


Figure 1. Carbohydrate biomass conversion to useful bio-products.

of tungstated mesoporous zirconia was enhanced by doping it with aluminium, which allowed further improvements in Fur yields at high conversions. The acidity of mesoporous aluminosilicate Al-TUD-1 was modified by varying the Si/Al ratio and applying post-synthesis acid treatment, for producing targeted bioproducts.<sup>[4]</sup> Al-TUD-1 exhibited superior catalytic performance in the conversion of HMF and FA to FEs and LEs, in comparison to zeolites and modified versions of zeolites. The sulfonated carbon S-RGO exhibited outstanding catalytic performance (activity, stability) in the reaction of HMF with ethanol to the corresponding

FE and LE, in comparison to other carbon and organic catalysts (e.g. carbon nanotubes, carbon black, Amberlyst<sup>TM</sup>-15). Cooperative effects of strong sulfonic acid groups and other acid sites in their surroundings contributed to the superior performance of S-RGO.<sup>[5]</sup>

<sup>1</sup> Department of Chemistry, CICECO, University of Aveiro, Campus Universitário de Santiago, 3810-193 Aveiro, Portugal

<sup>2</sup> Institute for Biotechnology and Bioengineering, Instituto Superior Técnico, Av. Rovisco Pais, 104900 Lisboa, Portugal

<sup>3</sup> Department of Chemistry, QOPNA, University of Aveiro, Campus Universitário de Santiago, 3810-193 Aveiro, Portugal

#### References

[1] Lima S, Antunes MM, Pillinger M, Valente AA, ChemCatChem, 2011, 3, 1686-1706.

[2] Ferreira LR, Lima S, Neves P, Antunes MM, Rocha SM, Pillinger M, Portugal I, Valente AA, Chemical Engineering Journal, 2013, 215-216, 772-783.

[3] Antunes MM, Lima S, Fernandes A, Candeias J, Pillinger M, Rocha SM, Ribeiro MF, Valente AA, Catalysis Today, 2012, 195, 127-135.

[4] Neves P, Antunes MM, Russo PA, Abrantes JP, Lima S, Fernandes A, Pillinger M, Rocha SM, Ribeiro MF, Valente AA, Green Chemistry, 2013, 15, 3367-3376.

[5] Antunes MM, Russo PA, Wiper PV, Veiga JM, Pillinger M, Mafra L, Evtuguin DV, Pinna N, Valente AA, ChemSusChem, 2014, 7, 804-812.

#### Acknowledgments

The funding institutions indicated in refs 1-5 are acknowledged, including European Union-FEDER-COMPETE, FCT, CICECO – FCOMP-01-0124-FEDER-03727 [FCT PEst-C/CTM/LA0011/2013].

## INVESTIGATION OF A DICHLORODIOXOMOLYBDENUM (VI)-PYRAZOLYLPYRIDINE COMPLEX AND A HYBRID DERIVATIVE AS CATALYSTS IN OLEFIN EPOXIDATION

Amarante TR<sup>1</sup>, Neves P<sup>1</sup>, Paz FAA<sup>1</sup>, Valente AA<sup>1</sup>, Pillinger M<sup>2</sup>, Gonçalves IS<sup>3</sup>

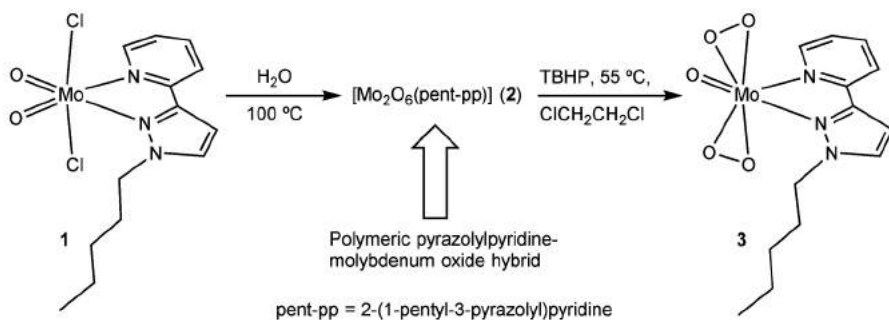


Figure 1. Hydrolysis of 1 to give the hybrid material 2, and formation of the oxodiperoxo complex 3 from 2 under conditions equivalent to those used for catalytic olefin epoxidation with material 2 as the (pre)catalyst.

Among the various oxyhalides of molybdenum, dichlorodioxomolybdenum(VI) ( $\text{MoO}_2\text{Cl}_2$ ) has received much attention especially as a catalyst for organic transformations. Treatment of  $\text{MoO}_2\text{Cl}_2$  with bidentate nitrogen donor ligands gives adducts with the general formula  $[\text{MoO}_2\text{Cl}_2\text{L}]$ . Depending on the choice of ligand (L), the complexes exhibit moderate to excellent catalytic performance for the liquid-phase epoxidation of olefins using *tert*-butylhydroperoxide (TBHP) as oxidant. Substituted pyrazolylpyridines stand out as being particularly effective organic ligands. In the present

work the chemistry and catalytic potential of molybdenum(VI)-pyrazolylpyridine compounds was further advanced by employing the ligand 2-(1-pentyl-3-pyrazolyl)pyridine (pent-pp) to prepare a complex of the type  $[\text{MoO}_2\text{Cl}_2(\text{pent-pp})]$  (1) (Fig. 1)<sup>[1]</sup>.

During the last few years we have determined that the hydrolysis of complexes of the type  $[\text{MoO}_2\text{Cl}_2\text{L}]$  is a route to novel molybdenum oxide-based organic-inorganic hybrid materials, which are of interest due to their potential application in important fields such as catalysis, sorption, electrical conductivity, mag-

netism, electronics, and optical materials<sup>[2-5]</sup>. Reaction of 1 with water in a digestion bomb at 100 °C gave a molybdenum oxide/pyrazolylpyridine hybrid material with the composition  $[\text{Mo}_2\text{O}_6(\text{pent-pp})]$  (2). Although the structure of 2 is presently unknown, the characterization data point towards a polymeric molybdenum oxide hybrid in which the organic ligands are coordinated to oxomolybdenum(VI) centers.

When used as (pre)catalysts for the epoxidation of *cis*-cyclooctene at 55 °C with TBHP as oxidant, compounds 1 and 2 exhibit excellent selectivity (100%) towards the epoxide product until 100% conversion (reached within 1-2 h). Very good catalytic results were also obtained with 2 as (pre)catalyst for the epoxidation of the bio-derived olefins DL-limonene (Lim), a cyclic monoterpene present in citrus peel oil, and methyl oleate (Ole), present in, for example, soybean oil (Fig. 2). The epoxides formed from these olefins have numerous possible uses, such as intermediates in the production of flavors and fragrances, as precursors to polyurethanes, and as biofuel additives. The catalytic reactions were found to be homogeneous in nature. Starting with material 2, the oxodiperoxo complex  $[\text{MoO}(\text{O}_2)_2(\text{pent-pp})]$  (3) was isolated from solution after a catalytic run (Fig. 1), suggesting that it is formed from 2 and plays a catalytic role. While most of the molybdenum oxide/organic hy-

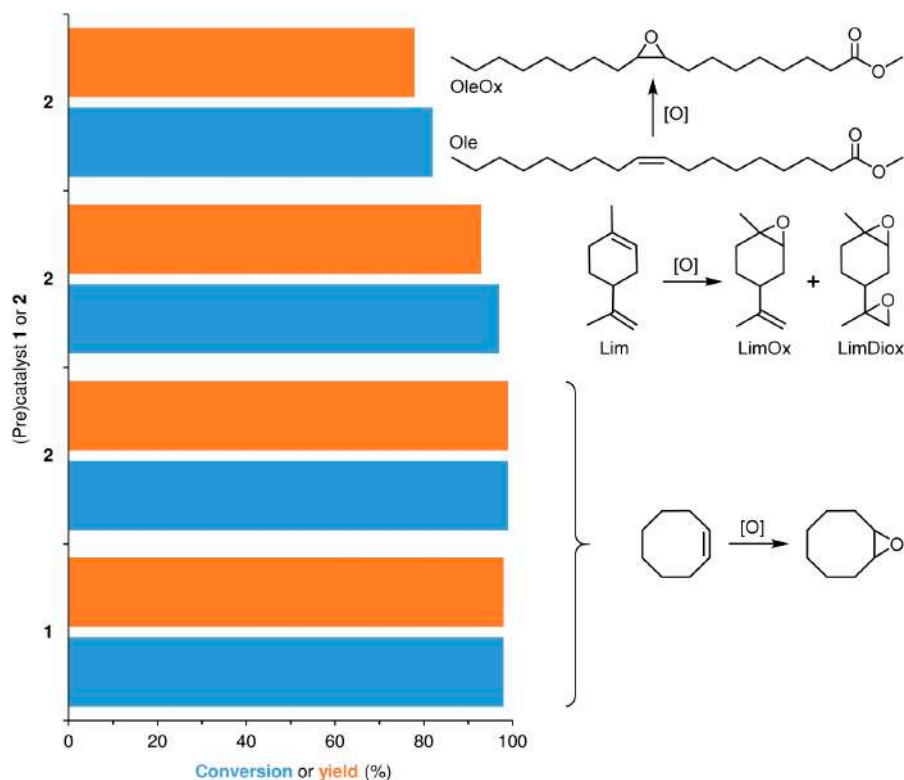


Figure 2. Catalytic results for olefin epoxidation using 1 or 2 as (pre)catalysts, TBHP as oxidant and 1,2-dichloroethane as cosolvent (55 °C, 6 h).

brid materials studied recently by us in catalytic olefin epoxidation behave in a

similar way to 2, i.e., the materials act as a source of soluble active species, some

materials act as heterogeneous catalysts. By modifying the synthesis procedures and/or the organic ligands employed it may be possible to obtain porous materials that function effectively as heterogeneous catalysts. This would be a major breakthrough and is currently a focus of study in our laboratory.

<sup>1</sup> Department of Chemistry, CICECO, University of Aveiro, 3810-193 Aveiro, Portugal

#### References

- <sup>[1]</sup> Amarante TR, Neves P, Paz FAA, Valente AA, Pillinger M, Gonçalves IS, *Dalton Transactions*, 2014, 43, 6059-6069.
- <sup>[2]</sup> Abrantes M, Amarante TR, Antunes MM, Gago S, Paz FAA, Margiolaki I, Rodrigues AE, Pillinger M, Valente AA, Gonçalves IS, *Inorganic Chemistry*, 2010, 49, 6865-6873.
- <sup>[3]</sup> Amarante TR, Neves P, Tomé C, Abrantes M, Valente AA, Paz FAA, Pillinger M, Gonçalves IS, *Inorganic Chemistry*, 2012, 51, 3666-3676.
- <sup>[4]</sup> Figueiredo S, Gomes AC, Neves P, Amarante TR, Paz FAA, Soares R, Lopes AD, Valente AA, Pillinger M, Gonçalves IS, *Inorganic Chemistry*, 2012, 51, 8629-8635.
- <sup>[5]</sup> Amarante TR, Neves P, Gomes AC, Nolasco MM, Ribeiro-Claro P, Coelho AC, Valente AA, Paz FAA, Smeets S, McCusker LB, Pillinger M, Gonçalves IS, *Inorganic Chemistry*, 2014, 53, 2652-2665.

#### Acknowledgments

The authors acknowledge FEDER, COMPETE and the FCT for the projects CICECO – FCOMP-01-0124-FEDER-037271 [FCT ref. PEst-C/CTM/LA0011/2013], FCOMP-01-0124-FEDER-029779 [FCT ref. PTDC/QEQ-SUP/1906/2012], and FCOMP-01-0124-FEDER-020658 [FCT ref. PTDC/EQU-EQU/121677/2010].

## IRON-SUBSTITUTED POLYOXOTUNGSTATES AND THEIR CATALYTIC APPLICATIONS

Cavaleiro, AMV<sup>1</sup>, Nogueira HIS<sup>1</sup>

Iron-substituted polyoxometalates (Fe-POM) are an interesting group of anions with quite a large variation in structure, size, composition, and properties. A systematic study of some iron(III)-substituted polyoxotungstates (Fe-POT) for catalytic applications has been taking place in CICECO during the last years. Recent work focused on the immobilization of Keggin-type Fe-POT on silica<sup>[1,2]</sup> or films<sup>[3]</sup> and the preparation of ionic liquid-type compounds<sup>[4]</sup> with these anions.

Silica nanoparticles supporting  $[\text{PW}_{11}\text{Fe}(\text{H}_2\text{O})\text{O}_{39}]^{4-}$  ( $\text{PW}_{11}\text{Fe}$ ) and  $[(\text{PW}_{9}\text{O}_{34})_2\text{Fe}_4(\text{H}_2\text{O})_2]^{6-}$  were obtained by alkaline hydrolysis of tetraethoxysi-

lane using a reverse micelle and sol-gel technique. The catalytic activity of these Fe-POT/SiO<sub>2</sub> nanomaterials (Fig. 1) was established in the epoxidation of geraniol with H<sub>2</sub>O<sub>2</sub> as oxygen donor. The  $\text{PW}_{11}\text{Fe}/\text{SiO}_2$  nanocomposite was the most efficient, with high geraniol conversion (96% after 3 h at room temperature) and good regioselectivity for 2,3-epoxygeraniol. Polyoxotungstates  $[\text{XW}_{11}\text{Fe}(\text{H}_2\text{O})\text{O}_{39}]^{n-}$  (X = P, Si or B) were also immobilized on a functionalized silica matrix. The obtained materials catalysed the oxidation of cyclooctane with H<sub>2</sub>O<sub>2</sub> at 80 °C, with conversion as high as 71–74%. The reaction products varied with X, and were

somewhat different from those obtained in homogeneous systems. Both types of silica supported Fe-POT catalysts could be reused several times.

Hybrid organic/inorganic films composed of the conducting polymers poly(3,4-ethylenedioxythiophene) or poly(brilliant cresyl blue) with  $[\text{SiW}_{11}\text{Fe}(\text{H}_2\text{O})\text{O}_{39}]^{5-}$  were

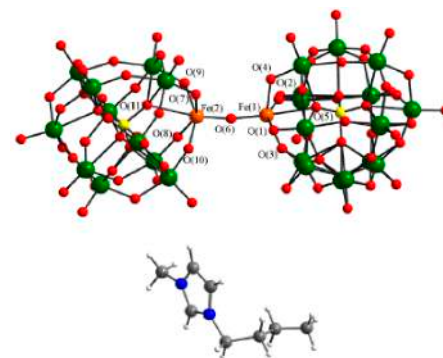


Figure 2. Molecular structures of dimer  $[(\text{PW}_{11}\text{O}_{39}\text{Fe}_2)\text{O}]^{10-}$  (top) and 1-butyl-3-methylimidazolium cation. Colour scheme: C, grey; N, blue; O, red; H, white; P, yellow; W, green and Fe, orange.

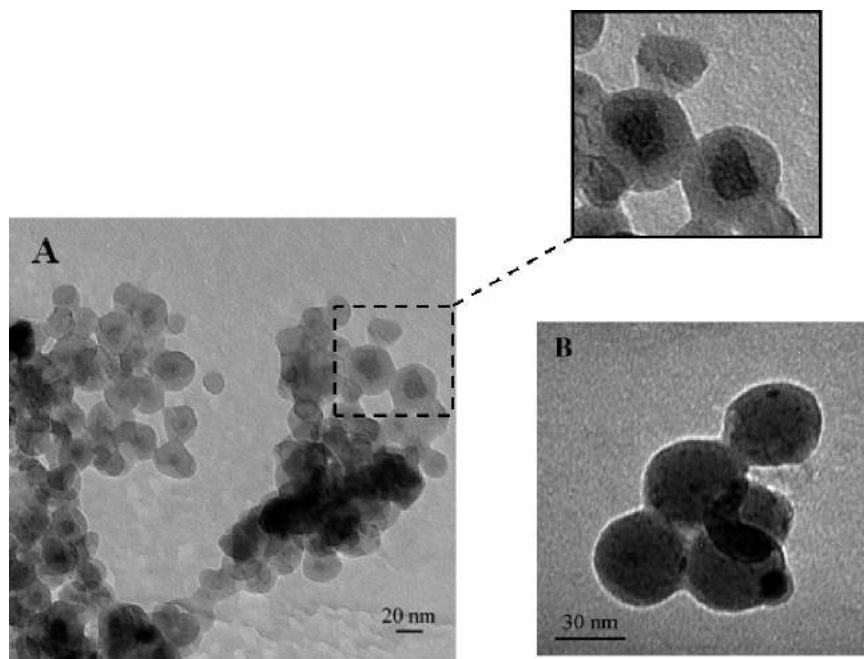


Figure 1. TEM images of  $[PW_{11}O_{39}Fe_2]/SiO_2$  (A) and  $PW_{11}Fe/SiO_2$  (B) nanocomposites.

synthesized on the surface of glassy carbon electrodes by electrochemical polymerization in aqueous solution, and characterized by several techniques. The chemically modified electrodes were stable and their preparation was easy to perform. The results provided valuable information for exploring future applications of these films in electrochemical sensors or electrocatalysis.

The combination of cations typical of ionic liquids with polyoxoanions originates com-

pounds with interesting properties for use in catalytic studies. The comparatively high charge of most POMs hampers the formation of true ionic liquids, and our studies on the combination of  $\alpha-[XW_{11}Fe(H_2O)_O_{39}]^{n-}$  ( $X = P, Si$ ) with 1-butyl-3-methylimidazolium (bmim) yielded compounds with melting points around 210–220°C. In the course of these studies, the compound  $(Bmim)_{10}[(PW_{11}O_{39}Fe_2)O] \cdot 0.5H_2O$  (1) was isolated and characterized crystallographically. For the first time, a salt of a  $\mu$ -oxo

iron(III) polyoxometalate dimer (Fig. 2) was obtained by simple bench top techniques. It was possible to compare (1) and  $(Bmim)_4[PW_{11}O_{39}Fe(H_2O)] \cdot H_2O$  (2) and to identify techniques that could distinguish them (e.g., solid state spectroscopic and magnetic techniques) and others that were inappropriate for this distinction. This study contributed to the understanding of iron  $\mu$ -oxo-dimer formation in polyoxometalate chemistry, and showed that the influence of counter-cations and solution composition on the precipitation of different salts from solutions of iron-substituted Keggin anions must be considered carefully.

<sup>1</sup> Department of Chemistry, CICECO, University of Aveiro, 3810-193 Aveiro, Portugal

#### References

- [1] Sousa JLC, Santos ICMS, Simões MMQ, Cavaleiro JAS, Nogueira HIS, Cavaleiro AMV, *Catalysis Communications*, 2011, 12, 459–463.
- [2] Estrada AC, Santos ICMS, Simões MMQ, Neves MGPM, Cavaleiro JAS, Cavaleiro AMV, *Applied Catalysis A*, 2011, 392 28–35.
- [3] Fernandes DM, Brett CMA, Cavaleiro AMV, *Journal of Solid State Electrochemistry*, 2012, 16, 2267–2273.
- [4] Santos FM, Brandão P, Félix V., Domingues MRM, Amaral JS, Amaral VS, Nogueira HIS, Cavaleiro, AMV, *Dalton Transactions*, 2012, 41, 12145–12155.

#### Acknowledgments

This work was performed in collaboration with Prof Mário Simões and Graça Neves of the University of Aveiro [QOPNA].

## COPPER(II) BIS(OXAZOLINE)-TYPE LIGANDS IMMOBILIZED ONTO MESOPOROUS SILICAS AND THEIR CARBON REPLICAS AS EFFICIENT ASYMMETRIC HETEROGENEOUS CATALYSTS FOR ORGANIC TRANSFORMATIONS

Silva AR<sup>1</sup>, Carneiro L<sup>1</sup>, Guimarães V<sup>1</sup>, Carvalho AP<sup>2</sup>, Pires J<sup>2</sup>

The preparation of robust and efficient asymmetric heterogeneous catalysts based on the immobilization of expensive privileged chiral ligands onto porous supports is of great interest to their use in industry. Copper(II) complexes with chiral bis(oxazoline)-type ligands are versatile homogeneous catalysts for a broad range

of asymmetric organic transformations. Although some bis(oxazoline) ligands are commercially available they are of high cost. A copper(II) complex with a commercial chiral bis(oxazoline) (CuPhBox) was anchored onto ordered mesoporous silica materials and their respective carbon replicas (Fig. 1) [1]. For the first time the

asymmetric benzoylation of a 1,2-diol was performed in the heterogeneous phase by using an anchored commercial bis(oxazoline) ligand [1]. All the composites prepared were active, selective and enantioselective in this asymmetric organic transformation. Using the two ordered mesoporous silicas as supports good selectivities, with comparable yields and TONs to the homogeneous phase reaction, were obtained. Furthermore these two heterogeneous catalysts are more stable upon reuse than the corresponding ordered carbon replica materials. One of the former heterogeneous catalysts, with mesoporous silica as a support, could be further reused for 4 consecutive cycles without significant loss of selectivity, the TON or enantioselectivity [1].

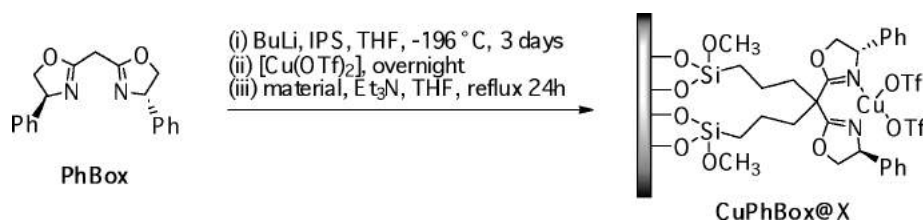


Figure 1. Anchoring a copper(II) chiral bis(oxazoline) catalyst onto mesoporous materials.

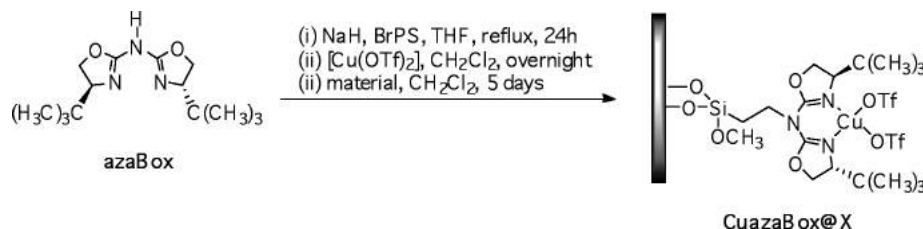


Figure 2. Anchoring of a copper(II) chiral aza-bis(oxazoline) catalyst onto mesoporous materials.

A copper(II) chiral aza-bis(oxazoline) catalyst (CuazaBox) was synthesised and anchored onto ordered mesoporous silicas and their carbon replicas (Fig. 2) [2]. The materials were tested as heterogeneous catalysts in the reaction of cyclopropana-

tion of styrene [2]. Generally, the composites were more active and enantioselective in the cyclopropanation of styrene than the corresponding homogeneous phase reaction run under similar experimental conditions. The materials pHpzc proved

to be an important factor not only in the CuazaBox anchoring yields, but also in their catalytic performance. Less acidic surfaces yielded heterogeneous catalysts with higher styrene conversion and enantioselectivity. The materials could also be recycled with comparable enantioselectivities or generally a slight decrease in the enantioselectivity [2].

<sup>1</sup> Department of Chemistry, CICECO, University of Aveiro, 3810-193 Aveiro, Portugal

<sup>2</sup> COB, Departamento de Química e Bioquímica, Faculdade de Ciências, Universidade de Lisboa, 1749-016 Lisboa, Portugal

#### References

[1] Silva AR, Carneiro L, Carvalho AP, Pires J, *Catalysis Science & Technology*, 2013, 3, 2415-2424.

[2] Silva AR, Guimarães V, Carvalho AP, Pires J, *Catalysis Science & Technology*, 2013, 3, 659-672.

#### Acknowledgments

This work was funded by FCT through the project PTDC/QUI/64770/2006.

## INTERCALATION OF MOLYBDENUM CARBONYL COMPLEXES IN LAYERED DOUBLE HYDROXIDES

Gomes AC<sup>1</sup>, Bruno SM<sup>1</sup>, Gamelas CA<sup>2</sup>, Valente AA<sup>1</sup>, Abrantes M<sup>2</sup>, Gonçalves IS<sup>1</sup>, Romão CC<sup>2</sup>, Pillinger M<sup>1</sup>

Transition metal carbonyl complexes are one of the most important families of compounds in organometallic chemistry. Interest in molybdenum  $\pi$ -allyl complexes of the type  $[\text{Mo}(\eta^3\text{-C}_3\text{H}_5)\text{X}(\text{CO})_2(\text{L})_n]$  ( $\text{X} = \text{Cl}, \text{Br}, \text{I}$  or pseudohalide;  $\text{L} =$  monodentate or bidentate ligand) stems mainly from their use as precursors for the preparation of other organometallic complexes, or as (pre)catalysts in homogeneous catalysis. Molybdenum carbonyl complexes have also been studied as anti-cancer agents, biomarkers, and carbon monoxide releasing molecules. In all these applications the immobilization of the metal carbonyls is desirable for many reasons, e.g. to facilitate catalyst recycling and cellular delivery of drugs. In the present work a molybdenum  $\pi$ -allyl dicarbonyl complex (**1**) containing the ligand 2,2'-bipyridine-5,5'-dicarboxylate (bpdc) was successfully intercalated in a layered double hydroxide (LDH) host by using a spontaneous

self-assembly/coprecipitation method<sup>[1]</sup>. Comprehensive characterization of the resultant inorganic-organometallic hybrid nanocomposite (**1**@LDH) supported the formation of a highly organized intercalate containing anisotropically oriented guest molecules at the nanoscale (Fig. 1). The intracrystalline reactivity of intercalated dicarbonyl complexes was probed

by using **1**@LDH as a precatalyst in the epoxidation of *cis*-cyclooctene with *tert*-butylhydroperoxide (TBHP) as oxidant (Fig. 2). Oxidative decarbonylation of the guest molecules takes place *in situ* to give intercalated molybdenum oxide/bipyridine species that selectively catalyze the epoxidation reaction. On the basis of previous studies in which the reaction of the complex  $[\text{Mo}(\eta^3\text{-C}_3\text{H}_5)\text{Cl}(\text{CO})_2(\text{bipy})]$  (bipy = 2,2'-bipyridine) with TBHP under certain conditions was found to give the polymeric molybdenum oxide/bipyridine hybrid material  $[\text{MoO}_3(\text{bipy})]_n$ <sup>[2]</sup>, we proposed that polymeric species of the type  $[\text{MoO}_3(\text{bpdc})]_n$  could form be-

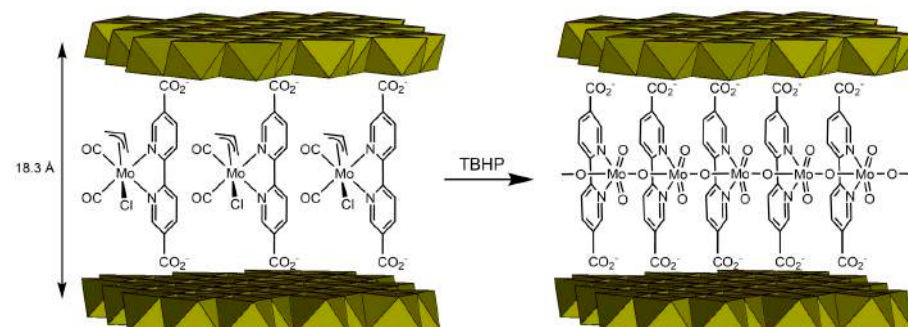


Figure 1. Schematic representations of the interlayer arrangement of guest anions in the material **1**@LDH and the polymeric species of the type  $[\text{MoO}_3(\text{L})]_n$  that could form between the LDH layers upon reaction of **1**@LDH with TBHP.

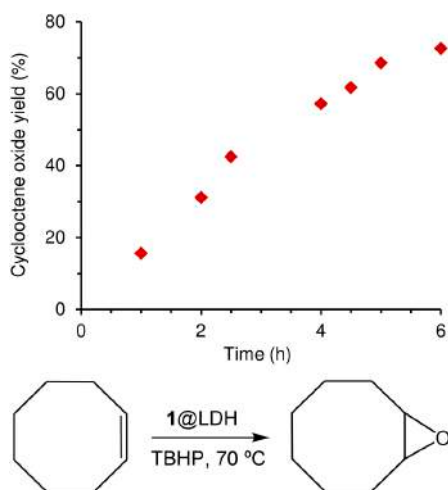


Figure 2. Dependence of cyclooctene oxide yield (or olefin conversion) on time of reaction of cyclooctene (Cy) with TBHP at 70 °C using 1@LDH as catalyst precursor [Mo : Cy : TBHP molar ratio of 1 : 150 : 230].

tween the LDH layers upon reaction of the intercalated dicarbonyl complexes with TBHP (Fig. 1).

Following this work, we have successfully immobilized other molybdenum carbonyl complexes in LDHs, namely the tetracarbonyl complex *cis*-[Mo(CO)<sub>4</sub>(bpdc)] by an ion-exchange method, and the cyclopentadienyl complex ( $\eta^5$ -C<sub>5</sub>H<sub>5</sub>)Mo(CO)<sub>3</sub>(CH<sub>2</sub>COO<sup>-</sup>) by a direct coprecipitation route. These inorganic/organometallic host-guest systems may find applications in several important fields such as nonlinear optics and biomedicine.

<sup>1</sup> Department of Chemistry, CICECO, University of Aveiro, 3810-193 Aveiro, Portugal

<sup>2</sup> Instituto de Tecnologia Química e Biológica da Universidade Nova de Lisboa, 2780-157 Oeiras, Portugal

<sup>3</sup> Centro de Química Estrutural, Complexo Interdisciplinar, Instituto Superior Técnico, Universidade Técnica de Lisboa, 1049-001 Lisboa, Portugal

#### References

[1] Gomes AC, Bruno SM, Gamelas CA, Valente AA, Abrantes M, Gonçalves IS, Romão CC, Pillinger M, *Dalton Transactions*, 2013, 42, 8231-8240.

[2] Gamelas CA, Gomes AC, Bruno SM, Paz FAA, Valente AA, Pillinger M, Romão CC, Gonçalves IS, *Dalton Transactions*, 2012, 41, 3474-3484.

#### Acknowledgments

The authors acknowledge FEDER, COMPETE and the FCT for the projects CICECO - FCOMP-01-0124-FEDER-037271 (FCT ref. PEst-C/CTM/LA0011/2013) and FCOMP-01-0124-FEDER-029779 (FCT ref. PTDC/OEQ-SUP/1906/2012).

## CO<sub>2</sub> ADSORPTION AND ACTIVATION BY AMINE-MODIFIED NANOPOROUS MATERIALS STUDIED BY NMR AND <sup>13</sup>CO<sub>2</sub> ADSORPTION

Pinto ML<sup>1</sup>, Mafra L<sup>1</sup>, Guil JM<sup>2</sup>, Pires J<sup>2</sup>, Rocha J<sup>1</sup>

Adsorption of CO<sub>2</sub> experiments and adsorption microcalorimetry revealed high adsorption capacity and strong interaction with the clays surfaces at low pressures, due to the presence of amine groups (Figure 1). Considerable surface heterogeneity and high initial adsorption heat (125 kJ mol<sup>-1</sup>) were observed, although the adsorption was reversible with hysteresis at low pressures and very slow desorption kinetics. The interaction between <sup>13</sup>CO<sub>2</sub> and the surface of the nanoporous clay materials was investigated by <sup>13</sup>C and <sup>15</sup>N magic-angle spinning NMR. <sup>13</sup>C NMR resonances at *ca.* 164 and 160 ppm were assigned to, respectively, carbamate and carbamic acid, and the stability of these species have been studied (Figure 2). Peak areas and the amount of <sup>13</sup>CO<sub>2</sub> adsorbed allowed the determination of the concentration of carbamate and

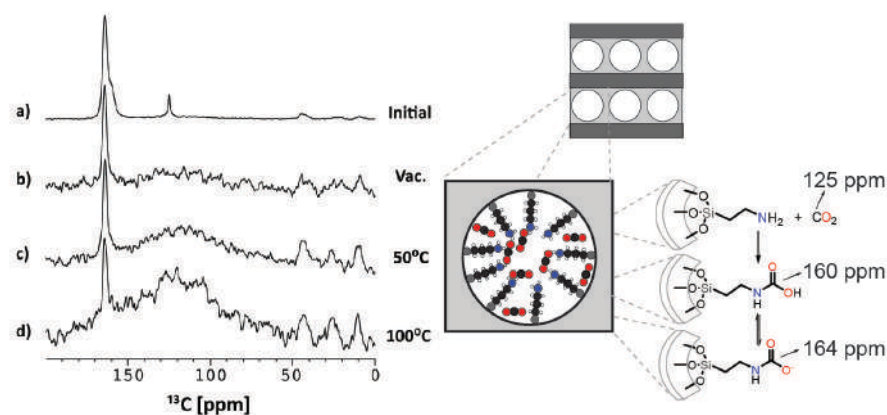


Figure 1. Differential calorimetric isotherms of CO<sub>2</sub> adsorption on nanoporous clay with primary amines. The data corresponds to adsorption (circles), readsorption after vacuum outgassing for 1 night (squares), and with readsorption points displaced 0.06 mmol g<sup>-1</sup> to the right along the x-axis (crosses).

Global warming and climate changes are probably among the most difficult challenges for the humankind in the next century. Carbon dioxide emissions from anthropogenic sources are the main causes of the greenhouse effect and associated climate changes. Nanoporous materials functionalized with amine groups selectively retain large amounts of CO<sub>2</sub> and may be regenerated, suggesting that they be used in cyclic processes for the

CO<sub>2</sub> separation from the remaining flue gases. The interaction of CO<sub>2</sub> with the amine groups at the gas/solid interface is, however, not well understood, hindering the design of improved material for its capture or conversion to other high-value chemicals.

In this work we have studied the interaction of gaseous CO<sub>2</sub> with the surface of nanoporous clays functionalized with primary amines using several techniques.

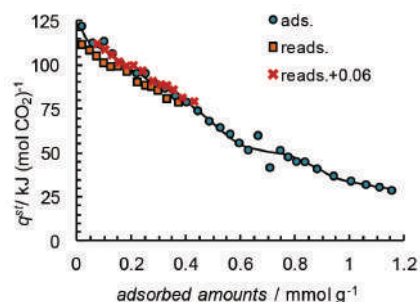


Figure 2. Single-pulse <sup>13</sup>C [<sup>1</sup>H decoupled] NMR spectra of nanoporous clay with a) adsorbed <sup>13</sup>CO<sub>2</sub>, b)-d) submitted to vacuum and heated 50 and 100 °C, for 4 hours [raise baseline at 100-140 ppm is probe background]. Representation of the species formed in the pores of the amine functionalized material.

carbamic acid. To the best of our knowledge, this is the first time that solid-state NMR is used to establish the amine-CO<sub>2</sub> bonding at the surface of amine-modified nanoporous materials and to identify the nature of the species formed. The results shed light on the mechanism of CO<sub>2</sub> activation, because the adsorption of CO<sub>2</sub>

on the surface of these materials is the activation step allowing further reactions to occur. The instability of the carbamate and carbamic acid species formed at the surface is important in explaining the reactivity of these intermediates and supports the application of these materials in CO<sub>2</sub> activation.

<sup>1</sup> Department of Chemistry, CICECO, University of Aveiro, 3810-193 Aveiro, Portugal

<sup>2</sup> Department of Chemistry and Biochemistry, and CQB, Faculty of Sciences, University of Lisbon, 1749-016 Lisboa, Portugal

<sup>3</sup> Instituto de Química Física 'Rocasolano', CSIC, E-28006 Madrid, Spain

#### Reference

<sup>[1]</sup> Pinto, M. L., Mafra, L., Guil, J. M., Pires, J., Rocha, *Chemistry of Materials*, 2011, 23, 1387–1395.

## CARBOHYDRATES AND IONIC LIQUIDS IN AQUEOUS MEDIA: A MAJOR PATH TOWARDS A SUSTAINABLE DEVELOPMENT

Freire MG,<sup>1</sup> Louros CLS,<sup>1</sup> Rebelo LPN,<sup>2</sup> Coutinho JAP<sup>1</sup>

Sustainability concerns have led to intense activity in the development of unconventional solvents and extraction techniques. Aqueous biphasic systems (ABS) are an efficient and clean alternative for the separation and purification of a broad range of biomolecules through their partitioning between two aqueous liquid phases. Due to the aqueous environment, ABS are regarded as biocompatible systems. Recent advances in ABS have suggested that ionic liquids are viable replacements to polymers commonly employed. The interest on using ionic liquids in ABS stems from their unique combination of physicochemical properties (negligible volatility, non-flammability, and high thermal and chemical stability), which make them benign solvents. However, the major advantage of using ionic liquids as the phase-forming component of ABS is their improved solvation/extraction ability. The judicious design of the ionic liquid's cation/anion combination allows tailoring the polarities of the co-existing phases and, thus, to optimize the extraction efficiencies of various types of biomolecules and added-value products. Besides the interest devoted to ionic liquids-based ABS formed by the addition of salts, the use of much less investigated carbohydrates can lead to more biocom-

patible and benign extraction routes. Carbohydrates are a non-charged, biodegradable, nontoxic and renewable feedstock. The combination of non-volatile and tailored ionic liquids with renewable bio-sourced organic compounds (carbohydrates) may lead to greener processes. In this work, we proposed novel ionic liquids-carbohydrate-based ABS by combining the water-stable ionic liquid 1-butyl-3-methylimidazolium trifluoromethanesulfonate ([C<sub>4</sub>mim][CF<sub>3</sub>SO<sub>3</sub>]) and a plethora of carbohydrates (monosaccharides, disaccharides and polyols). The phase diagrams, tie-lines and tie-line lengths were determined at 25 °C to infer on the monophasic/biphasic regimes in which ABS may be applied as liquid-liquid extractive strategies. Aiming at evaluating these novel ionic liquids-carbohydrate-based ABS as potential extractive media, from biomass matrices and biorefinery processes, three representative model biomolecules were screened *via* their partitioning between the two aqueous phases. Caffeine and  $\beta$ -carotene were chosen as bioactive substances belonging to the alkaloids and terpenoids families. These compounds are usually present in the biomass and have multiple therapeutic effects and pharmacological activities. L-tryptophan is an aminoacid essential to

humans, required for the production of the neurotransmitter serotonin, that may be produced by fermentative processes. The novel systems investigated showed very high extraction efficiencies (50% - 95%, in a single step) for all the studied biomolecules. A macroscopic view of the almost complete extraction of the carotenoid into the IL-rich phase is depicted in Fig. 1.



Figure 1. Extraction of  $\beta$ -carotene using carbohydrate + ionic liquid aqueous biphasic systems.

The use of carbohydrates in ionic liquids-based ABS is a step forward into sustainable extractions from biomass, allowing the recovery of a broad range of bio-based products. We are now actively engaged in studies aiming at finding high-molecular weight polysaccharides and ionic liquids capable of forming ABS.

<sup>1</sup> Department of Chemistry, CICECO, University of Aveiro, 3810-193, Aveiro, Portugal

<sup>2</sup> Instituto de Tecnologia Química e Biológica, UNL, 2780-901, Oeiras, Portugal

#### Reference

<sup>[1]</sup> Freire MG, Louros CLS, Rebelo LPN, Coutinho JAP, *Green Chemistry*, 2011, 13, 1536.

# ZEOLITIC INORGANIC MEMBRANES

Lin Z<sup>1</sup>, Cardoso SP<sup>1</sup>, Silva CM<sup>1</sup>

The separation of H<sub>2</sub> from gaseous mixtures using inorganic membranes is still a matter of considerably effort. An affordable H<sub>2</sub>-permselective membrane could be a definitive advantage in the implementation of challenging processes, among them purification of hydrogen-containing streams and H<sub>2</sub> proton-exchange membrane (PEM) fuel cells. Small pore zeolitic materials, such as AM-3, grant them potential for the separation of H<sub>2</sub>-containing mixtures [1]. In our research, the zeolitic membranes were synthesized *in-situ* from a gel or clear solution, following the general procedure shown in Figure 1. The reagents are mixed to get a gel or clear solution first, and the zeolitic membranes are hydrothermally synthesized by using the seeded growth approach on the surface of porous support tubes. Seeding is performed by immersing the support into a water suspension of seeds and then dried at 150 °C for 20 minutes. The seeded support is put into an autoclave and then the precursor is added. In order to improve the quality of the membranes, samples can be prepared by repeating the preparation, i.e., after a certain synthesis

time, the sample is placed into fresh gel and all steps repeat. These efforts result in small pore AM-3 and AV-7 membranes on tubular alumina support [1]. The new membranes are then structurally and dynamically characterized to evaluate their performance, i.e. the existence of defects and the range of permeance values. Prior to the dynamic tests, several heating/cooling cycles are carried out between room temperature and ca. 120 °C, since the presence of adsorbed compounds, like water from air humidity, affects significantly the results. In Figure 2 it is shown a sequence of experiments of this kind for an AM-3 membrane. The dynamic tests involve not only the continuous measurement of pure gas permeance as function of temperature at fixed transmembrane pressure drop (e.g. in Figure 2) but also steady state measurements at fixed pressure and temperature. Our work comprehends also the phenomenological modelling of permeation of pure gases and mixtures through the zeolitic membranes, where the Maxwell-Stefan approach has been adopted with advantage [2-4]. The main transport mech-

anisms that prevail in porous media are primarily related with pore diameter,  $d_p$  (see Figure 3) [4]: viscous flow, Knudsen regime, and activated or configurational diffusion. In this case, if molecules retain their gaseous state inside small micropores, one has gas translational or activated gaseous diffusion; on the other hand, the strong interactions with the solid framework make them to move as an adsorbed phase (surface diffusion). For details, a deep and recent review may be consulted [4], where new expressions for thermodynamic and Maxwell-Stefan factors are also derived.

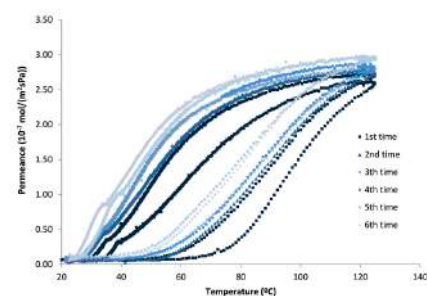


Figure 2. Sequences of heating and cooling cycles at programmed temperature of an AM-3 membrane. Transmembrane pressure drop = 0.5 bar, permeation gas = He.

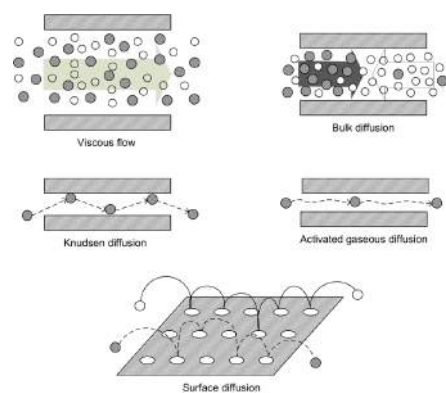


Figure 3. Mass transfer mechanisms involved in gas transport through porous materials [4].

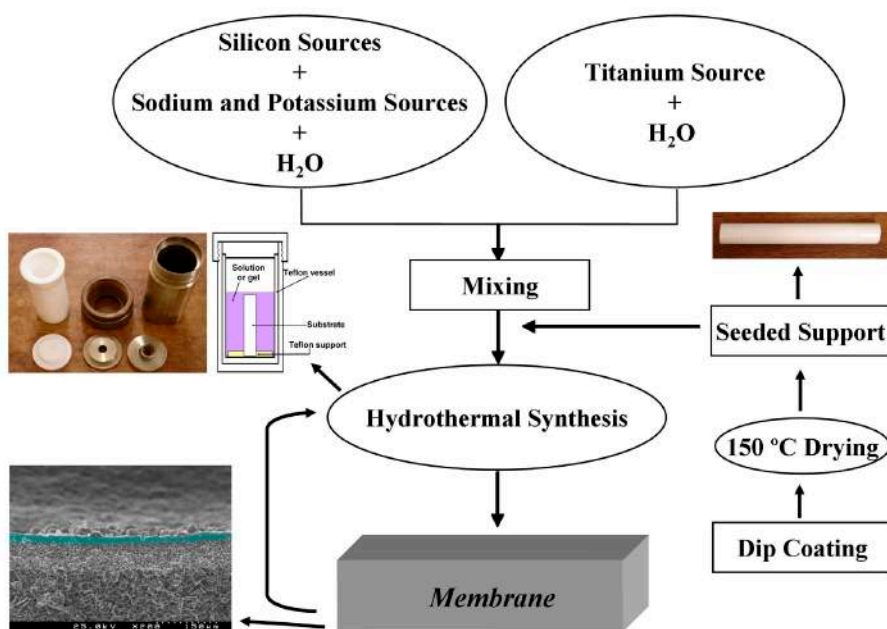


Figure 1. Flow chart of the synthesis procedure of zeolitic membranes.

<sup>1</sup> Department of Chemistry, CICECO, University of Aveiro, 3810-193, Aveiro, Portugal

## References

- [1] Li XW, Zhou CF, Lin Z, Rocha J, Lito PF, Santiago AS, Silva CM, *Microporous Mesoporous Materials*, 2011, 137, 43-48.
- [2] Lito PF, Zhou CF, Santiago AS, Rodrigues AE, Rocha J, Lin Z, Silva CM, *Chemical Engineering Journal*, 2010, 165, 395-404.
- [3] Lito PF, Santiago AS, Cardoso SP, Figueiredo BR, Silva CM, *Journal of Membrane Science*, 2011, 367, 21-32.
- [4] Lito PF, Cardoso SP, Rodrigues AE, Silva CM, *Separation and Purification Reviews*, 2014 (in Press).

## MODELING TRACER DIFFUSION COEFFICIENTS IN LIQUIDS, GASES AND SUPERCRITICAL FLUIDS

Vaz RV<sup>1</sup>, Magalhães AL<sup>1</sup>, Gomes JRB<sup>1</sup>, Silva CM<sup>1</sup>

The diffusion coefficient in dense phases is fundamental for simulation, design and scale-up of rate-controlled processes. Here, compressed gases and supercritical fluids get special attention due to their remarkable ability to be applied to mass-

and then extended to real substances; e.g. in Figure 1), semi-empirical expressions, free-volume equations, and improved hydrodynamic equations. To validate them, the largest database published in the literature has been compiled, including globally

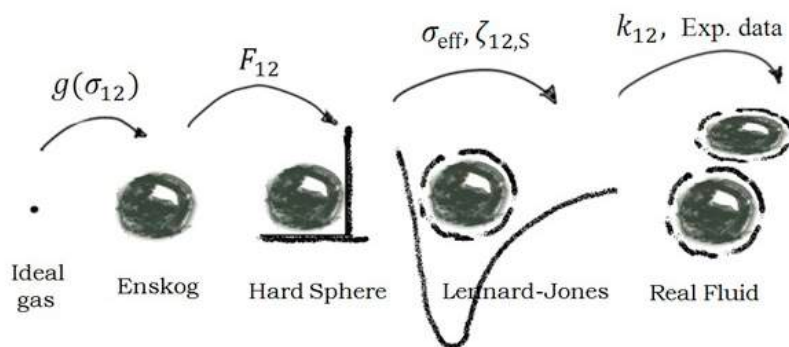


Figure 1. Example of the steps involved in the development of new tracer diffusion coefficient model for real systems.

transfer operations, phase transition processes, reactive systems, materials related processes, and nanostructured materials, either at industrial capacity application or yet under development.

During last years several models have been developed in our group for the calculation of tracer diffusion coefficient ( $D_{12}$ ) in liquids, supercritical fluids and gases. In the whole, they provide very reliable and accurate results for extremely different binary systems in terms of symmetry, mass, size and even polarity. They may be divided into molecular-based equations (derived for model fluids like hard spheres, Lennard-Jones, or Stockmayer,

630 binary systems, 9500 experimental points and 360 different molecules.

From previous models, the correlations provide very low deviations (2.70–4.40%)<sup>[1–6]</sup> but embody one or two system-specific parameters (e.g., solute/solvent diameters and interaction energy), which prevents their application to unknown systems. Therefore, recently, we are focusing predictive models for  $D_{12}$  estimation<sup>[7,8]</sup>. They are particularly desirable in supercritical solvents, since a large number of natural compounds and unknown systems are increasingly being identified and studied under the context of biorefinery. One may cite several Stokes-Einstein based

equations (e.g.<sup>[7]</sup>) and one model with improved behaviour near the critical point<sup>[8]</sup>. In this case,  $D_{12}$  is given by a regular or background equation plus a singular contribution specifically introduced to correct the behaviour of  $D_{12}$  in the critical region (error = 6.20%), particularly in the vicinity of the critical point where common models usually fail.

Presently, the phenomenological modelling is being complemented with classical molecular dynamics (MD) simulations in order to disclose the influence of solute chemical groups, substituents, alkyl chain size, and molecular symmetry upon  $D_{12}$  values. Accordingly, alkanes, alcohols and ketones in supercritical CO<sub>2</sub> are being computed to analyze their local structures based on radial distribution functions and coordination numbers. The MD simulations are based on boxes with several thousands of particles and are employing the Gromacs code together with potential parameters taken from the literature.

<sup>1</sup> Department of Chemistry, CICECO, University of Aveiro, 3810-193, Aveiro, Portugal

### References

- [1] Magalhães AL, Da Silva FA, Silva CM, *Chemical Engineering Journal*, 2011, 166, 49-72.
- [2] Magalhães AL, Da Silva FA, Silva CM, *The Journal of Supercritical Fluids*, 2011, 55, 898-923.
- [3] Magalhães AL, Da Silva FA, Silva CM, *Chemical Engineering Science*, 2012, 73, 151-168.
- [4] Magalhães AL, Da Silva FA, Silva CM, *The Journal of Supercritical Fluids*, 2013, 74, 89-104.
- [5] Magalhães AL, Lito PF, Da Silva FA, Silva CM, *The Journal of Supercritical Fluids*, 2013, 76, 94-114.
- [6] Lito PF, Magalhães AL, Gomes JRB, Silva CM, *Journal of Chromatography A*, 2013, 1290, 1-26.
- [7] Vaz RV, Magalhães AL, Silva CM, *Fluid Phase Equilibria*, 2013, 360, 401-415.
- [8] Vaz RV, Magalhães AL, Silva CM, *Journal of Supercritical Fluids*, 2014, 91, 24-36.

## IONIC LIQUIDS MICROEMULSIONS: THE KEY TO CANDIDA ANTARCTICA LIPASE B SUPERACTIVITY

Ventura SPM,<sup>1</sup> Santos LDF,<sup>1</sup> Saraiva JA,<sup>2</sup> Coutinho JAP<sup>1</sup>

An ionic liquid system compatible with the lipase *Candida antarctica* lipase B (CaLB) to enhance its activity was developed. The use of a simple method based on 1-decyl-3-methylimidazolium chloride

[C<sub>10</sub>mim]Cl to increase the lipase activity was reported. The effect of different ionic liquid molar concentrations on the relative lipase activity ( $Act_{IL}/Act_{BF}$ ) was investigated (Figure 1, green dots). The lipase

activity increases with the ionic liquid molar concentration, achieving a maximum six-fold increase for 0.090 M ionic liquid. These results suggest that the activity increment does not result from changes in the reaction mechanism or enzyme structure, since the enzyme activation energy is not affected by the ionic liquid presence but, instead, may be explained by the formation of microemulsions due to the ionic liquid alkyl chain self-aggregation

(Figure 2). In fact, the formation of microemulsions in long chain imidazolium ionic liquids, including this one, was previously demonstrated. To evaluate if the aggregation of  $[C_{10}\text{mim}]\text{Cl}$  was related with the observed activity increase, the critical micelle concentrations (CMC) of  $[C_{10}\text{mim}]\text{Cl}$  in the potassium phosphate buffer with and without the presence of

the substrate *p*-nitrophenyl laurate (*p*-NFL) were determined by electric conductivity ( $\text{mS}\cdot\text{cm}^{-1}$ ) measurements (Figure 1). Considering the CMC results in the presence (red diamonds) and absence (blue triangles) of the substrate, it is shown that the *p*-NFL significantly contributes to lower the system CMC. A comparison of the relative enzyme activity and conduc-

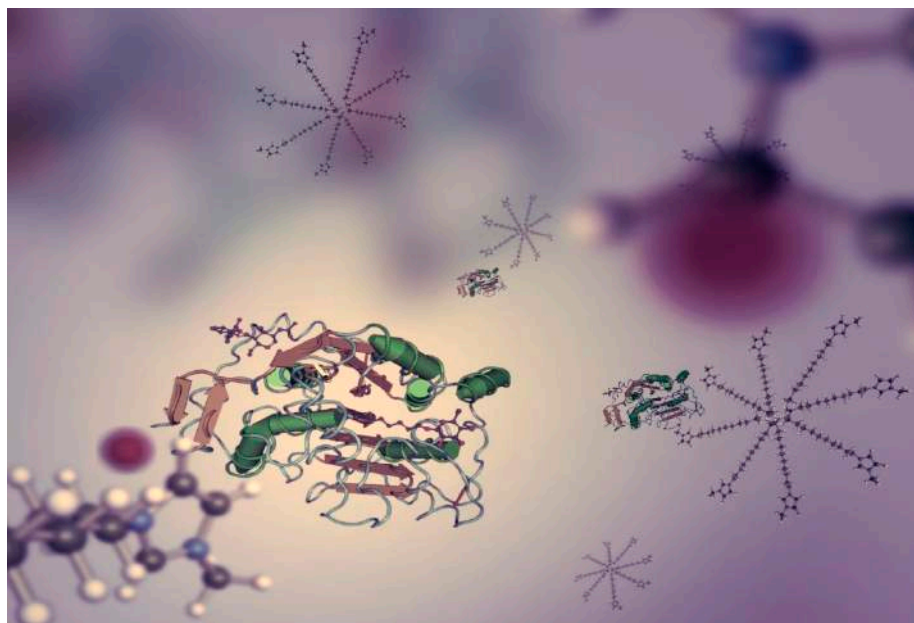


Figure 2. Illustration of the lipase in a microemulsion environment.

## SCALE-UP STUDIES OF THE SUPERCRITICAL FLUID EXTRACTION OF TRITERPENOIDS FROM EUCALYPTUS BARK

Melo MMR<sup>1</sup>, Silvestre AJD<sup>1</sup>, Silva CM<sup>1</sup>

The supercritical fluid extraction (SFE) of *Eucalyptus globulus* bark has been studied in order to produce *green* extracts enriched in triterpenic acids (TTAs) such as ursolic, oleanolic and betulinic acids (see

Figure 1)<sup>[1-4]</sup>. Recently we are focusing scale-up studies, by performing modeling and experiments at three different scales: nominal volumes of 0.5, 5.0 and 80.0 L

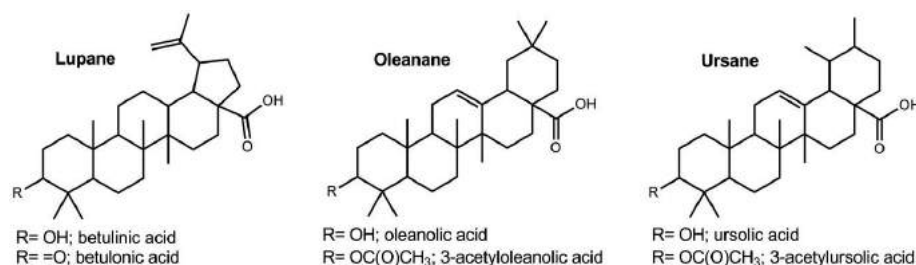


Figure 1. Main triterpenic acids found in the extracts of *E. globulus* bark.

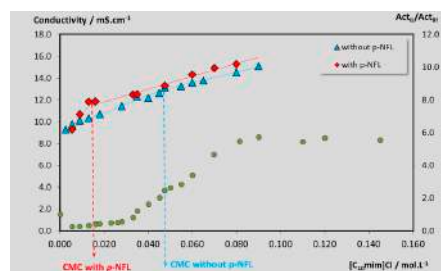


Figure 1. Relative enzyme activity of CaLB as function of the IL molar concentration and effect of the substrate (*p*-NFL) on the conductivity and CMC of  $[C_{10}\text{mim}]\text{Cl}$  aqueous solutions.

tivity data, presented in Figure 1, shows that the increase of  $\text{Act}_{\text{II}}/\text{Act}_{\text{BI}}$  is observed for molar concentrations of  $[C_{10}\text{mim}]\text{Cl}$  above the CMC for the system with the substrate *p*-NFL.

The behavior reported here is being studied as the basis for novel methodologies of enzyme activation using aqueous solutions of ionic liquids.

<sup>1</sup> Department of Chemistry, CICECO, University of Aveiro, 3810-193 Aveiro, Portugal

<sup>2</sup> Department of Chemistry, QOPNA, University of Aveiro, 3810-193 Aveiro, Portugal

### Reference

[1] Ventura SPM, Santos LDF, Saraiva JA, Coutinho JAP, *Green Chemistry*, 2012, 14, 1620-16-25.

(see Figure 2); the higher units belong to Natex, our industrial partner<sup>[5]</sup>.

The operating conditions of the SFE (pressure, temperature, ethanol content, and  $\text{CO}_2$  mass flow rate) have been optimized at lab scale (0.5 L) using design of experiments and response surface methodologies combined with phenomenological

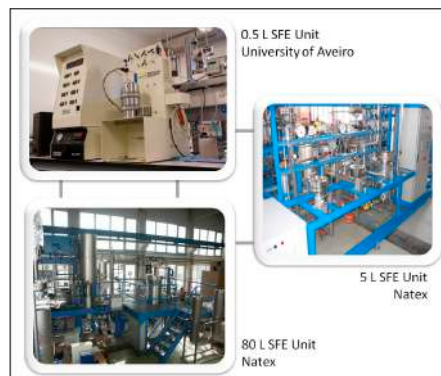


Figure 2. Supercritical fluid extraction units used in the scale-up studies.

modelling [3,4,6]. Several extraction curves have also been measured and modelled with the objective to disclose the dominant mechanisms of the process. The Logistic, Desorption, Simple Single Plate, and Diffusion equations have been selected for the calculations, and the higher adequacy of the last two expressions pointed that the intraparticle diffusion controls the separation [4]. In view of these results, the ratio between the  $\text{CO}_2$  flow rate and the bark weight was fixed in  $10 \text{ h}^{-1}$ , being established as the appropriate scale-up

criterion. The remaining variables were 200 bar,  $40^\circ\text{C}$ , 2.5 wt.% ethanol. The alcohol plays an important role, since it improves the affinity of TTAs to the supercritical solvent, increases the extraction yield, and thus allows lower operating pressure.

The total extraction yield and the TTAs concentration in the extracts obtained at 0.5, 5.0 and 80.0 L are plotted in Figure 3. The results evidence good agreement, therefore confirming the validity of the adopted scale-up criterion and the techni-

cal viability of the process at commercial scale. In the whole, the scale-up results are essentially concordant, taking into account that they were obtained using three units with distinct geometries, packing efficiency, and operators.

<sup>1</sup> Department of Chemistry, CICECO, University of Aveiro, 3810-193 Aveiro, Portugal

#### References

- [1] Domingues RMA, Oliveira ELG, Freire CSR, Couto RM, Simões PC, Neto PC, Silvestre AJD, Silva CM, *International Journal of Molecular Sciences*, 2012, 13, 7648-7662.
- [2] Melo MMR, Oliveira ELG, Silvestre AJD, Silva CM, *The Journal of Supercritical Fluids*, 2012, 70, 137-145.
- [3] Domingues RMA, Melo MMR, Oliveira ELG, Neto CP, Silvestre AJD, Silva CM, *The Journal of Supercritical Fluids*, 2013, 74, 105-114.
- [4] Domingues RMA, Melo MMR, Neto CP, Silvestre AJD, Silva CM, *The Journal of Supercritical Fluids*, 2012, 72, 176-185.
- [5] NATEX Prozesstechnologie GesmbH ([www.natex.at](http://www.natex.at)).
- [6] Melo MMR, Silvestre AJD, Silva CM, *The Journal of Supercritical Fluids*, 2014, 92, 115-176.
- [7] Melo MMR, Domingues RMA, Sova M, Lack E, Seidlitz H, Lang JRF, Silvestre AJD, Silva CM, *The Journal of Supercritical Fluids*, submitted.

#### Acknowledgments

We acknowledge Associate Laboratory CICECO (Pest-C/CTM/LA0011/2013) and the 7<sup>th</sup> Framework Programme FP7/2007-2013 for funding project AF0RE (CP-IP 228589-2).

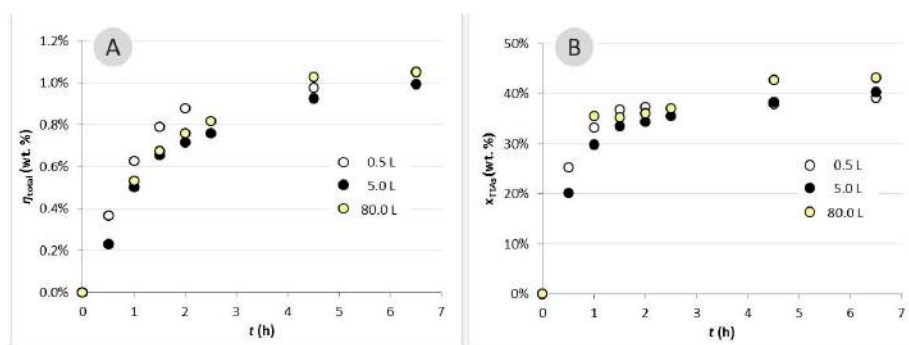


Figure 3. Cumulative curves of (A) total extraction yield and (B) TTAs concentration for the SFE of *E. globulus* bark at pilot (80.0 L), intermediate (5.0 L) and lab (0.5 L) scales. Operating conditions: 200 bar,  $40^\circ\text{C}$ , 2.5 wt.% ethanol,  $\theta_{\text{CO}_2}^{-1} w_{\text{bark}}^{-1} = 10 \text{ h}^{-1}$  [7].



# **Biorefineries and Materials from Renewable Sources**

## 2<sup>nd</sup> GENERATION BIOETHANOL PRODUCTION FROM DIFFERENT LIGNOCELLULOSIC RESIDUES

Pereira SR<sup>1</sup>, Fernandes MC<sup>2</sup>, Gorwa-Grauslund MF<sup>3</sup>, Evtugun DE<sup>1</sup>, Serafim LS<sup>1</sup>, Xavier AMRB<sup>1</sup>

According to the directive 2009/28/EC, biofuels should comprise at least 10 % of transport fuel in every Member State of European Union in 2020. In Portugal there is a search for bioethanol production in order to blend it with gasoline from the next year. Bioethanol is one of the most attractive biofuels and can be obtained from renewable lignocellulosic feedstocks, contributing to the decrease of fossil fuels dependence and the reduction of CO<sub>2</sub> build-up. Also, environmental concerns about the removal of industrial by-products and wastes are increasing the search for biotechnological integrated processes with the objective of obtaining their valorisation and economical profit via biorefinery namely by bioethanol production. Three different lignocellulosic residues produced in Portugal were tested for 2<sup>nd</sup>

generation bioethanol production, the first from paper pulp industry, the second from a winery and the third from forest managing to prevent forest fires.

Hardwood spent sulphite liquor (HSSL) is the main effluent resulting from the acidic sulphite pulping process and produced in large amounts. Besides other compounds HSSL is rich in monosaccharides that can be fermented to bioethanol by *Scheffersomyces stipitis*. Two different strategies were studied: the first one was focused in the bio-detoxification of HSSL with *Paecilomyces variotii* that would allow *S. stipitis* to grow in HSSL [1]. At the same time the fungal biomass produced was analysed for single-cell protein production. The second approach consisted in the adaptation of *S. stipitis* to the HSSL without the detoxification step. The

obtained adapted population was then studied and compared with the parental strain in order to optimise bioethanol production.

The study of bioprocess microaerophilic conditions is being developed in order to promote a fermentative metabolism of *S. stipitis* for bioethanol production optimization.

The winemaking sector produces high amounts of by-products with significant economic potential. Bioethanol production from grape skins from white grape pomaces was studied. Sugars aqueous extraction provided an extract rich in hexoses and suitable for yeast fermentation. *Saccharomyces cerevisiae* batch fermentation was successful attaining bioethanol productivity of 1.34 g ethanol L<sup>-1</sup> h<sup>-1</sup> and a high yield of 0.51 g ethanol per gram of sugar [2].

Thermochemical pretreatment, saccharification and fermentation of *Cistus ladanifer* (rockrose) wildy grown in Alentejo were studied in order to valorize this forest residue. Rockrose was subjected to steam explosion treatment (SE) and a subsequent alkali treatment (SE-OH). Enzymatic hydrolysis of untreated, SE and SE-OH materials was compared. The biomass resulting from the best pretreatment was used for a comparative study in Separate Hydrolysis and Fermentation (SHF), and Simultaneous Saccharification and Fermentation (SSF) assays. Fermentation was carried out in SHF and SSF modes with SE-OH rockrose, commercial cellulase and cellobiase, showing that SSF process is more efficient than SHF process with an overall efficiency of 66%, allowing the production of 14.8 g/L of bioethanol with a productivity of 0.62 g L<sup>-1</sup> h<sup>-1</sup> after 24h of saccharification and simultaneous fermentation.

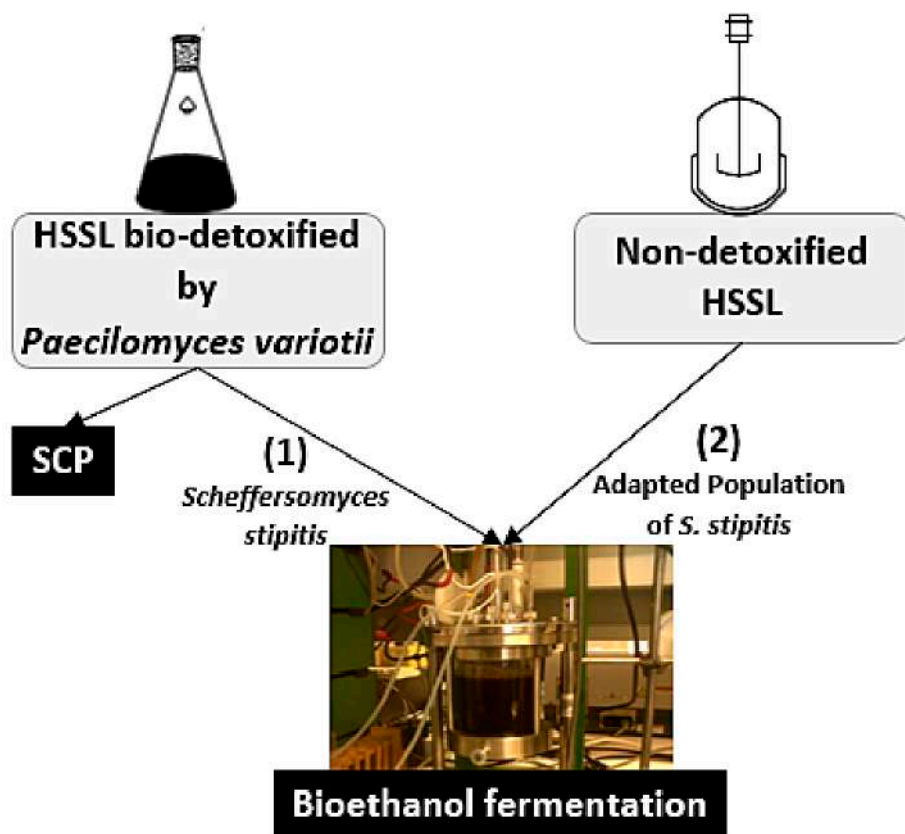


Figure 1. Bioethanol production from HSSL. Strategy 1: HSSL bio-detoxification by *Paecilomyces variotii* with production of single cell protein (SCP); Strategy 2: adaptation of *S. stipitis* to HSSL.

<sup>1</sup> Department of Chemistry, CICECO, University of Aveiro, 3810-193 Aveiro, Portugal

<sup>2</sup> Centro de Biotecnologia Agrícola e Agro-Alimentar do Alentejo (CEBAL)/ Instituto Politécnico de Beja, Portugal

<sup>3</sup> Division of Applied Microbiology, Department of Chemistry, Lund University, Sweden

### References

[1] Pereira SR, Ivanuša Š, Evtugun DV, Serafim LS, Xavier AMRB, *Bioresource Technology*, 2012, 103, 131–135.

[2] Mendes JAS, Xavier AMRB, Evtugun DV, Lopes LPC, *Industrial Crops and Products*, 2013, 49, 286–291.

## ADVANCED CELLULOSE/SILICA HYBRID MATERIALS

Evtuguin DV<sup>1</sup>, Portugal I<sup>1</sup>

Cellulosic fibres have been modified by a mild sol–gel process, at room temperature, using silicon alkoxides as silica precursors, an acidic catalyst and aqueous solution or aqueous organic solvents. Silica is deposited on the fiber surface as isolated or aggregated mesoparticles (0.1–2 μm diameter, Fig. 1.a) or as a discontinuous film comprising round-shape domains (0.05–0.3 μm, Fig. 1.b) depending on the synthesis conditions.<sup>[1]</sup> The strong hydrogen bonds formed between silica and the hydroxyl groups of cellulose create an impermeable interface that reduces water adsorption as revealed by the net isosteric heat of sorption.<sup>[2]</sup> Hence, cellulose silica hybrids (CSH) have lower hydrophilicity (expressed as water retention value) than the parent cellulosic fibers. At the same time, the presence of silica improves dimensional stability in water, fire resistance and bending strength. Altogether, these properties are appealing for packaging applications of CSHs materials that are being explored within the FP7 project nanobarrier.

The surface properties of CSHs may be radically changed if the silica formulations contain tetraethyl orthosilicate (TEOS) and smaller amounts of prehydrolyzed trialkoxysilanes bearing distinct functions (propylamine, allyl, alkyl, etc.). Some of these functionalities may be used to bind active substances (e.g. catalysts, sensors, scavengers, etc.) that widely expand the application areas of cellulosic hybrid materials. For instance CSHs possessing aminopropyl groups were examined as ion exchange materials for arsenates removal from aqueous solutions (in the range 26–172 μg As/L, at 25 fflC and pH 3.5) and revealed specific sorption properties that can be explored for water purification.<sup>[3]</sup> CSHs bearing amine groups chemically bonded to reversible redox catalysts such as polyoxometalates (Fig. 1.c) are suitable as barrier coatings, active filters, etc. In particular CSH materials functionalized with 2% of  $[\text{PMo}_{11}\text{VO}_{40}]^{4-}$  or  $[\text{PV}_2\text{Mo}_{10}\text{O}_{40}]^{5-}$  showed particularly high activity towards degradation of volatile organic compounds (VOC) present in urban and indoor air at

high concentration levels, thus anticipating future environmental applications.<sup>[4]</sup> Furthermore, the basic redox cycle of POM which includes VOCs oxidation via electron transfer and radical mechanisms, followed by room temperature catalyst re-oxidation with atmospheric O<sub>2</sub> (or O<sub>3</sub>), is easily visualized by CSHs colour change (from green to yellow) due to the reduction of vanadium atoms ( $\text{V}^{\text{V}} \rightarrow \text{V}^{\text{IV}}$ ).<sup>[4]</sup> In a further embodiment, 2–3 g/m<sup>2</sup> of silica-based formulations (*nanocoating*) were applied on the surface of paper sheets with a significant impact on surface properties related to printability. Adjusting the composition of the silica formulation enables the fine-tuning of surface microporosity and effective parameters (contact angle, surface energy and the corresponding polar and dispersive counterparts, among others) to improve colour reproduction and printing firmness (Fig. 2) when using both inkjet and

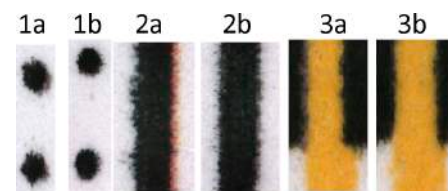


Figure 2. Ink jet printing tests of uncoated [series a] and DEDMS/TEAP/TEOS coated paper [series b]: firmness of point [1], firmness of line [2] and inter-color-bleeding [3]. [Silica formulation: 94% Tetraethoxysilane (TEOS) + 3% triethoxysilanaminopropyl (TEAP) + 3% diethoxydimethylsilane (DEDMS)]

laser printers. Thus paper surface modification by silica based formulations is suggested as a prospective tool for surface engineering towards tailored printing performance.

<sup>1</sup> Department of Chemistry, CICECO, University of Aveiro, 3810-193 Aveiro, Portugal

### References

- [1] Sequeira S, Evtuguin DV, Portugal I, Esculcas AP, *Materials Science and Engineering: C*, 2007, 27, 172–179.
- [2] Portugal I, Dias VM, Duarte RF, Evtuguin DV, *The Journal of Physical Chemistry B*, 2010, 114, 4047–4055.
- [3] Martins C, Duarte RF, Magalhães MCF., Evtuguin DV, *Materials Science Forum*, 2013, 730–732, 563–568.
- [4] Gamelas JAF, Evtugina MGI, Portugal I, Evtuguin DV, *RSC Advances*, 2012, 2 (3), 831–839.

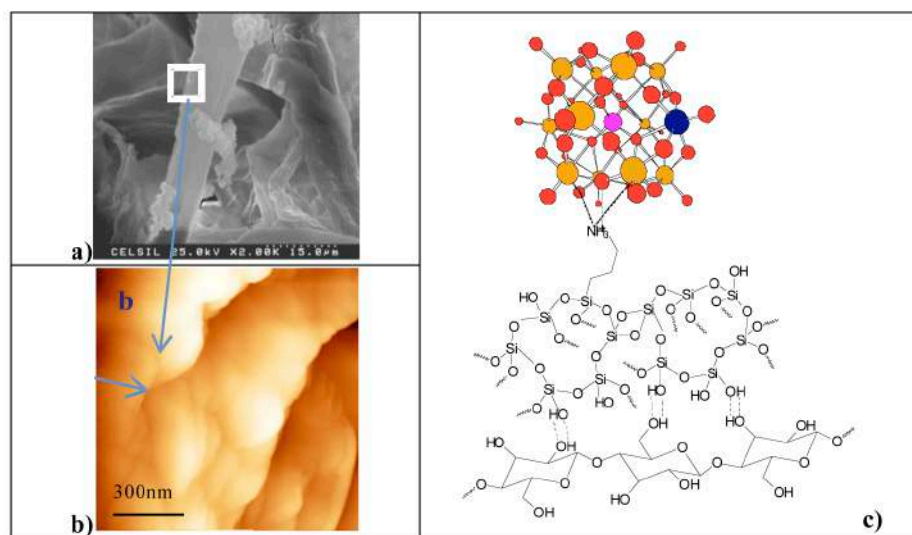
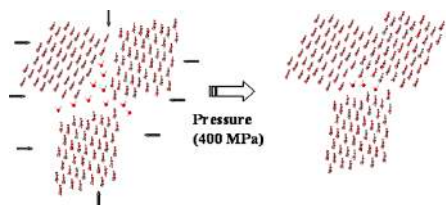


Figure 1. Cellulose/Silica Hybrids: (a) SEM image of cellulose fibres covered by silica; (b) the presence of a silica film was assessed by SEM/EDS and AFM applied in a tapping mode; covered by a silica film; (c) schematic representation of the cellulose chain bonded to a silica network functionalized with POM.

## TARGETED MODIFICATION OF CELLULOSIC MATERIALS USING ULTRAHIGH PRESSURE PROCESSING

Evtugin DV<sup>1</sup>, Saraiva JA<sup>2</sup>

Ultra high pressure (UHP) technology has been applied for many years in the production of ceramics, composite materials, plastics, artificial diamonds and is an expanding tool in food preservation and processing. Recently UHP was applied for the first time to the modification of physical structure of cellulosic fibres.<sup>1</sup> UHP treatment of pulps is pronouncedly endothermic, which explained by cleavage of strong hydrogen bonds between inaccessible cellulose surfaces since the free hydration enthalpy is lower than the enthalpy of intermolecular bounding between them. Hence, the treatment at high hydrostatic pressure opens initially inaccessible cellulose surfaces introducing water molecules that impossible to



**Figure 1.** Schematic representation of cross-section of microfibril assembled by three elementary fibrils. The hyperbaric treatment promotes the aggregation of appropriately oriented crystallites. Some water is trapped in internal cavities of fibril aggregates remaining upon drying (strongly bound water).

remove upon drying (strongly bound water) (Fig. 1). It was revealed that UHP treatment (200–500 MPa during 10–20 min) causes provided the rearrangement of elementary fibrils (EF) in a way that those became highly hydrated (contained increased amount of strongly bound water released at temperatures superior than 300 °C), thus promoting the fibrils disintegration and the accessibility of cellulose surfaces. EFs, which surfaces are free of concomitant hemicelluloses and appropriately oriented, suffer partial junction of adjacent cellulose crystallites (cocrySTALLIZATION). These physical changes in cellulose domains are reflected in the improved physical and chemical properties of cellulosic fibers.<sup>[1]</sup> Thus UHP treatment has a pronounced effect on the internal swelling of fibres improving their flexibility and elasticity thus practically “smoothing” the hornification features. UHP treatment may be highly advantageous to fibre materials which papermaking properties are drastically deteriorated upon drying due to the hornification (recycled fibres, acidic sulphite, organosolv pulps, etc.).

UHP treatment allows controlled radical improvement (2–10 times) of hydrolysis

of cellulosic fibres by hydrolytic enzymes (cellulases and xylanases) and the reactivity towards chemical reagents.<sup>[2,3]</sup> The rate of enzymatic reactions can be regulated by the conditions of UHP pre-treatment (pressure, time and temperature). UHP pre-treatment combined with enzymatic hydrolysis by xylanase leads to gelation of cellulosic fibres in water (Fig. 2) thus

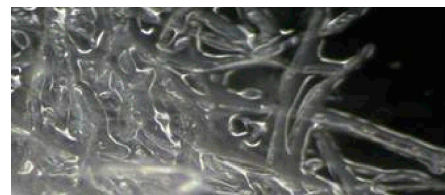


**Figure 2.** Optic microscope image of UHP-treated (400 MPa, 20 min) and xylanase hydrolyzed cellulosic fibres of *E. globulus* bleached kraft pulp.

allowing it easier disaggregation into fibrils/nanocrystals during the production of microfibrillated (MFC) by ultrahomogenisation and nanocrystalline celluloses (NCC) by acidic hydrolysis.<sup>[3]</sup>

<sup>1</sup> Department of Chemistry, CICECO, University of Aveiro, 3810-193 Aveiro, Portugal

<sup>2</sup> Department of Chemistry, QOPNA, University of Aveiro, 3810-193 Aveiro, Portugal

### References

- [1] Figueiredo A, Evtugin DV, Saraiva J, *Cellulose*, 2010, 17, 1193–1202.  
 [2] Ferreira ARFC, Figueiredo AB, Evtugin DV, Saraiva JA, *Green Chemistry*, 2011, 13, 2764–2767.  
 [3] Oliveira SCT, Figueiredo A, Evtugin DV, Saraiva JA, *Bioresource Technology*, 2012, 107, 530–534.

## POTENTIOMETRIC CHEMICAL SENSORS FROM LIGNIN-DERIVED NANOCOMPOSITES

Rudnitskaya A<sup>2</sup>, Evtugin DV<sup>1</sup>, Costa LC<sup>3</sup>, Graça MPF<sup>3</sup>, Correia MRP<sup>3</sup>, Fernandes AJS<sup>3</sup>

A set of technical lignins (modified kraft lignin (K), lignosulfonates (S) and organosolv lignin (OS)) doped with multi-walls carbon nanotubes (MWCNTs) were involved in step-growth polymerization with tolylene 2,4-diisocyanate terminated poly(propylene glycol) giving rise crosslinked elastomeric polyurethanes.

[1] Doping of lignin-based polyurethanes

with MWCNTs allowed radical enhancement of their electrical conductivity without significant deterioration of thermal and viscoelastic properties. The former polymer composites displayed low percolation threshold at MWCNT concentration of ca 0.18 % (w/w), which was explained by the oriented distribution of nanotubes along lignin clusters.

[1] Effect of the polymer interaction with MWCNTs was studied in more details using electrical impedance (EIS)<sup>[2,3]</sup> and UV-Resonance Raman (UV-RR) spectroscopy.<sup>[3]</sup> The percolation model theory was used to describe direct current (DC) and the low frequency behaviour, where the electrical conductivity and the dielectric constant were expressed by scaling laws near the threshold conduction. The dielectric analysis was carried out using the modulus formalism and the dielectric relaxation behaviour was modelled using the Cole–Cole expression.<sup>[2]</sup> Significant influence of the MWCNTs’

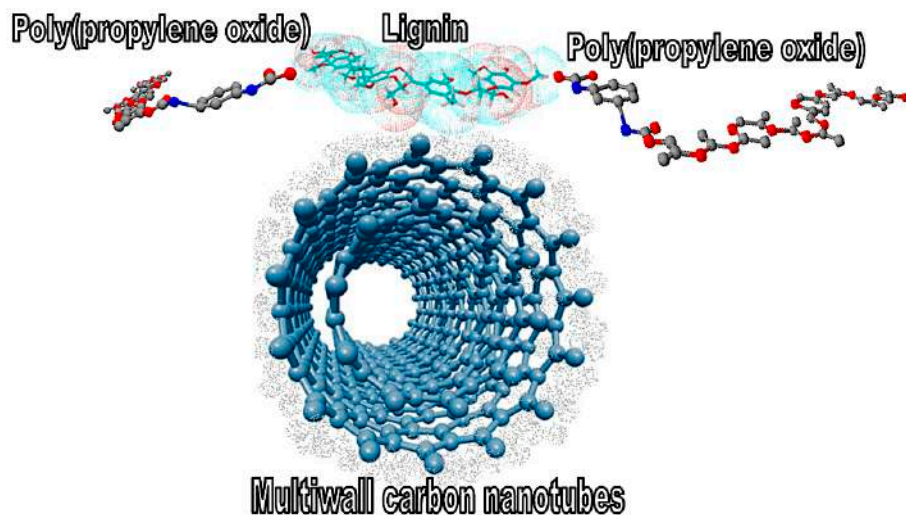


Figure 1. Schematic representation of lignin-MWCNT interaction in conductive polymer.

presence on the parameters of the low frequency relaxation process related to the polymer matrix indicated existence of the interaction between nanotubes and lignin, which affect dielectric properties of the polymer. According to results revealed by UV-RR spectroscopy, this interaction should be a  $\pi$ - $\pi$  stacking interaction between delocalized hybrid orbitals of aromatic ring and carbon nanotubes side wall leading to the increase of the electron delocalization and possibly change of lignin chain conformation allowing better  $\pi$ -overlap along the chain of lignin giving rise to the increased electric conductivity (Fig. 1).<sup>[3]</sup>

Potentiometric sensors were prepared by drop casting of liquid polymer on the surface of carbon glass or platinum electrodes. Lignin-based sensors displayed no or a very low sensitivity to all alkali, alkali-earth and transition metal cations except to Cr(VI) at pH 2 (Fig. 2).<sup>[3]</sup> Response to Cr(VI) of 39, 50 and 53 mV/pX for the sensors based on kraft, organosolv and lignosulphonates, respectively, was observed. Redox sensitivity close to theoretical of 20 and 21 mV/pX for organosolv and lignosulphonate based sensors respectively was detected in the Cr(III)/Cr(VI) solutions while a very low response was observed in the solutions

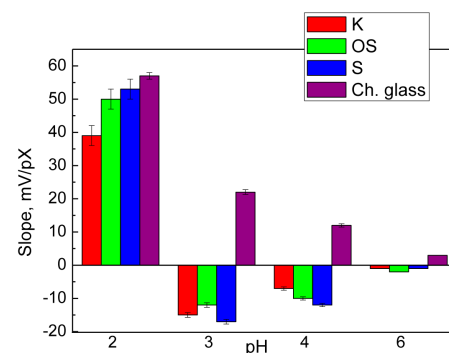


Figure 2. Sensitivity of lignin based polymeric sensors and chalcogenide glass Cr(VI)-selective electrode in the solutions of Cr(VI) at different pH.

containing  $\text{Fe}(\text{CN})_6^{3/4-}$ . Conducting composite lignin-based polyurethanes doped with MWCNTs were suggested to be promising materials for Cr(VI)-sensitive potentiometric sensors.

<sup>1</sup> Department of Chemistry, CICECO, University of Aveiro, 3810-193 Aveiro, Portugal

<sup>2</sup> Department of Chemistry, CESAM, University of Aveiro, 3810-193 Aveiro, Portugal

<sup>3</sup> Department of Physics, I3N, University of Aveiro, 3810-193 Aveiro, Portugal

#### References

- [<sup>1</sup>] Faria FAC, Evtuguin DV, Rudnitskaya A, Gomes MTSR, Oliveira JABP, Graça MPF, Costa LC, *Polymer International*, 2012, 61, 788-794.
- [<sup>2</sup>] Graça MPF, Rudnitskaya A, Faria FAC, Evtuguin DV, Gomes MTSR, Oliveira JABP, Costa LC, *Electrochimica Acta*, 2012, 76, 69-76.
- [<sup>3</sup>] Rudnitskaya A, Evtuguin DV, Costa LC, Graça LMPF, Fernandes AJS, Correia MRP, Gomes MTSR, Oliveira JABP, *Analyst*, 2013, 138, 501-508.

## GETTING VALUE FROM WASTES: BIOLOGICAL PRODUCTION OF BIODEGRADABLE PLASTICS

Queirós DC<sup>1</sup>, Xavier AMRB<sup>1</sup>, Evtuguin DE<sup>1</sup>, Rossetti S<sup>2</sup>, Serafim LS<sup>1</sup>

Several millions tons of synthetic plastics are discarded every year worldwide and only a small part can be recycled. For these reasons biodegradable materials obtained from renewable resources with similar properties are required. Polyhydroxyalkanoates (PHA) are a class of polymers with those characteristics with the additional advantage of being produced by a wide variety of microorganisms in their final form and their composition manipulated by choosing the appropriate substrate composition. Recently, the use

of industrial waste as nutrient source for PHA production attracted much attention, since substrates are a substantial contribution to production costs.

Two industrial wastes were tested as substrates for PHA production, namely hardwood spent sulfide liquor (HSSL) from pulp industry and grape skins from winery industry. HSSL is rich in xylose, acetic acid and phenolic compounds<sup>[1]</sup> and was tested as substrate to select a mixed microbial culture (MMC) collected in a wastewater treatment

plant under alternating conditions of feast and famine of carbon substrate.<sup>[2]</sup> MMCs are microbial communities with undefined composition enriched in PHA-storing organisms after being submitted to transient operational conditions under which polymer production ability represents a competitive advantage. GC analysis showed that the MMC produced poly-3-hydroxybutyrate (PHB) during the entire operational period reaching a maximum of 67.6% of cell dry weight.<sup>[2]</sup> Nile blue staining showed that the majority of bacteria were involved in PHA production (Fig. 1) and their characterization and identification by fluorescence *in situ* hybridization, and isolation are currently being attempted. The integration of PHA production within a HSSL based-biorefinery concept is being studied.<sup>[3]</sup>

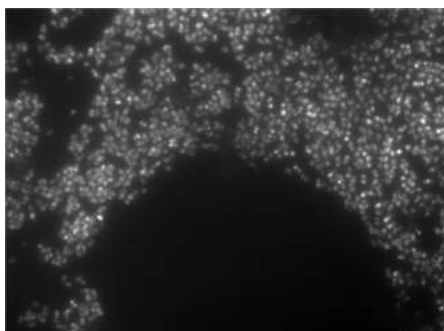


**Figure 1.** PHA granules stored intracellularly by MMC from HSSL observed under epifluorescence microscope after staining cells with Nile Blue.

Dried grape skins from white grapes were submitted to hot aqueous extraction and a sugar-rich mixture containing mainly glucose (75.0%) and mannose (21.9%) was obtained. The sugar-rich extract supplemented with essential nutrients was fed to a *Cupriavidus necator* strain that was able to grow, reaching a biomass concentration of 2.5 g/L, and accumulate 85.6% of PHAs of cell dry weight. FTIR analysis of the extracted polymer confirmed the production of PHB based on the characteristic pick profile.

<sup>1</sup> Department of Chemistry, CICECO, University of Aveiro, 3810-193 Aveiro, Portugal

<sup>2</sup> Water Research Institute, CNR, Monterotondo, Roma, Italy

#### References

[1] Pereira SR, Ivanusa S, Evtuguin DV, Serafim LS, Xavier AMRB, *Bioresource Technology*, 2012, 103, 131-135.

[2] Queiros DC, Rossetti S, Serafim LS, *Bioresource Technology*, 2014, 157, 197-205.

[3] Serafim LS, Hus S, Passos H, Lemos PC, Evtuguin D, Xavier AMRB, *Journal of Biotechnology*, 2010, 150, S264.

## PLANT OIL-BASED LONG-CHAIN MONOMERS AND THEIR POLYMERS

Vilela C<sup>1</sup>, Silvestre AJD<sup>1</sup>, Meier MAR<sup>2</sup>

Interest in monomers and polymers from renewable resources is increasing progressively, as part of the general awareness for sustainability. Among the numerous renewable resources used to generate macromolecular materials, plant oils occupy a leading position, as

evidenced by the growing research activities over the last several years,<sup>[1-3]</sup> mainly due to their ubiquitous availability and reactive functionalities.

Our research interest relies on the idea of exploring plant oil and its derivatives as building blocks in the synthesis of 100%

renewable aliphatic long-chain polyesters.

[4] For this purpose, erucic acid, a monounsaturated  $\omega$ -9 fatty acid readily available from rapeseed oil, was efficiently self-metathesized (and hydrogenated) to the linear saturated long-chain  $\alpha,\omega$ -dicarboxylic acid. The subsequent direct polycondensation of stoichiometric amounts of the previous C26 diacid with its corresponding C26 diol (obtained from the diacid via reduction), proved to be a straightforward method to prepare aliphatic long-chain polyesters that are 100% renewable. Their properties were investigated by means of various techniques, revealing high crystallinity, melting and degradation temperatures.

The possible biodegradability of the polyesters together with their renewable origin make them attractive candidates to be used as surrogate of polyethylene or other polyolefins in some specific applications.

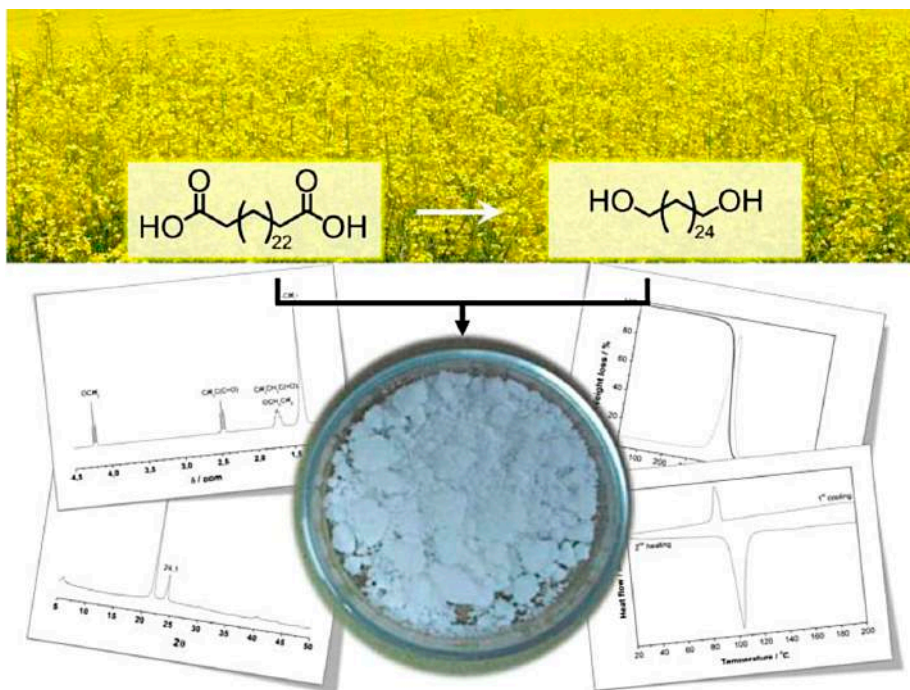


**Figure 1.** This work was front cover of issue 21/2012 on *Macromolecular Chemistry and Physics*, and was featured on *Materials Views*.

<sup>1</sup> Department of Chemistry, CICECO, University of Aveiro, 3810-193 Aveiro, Portugal

<sup>2</sup> Karlsruhe Institute of Technology (KIT), Institute of Organic Chemistry, 76131 Karlsruhe, Germany

#### References

[1] Vilela C, Sousa AF, Fonseca AC, Serra AC, Coelho JFJ, Freire CSR, Silvestre AJD, *Polymer Chemistry*, 2014, 5, 3119-3141.

[2] Lligadas G, Ronda JC, Galà M, Cádiz V, *Materials Today*, 2013, 16, 337-343.

[3] Biermann U, Bornscheuer U, Meier MAR, Metzger JO, Schäfer HJ, *Angewandte Chemie International Edition*, 2011, 50, 3854-3871.

[4] Vilela C, Silvestre AJD, Meier MAR, *Macromolecular Chemistry and Physics*, 2012, 213, 2220-2227.

#### Acknowledgments

FCT and POPH/FSE are acknowledged for the doctorate grant to C. Vilela [SFRH/BD/44884/2008] and for Associate Laboratory CICECO funding [PEst-C/CTM/LA0011/2013].

## TWO STEPS FORWARD IN THE DEVELOPMENT OF FURAN-BASED POLYESTERS

Sousa AF<sup>1,2</sup>, Matos M<sup>1</sup>, Freire CSR<sup>1</sup>, Silvestre AJD<sup>1</sup>, Coelho JFJ<sup>2</sup>

Polymer research based on renewable feedstocks has been asleep since the early years of polymer science, back in the 19th century, but in recent years it has emerged with a renewed strength. The demand for sustainable alternatives to fossil resources is motivating both scientific and industrial communities to turn back their attention to polymers from renewable resources. Indeed, the number of polymers partially or entirely renewable-based already commercialized, or which will be in a very near future, is increasing very fast. Poly(ethylene 2,5-furandicarboxylate)-PEF, due to its resemblance to the well-known poly(ethylene terephthalate) - PET, is one of the most promising renewable-based polyesters. However, the replacement of petroleum-based PET with PEF renewable counterpart, gives rise to a first question related with economical issues and cost-competitiveness. Indeed, in this matter any renewable chemical causes the very same question 'which is less expensive precursor of these polyesters petrole-

um-based terephthalic acid or renewable-based 2,5-furandicarboxylic acid (FDCA)?' A second relevant issue to any polymer is (bio)degradability, indeed a second question could be posed 'how to enhance (bio) degradability of FDCA-based polymers or any aromatic-like polyester?'

The present study<sup>[1,2]</sup> was conducted with the specific aim of answering to the above two questions (Figure 1). Therefore, in a first step, having in consideration that currently renewable-based chemicals are still expensive, one logical approach was to progressively replace PET with its furanic homologue, PEF, copolymerising them. A second step taken was to copolymerise PEF with a (bio)degradable aliphatic precursor which has introduced (bio)degradability properties to the ensuing copolyesters. Poly(lactic acid) (PLA) due to its high versatility, (bio)degradability and biocompatibility; besides being an aliphatic polyester obtained from renewable feedstocks, was the aliphatic counterpart chosen. These copolyesters

have been synthesised by polytransesterification reactions and characterised in detail. They displayed interesting thermal and mechanical properties showing to be adequate candidates to replace fossil-based counterparts. The PET-co-PEF copolyester incorporating 20% of renewable furanic units showed very similar properties to commercial PET, displaying glass transition, crystallisation and melting temperatures at 62.4, 125.2 and 220.1 °C, respectively; and thermal stability up to 260 °C. The operating temperature ranges (*c.a.* -40.9 to 67.5 °C) determined by DMA were very close to those of PET. PEF-co-PLA copolyester incorporating only 8% of lactyl units showed to have enhanced degradability compared both to PEF and to PET, and at the same time displayed very high degradation and glass transition temperatures (*c.a.* 324 and 76 °C, respectively) like its PEF homologue. The properties of PET-co-PEF and PEF-co-PLA open the way to the development of an entirely new generation of commodity polymers which are based on renewable resources and which are (bio)degradable. Hence, the next step forward is to go on exploring the realm these furanic copolyesters with emphasis on their potential applications.

<sup>1</sup> Department of Chemistry, CICECO, University of Aveiro, 3810-193 Aveiro, Portugal

<sup>2</sup> Department of Chemical Engineering, University of Coimbra, 3030-290 Coimbra, Portugal

### References

[1] Sousa AF, Matos M, Freire CSR, Silvestre AJD, Coelho JFJ, *Polymer*, 2013, 54, 513-519.

[2] Matos M, Sousa AF, Fonseca AC, Freire CSR, Coelho JFJ, Silvestre AJD, *Macromolecular Chemistry and Physics*, 2014, in press. DOI: 10.1002/macp.201400175.

### Acknowledgments

This work was financed by FEDER funds through the Operational Factors of competitiveness Programme-COMPETE and national funds through FCT under the CICECO project FCOMP-01-0124-FEDER-037271 (Ref. FCT Pest -C/CTM/LA0011/2013).

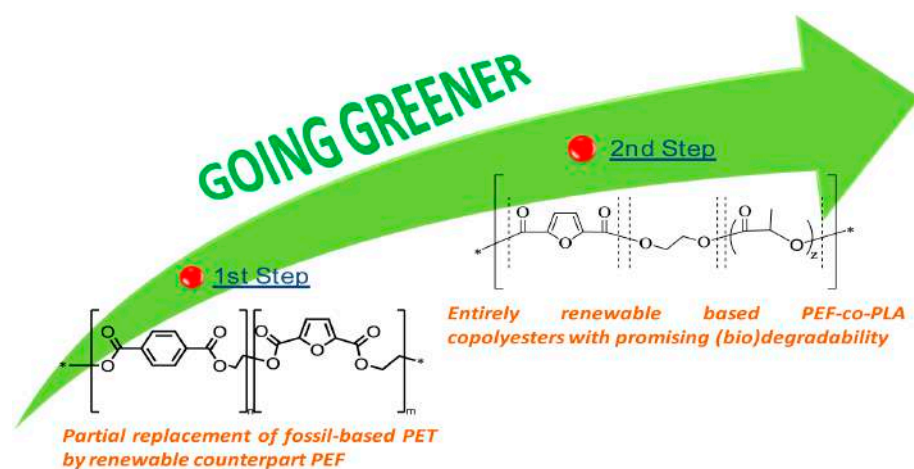


Figure 1. Two steps forward in furan-based polyesters.



# Biomedical Materials and Applications

## SLOW RELEASE OF NO BY MICROPOROUS TITANOSILICATE ETS-4

Pinto ML<sup>1,2</sup>, Rocha J<sup>1</sup>, Gomes RJB<sup>1</sup>, Pires J<sup>2</sup>

Nitric oxide (NO) acts as an important agent in the body for expanding blood vessels (its role in Viagra and related medicines for erectile dysfunction), preventing the formation of blood clots, aiding nerve signals, and repairing wounds. NO's multipurpose role makes it an exciting prospect for new drug development, but current NO delivery systems sometimes

cause undesirable side effects. Besides good NO adsorption capacity, materials must also present an appropriate releasing kinetics, to maintain a given concentration in the surrounding milieu. Often, a slow releasing kinetics is preferred because it allows for easier and safer control of the NO concentration, for longer periods. Clearly, new materials and technolo-

gies are needed to store and target-deliver NO in biological amounts. A novel approach to design nitric oxide storage and releasing microporous agents based on very stable, zeolite-type silicates possessing framework unsaturated (e.g., pentacoordinated Ti<sup>4+</sup>) transition-metal centers has been proposed<sup>[1]</sup>. This idea has been illustrated with ETS-4 [Na<sub>9</sub>Si<sub>12</sub>TiO<sub>38</sub>(OH)·xH<sub>2</sub>O], a titanosilicate (Fig. 1a) which displays excellent NO adsorption capacity and a slow relea-

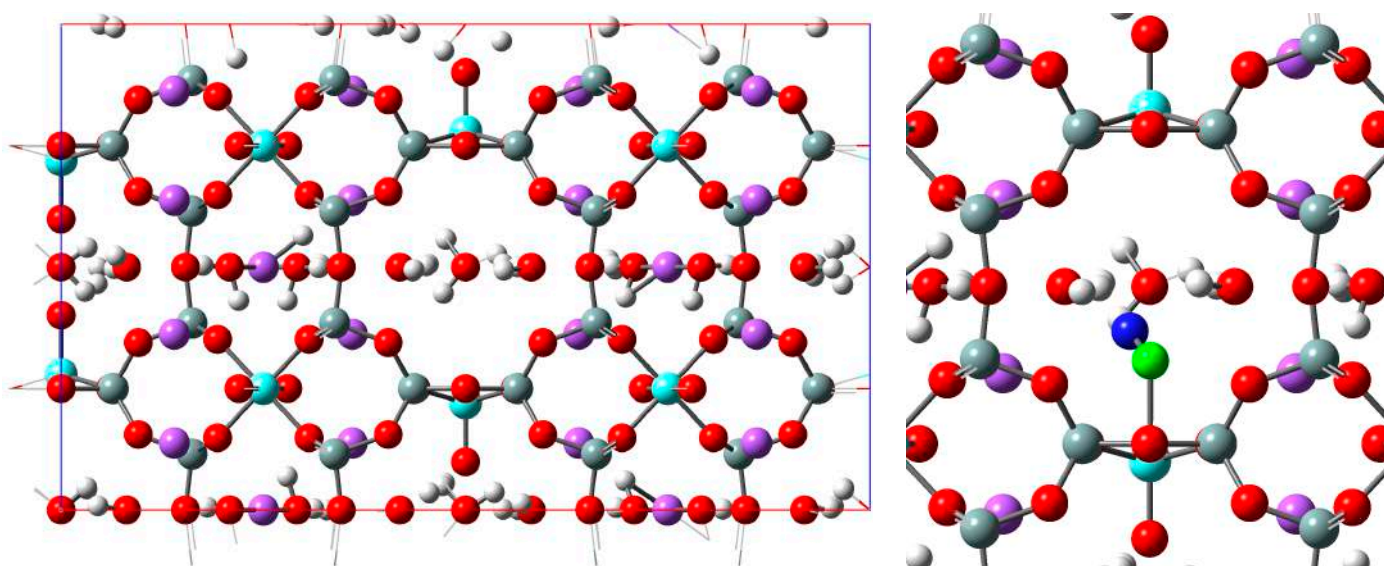


Figure 1. (Left) Model of the structure of ETS-4 used in the DFT calculations; (Right) coordination of NO to the pentacoordinated Ti<sup>4+</sup> centre. Colored spheres represent atoms of sodium (purple), hydrogen (white small), oxygen (red), silicon (grey) and titanium (cyan); NO: oxygen (dark blue), nitrogen (green).

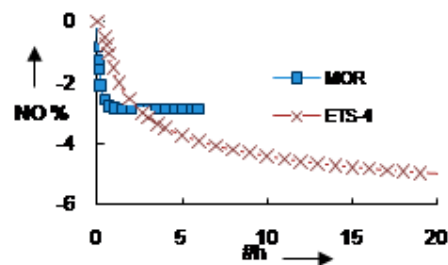


Figure 2. Kinetic profiles of NO desorption on the studied adsorbent materials, in high vacuum at 25 °C, after adsorption at 80 kPa.

gies are needed to store and target-deliver NO in biological amounts.

A novel approach to design nitric oxide storage and releasing microporous agents based on very stable, zeolite-type silicates possessing framework unsaturated (e.g., pentacoordinated Ti<sup>4+</sup>) transition-metal centers has been proposed<sup>[1]</sup>. This idea has been illustrated with ETS-4 [Na<sub>9</sub>Si<sub>12</sub>TiO<sub>38</sub>(OH)·xH<sub>2</sub>O], a titanosilicate (Fig. 1a) which displays excellent NO adsorption capacity and a slow relea-

ting kinetics (Fig. 2). The performance of these materials has been compared with the performance of titanosilicate ETS-10, [(Na,K)<sub>2</sub>Si<sub>5</sub>TiO<sub>13</sub>·xH<sub>2</sub>O], of benchmark zeolites mordenite and CaA, and of natural and pillared clays. DFT periodic calculations have shown that the presence of water in the pores of ETS-4 promotes the NO adsorption at the unsaturated (pentacoordinated) Ti<sup>4+</sup> framework ions (Fig. 1b). The ability of ETS-4 to release biologically relevant NO amounts was tested using the oxyhemoglobin method, which is based on the principal reaction of oxyhemoglobin with NO to form methemoglobin and

<sup>1</sup> Department of Chemistry, CICECO, University of Aveiro, 3810-193 Aveiro

<sup>2</sup> Departamento de Química e Bioquímica e COB, Faculdade de Ciências da Universidade de Lisboa, 1749-016 Lisboa

### Reference

[1] Pinto ML, Rocha J, Gomes RJB, Pires J, *Journal of the American Chemical Society*, 2011, 133, 6396–6402.

# QUANTIFYING WEAK PACKAGING INTERACTIONS IN THE HYDRATED AND ANHYDROUS FORMS OF ANTIBIOTIC CIPROFLOXACIN

Mafrá L<sup>1,2</sup>, Santos SM<sup>1</sup>, Siegel R<sup>1</sup>, Alves I<sup>1</sup>, Paz FAA<sup>1</sup>, Dudenko D<sup>2</sup>, Spiess HW<sup>2</sup>

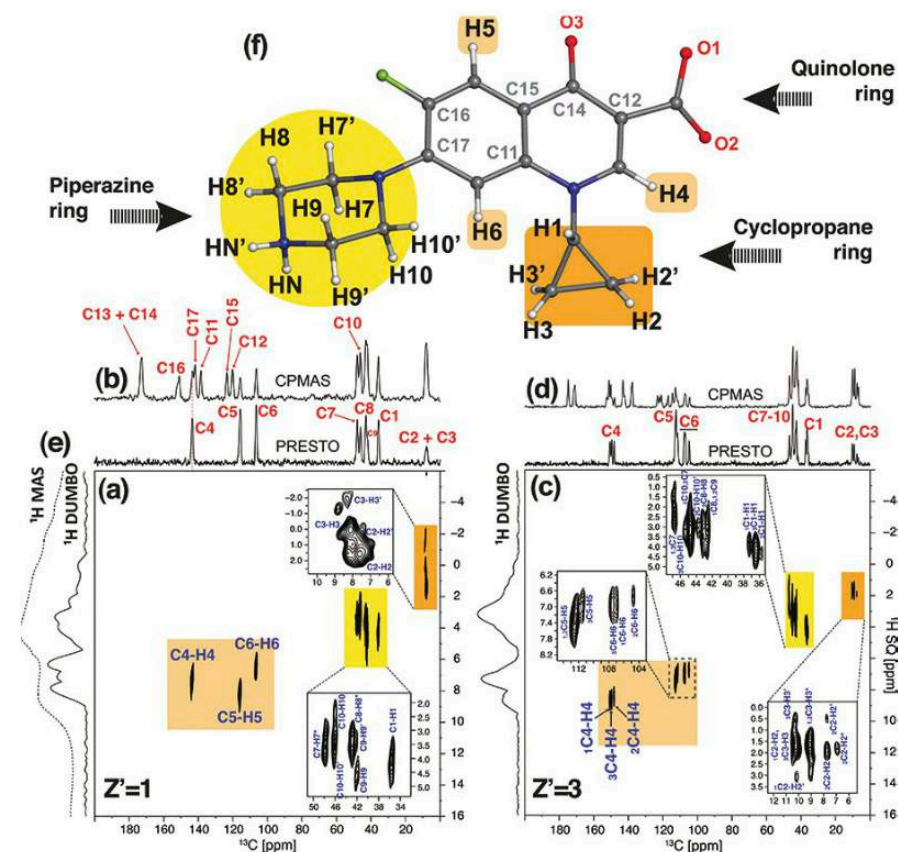


**Figure 1.** 2D  $^1\text{H}$ – $^{13}\text{C}$  PRESTO-HETCOR of ciprofloxacin forms (a) I and (c) II recorded at 800 MHz. (b, d)  $^{13}\text{C}$  CPMAS spectra recorded at 400 MHz. (e)  $^1\text{H}$  MAS and wDUMBO spectra of I are shown for comparison with the F1 projection of (a). (f) Labelling scheme adopted for ciprofloxacin. The capability of PRESTO transfer to select only the directly bonded C–H is manifested by comparison with the  $^{13}\text{C}$  CPMAS spectra [i.e., (a, c) vs. (b, d)]

Understanding how molecular systems self-assemble in the solid-state remains a challenge. In this regard, H bonding and van der Waals interactions play major roles as structure-driving entities in the construction of supramolecular arrangements. This is of particular relevance in pharmaceutical sciences, as multiple crystal forms of the same active pharmaceutical ingredient occur frequently, posing diverse problems in the pharmacokinetics, stability, and formulation of drugs.

In an attempt to better understand how drug hydrates self-assemble in the solid-state and reorganize to produce anhydrous forms, we presented a comprehensive NMR, X-ray diffraction (XRD), and computational study of packing interac-

tions of different types, such as weak/strong H-bonds and  $\pi$ – $\pi$  interactions,

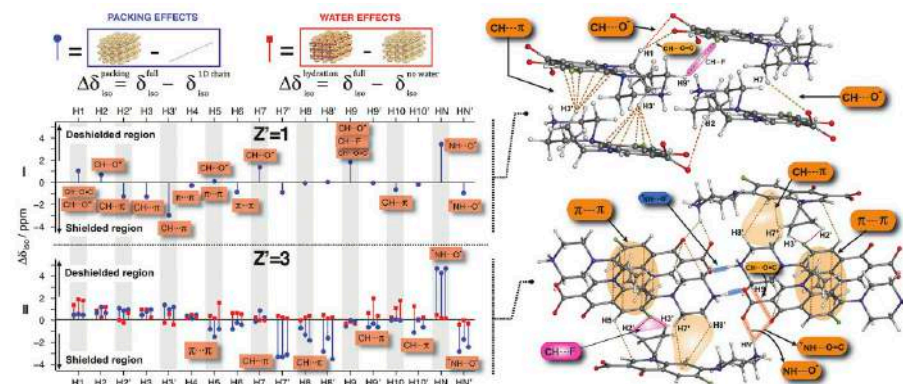


**Figure 2.** (Left) Stem plots showing the contribution of the crystal packing (blue stems) and water molecules (red stems) to the calculated  $^1\text{H}$  chemical shifts (positive  $\Delta\delta$  values indicate low-field shifts) of the ciprofloxacin forms I and II. In II, each of the three stems per nuclei corresponds to the crystallographically distinct ciprofloxacin molecules 1, 2, and 3 (from left to right); [right] detailed view of intermolecular interactions in packings of I and II.

that constitute the supramolecular assemblies of two crystalline forms of the antibiotic ciprofloxacin (Figure 1f)<sup>[1]</sup>: one anhydrate (form I) and one hydrate (form II) forming water wormholes, emphasizing the effect of nonconventional hydrogen bonds and water on NMR chemical shifts. The complete assignment of up to 51 and 54 distinct  $^{13}\text{C}$  and  $^1\text{H}$  resonances for the hydrate was reported, using a toolbox of advanced high-resolution 2D  $^1\text{H}$  CRAMPS-based NMR experiments and high magnetic fields (Figure 1a–e) combined with GIPAW calculations of  $^1\text{H}$ / $^{13}\text{C}$  chemical shifts. The effect of crystal packing on the  $^1\text{H}$  and  $^{13}\text{C}$  NMR chemical shifts, including weak interionic hydrogen bonds and  $\pi$ – $\pi$  interactions, was quantified through *in silico* structure deconstruction of I and II (Figure 2). For example,  $^1\text{H}$  chemical shift changes up to *ca.*  $-3.5$  ppm for  $\text{CH}\cdots\pi$  contacts and *ca.*  $+2$  ppm ( $\text{CH}\cdots\text{O}^{(-)}$ ); *ca.*  $+4.7$  ppm ( $^{(+)}\text{NH}\cdots\text{O}^{(-)}$ ) were estimated for hydrogen bonds. Water intake induced chemical shift changes up to 2 and 5 ppm for  $^1\text{H}$  and  $^{13}\text{C}$  nuclei, respectively. We showed that such chemical shifts are sensitive detectors of hydration/dehydration in the highly insoluble ciprofloxacin hydrates.

<sup>1</sup> Department of Chemistry, University of Aveiro, CICECO, 3810-193 Aveiro, Portugal

<sup>2</sup> Max-Planck-Institut für Polymerforschung, Ackermannweg 10, 55128 Mainz, Germany

## Reference

[1] Mafrá L, Santos SM, Siegel R, Alves I, Paz FAA, Dudenko D, Spiess HW, *Journal of the American Chemical Society*, 2012, 134, 71–74.

# BACTERIAL CELLULOSE AS TRANSDERMAL DRUG DELIVERY SYSTEMS

Silva NHCS<sup>1</sup>, Silvestre AJD<sup>1</sup>, Freire CSR<sup>1</sup>, Neto CP<sup>1</sup>

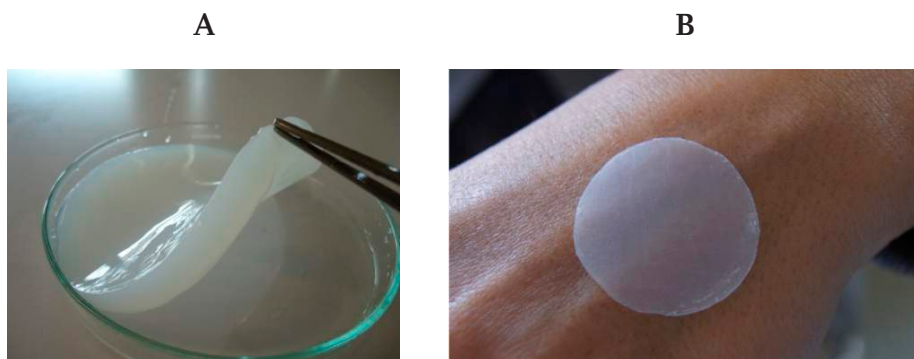


Figure 1. Visual image of a wet (A) and (B) drug loaded BC membrane applied over skin.

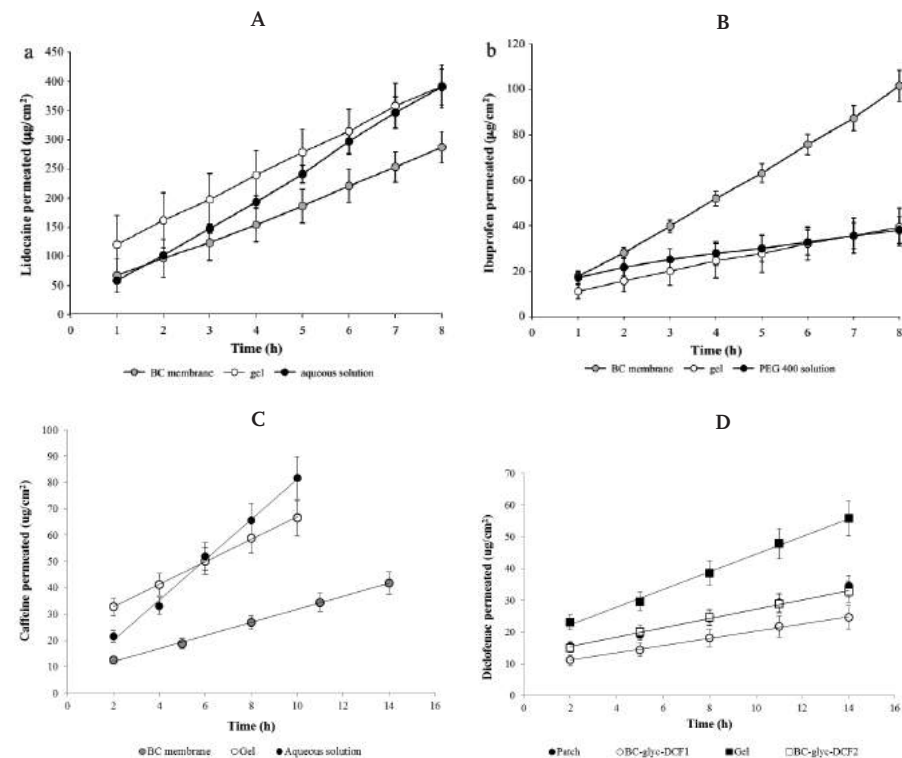


Figure 2. Drugs permeation profiles across human epidermis for A: lidocaine; B: ibuprofen; C: caffeine; D: diclofenac, compared with conventional formulations.

Cellulose is the most abundant biopolymer, and although it is mainly biosynthesized by plants, several bacteria (mainly of the *Gluconacetobacter* genus), can also produce an extra-cellular form of cellulose, commonly referred to as bacterial cellulose (BC), which is normally produced in the form of highly swollen

membranes. BC is obtained with high purity and shows remarkable properties, resulting from its unique tridimensional nanofibrillar structure, which have been explored in a wide range of applications<sup>[1]</sup>, notably in the biomedical field as wound healing membranes, scaffolds for tissue engineering, artificial blood vessels and

drug delivery systems. BC is particularly advantageous in the design of transdermal drug delivery systems because of the straightforwardness and effectiveness of preparation of the drug loaded BC membranes and the fact that they are only composed of a single layer. Furthermore, their ability to absorb exudates and to adhere to irregular skin surfaces, along with their conformability and intrinsic skin compatibility<sup>[2]</sup> are additional issues that are crucial for several clinical situations. In this vein BC membranes have been loaded by absorption of solutions of selected drugs (lidocaine<sup>[3-4]</sup>, ibuprofen<sup>[4]</sup>, caffeine<sup>[5]</sup> and diclofenac<sup>[6]</sup>), containing a few percent of glycerol (to improve flexibility of the membranes), followed by oven drying of the solvent. The drugs are uniformly distributed over the membranes, as confirmed by SEM analysis, and the *in vitro* skin permeation tests revealed that with the exception of ibuprofen, all the drugs have low permeation rates than conventional formulations [Figure 2], which is a clear advantage for situations where long term release of the drug is required. These results clearly demonstrate the potential of BC as a drug release system. New and promising perspectives might be opened with its testing on oral applications, particularly when combined in nanocomposite materials with other polymeric matrices.

<sup>1</sup> Department of Chemistry, CICECO, University of Aveiro, 3810-193 Aveiro

## References

- [1] Figueiredo ARP, Vilela C, Neto CP, Silvestre AJD, Freire CSR, *Bacterial cellulose based nanocomposites: a roadmap for innovative materials*, in: *Nanocellulose Polymer Nanocomposites: Fundamentals and Applications* (Kumar V. Ed.), Wiley, in press.
- [2] Almeida IF, Pereira T, Silva NHCS, Gomes FP, Silvestre AJD, Freire CSR, Sousa Lobo JM, Costa PC, *European Journal of Pharmaceutics and Biopharmaceutics*, 2014, 86, 332–336.
- [3] Trovatti E, Silva NHCS, Duarte IF, Rosado CF, Almeida IF, Costa P, Freire CSR, Silvestre AJD, Neto CP, *Biomacromolecules*, 2011, 12, 4162–8.
- [4] Trovatti E, Freire CSR, Pinto PC, Almeida IF, Costa P, Silvestre AJD, Neto CP, Rosado C, *International Journal of Pharmaceutics*, 2012, 435, 83–87.
- [5] Silva NHCS, Drumond I, Almeida IF, Costa P, Rosado CF, Neto CP, Freire CSR, Silvestre AJD, *Cellulose*, 2014, 21, 665–674.
- [6] Silva NHCS, Rodrigues AF, Almeida IF, Costa PC, Rosado C, Neto CP, Silvestre AJD, Freire CSR, *Carbohydrate Polymers*, 2014, 106, 264–269.

## Acknowledgments

FCT and POPH/FSE are acknowledged for the Associate Laboratory CICECO funding [PEst-C/CTM/LA0011/2013].

## PHOTOTHERMALLY ENHANCED DRUG RELEASE BY HYDROGELS REINFORCED WITH CARBON NANOTUBES

Estrada AC<sup>1</sup>, Daniel-da-Silva AL<sup>1</sup>, Trindade T<sup>1</sup>

One of the emerging strategies in drug delivery consists in the development of hydrogel carriers with remote controlled capabilities. The release of an encapsulated drug can be triggered remotely by external stimuli, providing a flexible control of the release rate and profile, according to the specific needs of the patient. Most studies on remotely triggered drug release have dealt with magnetically driven carriers upon the

exposure to an alternate magnetic field. Near-infrared (NIR) light is harmless and deeply penetrates in the living tissues, hence being an attractive stimulus source for remotely controlled bioapplications. Nevertheless the number of studies reporting NIR activated platforms for drug delivery is still modest. At the University of Aveiro, researchers from CICECO have succeeded in the fabrication of NIR responsive platforms

based on hydrogel nanocomposites. These composites comprised matrices of thermosensitive hydrogels reinforced with carbon nanotubes (CNTs), which absorb NIR light and convert the absorbed energy into heat very effectively. CNTs acted as multifunctional fillers by enhancing the mechanical properties of the hydrogels and conferring light responsive characteristics to the composites. The composite hydrogels showed reversible heat induced gel-to-sol phase transition, either by using temperature or NIR light irradiation as external stimuli. The release of a model drug from the hydrogels containing nanotubes could be induced by NIR irradiation, in which the CNTs acted as a nanoheater to raise the local temperature of the gel via the photothermal conversion of the CNTs.

In face of these promising results, these hydrogel composites are promising materials for the development of remotely controlled light activated drug delivery systems.

<sup>1</sup> Department of Chemistry, CICECO, University of Aveiro, 3810-193 Aveiro, Portugal

### Reference

[1] Estrada AC, Daniel-da-Silva AL, Trindade T, *RSC Advances*, 2013, 3, 10828-10836.

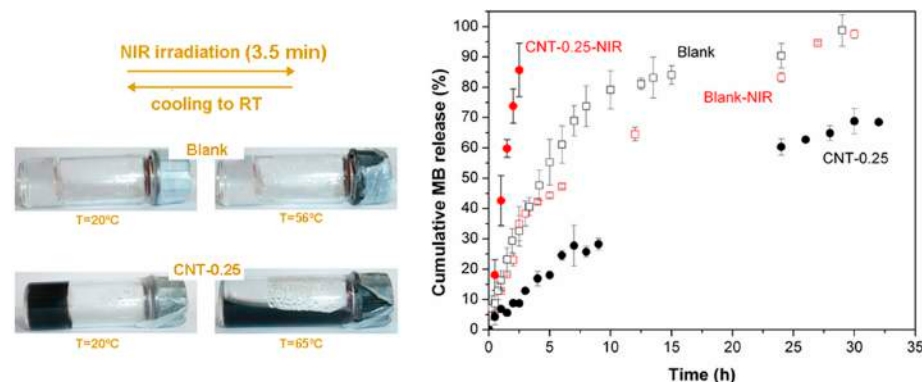


Figure 1. (left) Visual observation of the photoinduced gel-sol transition in hydrogels containing CNTs and (right) drug model release profiles in PBS at 37°C from the blank hydrogel and hydrogel composites, with and without exposure to NIR light.

## NOVEL BINUCLEAR COPPER COMPLEXES AS ALTERNATIVE ANTI-TUMORAL DRUGS: SYNTHESIS, CHARACTERISATION AND CYTOTOXIC STUDIES

Brandão P<sup>1</sup>, Ferreira, BJML<sup>1</sup>, Santos TM<sup>1</sup>, Meireles M<sup>2</sup>, Félix V<sup>1,3</sup>

Over the past decades, metal complexes have had enormous success as cytotoxic drugs against cancer related diseases. Cisplatin, cis-[Pt(NH<sub>3</sub>)<sub>2</sub>Cl<sub>2</sub>], is the paradigmatic example of a “small” transition metal complex which had been widely used as an anti-tumoral drug, particularly against testicular, ovarian, bladder, and head/neck tumours [1,2]. However, its effectiveness was early clouded by several undesirable side effects along with acquired drug resistance. This clearly

showed that selectivity and specificity are indeed the main keys to design and produce better and effective cytotoxic and anti-tumoral new drugs. Because of these drawbacks, the development of other anticancer metal-based drugs with more specificity and less toxicity is nowadays the object of the attention of a great number of researchers, who have directed their efforts towards the synthesis of polynuclear Pt, Ru, Rh, Pd, [3-5] and more recently to Au, Cu and Fe complexes [6-8],

which can overcome both the natural and the acquired resistance of human cancer cells to cisplatin and analogous drugs. Among this array of multi-metal centred complexes, those with copper have been much less explored, which seems to be a paradox taking into account the availability and bio-compatibility of both metals. A further benefit of the use of this metal is that is much cheaper than the “traditional” metals (platinum, ruthenium, rhodium and gold) currently used in the preparation of metal based anticancer agents.

Recent studies have demonstrated that certain dinuclear copper complexes showed much higher cleavage efficiency than their mononuclear analogues [9,10]. These recent findings prompted us to invest on the design of new polynuclear

transition metal complexes as an effort to discover new biologically active metalodrugs more selective and less toxic, when compared to classical drugs. The copper centres will be assembled using as bridging ligands DNA based motifs or pyridyl ligands with extended aromatics systems. The coordination sphere of copper centre will be completed with DNA type bases or

ancillary pyridyl ligands. The first ligands can interact with DNA through the formation of hydrogen bonds while the second ones can form T-T staking interactions with the base pairs. The presence of these two types of ligands in the same complex is a very important advantage: it can lead to a stronger binding affinity and to an increased selectivity for DNA.

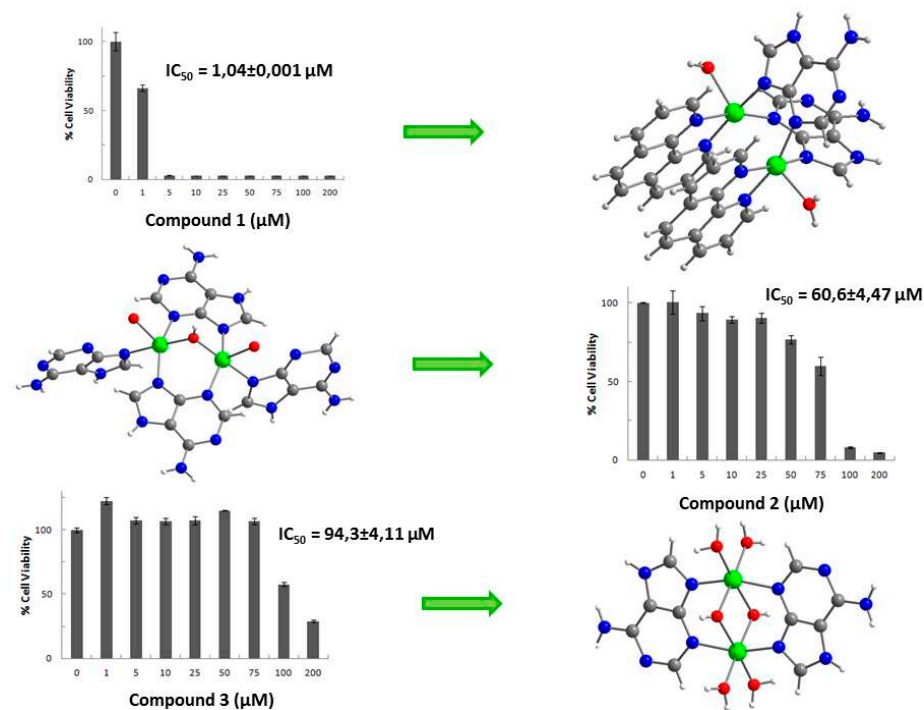


Figure 1. Molecular structure of copper compound 1  $[Cu_2(\mu\text{-adenine})_2(\text{phen})_2(\text{H}_2\text{O})_2] \cdot 4(\text{NO}_3) \cdot 2(\text{H}_2\text{O})$ ; copper compound 2  $[Cu_2(\mu\text{-adenine})_4(\mu\text{-OH})(\text{H}_2\text{O})_2] \cdot 3(\text{NO}_3) \cdot (\text{H}_2\text{O}) \cdot \text{adenine}$ ; and copper compound 3  $[Cu_2(\mu_2\text{-OH})_2(\mu\text{-adenine})_2(\text{H}_2\text{O})_4] \cdot 2(\text{NO}_3) \cdot \text{H}_2\text{O}$ , and in vitro cytotoxicity assays for all three copper complexes against HeLa cells.

For this purpose we have synthesized three binuclear copper complexes with adenine and 1-10-phenanthroline, compound 1, and only with adenine, compound 2 and 3 (figure 1). In these compounds the nucleobase adenine links the copper(II) atoms in a bridging mode by the N(3) and N(9) donor (as bi-dentate). All copper complexes exhibit significant anti-tumoral activity against HeLa cells, leading to  $IC_{50}$  values approximately of 1, 60 and 94  $\mu M$ , respectively (figure 1).

We believe that the study of such class of metal complexes can open the doors for new research toward the preparation of alternatives anti-tumoral drugs.

<sup>1</sup> Department of Chemistry, CICECO, University of Aveiro, 3810-193 Aveiro, Portugal

<sup>2</sup> Department of Chemistry and Biochemistry, University of Lisbon, Lisboa, Portugal

<sup>3</sup> Department of Health Sciences, University of Aveiro, 3810-193 Aveiro, Portugal

#### References

[1] Lippard SJ, et al., *Current Opinion in Chemical Biology*, 2003, 7, 481.

[2] Rosenberg B, et al., *Nature*, 1969, 222, 385.

[3] Kettunen, et al., *Current Opinion in Chemical Biology*, 2006, 13, 1337.

[4] Dyson PJ, et al., *Platinum Metals Review*, 2001, 45, 62.

[5] Hadjikakou SK, et al., *Coordination Chemistry Reviews*, 2009, 253, 235.

[6] Aldrich-Wright J, et al., *Chemical Communications*, 1018, 2004.

[7] Serratrice M, et al., *Inorganic Chemistry*, 2012, 51, 3161.

[8] Megens RP, et al., *Chemistry - A European Journal*, 2009, 15, 1723.

[9] Zhao Y, et al., *Chemistry - A European Journal*, 2006, 12, 6621.

[10] Medina-Molner A, et al., *Chemical Communications*, 2012 1961.

## BONE MECHANICAL STIMULATION WITH PIEZOELECTRIC MATERIALS

Reis J<sup>1,2</sup>, Frias C<sup>3</sup>, Capela-Silva F<sup>4,5</sup>, Potes J<sup>1,5</sup>, Simões JA<sup>6</sup>, Botelho ML<sup>7</sup>, Castro CC<sup>2</sup>, Marques ATM<sup>3</sup>

The commercially available biomaterials for bone replacement and reinforcement do not take into account the bone natural piezoelectric properties and thus its use is accompanied by a break in bone natural electro physiologic continuum<sup>[1]</sup>. Arthroplasty causes strong changes on adjacent bone strain levels and distribution.

The work explored in vitro and in vivo use of a piezoelectric polymer substrate for providing bone mechanical stimulation. Osteoblastic line cells MC3T3-E1 were seeded on the coated and electrically in-

ulated surface of polyvinylidene fluoride (PVDF) films and subjected to static and dynamic conditions, as described by Frias et al. (2010). In dynamic conditions the substrates were deformed by applying a 5 V current, at 1 Hz and 3 Hz for 15 min every 24 hours. Electronic speckle pattern interferometry method showed the maximum substrate displacement was 0.6  $\mu m$ , in the central area of the devices; displacement was minimum in the encastre (clamped) region. The assessment of cell viability and proliferation evidenced a material's poorer

performance when compared to control standard culture vessel. Higher viability values were registered on mechanically stimulated substrates, although the differences between static and dynamic samples were not statistically significant. To evaluate effectiveness of mechanical stimulation nitric oxide (NO) was measured in culture medium samples immediately after stimulation. NO is a messenger molecule produced in response to mechanical stimulation of osteoblasts and osteocytes, with a large variety of biological functions. Culture medium NO measurements in the samples subjected to mechanical stimulation were significantly higher than static samples.

The in vitro study showed therefore evidence of effective bone cell mechanical

stimulation, and the concept was further explored in vivo.

An actuator device was developed, composed of microcontroller (eZ430-RF2500, Texas Instruments, USA) and a set of six actuators. A similar, but static, control device was also developed, sterilized and implanted

The actuator device was implanted in the left hind limb and the control static device was implanted in the right hind limb of a 4 year old merino ewe, under general inhalatory anaesthesia. Six osteotomies were made on the tibial proximal physis and distal femoral physis, using especially metal designed guides. The biological response around the osteotomies was assessed through histology and histomorphometry in non-decalcified sections and histochemistry and immunohistochemistry in decalcified sections, namely through Masson's trichrome, and labeling of osteopontin, proliferating cell nuclear antigen and tartrate resistant acid phosphatase. After one-month implantation, total bone area and new bone area

were significantly higher around actuators when compared to static controls. Bone deposition rate was also significantly higher in the mechanically stimulated areas (Figure 1). In these areas, osteopontin increased expression was observed. The results suggest that piezoelectric materials and the converse piezoelectric effect may be used to effectively stimulate bone growth. Actuators with improved biocompatibility should be developed [2,3].

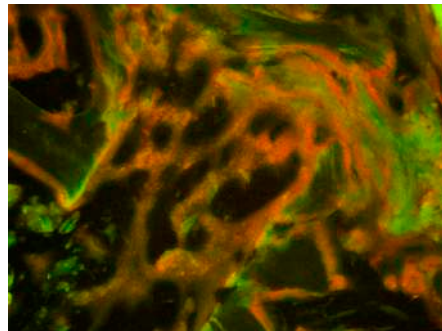


Figure 1. Newly formed bone around a piezoelectric actuator, labelled with calcein green and alizarin red, one month post-implantation in sheep (tibia, non-decalcified section).

<sup>1</sup> Department of Materials and Ceramics Engineering, CICECO, University of Aveiro, 3810-193 Aveiro, Portugal

<sup>2</sup> Department of Veterinary Medicine, University of Évora, 7002-554 Évora, Portugal

<sup>3</sup> Department of Mechanical Engineering, University of Porto, 4200-465 Porto, Portugal

<sup>4</sup> Department of Biology, University of Évora, 7002-554 Évora, Portugal

<sup>5</sup> Institute of Mediterranean Agricultural and Environmental Sciences (ICAAM), University of Évora, 7002-554 Évora, Portugal

<sup>6</sup> Department of Mechanical Engineering, University of Aveiro, 3810-193 Aveiro, Portugal

<sup>7</sup> Instituto Tecnológico e Nuclear, 2686-953 Sacavém, Portugal

References

[1] Reis J, Capela-Silva F, Queiroga C, Lucena, S, Potes J, *Journal of Biomedical and Bioengineering*, 2011, 2, 37-44.

[2] Reis J, Frias C, Castro CC, Botelho ML, Marques AT, Simões JA, Capela-Silva F, Potes J, *Journal of Biomedicine and Biotechnology*, 2012, ID 613403, 1-7.

[3] Reis J, Frias C, Capela-Silva F, Potes J, Simões JA, Botelho ML, Castro CC, Marques ATM, In *Natural Polymers, Biopolymers, Biomaterials, and Their Composites, Blends, and IPNs* (Thomas et al. Eds.), 2012, Chapter 25, 293-306.

Acknowledgments

The work was partially supported by FEDER Funds through the Operational Programme for Competitiveness Factors – COMPETE and National Funds through FCT – Foundation for Science and Technology under the Strategic Project PEst-C/AGR/UI0115/2011. Authors acknowledge also the financial support from the Portuguese Science Foundation (FCT) in the forms of projects PTDC/EME-PME/65749/2006 and PTDC/EME-PME/70824/2006; and BD/31895/2006.

## POLARIZATION SWITCHING IN HYDROXYAPATITE: BONES CAN GROW FASTER

Lang SB<sup>1</sup>, Tofail SAM<sup>2</sup>, Kholkin AL<sup>3</sup>, Wojta D M<sup>3</sup>, Gregor M<sup>4</sup>, Wang Y<sup>5</sup>, Bauer S<sup>6</sup>, Krause M<sup>6</sup>, Plecenik A<sup>4</sup>

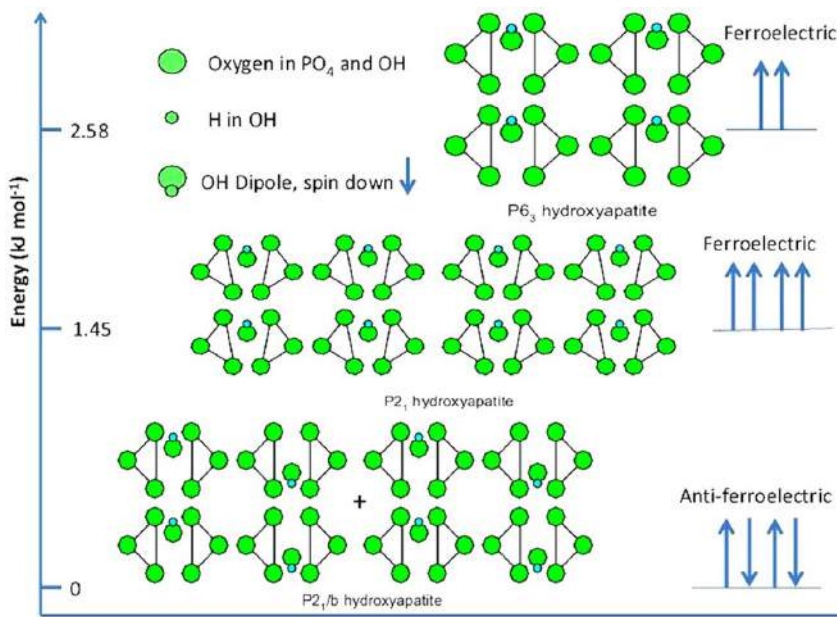


Figure 1. A schematic representation of the hydroxyl ion orientation and energetics of the nonpolar (P2<sub>1</sub>/b) and polar symmetries (P2<sub>1</sub> and P6<sub>3</sub>) of hydroxyapatite.

Ferroelectricity is a property of reversibility of spontaneous polarization (P<sub>s</sub>) by the application of a small electric field. Such property is shown by a small subset of pyroelectric materials that belongs to one of the ten crystal classes that possess no center of symmetry and a spontaneous polarization. Hydroxyapatite (HA) nanocrystals are one of the fundamental building blocks of bone and the primary determinant of bone density and mechanical stability. Hydroxyapatite concretions are even found in the pineal gland of the brain. Synthetic hydroxyapatite is widely used in bone grafts and prosthetic coatings as it binds strongly with natural bone –a critical requirement especially when the host bone-density is low due to age or diseases (e.g. osteoporosis). A piezoelectric effect in bone was first observed by Fukada and Yasuda in 1957 [1]. Until very recently, the effect was believed to be due to the collagen component of bone because another part of bone – hydroxyapatite was considered to be centrosymmetric [2]. It was contested in 2005 when Haverty *et al.* [3] proposed two polar

symmetries for HA: a monoclinic  $P2_1$  and a hexagonal  $P6_3$ , which are not restricted by the presence of a centre of symmetry. These polar, non-centrosymmetric structures originated from a ferroelectric ordering of the hydroxyl ions (OH) along the crystallographic  $c$  axis ( $[001]$

direction (Fig.1). The small energy difference between these polar symmetries and the centrosymmetric ( $P2_1/b$ ) meant that smaller size in HA crystals may lead to the stability of these polar structures due to the availability of large amount of surface energy [4].

Here we show that hydroxyapatite thin films show reversible spontaneous polarization of a ferroelectric nature [5]. The remnant polarization is about a quarter of that measured for a lead-zirconate-titanate film measured under similar conditions. While ferroelectricity in soft tissues such as aortic wall have been claimed for a long time, hard tissues (e.g. lamellar bone) and its constituents typically exhibited anti-ferroelectric order. In contrast, hydroxyapatite reveals a ferroelectric order, which is stabilized due to the nanoscale dimension of HA films. Figure 2 shows the local piezoresponse image ( $d_{33}$ ) and hysteretic dependences of  $d_{33}$  measured at two different locations. The amplitude of the piezoresponse and phase (which sign indicates polarization direction) were measured immediately after the application of poling pulses. The dependencies of both  $d_{33}$  and phase with respect to bias voltage show a strongly hysteretic dependence typical for polarization switching in ferroelectrics. This finding will stimulate new understanding on the mechanism of biomineralisation and the formation of the characteristic hierarchical structure of bone. Reversible spontaneous polarization in hydroxyapatite will also open up a number of novel technical applications such as in electronics, microelectromechanical systems (MEMS), *in vivo* energy harvesting and biosensors.

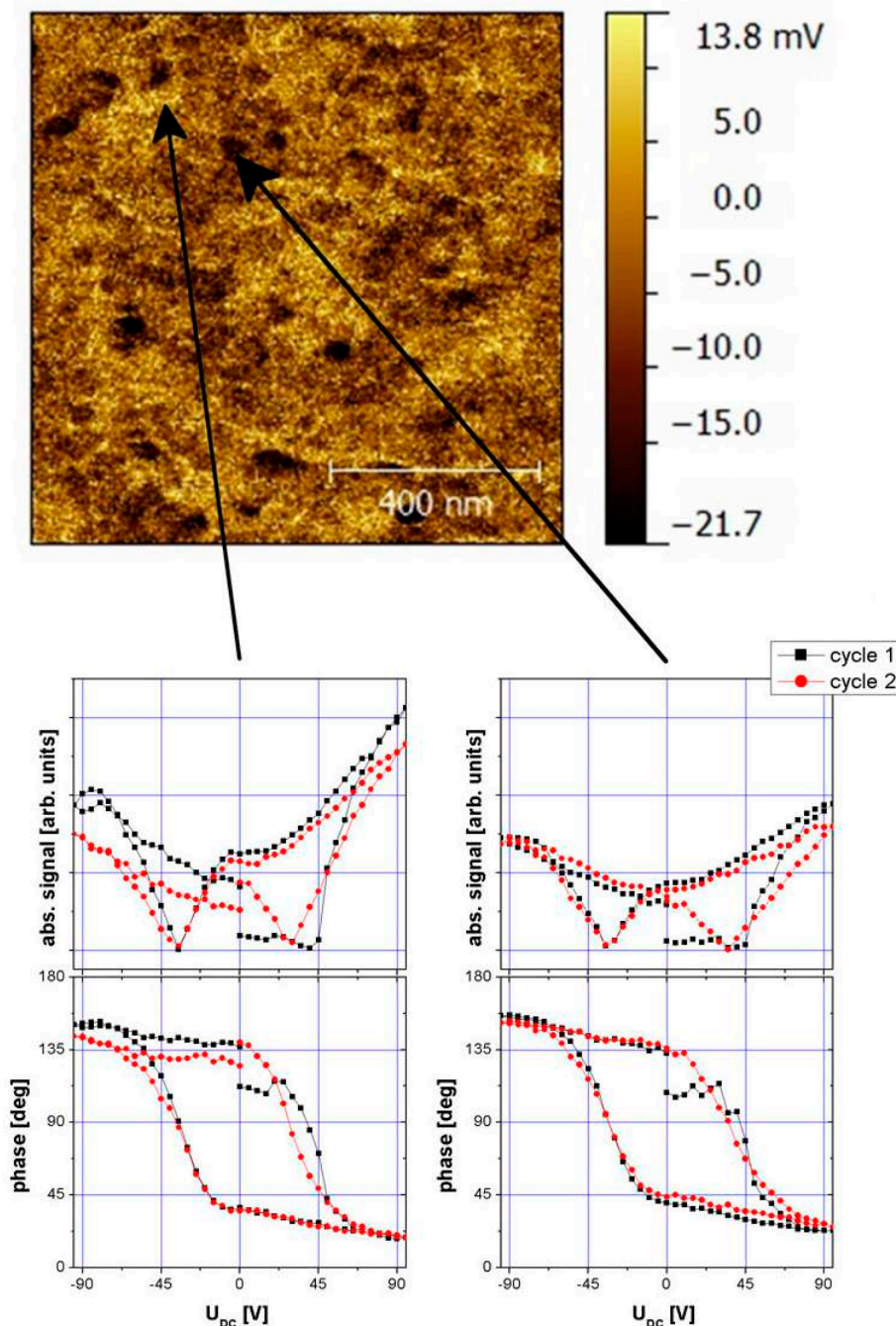


Figure 2. Representative PFM image (upper part) and recorded ferroelectric hysteresis loops (lower parts) in places indicated by arrows.

<sup>1</sup> Ben-Gurion University of the Negev, Beer Sheva, Israel

<sup>2</sup> Department of Physics and Energy, University of Limerick, Limerick, Ireland

<sup>3</sup> Department of Materials and Ceramic Engineering, CICECO, University of Aveiro, 3810-193 Aveiro, Portugal

<sup>4</sup> Comenius University, Bratislava, Slovakia

<sup>5</sup> Hong Kong Polytechnic University, Hong Kong

<sup>6</sup> Johannes Kepler University, Linz, Austria

#### References

- [1] Fukada E, Yasuda I, *Journal of the Physical Society of Japan*, 1957, 12, 1158-1162.
- [2] Kay MI, Young RA, Posner AS, *Nature*, 1964, 204, 1050.
- [3] Haverty D, Tofail SAM, Stanton KT, McMonagle JB, *Physical Review B*, 2005, 71, 9410.
- [4] Amis EJ, Rumble J, *Certificate of analysis*, SRM 2910: Calcium hydroxyapatite, 2003.
- [5] Lang SB, Tofail SAM, Kholkin AL, Wojta B M, Gregor M, Gandhi AA, Wang Y, Bauer S, Krause M, Plecenik A, *Scientific Reports* 3, 2013, 2215.

# CARBON NANOTUBE/BIOCERAMIC COMPOSITES FOR *IN SITU* ELECTRICAL STIMULATION OF BONE

Mata D<sup>1</sup>, Oliveira FJ<sup>1</sup>, Neto MA<sup>1</sup>, Belmonte M<sup>2</sup>, Bastos AC<sup>1</sup>, Lopes MA<sup>3</sup>, Gomes PS<sup>4</sup>, Fernandes MH<sup>4</sup>, Silva RF<sup>1</sup>

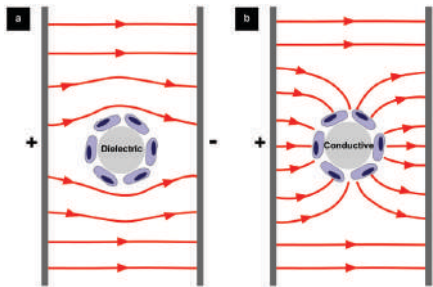


**Figure 1.** (a) Top view schematic images of the electric field (current density) lines distribution of a (a) dielectric and a (b) conductive spherical samples interfacing with osteoblastic cells (elliptical purple sketches) immersed in a homogeneous  $\alpha$ -MEM culture medium.

Bone regenerative medicine has noticed huge progress in the past decades driven by the great socioeconomic interest in treating skeletal diseases. Despite tremendous improvements of synthetic bone grafts, most are incapable of fully repair severe bone injuries. Yet, biomaterials can still be reinvented to become universal bone regeneration solutions. Following this roadmap, “smart” bone grafts have been designed with new functionalities able to stimulate specific bone cells responses. Regarding the beneficial effects of endogenous electrical signals in bone, electron conductivity emerge as an exciting functionality. The electrical currents found in healthy bone are not expected to exist at the fractured bone site. By applying exogenous electrical stimuli at the damaged bone together with conductive bone grafts is expectable an improved efficiency of charge transfer voltage at the substrate-cell interface allowing the spatial-temporal control of bone regeneration. This stimulation efficiency is thought to be related to the high density of electric field lines crossing the cell (Fig. 1), which boosts opening of voltage-gated channels at multi-locations in the cell membrane, and raises action potentials’ magnitude. Those conductive composite grafts containing metal fillers for such purpose are precluded due to corrosion phenomenon that induces cytotoxicity. Alternatively, the characteristics of carbon nanotubes (CNTs), namely low-cost, ultimate electrical conductivity and

low percolation thresholds, make them promising candidates to obtain conductive biomaterials with preserved biological profiles.

This work aims to develop a CNT/Bioglass/HA composite having adequate mechanical, electrical and, most important, biological characteristics, to be used as an electroconductive bone graft in the electrotherapy of injured bone. Composites with controlled CNT agglomeration were processed by an optimized functionalization-free route with minor contaminant levels and damage to CNTs. These phases worked as efficient toughening agents in composites improving the fracture toughness of the ceramic matrix, making it closer to the

one of cortical bone. The remaining mechanical and electrical properties of the composite outperformed those of the bone. The use of AC impedance spectroscopy (Figs. 2a and b) and of vibrating voltage probe measurements (Figs. 2c and d) in  $\alpha$ -MEM cell culture medium reveal the converging effects that the conductive composite material have on the electric field and current flow paths. *In vitro* studies evidence that CNT composites allowed cell adhesion and proliferation, further enhancing the functional activity and modulating the orientation of the cell growth along the alignment of the CNT agglomerates. The results on the *in vitro* AC electrical stimulation of bone cells highlight that the conductive CNT composite significantly improved cell functional activity under an appropriate electrical stimulation protocol, compared to the Bioglass/HA matrix. The cell metabolic activity and DNA content were increased by 130% and 60%, relatively to the non-stimulated condition, after only

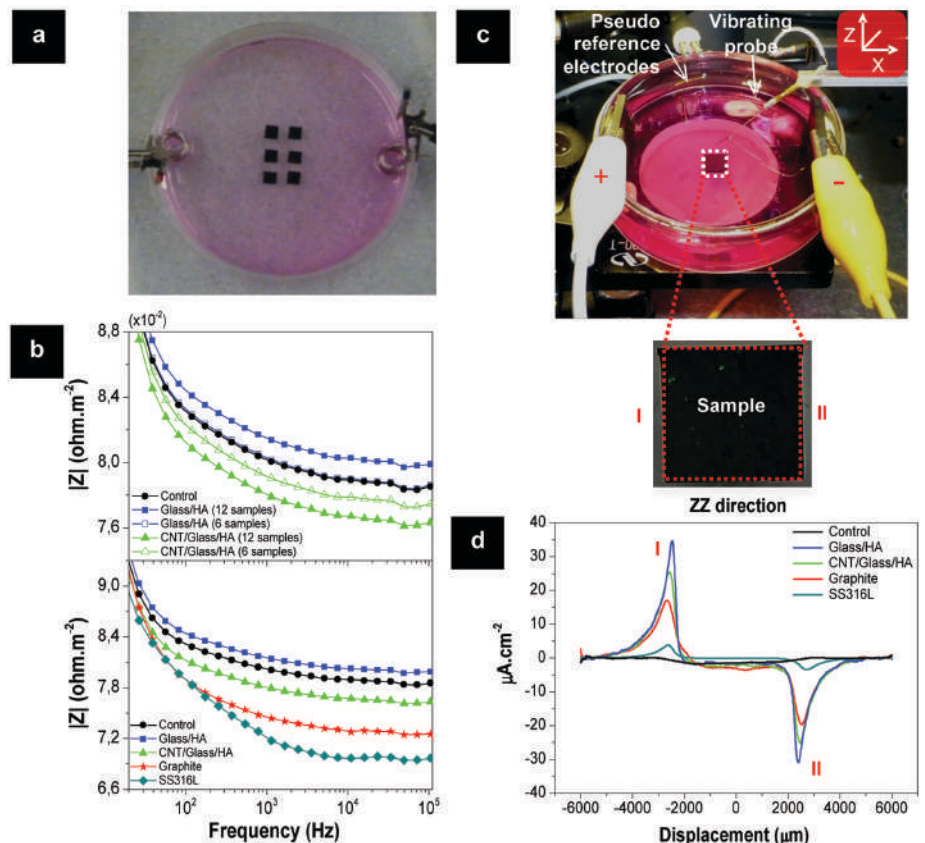


**Figure 2.** (a) Photographs of the electrochemical cells with six samples immersed in 12 ml of  $\alpha$ -MEM and platinum spiral electrodes. (b) Plots showing the dependence of the modulus of impedance  $|Z|$  of the electrochemical cells on the signal frequency. (c) Set-up of the vibrating voltage probe measuring system of a electrochemical cell containing one sample immersed in 12 ml of  $\alpha$ -MEM and parallel graphite electrodes. (d) Plot of the variation of the current density line profile (from I to II labels) in the zz direction with the electrical conductivity of the sample at a fixed sample-probe distance of 50  $\mu\text{m}$ .

3 days of daily stimulation of 15  $\mu$ A for 15 min (Figs. 3a-c). Moreover, the osteoblastic gene expression for Runx2, OC and ALP was enhanced by 80%, 50% and 25%, after 5 days of stimulation (Figs. 3d-f). These observations were related to the local increase of the  $\alpha$ -MEM conductivity and the confinement of electrical fields on the surface of the conductive material (Fig. 2).

The results validate the hypothesis that CNT/Bioglass/HA bone grafts could be used together with a non-invasive electrical stimulation technique to boost cell growth by an efficient stimuli delivering mechanism. Reducing the cost and time of bone treatment can make the elec-

trotherapies of clinical relevance. These novel non-metallic graft materials offer new possibilities, not only in bone regeneration, but also in other excitable tissues (e.g. neuronal). Future research should consider animal model tests applying the optimized *in vitro* stimulation protocol to validate the efficiency of bone formation on conductive bone grafts.

<sup>1</sup> Department of Materials and Ceramic Engineering, CICECO, University of Aveiro, 3810-193 Aveiro, Portugal

<sup>2</sup> Institute of Ceramics and Glass, CSIC, 28049 Madrid, Spain

<sup>3</sup> CEMUC, Metallurgical and Materials Engineering Department, Faculty of Engineering, University of Porto, 4200-465 Porto, Portugal

<sup>4</sup> Laboratory for Bone Metabolism and Regeneration, Faculty of Dental Medicine, University of Porto, 4200-465 Porto, Portugal

#### References

[1] Mata D, Silva MR, Fernandes AJS, Oliveira FJ, Costa PMFJ, Silva RF, *Carbon*, 2012, 50, 3585-3606.

[2] Mata D, Oliveira FJ, Ferro M, Gomes PS, Fernandes MH, Lopes MH, Silva RF, *Journal of Biomedical Nanotechnology*, 2013, 9, 1-19.

[3] Mata D, Horovistiz AL, Branco I, Ferro M, Ferreira NM, Belmonte M, Lopes MA, Silva RF, Oliveira FJ, *Materials Science and Engineering: C*, 2014, 34, 360-8.

[4] Mata D, Oliveira FJ, Ferreira NM, Araújo RF, Fernandes AJS, Lopes MA, Gomes PS, Fernandes MH, Silva RF, *Nanotechnology*, 2014, 25, 145602.

[5] Mata D, Oliveira FJ, Neto MA, Belmonte M, Bastos AC, Lopes MA, Gomes PS, Fernandes MH, Silva RF, *Nanomedicine: Nanotechnology, Biology and Medicine*, submitted.

#### Acknowledgments

The work was carried out with the financial support of FCT (SFRH/BD/36273/2007) and PEst-C/CTM/LA0011/2013.

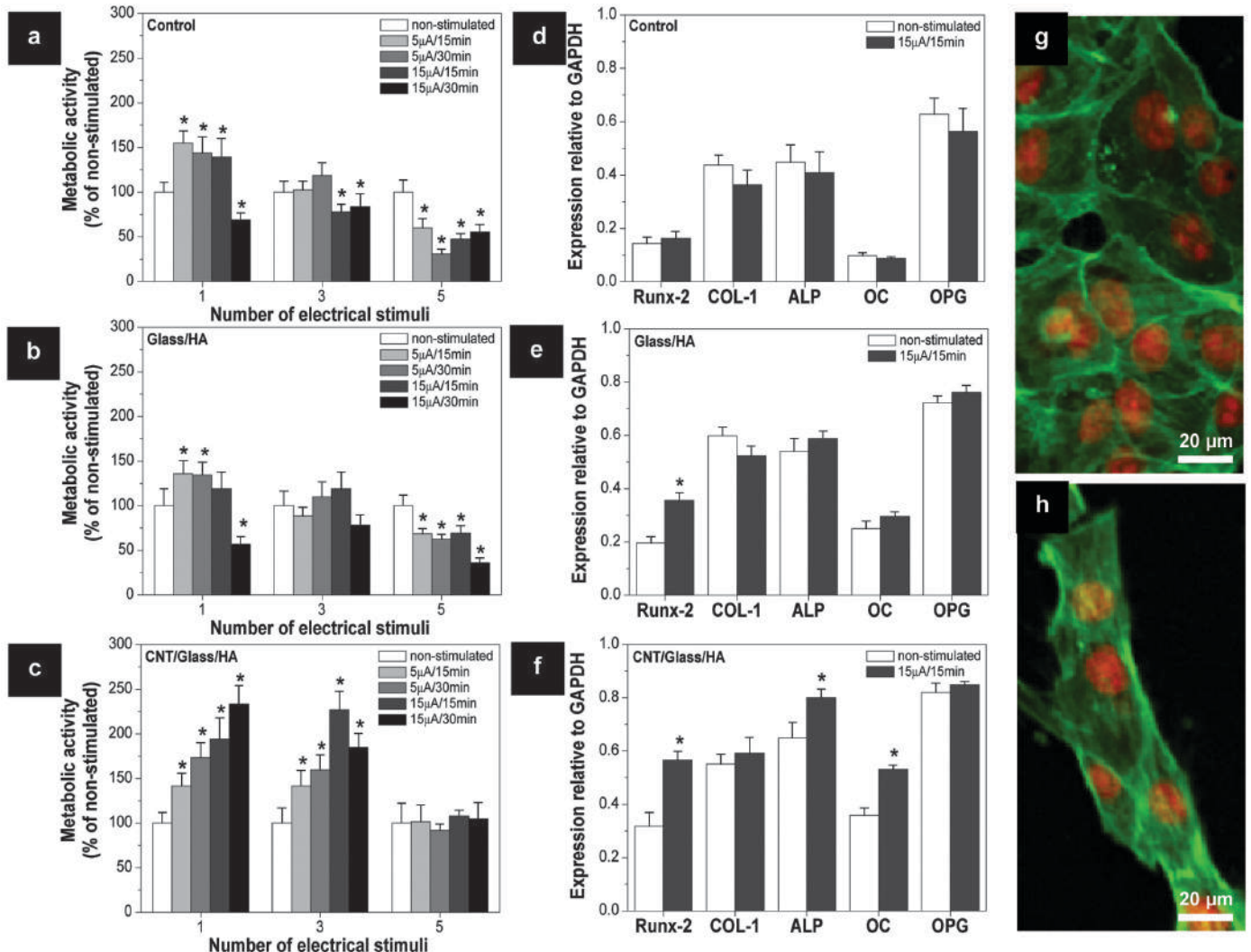


**Figure 3.** (a-c) Cell viability/proliferation of osteoblastic cell cultures grown over standard cell culture coverslips, Glass/HA matrix and CNT/Glass/HA composite, and characterized 24h after 1, 3, and 5 daily electrical stimuli, under different stimulation conditions. (d-f) Expression of osteoblastic-related genes by cell cultures characterized 24h after 5 daily electrical stimuli under 15  $\mu$ A, 15 min. Results are expressed as percentage of variation from non-stimulated cultures. Densitometric analysis of the RT-PCR bands normalized to the corresponding GAPDH value. \*Significantly different from non-stimulated cultures. CLSM appearance of osteoblastic cell cultures grown over (g) Glass/HA matrix and (h) CNT/Glass/HA composite, and observed 24h after 3 daily electrical stimuli, under 15  $\mu$ A, 15 min. Cells were stained for F-actin cytoskeleton (green) and nucleus (red).

## MODULATING CELLULAR RESPONSE WITH ENGINEERED HAP NANOPARTICLES

Costa MEV<sup>1</sup>, Almeida MM<sup>1</sup>, Santos C<sup>1</sup>

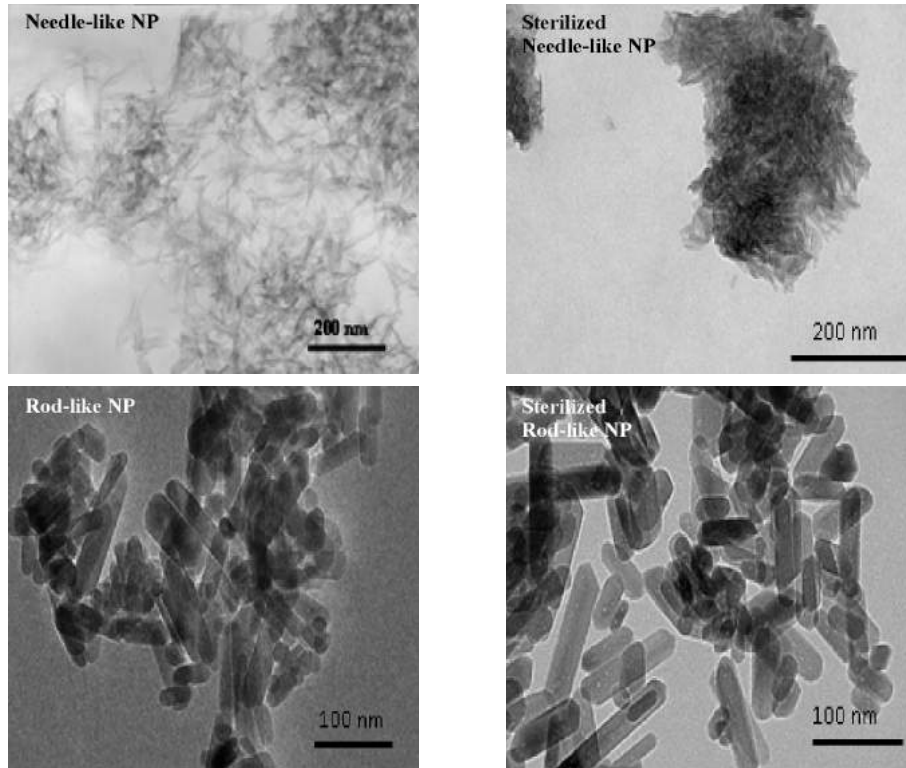


Figure 1. TEM images of Hap nanoparticles (NP): "as prepared" needle-like and rod-like NP and sterilized NPs.

phology by different synthesis methods are plentiful but the subsequent follow up of the bone cell response induced by the synthesized particles is still scarce. Consequently the correlations between the morphological characteristics of the individual NP and the elicited cell response are still poorly established. A research focused on Hap NP is thus crucial for mapping NP route and its interaction with cells and tissues and thus benefit the current applications of Hap like biomineralization processes associated to Hap NP based scaffolds or drug delivery efficiency of Hap NP based drug carriers, in which the implications of Hap NP morphology are not yet clarified. The synthesis of Hap NPs with different morphological features and their impact on the osteoblastic cell response are here addressed. Two different synthesis methods were used to produce Hap NPs with distinct shape and size: prismatic rod-like and needle-like NP with a specific surface area of  $55\text{m}^2/\text{g}$  and  $170\text{m}^2/\text{g}$ , respectively. In addition to their morphology features, the differences between the NPs also include their crystallinity, surface electrical charge and surface adsorbed species which are also dissimilar. Considering that the ultimate application requires the target NP to be sterilized before subsequent *in vivo* appli-

Hydroxyapatite (Hap) is a calcium phosphate (CaP) with a chemical composition  $(\text{Ca}_{10}(\text{PO}_4)_6(\text{OH})_2)$  that closely approaches that of the mineral constituents of hard tissues (i.e. teeth and bones) thus explaining its natural and excellent biocompatibility and hence its wide medical use. The biological genesis of bone mineral phase implies a deposition process mediated by a living tissue, consisting of a continuous synthesis, resorption and replacement of CaP under the action of living cells. This dynamic process modulates the composition and structure of bone mineral phase which are both space and time variable, reflecting the variability of body metabolism and the specificity of bone local cellular functions. The bone CaP consists of nanosized crystals of nonstoichiometric Hap, having a needle or plate like shape and thicknesses ranging from 30 to 120 nm, densely packed into woven collagen fibrils. The attempts to mimic the biological bone Hap nanoparticle (NP) mor-

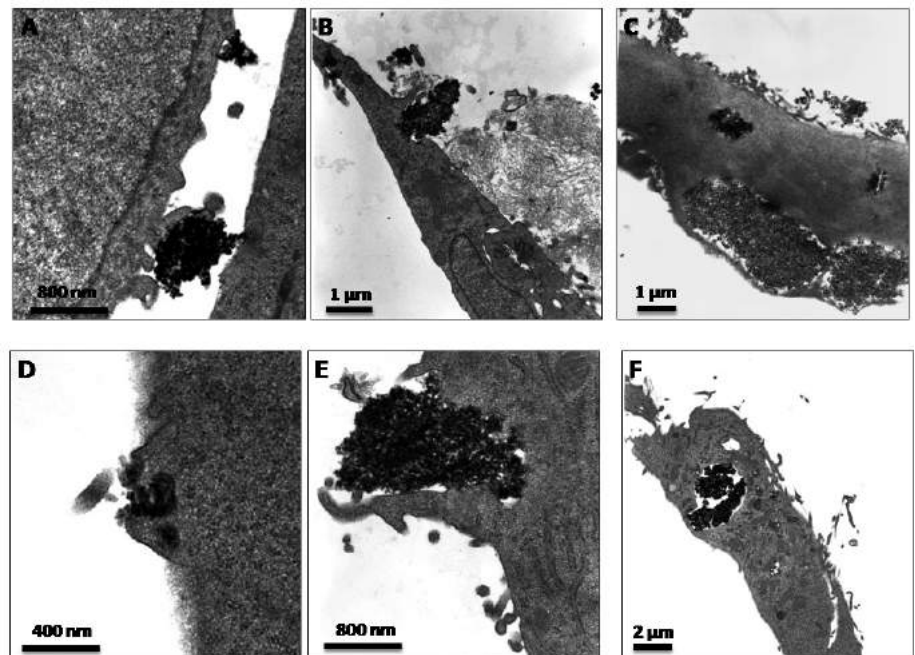


Figure 2. Representative TEM micrographs of osteoblastic cell cultures exposed to sterilized rod-like (A, B and C) and to needle-like Hap nanoparticles (E, F and G), 50 and  $500\mu\text{g}/\text{ml}$ , during different periods. The emission of pseudopods surrounding adjacent nanoparticles is observed in A and D (3 hours,  $50\mu\text{g}/\text{ml}$ ), B (3 days,  $50\mu\text{g}/\text{ml}$ ) and E (3 hours,  $500\mu\text{g}/\text{ml}$ ); C and F (24 hours,  $500\mu\text{g}/\text{ml}$ ) depicts clusters of nanoparticles entrapped in endosomes.

cations, the sterilized NPs were addressed as the true target for cell studies. The NPs were sterilized by autoclaving and sterilization was found to modify markedly the shape, size and aggregation state of the needle-like Hap NP which high surface area underwent a severe reduction to  $22\text{m}^2/\text{g}$  contrarily to a rod shaped NP which maintained the same surface area. The study of the interaction of the sterilized Hap NP with osteoblastic human cells showed that the two types of particles presented some differences in the elicited cell response [1]. Although both NPs were

readily internalized by an endocytosis pathway their degradation behavior after internalization could be differentiated and correlated with their crystallinity. It was also observed that the NP characteristics engineered via the manipulation of their synthesis conditions impacted their ability for inducing the gene expression of the osteoblastic markers ALP and BMP-2. The elicited cell response was thus conditioned by the physicochemical profiles of the used Hap NPs which affected protein adsorption, particle uptake, degradation/dissolution and intracellular trafficking

events. While predicting positive effects on osteoblastic differentiation and effective ability for internalization by certain cells, these results foreseen multivalent and useful applications such as in bone tissue engineering or as drug carriers targeted to specific tissues.

<sup>1</sup> Department of Materials and Ceramic Engineering, CICECO, University of Aveiro, 3810-193 Aveiro, Portugal

#### Reference

[1] Santos C, Gomes PS, Duarte JA, Franke RP, Almeida MM, Costa MEV, Fernandes MH, *Journal of the Royal Society Interface*, 2012, 9, 3397-3410.

## PIEZOELECTRIC PLLA AS A PLATFORM FOR TISSUE GROWTH

Barroca N<sup>1</sup>, Vilarinho PM<sup>1</sup>, Daniel-da-Silva AL<sup>1</sup>, Wu A<sup>1</sup>, Fernandes MHV<sup>1</sup>, Gruverman A<sup>2</sup>

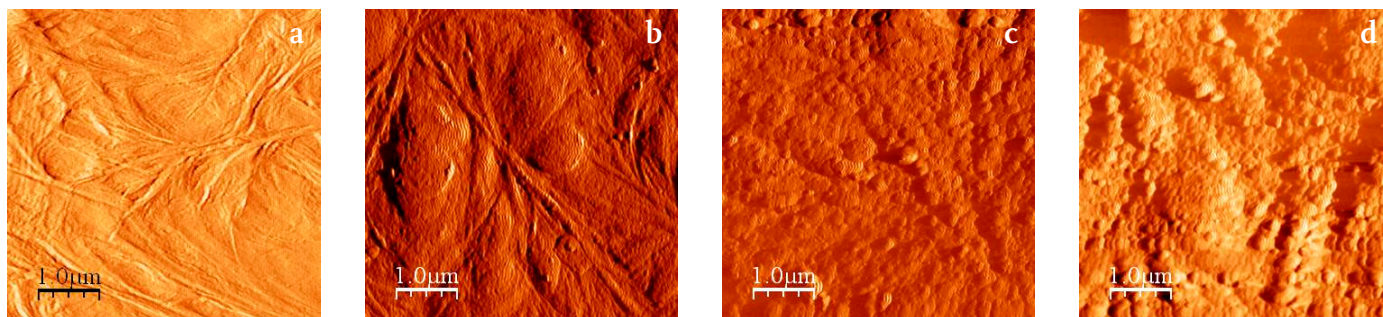


Figure 1. Topography images of PLLA thin film surfaces acquired in AFM tapping mode in liquid: (a) non-poled area before protein adsorption; (b) non-poled area after protein adsorption; (c) positively poled area after protein adsorption; (d) negatively poled area after protein adsorption.

Imagine an implantable platform made of an intelligent material capable of thwarting bone resorption by simple electrical stimulation: PLLA, a FDA approved biomaterial, is one of the few candidates than may fulfil the challenge.

Although physical exercise is known to increase bone mass, the exact processes

responsible for the bone growth remain elusive. The piezoelectric character of the organic component in bone has been identified as a possible ‘transducer’ (converter of mechanical to electrical energy and vice-versa) in bone tissue synthesis but the mechanisms are still largely unknown. The use of some piezoelectric materials

to correct bone defects has been shown to promote a faster bone growth as compared with non-piezoelectric materials.

Poly (L-lactic acid) (PLLA), a semi-crystalline polymer, is currently being investigated for bone regeneration because it possesses a valuable combination of properties. Besides its biocompatibility, biodegradability and adjustable physical properties, PLLA is piezoelectric. *In vivo* piezo effect is expected to create charges in the area surrounding the bone and enhance the regeneration processes. This research aims at understanding how the polarization of a piezoelectric substrate influences the bone-growth processes.

Spin-coated and solvent-casted films, nanofibers and scaffolds of PLLA were prepared. PLLA was poled by corona poling

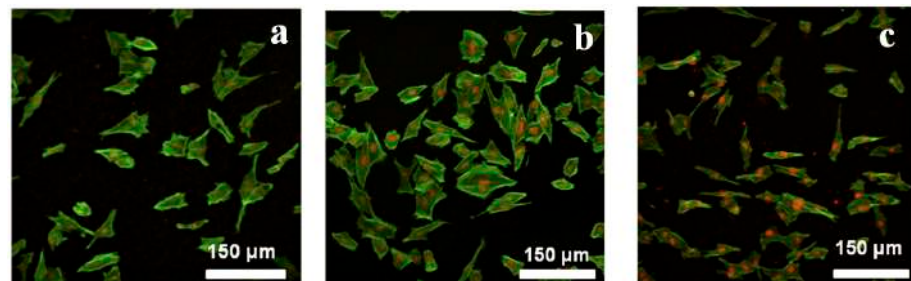


Figure 2. Confocal Laser Scanning Microscopy (CLSM) micrographs of cultures stained for F-actin cytoskeleton (green) and nucleus (red). Proliferation of MG63 osteoblast-like cells over PLLA films, pre-coated with fibronectin: (a) non-poled, (b) negatively charged and (c) positively charged PLLA (+).

for macroscopic polarization, or locally poled at the nanoscale by applying a DC field through a piezoresponse force microscopy tip. The molecular orientation induced by the electrical field was checked by piezoresponse force microscopy imaging. The electrically-induced polarization of PLLA was investigated regarding its stability over time and effect on human proteins and osteoblast-like cells. *In vitro*, we

have shown that polarization and surface charges in PLLA have an effect on biological events occurring during bone regeneration. Polarization significantly enhances the fibronectin adsorption (Figure 1) and the adhesion, spreading and proliferation of osteoblast-like cells (Figure 2). We have also demonstrated that in semi crystalline PLLA the polarization decay starts only after 10 days, enough time to trigger and

maintain the adhesion of proteins and proliferation of cells.

<sup>1</sup> Department of Materials and Ceramic Engineering, CICECO, University of Aveiro, 3810-193 Aveiro, Portugal

<sup>2</sup> Department of Physics and Astronomy, University of Nebraska-Lincoln, USA

#### Reference

[1] Barroca N, Vilarinho PM, Fernandes MHV, Sharma P, Gruverman A, *Applied Physics Letters*, 2012, 101, 023701.

## A NEW APPROACH TO THE PREPARATION OF PDMS-SiO<sub>2</sub> BASED HYBRIDS – A STRUCTURAL STUDY

Almeida JC<sup>1</sup>, Castro AGB<sup>1</sup>, Salvado IMM<sup>1</sup>, Margaça FMA<sup>2</sup>, Fernandes MHV<sup>1</sup>

Due to its elasticity, transparency and biocompatibility, polydimethylsiloxane (PDMS) has been used as the organic component of hybrid materials in different fields of application such as photonics or biomaterials. Typically an acidic medium is used in the sol-gel processing of PDMS-metal oxide systems due to its catalytic effect. Furthermore, when dealing with highly reactive transition metal alkoxides, a chelating agent is pointed out as being necessary to avoid phase separation. In this work a new approach to the preparation procedure of hybrid materials, based on the system PDMS-SiO<sub>2</sub>-

MO<sub>2</sub>, with M=Ti or Zr, was used, which does not require the hydrolysis step and also provided strategies to modulate material structures by altering metal types and pH environment [1]. Tetraethyl orthosilicate (TEOS), polydimethylsiloxane (PDMS-OH) silanol terminated (550 g mol<sup>-1</sup> average molecular weight), isopropanol (IPA), titanium isopropoxide (TiPr), zirconium propoxide (ZrPr) (70 wt.% solution in 1-propanol), all from Sigma-Aldrich, ethyl acetoacetate (EtAcAc) and ammonia (25% solution) from Merck, were used as raw materials, in the molar proportions TEOS:PDMS:MPr (M=Ti or

Zr):IPA:EtAcAc of 1:1:0.5:10:1. Materials were named “MpH”, being M=T for Ti, or Z for Zr, followed by a number that is the final pH value measured. The final pH was adjusted to 10 or 13 with addition of ammonia. The obtained samples were homogeneous and transparent, even at high pH and without the use of EtAcAc (Figure 1). ATR-IR, <sup>29</sup>Si-NMR MAS and <sup>29</sup>Si-{<sup>1</sup>H} CP-MAS were used for the characterization of the obtained samples. According to the <sup>29</sup>Si-{<sup>1</sup>H} CP-MAS results some differences in the nature of difunctional D ((CH<sub>3</sub>)<sub>2</sub>SiO<sub>2</sub>) and tetrafunctional (SiO<sub>4</sub>) Q structural units were observed. The presence of Ti-O-Si and Zr-O-Si bonds was confirmed by ATR-IR analysis. No marked differences were observed when comparing ATR-FT or CP-MAS spectra of compositions prepared at pH 13 containing, or not, the chelating agent. This is a good evidence that titanium and zirconium alkoxides react with OH-PDMS during the earlier stages of sol-gel process forming stable metal-O-Si(CH<sub>3</sub>)<sub>2</sub> bonds.

<sup>1</sup> Department of Materials and Ceramic Engineering, CICECO, University of Aveiro, 3810-193 Aveiro, Portugal

<sup>2</sup> Campus Tecnológico e Nuclear, IST, University of Lisbon, E.N 10, 2686-953 Sacavém, Portugal

#### Reference

[1] Almeida JC, Castro AGB, Salvado IMM, Margaça FMA, Fernandes MHV, *Materials Letters*, 2014, 128, 105–109.

#### Acknowledgments

This work is financed by FEDER funds (Program COMPETE) and by FCT funds, on the project PTDC/CTM/101115/2008 and by the grant SFRH/BD/72074/2010. We also acknowledge the program financing CICECO, Pest-C/CTM/LA0011/2013.

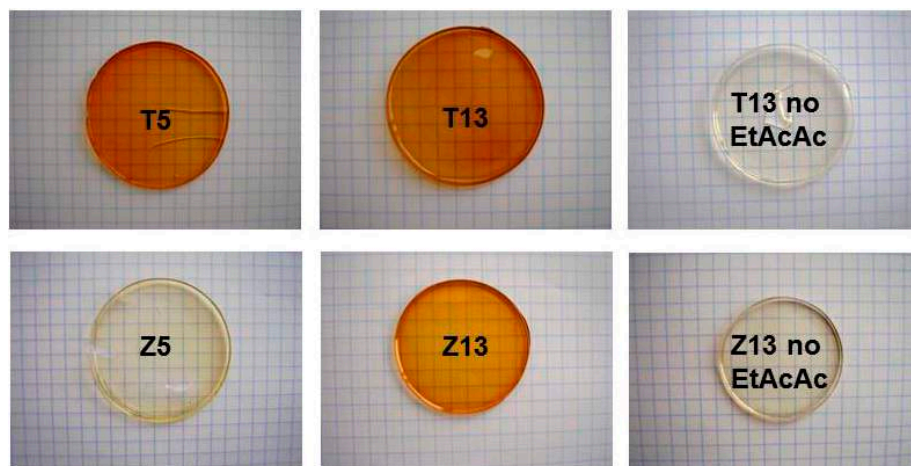


Figure 1. Bulk samples obtained for compositions with titanium [T5, T13 and T13 without EtAcAc] and zirconium [Z5, Z13 and Z13 without EtAcAc]

## SELECTIVE, ULTRASHARP, BORON DOPED DIAMOND MICROELECTRODES

Silva EL<sup>1</sup>, Bastos AC<sup>1</sup>, Neto MA<sup>1</sup>, Silva RF<sup>1</sup>, Ferreira MGS<sup>1</sup>, Zheludkevich ML<sup>1,2</sup>, Oliveira FJ<sup>1</sup>

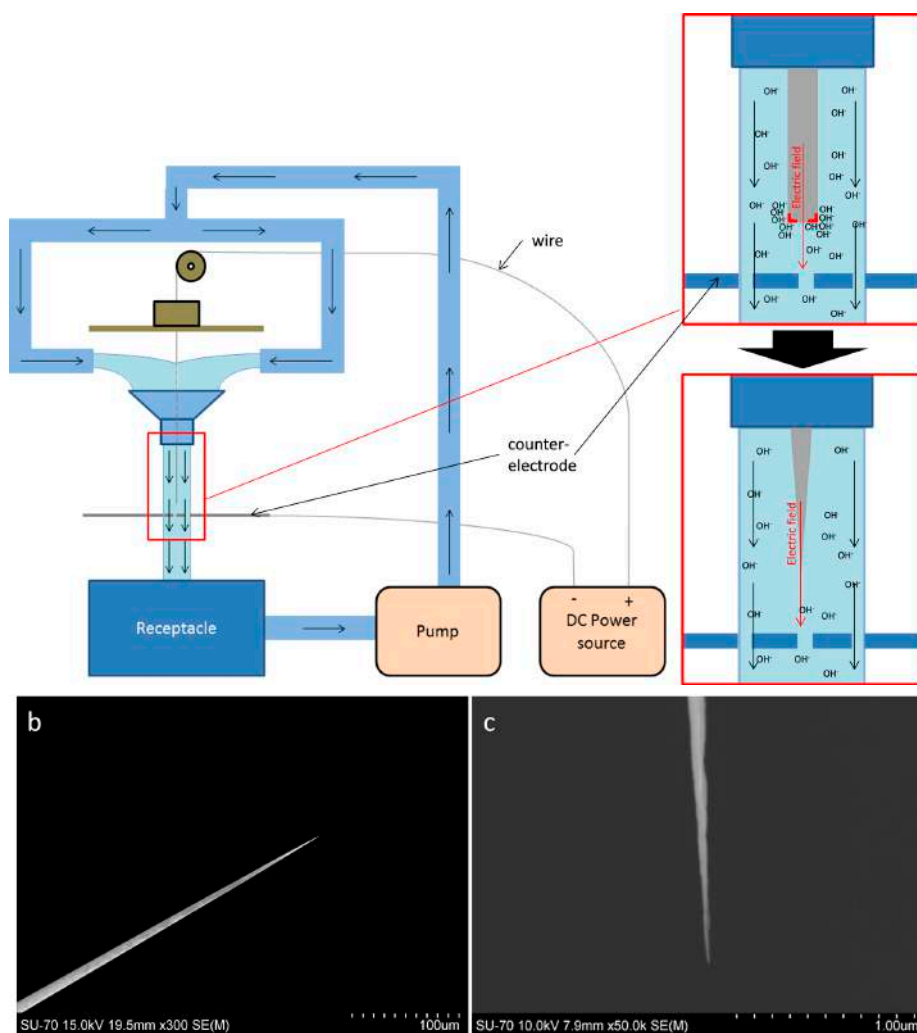


Figure 1. a) Electrochemical etching assembly, evidencing the etching mechanism (inset); electrochemically etched tungsten nanowire in b) low magnification and c) high magnification.

Microprobes are very important tools when it is necessary to perform electrical or electrochemical operations in confined volumes of the microscale with minimum or no damage to the surrounding environment. The fabrication of micro/nano probes has revolutionized the way research is done in various fields such as electroanalysis, biotechnology, medicine, imaging technology. A novel, simple, electrochemical etching method was successfully developed without requiring any complex apparatus or electronic/mechanical system (Fig. 1a) and a patent application was submitted. Taking a tungsten wire of 125  $\mu\text{m}$  diameter and

optimized parameters, this method can reproducibly deliver nanoelectrodes with aspect ratio up to 15:1 and as sharp as 10 nm tip curvature radius or less under 60 seconds (Fig. 1b,c). This was the basis for the development of microelectrodes (MEs) based in boron doped diamond (BDD) thin films grown by HFCVD (Hot Filament Chemical Vapour Deposition) on sharp tungsten filaments.

The BDD MEs were used in the as-grown form, with hydrogen terminated surface and also with surface modification, by RF-plasma, using  $\text{CF}_4$  and  $\text{O}_2$  for inducing different surface terminations, C-F bonds in the first case and C=O, C-O-C

and C-OH in the second. The MEs modified by  $\text{CF}_4$  plasma are oxygen sensors with a sensitivity of 0.1422 nA/ $\mu\text{M}$  of dissolved  $\text{O}_2$  and a detection limit of 0.63  $\mu\text{M}$ . During galvanic corrosion of Zn-Fe model couples long term stability was observed together with a faster response than as-grown MEs, especially when higher scanning rates are used (Fig. 2). This allows gathering a localized oxygen distribution map in a few minutes. Upon fluorination in  $\text{CF}_4$  plasma, diamond surfaces exhibited an improved sensing ability, limit of detection and response time for localized amperometric detection of dissolved oxygen in aqueous electrolyte solutions. For the  $\text{O}_2$  plasma treated MEs it was possible to detect, by zero-current chronopotentiometry, a pH sensitivity of 51 mV/pH in the range pH 2 to pH 12. This behaviour was attributed to the contribution of the C-O and C=O groups. The diamond microelectrodes were tested by micropotentiometry on a galvanic Fe-Zn couple immersed in 0.05M NaCl (Fig. 3a-b). At the iron cathode  $\text{OH}^-$  is generated by the reduction of oxygen at the iron surface. The pH above zinc is mostly determined by the concentration of  $\text{Zn}^{2+}$ , which conducts the hydrolysis of water with generation of  $\text{H}^+$ , leading to local acidification. The diamond microelectrodes were able to map the pH distribution which varies from ca. 4.8 above the zinc under anodic dissolution and 9.3 over the iron cathodic area due to the high  $\text{OH}^-$  concentration developing from the reduction of oxygen (Fig. 3c).

The developed microelectrodes are promising when compared to glass-based microelectrodes for various localized measurements in systems where fast response, high mechanical and chemical stability is required and micro-scale dimension is a key issue. These measurements confirm the usability of diamond microelectrodes for both discrete and continuous dissolved  $\text{O}_2$  and pH measurements, despite the complexity of the corroding media. Hence, the wide linearity range in comparison to the state-of-the-art for liquid membrane and solid contact microelectrodes and the simple two-step fabrication of diamond microelectrodes provide a robust, highly stable microelectrode, adequate for working in corrosion environments and possibly in the always challenging biological environments.

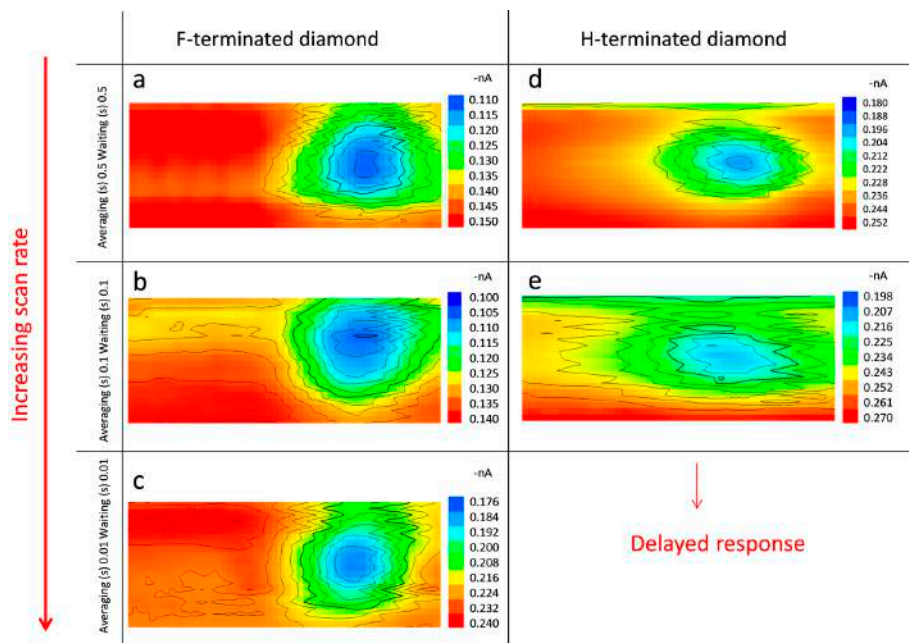


Figure 2. Dissolved oxygen concentration maps recorded with a diamond ME treated with  $CF_4$  plasma and an as-grown ME, polarized at  $-1.3$  and  $-0.9$  V, respectively, with varying averaging-waiting times.

<sup>1</sup> Department of Materials and Ceramic Engineering, CICECO, University of Aveiro, 3810-193 Aveiro, Portugal

<sup>2</sup> MagIC, Institute of Materials Research, Helmholtz-Zentrum Geesthacht, Max-Planck Str. 1, 21502 Geesthacht, Germany

#### References

- [<sup>1</sup>] Silva EL, Bastos AC, Neto MA, Silva RF, Ferreira MGS, Zheludkevich ML, Oliveira FJ, *Electrochemistry Communications*, 2014, 40, 31-34.
- [<sup>2</sup>] Silva EL, Bastos AC, Neto MA, Silva RF, Zheludkevich ML, Ferreira MGS, Oliveira FJ, *Electrochimica Acta*, 2012, 76, 487-494.
- [<sup>3</sup>] Silva EL, Bastos AC, Neto MA, Silva RF, Ferreira MGS, Zheludkevich ML, Oliveira FJ, *Analytical Chemistry*, submitted.

## BIOMATERIALS FROM THE VALORISATION OF WASTE COD FISH BONES WITH APPLICATIONS IN PHOTOCATALYSIS, POLLUTION REMEDIATION AND SELF-STERILISING MATERIALS

Piccirillo C<sup>2</sup>, Pullar RC<sup>1</sup>, Silva MF<sup>2</sup>, Tobaldi DM<sup>1</sup>, Pereira SIA<sup>2</sup>, Cruz IB<sup>2,3</sup>, Marques APGC<sup>2</sup>, Jorge R<sup>3</sup>, Dunnill CW<sup>4</sup>, Parkin IP<sup>4</sup>, Labrincha JA<sup>1</sup>, Castro PML<sup>2</sup>, Pintado MME<sup>2</sup>

Useful biomaterials were produced from the valorisation of cod fish bones, a typical Portuguese fisheries by-product. By simple room temperature treatments with  $CaCl_2$  or NaF solutions and subsequent heating to  $1000^\circ C$  these formed either pure HAp (hydroxyapatite,  $Ca_{10}(PO_4)_6(OH)_2$ ), FAp (fluorapatite,  $Ca_{10}(PO_4)_6F_2$ ) or ClAp (chlorapatite,  $Ca_{10}(PO_4)_6Cl_2$ ). Mixed HAp and  $\beta$ -TCP ( $\beta$ -Ca( $PO_3$ )<sub>3</sub>) was obtained if untreated bones were just heated. These are all valuable materials, as HAp is the main con-

stituent of human bone, and is used as a bioceramic in implants, bone scaffolds and biocompatible coatings. The 75:25

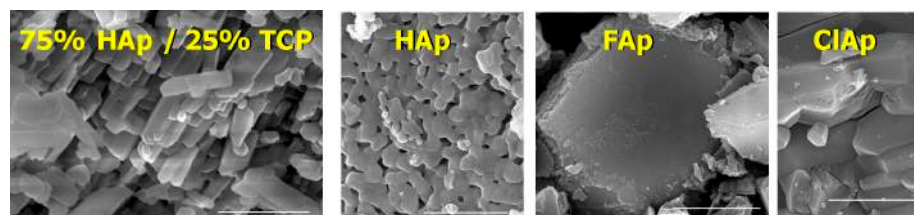


Figure 1. SEM images of 75% HAp/25%  $\beta$ -TCP made from heating cod fish bones at  $1000^\circ C$ , and pure HAp, FAp and ClAp made from treatment with solution of  $CaCl_2$  or NaF followed by heating to  $1000^\circ C$ . The scale bar is  $3 \mu m$ .

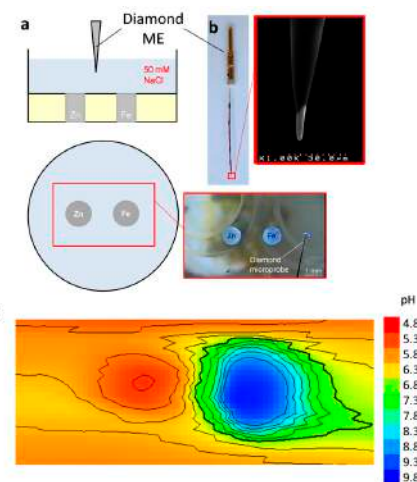


Figure 3. Micropotentiometric measurements showing: a) the Zn-Fe galvanic couple immersed in 50 mM NaCl and corresponding area scanned for pH mapping; b) the B-doped diamond microsensor; c) pH map of the galvanic couple showing the alkaline cathodic region due to higher concentration of  $OH^-$  from oxygen reduction and the acidic region due to hydrolysis of water by  $Zn^{2+}$  forming  $ZnOH^+$  and  $H^+$ .

#### Acknowledgments

Silva EL, Neto MA, would like to acknowledge FCT for the grants SFRH/BD/61675/2009, and SFRH/BPD/45610/2008, respectively. This work was supported by projects PTDC/CTM/108446/2008, PTDC/CTM-MET/113645/2009, funded by FEDER /COMPETE programme- Portuguese Science and Technology Foundation and by the Siset project (FP7-PEOPLE-2010-IRSES Reference 269282) and PESt-CTM/LA0011/2013.

mix of HAp and  $\beta$ -TCP produced from the untreated bones heated to  $1000^\circ C$  is preferred for many biomedical applications, FAp is used in dental implants and ClAp can form a phosphor material. When 2 mol%  $TiO_2$  was added to the bones during processing, titania-doped HAp/ $\beta$ -TCP materials were produced with excellent photocatalytic and antibacterial properties, with a band gap energy around 3.42 eV. These were able to remove polluting dyes from waste waters under UV or visible light, completely removing the dye after 1

hour under UV light, and degrading 75% after 8 hours under white (indoor) lighting. They also deactivated dangerous bacteria such as *MRSA* and *E. coli* in only 2 hours under UV light, with a reduction by 80% and 87%, respectively. Calcium doping of the bones also produced a pure HAp which deactivated 97% *E. coli* and 88% *MRSA* after 2 hours of UV exposure. The HAp from waste bones has also been combined with bacteria from polluted industrial sites in Portugal, and used to remove heavy metal pollutants through a synergistic process,

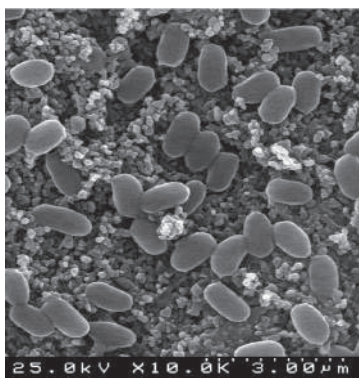


Figure 2. Photocatalytic properties of 2 mol% TiO<sub>2</sub> doped HAp from valorised waste cod fish bones. Degradation of methylene blue dye under a) UV light and b) white (artificial indoor) light, and deactivation of harmful bacteria c) *MRSA* and d) *E. coli*.

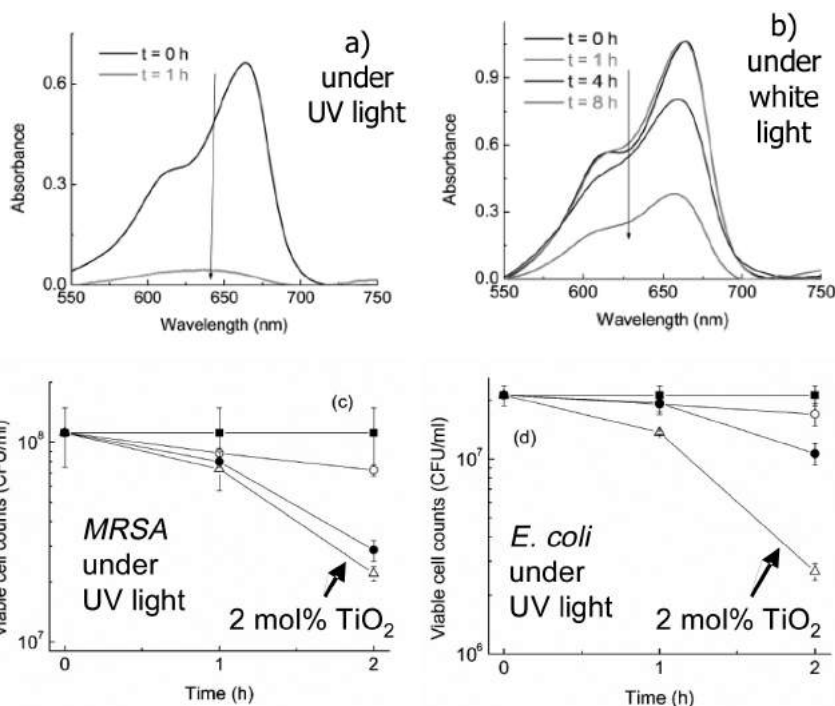
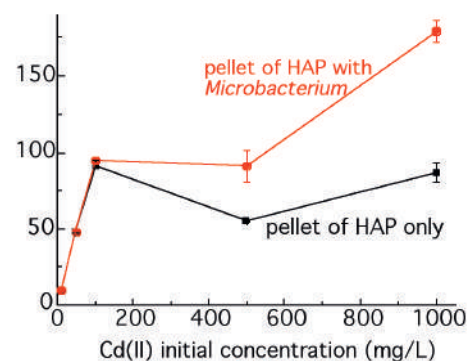


Figure 3 SEM image of *Microbacterium oxydans* immobilized on the surface of untreated HAp made from cod fish bone heated to 600 °C, and the synergistic effect of HAp + bacteria increasing the absorption of cadmium (II) ions.

greatly increasing the effect that the HAp had by itself. A four-fold increase in the amount of zinc (II) and a three-fold increase

in the amount of cadmium (II) adsorbed was observed, for the bones modified with the immobilised bacteria *Cupriavidus sp.*

and *Microbacterium oxydans*, respectively. The effect also increased with higher levels of heavy metal contaminants.

<sup>1</sup> Department of Materials and Ceramic Engineering, CICECO, University of Aveiro, 3810-193 Aveiro, Portugal

<sup>2</sup> CBQF / Escola Superior de Biotecnologia, Universidade Católica Portuguesa, 4200-072 Porto, Portugal

<sup>3</sup> WeDoTech, CiDEB / Escola Superior de Biotecnologia, Universidade Católica Portuguesa, 4200-072 Porto, Portugal

<sup>4</sup> Chemistry Department, University College London, London, WC1E 6BT, UK

#### References

- [1] Piccirillo C, Silva MF, Pullar RC, Cruz IB, Jorge R, Pintado MME, Castro PML, *Materials Science and Engineering C*, 2013, 33, 103-110.
- [2] Piccirillo C, Pereira SIA, Marques AP, Pullar RC, Tobaldi DM, Castro PML, *Journal of Environmental Management*, 2013, 121, 87-95.
- [3] Piccirillo C, Dunnill CW, Pullar RC, Tobaldi DM, Labrincha JA, Parkin IP, Pintado MM, Castro PML, *Journal of Materials Chemistry A*, 2013, 1, 6452-6461.

#### Acknowledgments

R.C. Pullar was supported by the FCT Ciência 2008 programme. This work was performed under the networks InSolEx (Innovative Solutions for Extracting High Value Natural Compounds, funded by the European Union, contract MRT-CT-2006-036053) and iCOD (Inovadora Tecnologias para a Valorização de Subprodutos do Processamento do Bacalhau, funded by FTC, contract OREN AdI IRI466), and was also supported by the FCT project PEst-OE/EQB/LA0016/2011 and the FCT research grants SFRH/BPD/34585/2007 and SFRH/BPD/65134/2009. We thank Pascoal & Filhos S.A. for supplying the cod fish bones.

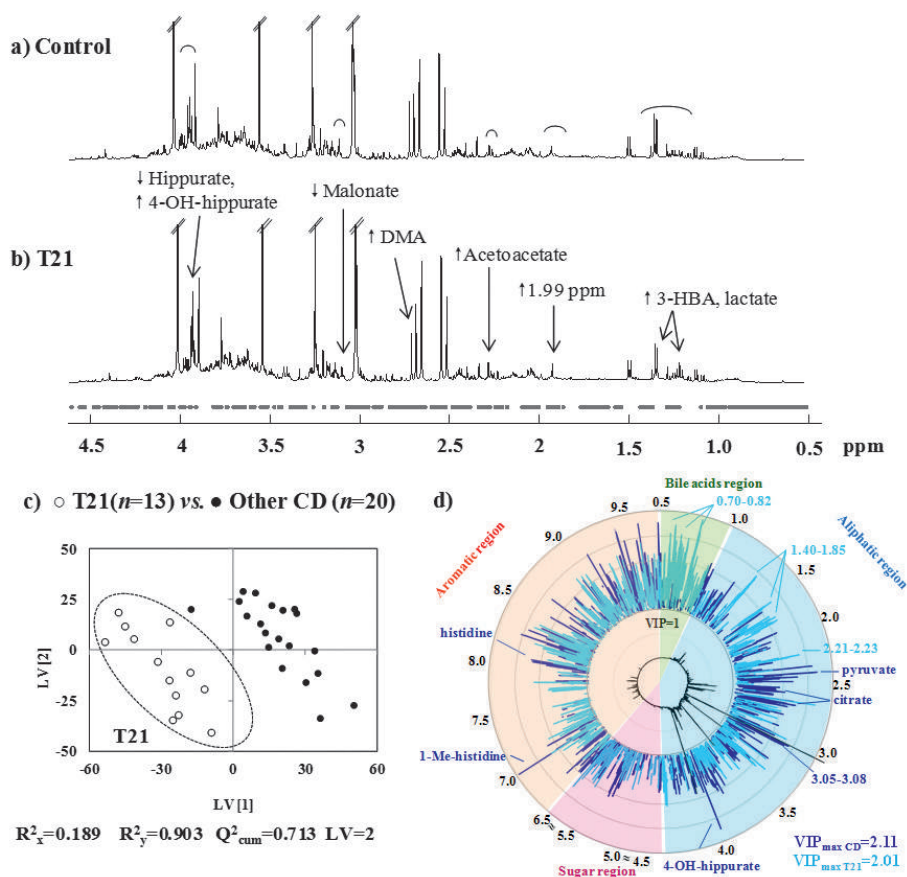
## SECOND TRIMESTER MATERNAL URINE FOR THE DIAGNOSIS OF TRISOMY 21 AND PREDICTION OF POOR PREGNANCY OUTCOMES

Diaz S<sup>01</sup>, Barros AS<sup>2</sup>, Goodfellow BJ<sup>1</sup>, Duarte IF<sup>1</sup>, Galhano E<sup>4</sup>, Pita C<sup>4</sup>, Almeida MC<sup>4</sup>, Carreira IM<sup>3</sup>, Gil AM<sup>1</sup>

A novel strategy was presented for the detection of deviations in the composition of maternal urine, to define metabolite fin-

gerprints for the recognition of trisomy 21 (T21) and fetal malformations (FM) and prediction of preterm delivery (PTD),

intra-uterine growth restriction (IUGR), preeclampsia (PE) and gestational diabetes mellitus (GDM) [1]. The challenge is set by the hundreds of metabolites present in urine, which result in complex analytical records from which meaningful variations are to be retrieved/quantified. The tools/strategies used here are applicable not only to biofluids in disease research, such as the present study, but also to other biological samples (tissues, cells) in



intensities. Although visual differences are noted between control and disease spectra (Figure 1a,b), comparison of full matrixes was handled by partial least squares discriminant analysis (PLS-DA) and subsequent Monte Carlo cross validation (MCCV) and permutation tests. Analysis of original datasets resulted in weak models and, hence, several variable importance to the projection (VIP)- and b-coefficient-based variable selection methods were tested (gray dots in Figure 1b represent variables selected for T21 identification). The variable selected subsets led to improved PLS-DA models and specific metabolite signatures (Figure 1c,d), with applicability in T21 and FM diagnosis and identification of PTD, IUGR, PE and GDM *pre-clinical* markers. This work demonstrated, for the first time, the value of maternal urine profiling as a complementary means of prenatal diagnostics and early prediction of several poor pregnancy outcomes.

<sup>1</sup> Department of Chemistry, CICECO, University of Aveiro, 3810-193 Aveiro, Portugal

<sup>2</sup> Department of Chemistry, QOPNA, University of Aveiro, 3810-193 Aveiro, Portugal

<sup>3</sup> Cytogenetics and Genomics Laboratory, Faculty of Medicine, University of Coimbra, Portugal and CIMAGO Center for Research in Environment, Genetics and Oncobiology, Portugal

<sup>4</sup> Maternidade Bissaya Barreto, Centro Hospitalar e Universitário de Coimbra, 3000 Coimbra, Portugal

#### Reference

<sup>[1]</sup> Dias SO, Barros AS, Goodfellow BJ, Duarte IF, Galhano E, Pita C, Almeida MC, Carreira IM, Gil AM, *Journal of Proteome Research*, 2013, 12, 2946–2957.

contexts as varied as exposure to contaminants, pharmaceuticals or (bio)materials. In this work,  $^1\text{H}$  NMR metabolomics was used to find specific metabolic excretory sig-

natures of the conditions specified above. Figure 1a shows an expansion of the NMR spectrum of control urine, with a large number of signals covering a wide range of

## METABOLOMICS OF BLOOD PLASMA AND URINE SHOWS PROMISE IN LUNG CANCER DIAGNOSIS

Rocha CM<sup>1</sup>, Carrola J<sup>1</sup>, Barros AS<sup>2</sup>, Gil AM<sup>1</sup>, Goodfellow BJ<sup>1</sup>, Carreira IM<sup>3,4</sup>, Bernardo J<sup>4,5</sup>, Gomes A<sup>4,5</sup>, Sousa V<sup>4,5,6</sup>, Carvalho L<sup>4,5,6</sup>, Duarte IF<sup>1</sup>

Lung cancer is one of the most prevalent and fatal types of cancer, its poor prognosis being typically related to asymptomatic development and late detection. New methods that can aid in the early, minimally invasive detection of this disease are, thus, greatly needed. Altered metabolism is currently viewed as an emer-

gent cancer hallmark, with tumour cells exhibiting a distinct metabolic behaviour and impacting on systemic metabolism. Therefore, assessing metabolic changes related to tumour onset and progression has been embraced as a promising tool in cancer detection and monitoring <sup>[1,2]</sup>. Our group has been investigating lung can-

cer metabolic signatures in easily accessible biofluids through Nuclear Magnetic Resonance (NMR) spectroscopy combined with multivariate analysis i.e. using a metabolomics approach. In particular, we have shown that, based on plasma profiles, cancer patients could be clearly differentiated from healthy subjects with sensitivity and specificity levels of about 90%, permutation testing having further confirmed the predictive ability of this model <sup>[3]</sup>. The main distinctive features in the patients' plasma were lower HDL and higher VLDL+LDL lipoproteins, together with increased lactate and pyruvate and de-

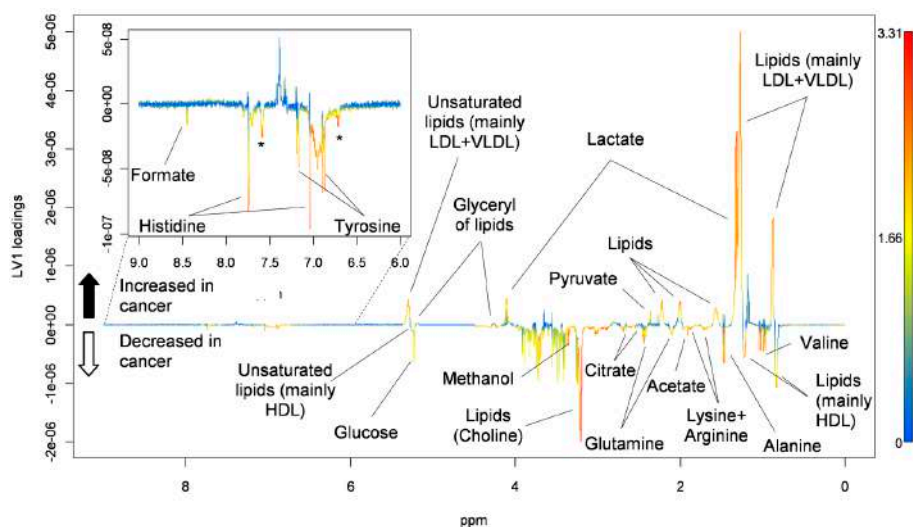


**Figure 1.** Loadings plot obtained by Partial Least Squares Discriminant Analysis (PLS-DA) of  $^1\text{H}$  NMR plasma spectra of healthy subjects ( $n = 78$ ) and lung cancer patients ( $n = 85$ ). Positive/negative signals refer, respectively, to compounds increased/decreased in patients relatively to controls. The colour scale reflects the importance of variables for class discrimination.

creased glucose, citrate, formate, acetate, several amino acids (alanine, glutamine, histidine, tyrosine, valine) and methanol (Figure 1). An equally good discrimination between lung cancer and healthy subjects was obtained by NMR profiling of urine [4], highlighting a number

of consistently altered metabolites, such as hippurate and trigonelline (reduced in patients), and  $\beta$ -hydroxyisovalerate,  $\alpha$ -hydroxyisobutyrate, N-acetylglutamine and creatinine (elevated in patients relatively to controls). Notably, possible confounders (age, gender, smoking habits)

were found to have a lower impact on the biofluids composition compared to the presence of the disease. Moreover, the changes detected in both plasma and urine were present at initial disease stages, thus supporting the promising value of NMR metabolomics in lung cancer screening and early detection.

<sup>1</sup> Department of Chemistry, CICECO, University of Aveiro, 3810-193 Aveiro, Portugal

<sup>2</sup> Department of Chemistry, QOPNA, University of Aveiro, 3810-193 Aveiro, Portugal

<sup>3</sup> Laboratory of Cytogenetics and Genomics, Faculty of Medicine, University of Coimbra, 3000 Coimbra, Portugal

<sup>4</sup> CIMAGO, Faculty of Medicine, University of Coimbra, 3000 Coimbra, Portugal

<sup>5</sup> University Hospitals of Coimbra, 3000-075 Coimbra, Portugal

<sup>6</sup> Institute of Pathological Anatomy, Faculty of Medicine, University of Coimbra, 3000 Coimbra, Portugal

## References

[1] Duarte IF, Gil AM, *Progress in Nuclear Magnetic Resonance Spectroscopy*, 2012, 51-74.

[2] Duarte IF, Rocha CM, Gil AM, *Expert Review of Molecular Diagnostics*, 2013, 13[?], 737-48.

[3] Rocha CM, Carrola J, Barros AS, Gil AM, Goodfellow BJ, Carreira IM, Bernardo J, Gomes A, Sousa V, Carvalho L, Duarte IF, *Journal of Proteome Research*, 2011, 10[9], 4314-4324.

[4] Carrola J, Rocha CM, Barros AS, Gil AM, Goodfellow BJ, Carreira IM, Bernardo J, Gomes A, Sousa V, Carvalho L, Duarte IF, *Journal of Proteome Research*, 2011, 10[1], 221-230.

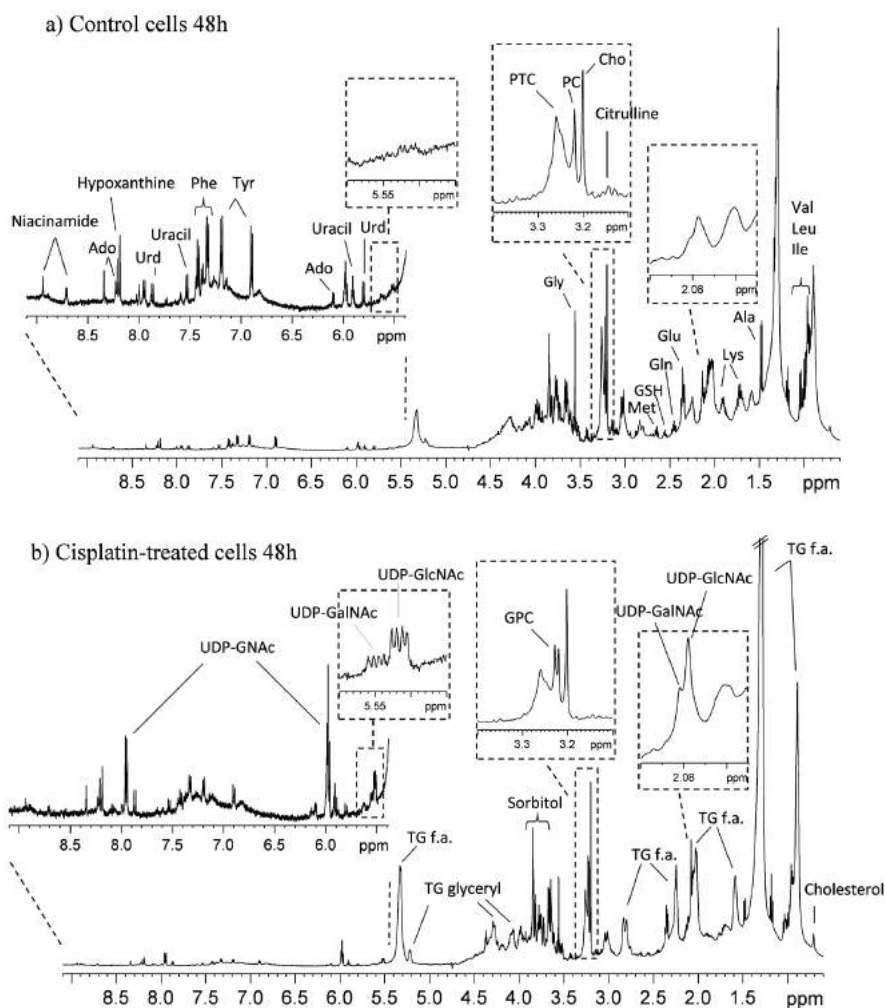
## POTENTIAL MARKERS OF CISPLATIN TREATMENT RESPONSE UNVEILED BY NMR METABOLOMICS OF HUMAN LUNG CELLS

Duarte IF<sup>1</sup>, Ladeirinha AF<sup>2</sup>, Lamego I<sup>1</sup>, Gil AM<sup>1</sup>, Carvalho L<sup>3,4,5</sup>, Carreira IM<sup>2,5</sup>, Melo JB<sup>2,5</sup>

Based on the premise that drugs consistently affect cellular metabolism, metabolic profiling (or metabolomics) of cultured cells has the potential to provide new insights about drugs' mechanisms of action and to reveal new endpoint markers of drug toxicity and/or efficacy.  $^1\text{H}$  High Resolution Magic Angle Spinning (HRMAS) Nuclear Magnetic Resonance (NMR) spectroscopy is particularly powerful in this context, as it allows well-resolved spectra to be obtained directly from cells (or cell lysates), providing rapid information on the quantitative variations in both small metabolites and mobile lipids, simultaneously (Figure 1). In this work,  $^1\text{H}$  HRMAS NMR was used to

characterize the intracellular composition (endometabolome) of A549 human lung adenocarcinoma cells exposed to cisplatin, an alkylating drug commonly used in chemotherapy for several cancer types (including lung cancer) [1]. One of the most striking differences between control and treated cells regarded lipid signals, namely those arising from triglycerides (TG) and cholesterol esters, which significantly increased upon cisplatin exposure. Moreover, TG accumulating in treated cells were shown to have greater average fatty acyl chain length and unsaturation degree, compared to those detected in control cells. Other than lipid-related changes, consistent varia-

tions were observed for nucleotide sugars (UDP-GNAc) and sorbitol (increased in treated cells), niacinamide and several amino acids (decreased in treated cells). The marked increase in nucleotide sugars, especially in uridine diphosphate N-acetylglucosamine (UDP-GlcNAc), was a particularly interesting observation as these compounds, produced from glucose *via* the hexosamine biosynthetic pathway (HBP), act as donor molecules for glycosylation of proteins and lipids, a modification known to be important in a number of biological processes and diseases, including cancer. Moreover, a strong correlation was observed between lipids and nucleotide sugars' variations, suggesting that the biogenesis of lipid droplets and the hexosamine biosynthesis and/or glycosylation pathways may be mechanistically associated. Overall, these results show that *in vitro* NMR metabolomics is a powerful tool for detecting variations in a range of intracellular compounds upon drug exposure, thus offering the possi-



bility of identifying candidate metabolite markers for *in vivo* monitoring of tumour responsiveness to treatment.

<sup>1</sup> Department of Chemistry, CICECO, University of Aveiro, 3810-193 Aveiro, Portugal

<sup>2</sup> Laboratory of Cytogenetics and Genomics, Faculty of Medicine, University of Coimbra, 3000 Coimbra, Portugal

<sup>3</sup> University Hospitals of Coimbra, 3000-075 Coimbra, Portugal

<sup>4</sup> Institute of Pathological Anatomy, Faculty of Medicine, University of Coimbra, 3000 Coimbra, Portugal

<sup>5</sup> CIMAGO, Faculty of Medicine, University of Coimbra, 3000 Coimbra, Portugal.

#### Reference

[1] Duarte IF, Ladeirainha A, Lamego I, Gil AM, Carvalho L, Carreira IM, Melo JB, *Molecular Pharmaceutics*, 2013, 10(11), 4242-4251.

**Figure 1.** Average <sup>1</sup>H HRMAS NMR spectra of a) control and b) cisplatin-treated A549 lung cells, at 48 hours. Some assignments are indicated: Three-letter code used for amino acids, Ado adenosine, Cho choline, f.a. fatty acyl groups, GPC glycerophosphocholine, GSH reduced glutathione, PC phosphocholine, PTC phosphatidylcholine, TG triglycerides, UDP-GalNAc uridine diphosphate galactosamine, UDP-GlcNAc uridine diphosphate glucosamine, UDP-GNAc uridine diphosphate hexosamine, Urd uridine.



# Computational Methods and Theory

## HALOGEN-BONDING IN ANION RECOGNITION

Costa PJ<sup>1</sup>, Félix V<sup>1</sup>, Beer PD<sup>2</sup>

Halogen bonding is the attractive intermolecular interaction between an electron deficient positively polarized halogen atom and a Lewis base. Although anion recognition in solution takes advantage of the ubiquitous hydrogen bonding, the halogen bonding is rapidly becoming an established field in its own right. An extensive collaboration between our group and the group of Prof. Paul Beer (University of Oxford) resulted in the development and application of halogen bonding in the field of anion recognition. In our first work, anion templation was used to prepare the first halogen bonding catenane, which binds and senses selectively chloride and bromide in  $\text{CH}_3\text{CN}$  solution [1]. Molecular dynamics simulations

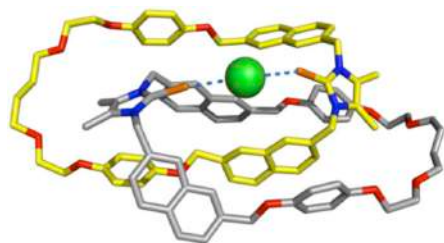


Figure 1 Representative co-conformation of the XB catenane bound to chloride in  $\text{CH}_3\text{CN}$  solution. The two  $\text{C-Br}\cdots\text{Cl}^-$  halogen bonds are drawn as light blue dashed lines.

were performed in explicit  $\text{CH}_3\text{CN}$  using the structure of the halogen bonding catenane bound to chloride and, among other analyses, a representative snapshot was extracted (Fig. 1). Two simultaneous halogen bonds are established between the bromine atoms of both macrocycles and the chloride anion. A  $\pi$ - $\pi$  stacking interaction between one hydroquinone and a naphthalene group was also observed throughout the course of a molecular dynamics simulation, corroborating the experimental data.

In our second work, a new family of fluorescent halogen bonding macrocyclic halo-imidazolium receptors was described showing that the bromo- and iodo- receptors bind selectively iodide and bromide, respectively, in the competitive  $\text{CD}_3\text{OD}/\text{D}_2\text{O}$  (9:1) aqueous solvent mixture, sensing these anions exclusively via a fluorescence response [2]. The remarkable affinity of both receptors towards bromide was investigated by means of Density Functional Theory calculations and molecular dynamics simulations. The DFT optimized structure of the iodo-imidazolium receptor binding bromide is depicted in Fig. 2 and show that indeed the receptor is able

to bind bromide with great affinity and relatively short  $\text{C-I}\cdots\text{Br}^-$  distances (3.192 Å). The subsequent molecular dynamics simulations showed that those two simultaneous halogen bondings were stable in explicit  $\text{CH}_3\text{OH}/\text{H}_2\text{O}$  mixtures, helping to complement the experimental characterization.

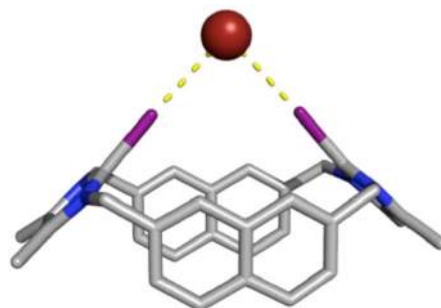


Figure 2 DFT optimized structure of the iodo-imidazolium receptor binding bromide, showing the corresponding halogen bonding interactions as yellow dashed lines.

<sup>1</sup> Department of Chemistry and Secção Autónoma de Ciências da Saúde, CICECO, University of Aveiro, 3810-193 Aveiro, Portugal

<sup>2</sup> Chemistry Research Laboratory, Department of Chemistry, University of Oxford, Mansfield Road, Oxford, OX1 3TA, UK

### References

[1] Caballero A, Zapata F, White NG, Costa PJ, Félix V, Beer PD, *Angewandte Chemie International Edition*, 2012, 51, 1876-1880.

[2] Zapata F, Caballero A, White NG, Claridge TDW, Costa PJ, Félix V, Beer PD, *Journal of the American Chemical Society*, 2012, 134, 11533-1154.

## DEVELOPMENT OF SYNTHETIC ANION CARRIERS FOR REPLACEMENT THERAPIES: A COMPUTATIONAL APPROACH

Félix V<sup>1</sup>, Marques I<sup>1</sup>, Colaço AR<sup>1</sup>, Costa PJ<sup>2</sup>, Busschaert N<sup>3</sup>, Gale PA<sup>3,4</sup>

The anion transmembrane transport is essential to cell functioning and depends on several mechanisms, such as anions channels. The dysfunction of these channels is currently linked with the occurrence of several pathologies, including cystic fibrosis and male infertility, caused by defective transmembrane transport of chloride and bicarbonate anions. The lack of natural alternative anionophores led to great interest in the development of syn-

thetic molecules able to promote passive anion transport with the potential to be applied as replacement therapeutics. Molecular Dynamics (MD) simulations are a powerful tool to investigate the impact of the artificial transporters on the structural and dynamic properties of the phospholipid bilayers. Moreover, MD simulations also give valuable insights on how these molecules mediate the anion transmembrane transport.

Following our research interests on this field of supramolecular chemistry, we have studied the potential of a calix<sup>[4]</sup>arene derivative (1) as chloride anion transporter by MD simulations in a DOPC bilayer. This putative transporter has four protonated  $\text{NH}_3^+$  binding groups in the upper rim and four hydrophobic aliphatic tails in the lower rim. Unconstrained MD simulations show that the interaction of 1 with DOPC occurs *via* the  $\text{NH}_3^+$  groups, which are able to establish electrostatic interactions and multiple hydrogen bonds with the DOPC phosphate groups, while the aliphatic tails point towards the water phase (when 1 was initially positioned in the water phase) or to the membrane (when 1 starts within the bilayer). The interaction does not induce any relevant

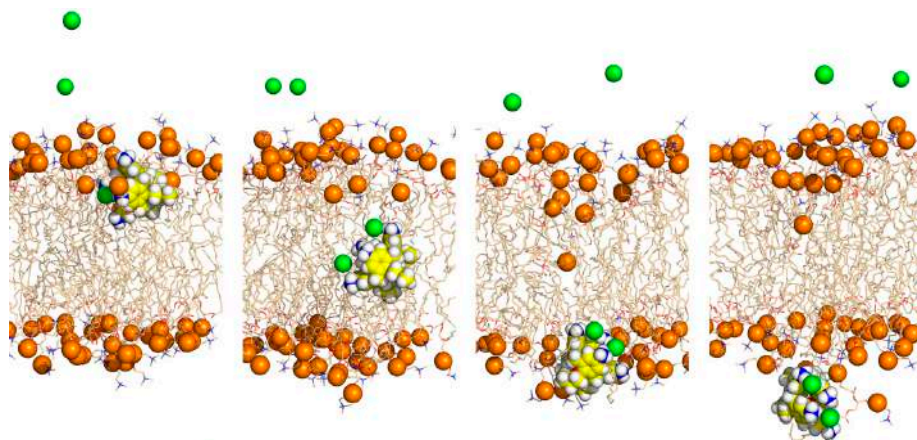


**Figure 1.** The transmembrane transport of two chloride anions assisted by **1** is illustrated with four consecutive snapshots. The transporter and phosphorus atoms are represented in spheres with hydrogen atoms in white, oxygen atoms in red, nitrogen atoms in blue and carbon atoms in yellow (transporter) or wheat (phospholipids) colour, while the chloride ions are shown as green spheres. The lipids C–H atoms and the water slabs were omitted for clarity.

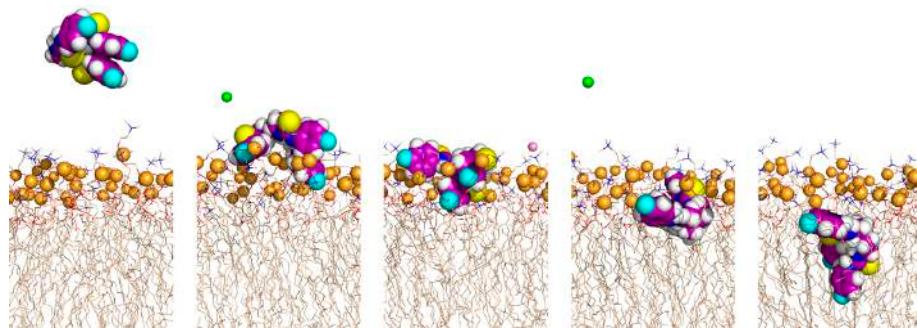


**Figure 2.** The approach of **4** to the water–lipid interface of the bilayer is illustrated with five consecutive snapshots. The transporter and phosphorus atoms are represented in spheres with hydrogen atoms in white, oxygen atoms in red, nitrogen atoms in blue and carbon atoms in purple (transporter) or wheat (phospholipids) colour, while the chloride and sodium ions are shown as green and pink spheres, respectively. The lipids C–H atoms and the water slabs were omitted for clarity.

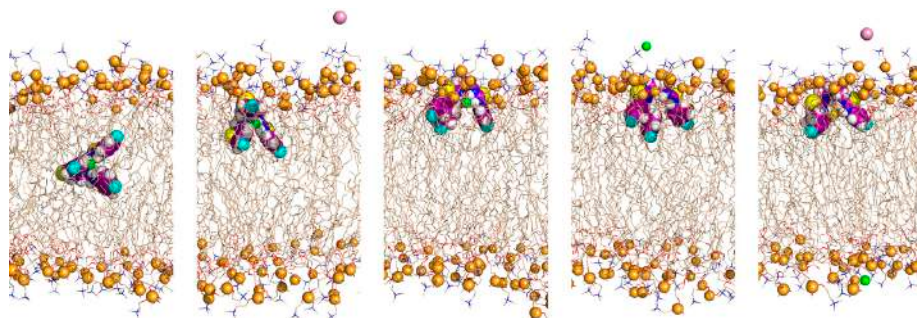


**Figure 3.** The diffusion of **4** from the bilayer core and the release of the chloride anion is illustrated with five consecutive snapshots. The transporter and phosphorus atoms are represented in spheres with hydrogen atoms in white, oxygen atoms in red, nitrogen atoms in blue and carbon atoms in purple (transporter) or wheat (phospholipids) colour, while the chloride and sodium ions are shown as green and pink spheres, respectively. The lipids C–H atoms and the water slabs were omitted for clarity.

perturbation on the biophysical properties of the bilayer, apart from a systematic increase in the order parameter of the C<sub>2</sub> carbon atom of the *sn*-1 lipid tail. Steered Molecular Dynamics (SMD) simulations were performed in order to simulate the permeation of the bilayer by **1** and as well to evaluate the energy barrier associated with this event. To the best of our knowledge, this SMD simulation is the first evi-

dence at molecular level of the occurrence of chloride transport assisted by a synthetic molecule, as illustrated by the sequence of events shown in Figure 1, in agreement with anion carrier mechanism. Furthermore, the Potential of Mean Force (PMF) indicates a barrier of *ca.* 58 kJ mol<sup>-1</sup> for **1** to cross the membrane.<sup>[1]</sup> Moreover, we are also in collaboration with the colleague Philip Gale (University

of Southampton), in an effort to obtain insights regarding several series of potential anion transmembrane transporters. One highlight of this combination of theoretical and experimental efforts is the study of the interaction of six synthetic chloride transmembrane transporters with a POPC bilayer by means of MD simulations. The general Amber force field (GAFF) was set to describe the transporters, while LIPID11 was used for the POPC lipids. These transporters are structurally simple molecules, based on the tris(2-aminoethyl)amine scaffold, containing three thiourea binding units coupled with three *n*-butyl (2), phenyl (3), fluorophenyl (4), pentafluorophenyl (5), trifluoromethylphenyl (6), or bis(trifluoromethyl)phenyl (7) substituents. The passive diffusion of 2–7 ⊃ Cl<sup>-</sup> was evaluated with the complexes initially positioned either in the water phase or inside the bilayer. In the first scenario the chloride is released in the water solution before the synthetic molecules achieve the water–lipid interface and permeate the membrane (Figure 2). In the second scenario, the anion is released to the water phase only when the chloride complex reaches the interface (Figure 3). Independently of the transporter used in the membrane system, the bilayer structure is preserved and the synthetic molecules interact with the POPC molecules at the phosphate head-group level, *via* N–H⋯O hydrogen bonds. Overall, the MD simulations' results indicate that the small tripodal molecules in this series have a low impact on the bilayer and are able to diffuse with chloride inside the lipid environment, potentially as anion carriers.<sup>[2]</sup>

<sup>1</sup> Department of Chemistry and Secção Autónoma de Ciências da Saúde, CICECO, University of Aveiro, 3810-193 Aveiro, Portugal

<sup>2</sup> Department of Chemistry and Secção Autónoma de Ciências da Saúde, OOPNA, University of Aveiro, 3810-193 Aveiro, Portugal

<sup>3</sup> Chemistry, University of Southampton, Southampton, UK

<sup>4</sup> Department of Chemistry, Faculty of Science, King Abdulaziz University, Jeddah 21589, Saudi Arabia

#### References

<sup>[1]</sup> Costa PJ, Marques I, Felix V, *Biochimica et Biophysica Acta*, 2014, 1838, 890-901.

<sup>[2]</sup> Marques I, Colaco AR, Costa PJ, Busschaert N, Gale PA, Felix V, *Soft Matter*, 2014, 10, 3608-3621.

# DINUCLER RUTHENIUM(II) COMPLEXES FOR STABILIZING AND IMAGING AN ANTIPARALLEL FOLDED HUMAN TELOMERE SEQUENCE

Félix V<sup>1,3</sup>, Costa PJ<sup>2,3</sup>, Williamson MP<sup>4</sup>, Thomas JA<sup>5</sup>, Wilson T<sup>4,5</sup>

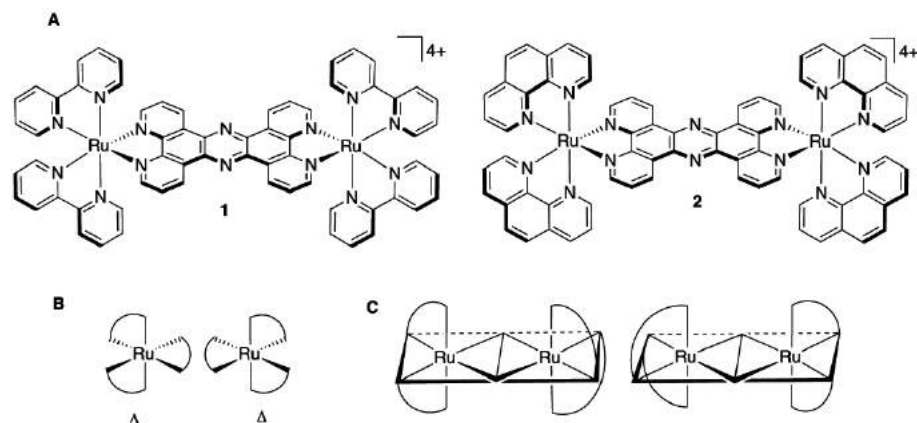


Figure 1. (A) Structures of complexes studied. (B) The two possible enantiomers of each of the metal centers in 1 and 2. (C) Schematic of the two diastereomers of 1 and 2 relevant to this study: left  $\Lambda\Lambda$ ; right  $\Delta\Delta$ .

Telomeres can fold into quadruplex structures *in vivo* and shortening of telomeres on chromosomal replication is considered to be a major cause of senescence. Additionally, cancer cells have been shown to generate an immortal phenotype by up-regulating telomerase. Since the activity of telomerase is inhibited by the presence of G-quadruplexes there is a great potential in novel compounds able to bind and stabilize quadruplexes as anticancer agents.

This Highlight focuses on an ongoing collaboration between the group of Macromolecular Modelling and Computational Biophysics (UA) and colleagues from University of Sheffield which ambitions to develop luminescent metal complexes as sequence and structure specific DNA binding substrates. In this context, the quadruplex binding properties of dinuclear ruthenium(II) complexes containing the tetrapyrido[3,2-

*a:2',3'-c:3'',2''-h:2''',3'''-j*]phenazine (tp-phz) depicted in Figure 1 were studied using a combination of NMR experiments and Molecular Dynamics (MD) simulations. Both  $[\{\text{Ru}(\text{bipy})_2\}_2\text{tpphz}]^{4+}$ , 1, and  $[\{\text{Ru}(\text{phen})_2\}_2\text{tpphz}]^{4+}$ , 2, (where bipy = 2,2'-bipyridine, phen = 1,10-phenanthroline), bind to quadruplex DNA but the  $\Lambda\Lambda$  isomer binds approximately 40 times more tightly than the  $\Delta\Delta$ , with a stronger luminescence.

The structures based on NMR experimentally derived restraints show that the  $\Lambda\Lambda$  isomer fits neatly under the diagonal loop, whereas the  $\Delta\Delta$  isomer is unable to bind here and binds at the lateral loop end. In order to try to explain this selectivity, we performed unrestrained MD simulations to evaluate the impact of  $\Lambda\Lambda$ -1 and  $\Delta\Delta$ -1 complexes on the quadruplex structure when binding under the diagonal loop. The results suggest that, although both  $\Lambda\Lambda$ -1 and  $\Delta\Delta$ -1 complexes can fit under the loop (see Figure 2), sufficient HTS loop conformational freedom to permit the complex entrance into the prefolded G-DNA structure is only present for  $\Lambda\Lambda$ -1. In contrast, the stereochemistry of  $\Delta\Delta$ -1 appears to induce increased rigidity on the loop, preventing complex entrance into the loop arch. This structural feature is depicted in Figure 3, which shows a surface representation built from the positions occupied by the tp-phz ligand (excluding the hydrogen atoms) over a 50 ns collection period for the HTS association with each one of the diastereomers. In  $\Lambda\Lambda$ -1-HTS, the tp-phz ligand is able to “float” over the G-tetrad interacting with the four guanines. In contrast, in  $\Delta\Delta$ -1-HTS, the tp-phz ligand remains “locked” over two guanines of the G-tetrad throughout the entire simulation time. In other words,  $\Delta\Delta$ -1 does not bind under the diagonal loop because the loop arch does not fulfill the complex’s “stereochemical requirements”.

In summary, this work showed that  $\Lambda\Lambda$ -1, as well as  $\Lambda\Lambda$ -2, is a useful tool for specifically stabilizing and imaging antiparallel basket structures with a diagonal loop and confirms that the antiparallel structure of HTS can be selectively targeted.

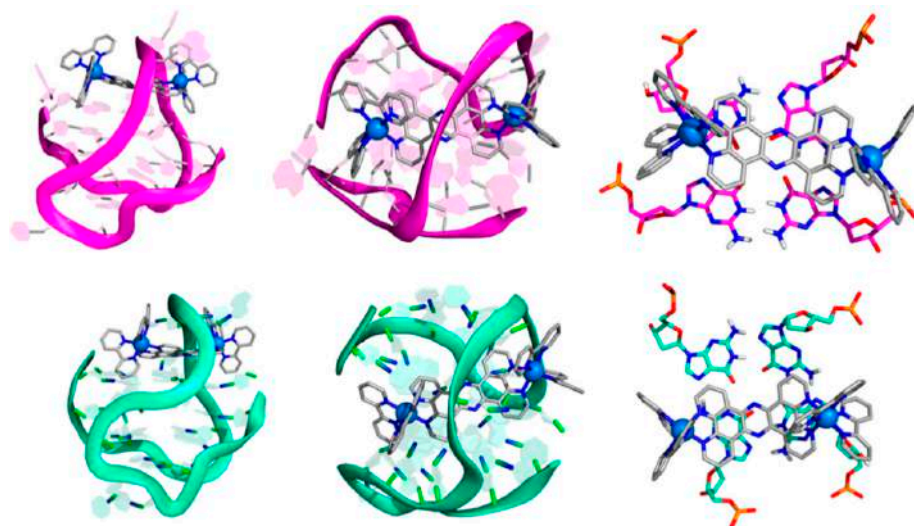


Figure 2. Representative snapshots of simulations  $\Lambda\Lambda$ -1-HTS (top, magenta) and  $\Delta\Delta$ -1-HTS (bottom, aquamarine) showing both complexes under the diagonal loop. Side and top views are presented on the left and center, respectively. Right pictures represent the complexes stacked over the top G-quartet.

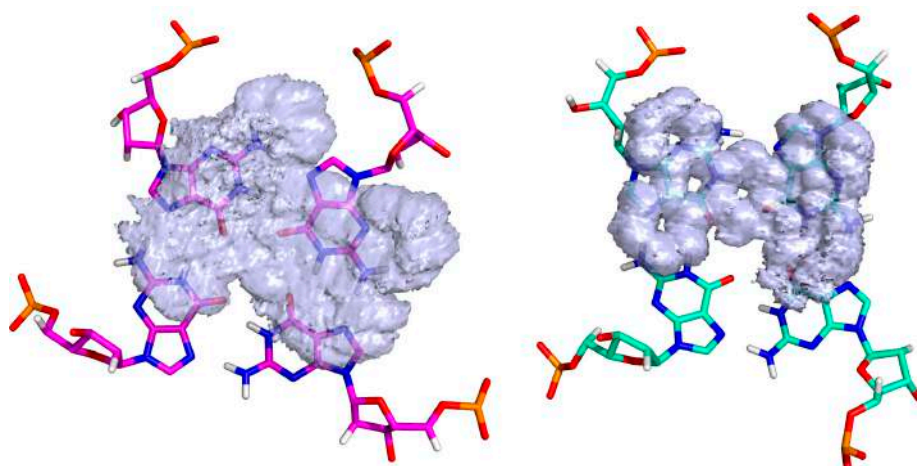


Figure 3. Surface representing the histogram of positions occupied by the tpphz atoms over the 50 ns collection period in  $\Delta\Delta$ -1-HTS (left) and  $\Delta\Delta$ -1-HTS (right).

<sup>1</sup> Department of Chemistry, CICECO, University of Aveiro, 3810-193 Aveiro, Portugal

<sup>2</sup> Department of Chemistry, QOPNA, University of Aveiro, 3810-193 Aveiro, Portugal

<sup>3</sup> Secção Autónoma de Ciências da Saúde, University of Aveiro, 3810-193 Aveiro, Portugal

<sup>4</sup> Department of Molecular Biology and Biotechnology, University of Sheffield, UK

<sup>5</sup> Department of Chemistry, University of Sheffield, UK

#### Reference

<sup>[1]</sup> Wilson T, Costa PJ, Félix V, Williamson MP, Thomas JA, *Journal of Medicinal Chemistry*, 2013, 56, 8674–8683.

## SIMPLE DESCRIPTORS FOR PREDICTING THE CATALYTIC ACTIVITY OF TRANSITION METAL SURFACES FOR O-H BOND DISSOCIATION REACTIONS

Fajin JLC<sup>1</sup>, Cordeiro MNDS<sup>1</sup>, Illas F<sup>2</sup>, Gomes JRB<sup>3</sup>

Chemical processes often consist of a number of elementary reaction steps where bond making and bond breaking occur. One of such important elementary steps concerns the cleavage of the RO—H functional group since this is present in many common compounds such as alco-

hols, organic acids or even water. There are several heterogeneous catalytic processes where elementary steps involving the cleavage of O—H bonds either in reactants or intermediate species play a key role. The water gas shift reaction (WGS:  $\text{CO} + \text{H}_2\text{O} \rightarrow \text{CO}_2 + \text{H}_2$ ) is essen-

tial in the production of clean hydrogen, and the ability of the catalyst to dissociate the O—H bonds in the water molecule becomes crucial. The scission of O—H bonds is also involved in the selective oxidation of alcohols to carboxylic compounds over heterogeneous recyclable catalysts and, in general, the mechanism for alcohol oxidation involves the formation of an adsorbed alkoxy species.

Due to the important role of the O—H bond in many chemical processes it would be important to rationalize the vast number of available results and to develop tools for predicting the activities of catalysts towards the reaction of O—H bond dissociation. Previously, based on energetic data calculated through density functional theory (DFT), we have found that it is possible to estimate/predict the activity of metal-based surfaces for the catalysis of the O—H bond scission in water by consideration of Brønsted-Evans-Polanyi (BEP) type relationships connecting the energy barrier required to break the bond and several descriptors that may be easily calculated or found in the literature, such as the reaction energy, the adsorption energy of the reaction products, or even the adsorption energy of an oxygen atom <sup>[1]</sup>. Now, we extended these ideas and developed a new BEP relationship for predicting the activities of planar or stepped metal surfaces and metal particles towards the catalysis of the O—H bond scission in any compound <sup>[2]</sup>. The adsorption energy of the reaction products was found

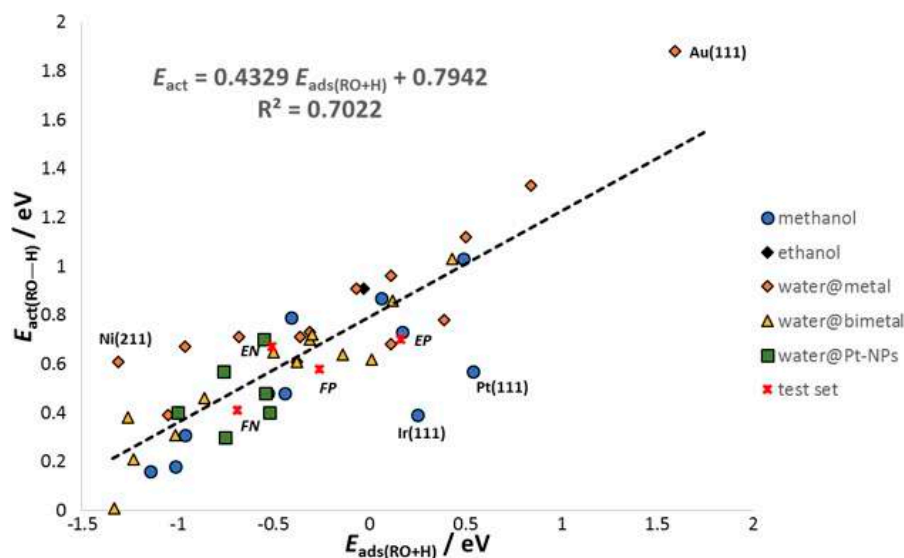


Figure 1. Relationship between the activation energy barrier for the  $\text{ROH}^* + * \rightarrow \text{RO}^* + \text{H}^*$  reaction and the co-adsorption energy of the RO and H species on planar and stepped metallic or bimetallic surfaces and platinum nanoparticles, with  $\text{R} = \text{H}_0, \text{CH}_3, \text{CH}_2\text{CH}_2, \text{O}$  and  $\text{ROH} = \text{water, methanol and ethanol, respectively}$ . E, F, N and P stand for ethanol, formic acid, Ni(111) and Pd(111), respectively. \* denotes an adsorption site available on the catalyst model surface.

to be the most convenient descriptor for the RO—H bond break with the resulting fitting shown in Figure 1. The validity of the relationship has been explored by considering cases not included in the database of energy barriers and adsorption energies used to its development. The use of this descriptor allows a fast and easy screening of the cases of interest on a rather large number of metallic sur-

faces, bimetallic surfaces and nanoparticles without needing to carry out tedious calculations for transition state structure location and characterizations or keeping this to a minimum number on potential candidate systems. Therefore, explicit calculation of the activation energy barriers are limited to a few, previously detected, interesting cases only.

## ON THE ORIGINS OF THE MOLECULAR-SCALE PERIODICITY IN THE PORE WALLS OF PERIODIC MESOPOROUS ORGANOSILICAS

Futamura R<sup>1</sup>, Jorge M<sup>2</sup>, Gomes JRB<sup>1</sup>

Periodic mesoporous organosilicas (PMOs) are materials presenting unique structural properties due to their hybrid building blocks, based on organic and inorganic (silicate) moieties, which self-assemble in aqueous solutions of surfactants under basic conditions to create ordered architectures with nanometer-thick walls and uniform pores between 2 - 30 nm in width. The syntheses of the first examples of PMOs were accomplished from bis(trialkoxysilyl) ethane, or bis(trialkoxysilyl)ethylene or bis(trialkoxysilyl)benzene precursors and solutions containing alkyltrimethylammonium bromide surfactants. The benzenesilica and ethylenesilica materials display both meso- and molecular-scale periodicity, with clearly alternating organic and inorganic layers on the pore surface. Molecular scale is absent when the materials were prepared from ethanesilica. Differences were attributed to the size of the organic linker and to the strength of the organosilicate–organosilicate interactions but no explicit evidence was presented.

Molecular dynamics (MD) simulations using atomistic models were performed with the aim of unveiling the role of the organic linker in the structural differences observed between PMOs synthesized with different organosilicates.<sup>[1]</sup> The simulations considered three different high-pH decyltrimethylammonium bromide, water and organosilica solutions, where

the linker is benzene, ethylene or ethane, i.e., linkers that were found to lead to a high degree, to a lower degree, and to no molecular-scale periodicity, respectively. Figure 1 shows the evolution of the mass average micelle size with simulation time, where it is clear that benzenesilica or ethylenesilica promote the formation of larger aggregates than those seen in the solution with ethanesilica. This most probably originates from the higher concentration of silica species in the regions close to the surfactant heads in the two former cases as can be seen in the density profiles shown in Figure 2. Note that not only the inorganic but also the organic parts of the organosilicates are found in the space between the surfactant heads, but the densities of the silicate moieties in the tail/head interface region are visibly larger when the linker is benzene or ethylene than when the linker is ethane.

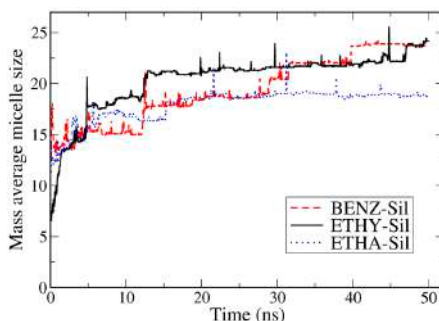


Figure 1. Mass-average micelle size as a function of simulation time for the solutions with benzenesilica, ethylenesilica and ethanesilica.

<sup>1</sup> Department of Chemistry, REQUIMTE, Faculty of Sciences, University of Porto, Portugal

<sup>2</sup> Department of Chemistry, IQTUB, Faculty of Chemistry, University of Barcelona, Spain

<sup>3</sup> Department of Chemistry, CICECO, University of Aveiro, 3810-193 Aveiro, Portugal

### References

[1] Fajin JLC, Cordeiro MNDS, Illas F, Gomes JRB, *Journal of Catalysis*, 2010, 276, 92-100.

[2] Fajin JLC, Cordeiro MNDS, Illas F, Gomes JRB, *Journal of Catalysis*, 2014, 313, 24-33.

The density profiles for the organic linkers follow closely the behavior observed for the inorganic parts of the organosilicates, i.e., for the solution containing benzenesilica there is a well-defined peak for the organic part and the peak becomes visibly broader in the case of ethylenesilica and virtually disappears in the case of

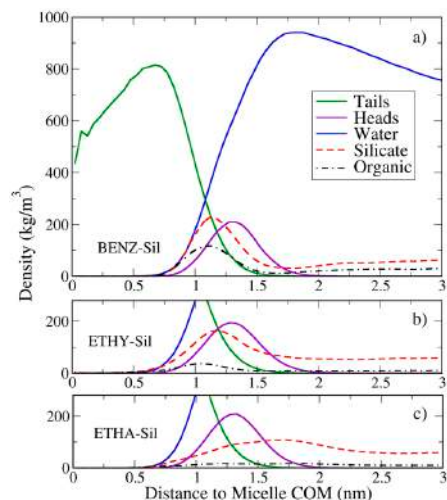


Figure 2. Density profiles of micelles with ff20 surfactants formed in solutions with a) benzenesilica, b) ethylenesilica and c) ethanesilica.

ethanesilica. Thus, most of the organosilicates interact with the micelle surface and are located in between the head groups in the former cases. A contrasting behavior is found for the solution with ethanesilica, for which the maximum of the silica density is outside the highest density region for the surfactant head groups. In this case, the organic linkers seem to be much more mobile and a well-defined peak is absent. Thus, results show that the presence or absence of molecular-scale periodicity in the pore walls of the PMO materials is due to different mechanisms of interaction between surfactant

micelles and organosilicates at the very early stages of the templated synthesis process. Precursors that adsorb strongly and orient their Si–Org–Si axis parallel to the micelle surface may lead to materials with molecular-scale periodicity, while

with more flexible precursors that are less ordered this periodicity is not observed.

<sup>1</sup> Department of Chemistry, CICECO, University of Aveiro, 3810-193 Aveiro, Portugal

<sup>2</sup> LSRE/LCM, Faculty of Engineering, University of Porto, Portugal

#### Reference

[1] Futamura R, Jorge M, Gomes JRB, *Physical Chemistry Chemical Physics*, 2013, 15, 6166-6169.

## COMBINING QUANTUM MECHANICS WITH MOLECULAR SIMULATION FOR PREDICTING ADSORPTION IN MOFS WITH UNSATURATED METAL SITES

Jorge M<sup>1</sup>, Fischer M<sup>2</sup>, Gomes JRB<sup>3</sup>

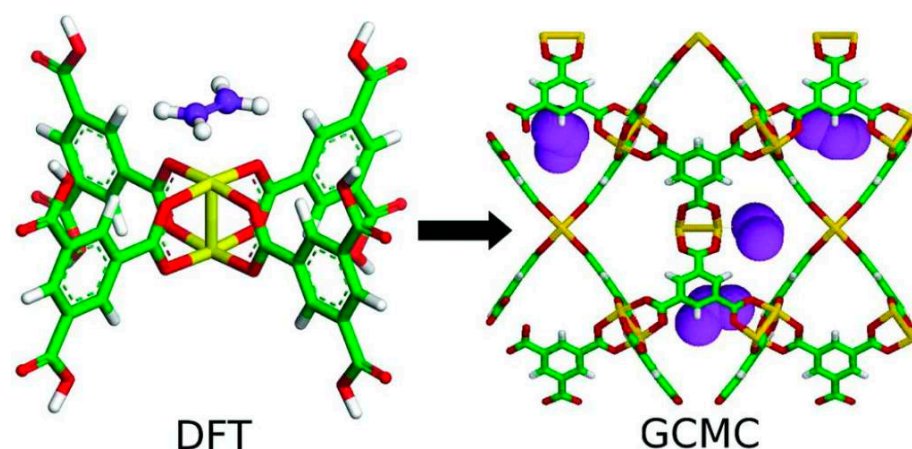


Figure 1. On the left it is shown the geometry used for the DFT calculations of ethylene adsorbing onto a  $\text{Cu}_2(\text{btc})_2$  cluster (btc= benzene-tricarboxylate) while on the right it is shown a typical snapshot from the GCMC simulations on propylene adsorption in CuBTC. Color coding is green for C in the framework, purple for C in the sorbate, white for H, red for O, and yellow for Cu.

Metal-Organic Frameworks (MOFs) allow for simultaneously tuning the pore structure and the surface chemistry of the adsorbent, thus opening the possibility of a priori material design to suit particular adsorption applications, including gas storage and separation. MOFs have shown tremendous potential for challenging gas separation applications, an example of which is the separation of olefins from paraffins. Some of the most promising MOFs show enhanced selectivity for olefins due to the presence of coordinatively unsaturated metal sites. CuBTC, or HKUST-1, is a commercial MOF containing unsaturated Cu sites that are able to selectively bind unsaturated hydrocarbons by interacting with the  $\pi$ -orbitals of these molecules. Unfortunately, it is still not possible to accurately predict adsorption in MOFs with unsaturated metal sites, since most classical models are unable to cope with this phenomenon.

A new approach to model adsorption in MOFs with unsaturated metal sites in

CuBTC is presented [1,2]. It combines electronic density functional theory (DFT) calculations with grand canonical Monte Carlo (GCMC) simulations at the classical level (Figure 1). The DFT calculations were used to calculate the energy profile for ethylene adsorption on the unsaturated metal sites of CuBTC. Then, an empirical function for modelling the specific Cu- $\pi$  interaction energy profile was calculated from  $U_{\text{Cu}-\pi}(\mathbf{r}) = U_{\text{DFT}}(\mathbf{r}) - U_{\text{Rep}}(\mathbf{r})$ , where  $U_{\text{DFT}}$  is the DFT interaction energy between ethylene and the CuBTC cluster,  $U_{\text{Cu}-\pi}$  is the contribution to the energy due to the specific interaction between the Cu atom and the olefin double bond,  $U_{\text{Rep}}$  is the repulsion contribution and made equal to the repulsive contribution of the Lennard-Jones potential, and  $r$  is the distance between the center of the double bond and the closest Cu atom of the MOF. With this approach, the remainder of the model, i.e., the LJ interactions between each adsorbate site and all the other adsorbate and adsorbent sites in the system (including the metal), were

kept unchanged relatively to the standard DREIDING force field that can tackle correctly the interaction between alkanes and CuBTC. It presents obvious advantages: i) it allows to simplify the problem, without the need for a full reparameterization of all the fluid-solid potential parameters; ii) it increases the chances that the model will be transferable to other MOFs; and iii) the model will benefit directly from independent force field developments.

Using this new approach, it was possible to accurately predict adsorption isotherms not only for ethylene on CuBTC, which was the adsorbate used to derive the new function,

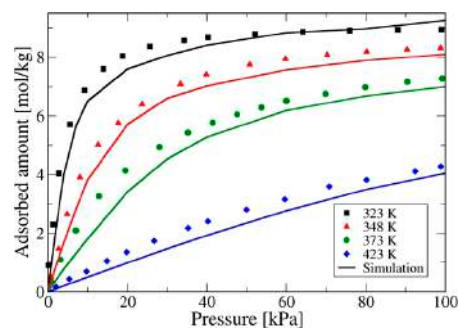


Figure 2. Comparison between experimental (points) and simulated (lines) adsorption isotherms for propylene on CuBTC at several temperatures.

but also for ethane, propane and propylene (Figure 2). Crucially, it was found that good predictions can only be obtained in the case of the olefins only when the specific interactions between the metal sites and the olefin double bonds are explicitly taken into account in the simulations.

<sup>1</sup> Department of Chemical and Process Engineering, University of Strathclyde, United Kingdom

<sup>2</sup> Fachbereich Geowissenschaften, University of Bremen, Germany

<sup>3</sup> Department of Chemistry, CICECO, University of Aveiro, 3810-193 Aveiro, Portugal

#### References

- [1] Fischer M, Gomes JRB, Fröba M, Jorge M, *Langmuir*, 2012, 28, 8537-8549.  
 [2] Jorge M, Fischer M, Gomes JRB, Siquet C, Santos JC, Rodrigues AE, *Industrial and Engineering Chemistry Research*, 2014, in press. DOI: 10.1021/ie500310c

# AB-INITIO VALIDATION OF A RELATION BETWEEN LOCAL ELECTRIC FIELD AND GLOBAL POLARIZATION IN FERROELECTRICS

Gonçalves JN<sup>1</sup>, Stroppa A<sup>2</sup>, Correia JG<sup>3</sup>, Butz T<sup>4</sup>, Picozzi S<sup>2</sup>, Fenta AS<sup>1</sup>, Amaral VS<sup>1</sup>

Atomic nuclei with non-spherical shape interact, via its quadrupole moment, with the electric field gradient (EFG) at the nucleus due to their local extranuclear environment. This interaction can be measured by several hyperfine experimental techniques such as nuclear magnetic/quadrupolar resonance, perturbed angular correlations and Mössbauer spectroscopy, and with knowledge of the nuclear quadrupole momenta it becomes a sensitive quantitative atomic scale probe of electronic distribution in molecules and solids. EFG is a second-rank tensor, quantified by the second derivative of the electrostatic potential at the nuclear position that is accurately calculated using state-of-the-art density functional theory (DFT) methods. Some works can be found in literature back to the 1960s and 1970s where the quadrupole hyperfine interaction was measured in ferroelectrics, materials which lose spatial inversion symmetry and order spontaneously with an electric polarization ( $P$ ). At the time, the results provided the hint that a relation between the EFG and  $P$  could be established in some materials. This quantity has recently achieved a full understanding with the modern theory [see for example, Rabe et al (Eds), *Physics of Ferroelectrics: A Modern Perspective* (Springer, Berlin, 2007)], in which the absolute value of  $P$  is not uniquely defined, but its variations are unique, a consequence of an integrated current over time, related to the Berry phase, a geometrical phase acquired by the electrons in the adiabatic path connecting two states with different values of polarization. At the time of these first hyperfine measurements in ferroelectrics, only empirical or simplified models could

be implemented and discussed. With the improved conceptual framework of both properties, it is possible now to calculate them accurately by ab-initio DFT without adjustable parameters and in a systematic way. We studied simple ferroelectrics with several different cations and with perovskite-based structures, varying in each the polar distortion in small step, between 0% (paraelectric) to 120% (experimental ferroelectric + 20% distortion). The results revealed that the EFG is linearly proportional to  $P$  squared, matching the previous experiments and models. The figure shows this relation for the

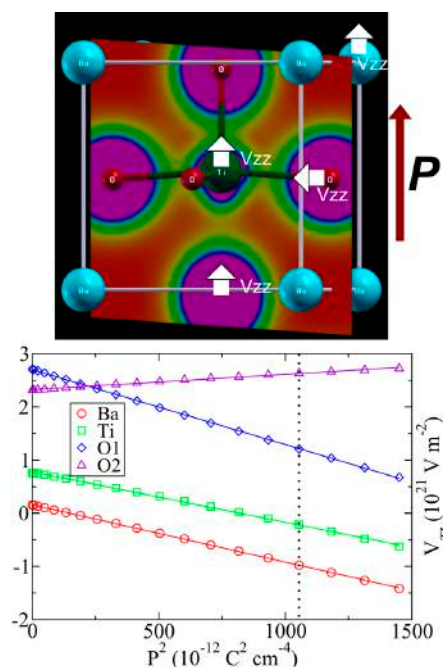


Figure 1. Top) picture of the experimental structure of BaTiO<sub>3</sub>, showing the direction of  $V_{zz}$  (largest EFG principal component) at some atoms and the electric polarization. Bottom)  $V_{zz}$  as a function of the polarization squared, showing the linear relationship. The dotted line corresponds to the values calculated with the experimental tetragonal structure at equilibrium conditions.

Ba, Ti and O atoms in tetragonal barium titanate, a classical ferroelectric, where Ti and O atoms have average displacement of 8 picometers. In some cases, an additional higher order term is needed only for very large distortion ranges, for which there is not yet experimental data available. Our computational “experiments” for a wide range of materials also allowed the accurate characterization of the EFG tensor, which established a linear relationship between the EFG tensor components, and a variation of EFG with the square of the atomic number at the corner site of the perovskite lattice, a very general relation which is still not well understood.  $P$  is sometimes a difficult property to quantitatively measure with the more conventional techniques due to non-homogeneity effects and leakage currents. The EFG, in contrast, can be measured in a wide range of conditions at the local atomic scale, which makes a deeper study of this relationship worthwhile. ISOLDE (Isotope Separator On-Line, at CERN), with the large number of radioactive Perturbed Angular Correlation probe nuclei, is one of the places available to carry experiments even under extreme conditions to understand polarization and phase transitions in materials via hyperfine interactions probing. The extension of this relation to more complex multiferroic and magnetoelectric cases is being theoretically studied along with EFG measurements at ISOLDE-CERN.

<sup>1</sup> Department of Physics, CICECO, University of Aveiro, 3810-193 Aveiro, Portugal

<sup>2</sup> CNR-SPIN, 67100 L'Aquila, Italy

<sup>3</sup> Centro de Ciências e Tecnologias Nucleares, Instituto Superior Técnico, University of Lisboa, Portugal

<sup>4</sup> Fakultät für Physik und Geowissenschaften, Institut für Experimentelle Physik II, Universität Leipzig, Germany

## Reference

[1] Gonçalves JN, Stroppa A, Correia JG, Butz T, Picozzi S, Fenta AS, Amaral VS, *Physical Review B*, 2012, 86, 035145.

## Acknowledgments

Work supported by FCT research projects [PTDC/FIS/105416/2008, CERN/FP/116320/2010] and Grant SFRH/BD/42194/2007.

# Outreach

## “THE CHEMISTRY OF THINGS” MULTIMEDIA PROJECT

Ribeiro-Claro P<sup>1</sup>



Figure 1. “The Chemistry of Things” logo composition

“The Chemistry of Things” is a multimedia project that reveals the chemistry hidden in our day-to-day activities and shows how recent scientific developments have improved our lives. A total of 26 episodes, each of three minutes, have been produced. The topics covered include breakfast cereals, computers, fireworks, and even romantic love. To accompany these episodes a number of leaflets entitled “if you want to know more about...” have also been produced. The target audience for this project was the general public and special attention was given to the original texts in which the screenplays were based. As all the episodes include some chemical/scientific content an effort was made to keep the language clear and simple. The use of animation effects to demonstrate scientific principles, the use of molecular models, and the choice of entertaining examples of where chemistry can be found also allow the episodes to be used in high schools. Overall the quality of the videos was recognised as being of added value among young people.

“The Chemistry of Things” was available on television, radio, internet, social networks, and iPad. The original video episodes were broadcast by the national channel RTP2 (2012) and by the cable channel SICKkids (2013). These episodes are also still accessible on the dedicated channel MEO 606600. The radio version

was transmitted on RDP International and RDP Africa “Científica Mente” (March-December 2012).

A website was produced for the project ([aquimicadascoisas.org/en/](http://aquimicadascoisas.org/en/)) and social networks, such as YouTube ([youtube.com/user/quimicadascoisas](http://youtube.com/user/quimicadascoisas)) and Facebook ([facebook.com/AQuimica dasCoisas](http://facebook.com/AQuimica dasCoisas)) have been used to ensure the continued visibility of the project. By the end of 2013, the website registered *ca.* 75.000 visits, the YouTube videos have collected more than 60.000 views, and the Facebook page more than 10.000 fans. These numbers are still increasing at a good rate! Finally an application was developed for iPad (it has been downloaded more than 5000 times) and the leaflets accompanying the programs are available as an e-Book, in both *pdf* and *iBook* versions.

The national and international impact of the project can be measured via the geographical origin of internet access and downloads and through the comments and reviews on educational resources sites, such as “Casa das Ciências” ([casadasciencias.org](http://casadasciencias.org)) and “Chemistry Is All Around Us Network” ([chemistrynetwork.pixel-online.org](http://chemistrynetwork.pixel-online.org)). Another indication of the impact of the project comes from its participation in international science

festivals. “The Chemistry of Things” programs have been shortlisted for the science film festival “Scinema” (Australia) in 2012, and were included (in two categories) in the first shortlists for the

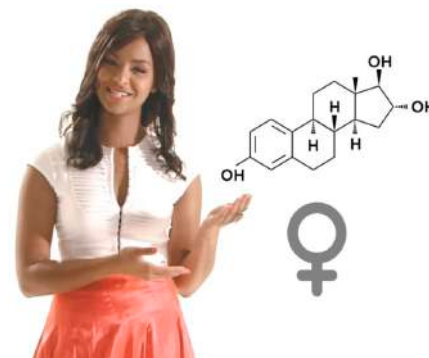


Figure 2. Snapshot of video episode, with presenter Claudia Semedo

“European Science TV and New Media Awards” in 2013 ([europaws.org/archive/festival-2013/2013-shortlist/](http://europaws.org/archive/festival-2013/2013-shortlist/)) where they faced competition from major European TV producers such as the BBC (UK), ARTE (France) and ZDF (Germany). The project was produced as an “official activity” of the International Year of Chemistry 2011 and was funded by COMPETE – Competitive Factors Operational Programme and by Ciência Viva, Media Science Programme.

<sup>1</sup> Department of Chemistry, CICECO, University of Aveiro, 3810-193 Aveiro, Portugal

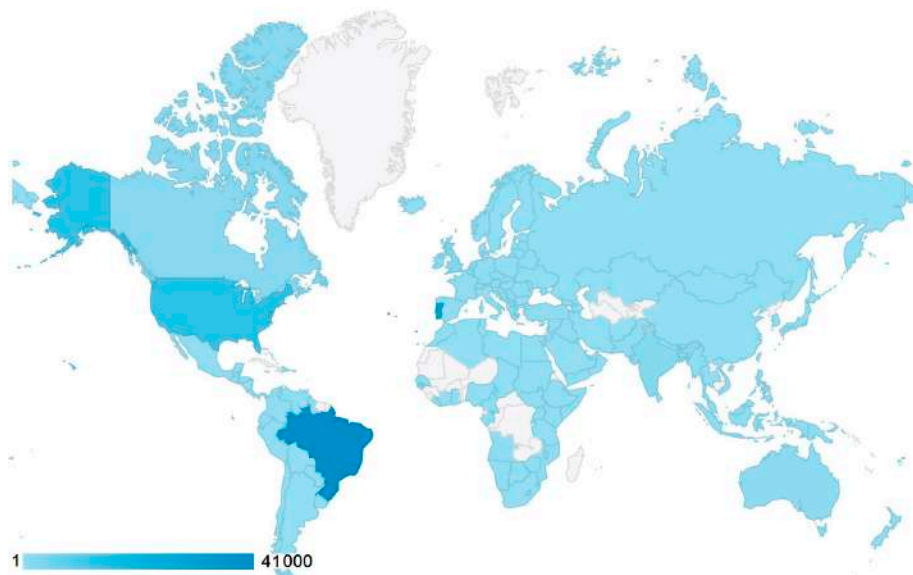


Figure 3. Geographical distribution of website visitors

## WEBCAM-BASED SPECTROGRAPH FOR A STUDENT PROJECT

Ferreira RAS<sup>1</sup>, André PS<sup>2</sup>

This work describes the implementation of a low-cost spectrometer produced with common objects (Figure 1) and proposed as a pedagogical students' project [1]. The development of this project in the classroom environment is an important diagnostic tool for the students' performance and skills but is also a pedagogical technique in a teaching-learning context, being used to explain new basic concepts to the students, such as optical diffraction, CCD operation and colour quantification.

The goals of this project are introduce the theme of image detection and to stimulate the students to develop skills in the field of optics and photonics. The emission spectra of light emitting diodes (LEDs) operating

in the visible spectral range were used to evaluate the performance of the developed spectrometer (Figure 1c). The implemented

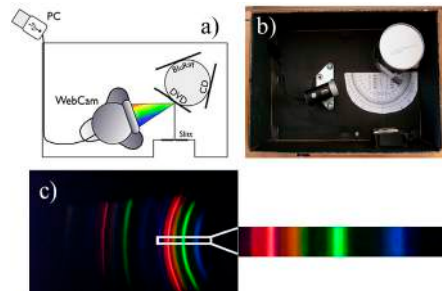


Figure 1. a) Scheme and b) photography of the implemented spectrometer layout with real dimensions of  $15 \times 10$  cm<sup>2</sup>. c) Native image acquired for the CFL lamp with  $960 \times 44$  pixels and [right side] cropped image for data processing with  $250 \times 25$  pixels.

device was also useful for demonstrations allowing colour coordinate calculations, which can help students to make the distinction between a graphical representation of a spectrum and the visual colour emission. The results pointed out that the proposed methodology provides good resolution and precision in the calculation of the CIE colour coordinates. This project was offered with success in 2010 to students from the Optoelectronics unit of the Physics Engineering Masters degree at Aveiro University, Portugal.

<sup>1</sup> Department of Physics, CICECO, University of Aveiro, 3810-193 Aveiro, Portugal

<sup>2</sup> Department of Electric and Computer Engineering and Instituto de Telecomunicações Instituto Superior Técnico, Universidade de Lisboa, Lisbon, Portugal

### Reference

[1] Trindade A, Falcão B, Carramate LFND, Marques MISF, Ferreira RAS, André PS, *International Journal of Electrical Engineering Education*, 2014, 51, IJEEE.51.1.1.

## BRING DISCOVERY INTO THE CLASSROOM: HOW TO EVALUATE PLANCK'S CONSTANT USING SIMPLE EQUIPMENT

Ferreira RAS<sup>1</sup>, André PS<sup>2</sup>

When we think of the evaluation of fundamental physical constants, such as the speed of light or the force of gravity, we probably think of famous, large-scale experiments – but classroom equipment can also be used to calculate these unvary-

ing values [1]. A simple and practical experiment was described and implemented to enable the determination of the value of the Planck constant, which is widely used in quantum physics. The experimental set-up (Figure 1) is easily reproducible in

class or used by students in an independent research project, as the materials used are commonly found in physics labs. In particular, light emitting diodes (LEDs) operating in the visible are used in this experiment because each LED has a different threshold voltage at which photons start being produced. Measuring this voltage, together with known values for the emission wavelengths, provide a path to finding a value for the Planck constant (Figure 1). The experimental activities will help students to understand important concepts, such as: the photo-electric effect, where 'packets of energy' are absorbed by a material and consequently cause a diode to emit electromagnetic waves; the activation voltage in diodes; calculation of the Planck constant [1].

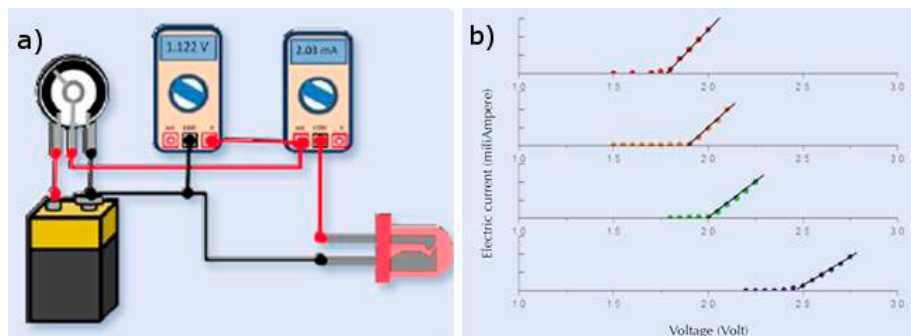


Figure 1. a) Electric circuit for measuring the voltage-current response of each LED. From left to right: battery, potentiometer or rheostat, voltmeter, ammeter, LED. b) Voltage-current response of LEDs emitting red, orange, green and blue light linear response region backwards (from top to bottom).

<sup>1</sup> Department of Physics, CICECO, University of Aveiro, 3810-193 Aveiro, Portugal

<sup>2</sup> Department of Electric and Computer Engineering and Instituto de Telecomunicações Instituto Superior Técnico, Universidade de Lisboa, Lisbon, Portugal

### Reference

[1] Ferreira RAS, André PS, *Science in School*, 2014, 28, 28.

**Editorial coordination**

João Rocha, Luís Dias Carlos, Joaquim Vieira and Ruben Silva

**Cover design**

Álvaro Sousa and Ruben Silva

**Print process**

Gráfica Maiadouro S.A.

**Number of copies**

1000

**This publication was financially supported by**

FEDER through Programa Operacional Fatores de Competitividade – COMPETE and national funds through FCT – Fundação para a Ciência e Tecnologia within CICECO project – FCOMP-01-0124-FEDER-037271 (FCT Ref. PEst-C/CTM/LA0011/2013)



